Nonlinear Response of Cantilever Beams

Haider N. Arafat

Dissertation submitted to the Faculty of the
Virginia Polytechnic Institute and State University
in partial fulfillment of the requirements for the degree of

Doctor of Philosophy
in
Engineering Mechanics

Ali H. Nayfeh, Chairman
L. Glenn Kraige
Dean T. Mook
Scott L. Hendricks
Muhammad R. Hajj
Mehdi Ahmadian

April 9, 1999
Blacksburg, Virginia

Keywords: Nonlinear Responses, Beams, Vibrations, Modal Interactions, Resonances.

Nonlinear Response of Cantilever Beams

Haider N. Arafat

(ABSTRACT)

The nonlinear nonplanar steady-state responses of cantilever beams to direct and parametric harmonic excitations are investigated using perturbation techniques. Modal interactions between the bending-bending and bending-bending-twisting motions are studied. Using a variational formulation, we obtained the governing equations of motion and associated boundary conditions for monoclinic composite and isotropic metallic inextensional beams. The method of multiple scales is applied either to the governing system of equations and associated boundary conditions or to the Lagrangian and virtual-work term to determine the modulation equations that govern the slow dynamics of the responses. These equations are shown to exhibit symmetry properties, reflecting the conservative nature of the beams in the absence of damping.

It is popular to first discretize the partial-differential equations of motion and then apply a perturbation technique to the resulting ordinary-differential equations to determine the modulation equations. Due to the presence of quadratic as well as cubic nonlinearities in the governing system for the bending-bending-twisting oscillations of beams, it is shown that this approach leads to erroneous results. Furthermore, the symmetries are lost in the resulting equations.

Nontrivial fixed points of the modulation equations correspond, generally, to periodic responses of the beams, whereas limit-cycle solutions of the modulation equations correspond to aperiodic responses of the beams. A pseudo-arclength scheme is used to determine the fixed points and their stability. In some cases, they are found to undergo Hopf bifurcations, which result in limit cycles. A combination of a long-time integration, a two-point boundary-value continuation scheme, and Floquet theory is used to determine in detail branches of periodic and chaotic solutions and

assess their stability. The limit cycles undergo symmetry-breaking, cyclic-fold, and period-doubling bifurcations. The chaotic attractors undergo attractor-merging and boundary crises as well as explosive bifurcations.

For certain cases, it is determined that the response of a beam to a high-frequency excitation is not necessarily a high-frequency low-amplitude oscillation. In fact, low-frequency high-amplitude components that dominate the responses may be activated by resonant and nonresonant mechanisms. In such cases, the overall oscillations of the beam may be significantly large and cannot be neglected.

In the Name of God (Allah), the Benevolent, the Merciful.

Dedication

To my Mother and Father, with love, admiration, and gratitude.

Acknowledgments

I would like to thank Dr. Ali Nayfeh for his invaluable guidance and advice throughout my Ph. D. studies. His encouragement, thoughtfulness, and willingness to help are deeply appreciated. His brilliance, resourcefulness, and patience are greatly admired. It has been my pleasure to have him as a friend as well as a mentor.

I would also like to thank my committee members: Dr. Glenn Kraige for his support and belief in me, it is an honor to have worked with him and learned from him; Dr. Dean Mook for his advice and encouragement; Dr. Scott Hendricks for giving me an invaluable understanding and appreciation for dynamics, his skillful and clear approach to teaching such a challenging material is unique; Dr. Muhammad Hajj for his friendship, understanding, and caring attitude; and Dr. Mehdi Ahmadian for his thoughtfulness, invaluable comments, and fresh ideas.

I would like to thank all of the people and friends I have met as part of the Nonlinear Dynamics Group. In particular, I would like to thank Mr. Ryan Krauss for his unselfishness and for teaching me how to conduct experiments; I thank Mr. Mohammed Al-Fayyoumi, Mr. Ayman El-Badawi, Dr. Shafic Oueini, Mr. Nader Nayfeh, Mr. Sean Fahey, and Mr. Ben Hall for their friendship and inspiring ideas. Thanks are also due to Dr. Char-Ming Chin for his patience and expert advice and to Mrs. Sally Shrader for her friendship and help in administrative matters.

I would like to thank the National Science Foundation and the Air Force Office of Scientific Research for their support of this research under Grants No. CMS-9423774 and No. F49620-95-1-0254, respectively.

Special acknowledgements are due to the following persons: Dr. Fred Just for being the nicest

person I have ever known and for his continuous encouragement and belief in me; Drs. Hung-Peng Li and Jay Warren for their friendship and companionship; Dr. Eihab Abdel-Rahman for his tolerant behavior and interesting personality; Mr. Naim Jaber for his generosity, hospitality, and the fun times we had playing basketball; Mr. Osama Ashour for his cheerful attitude and kindness; and Mr. Sami Al-Masalha for being an exciting, fun, and resourceful friend.

Most importantly, I would like to thank my family without whose support, I would have never reached this point: my father, Mr. Nabhan Arafat, whose accomplishments, boundless energy, and words of wisdom are great sources of inspiration to me; my mother, Mrs. Siham Arafat, to whom I am forever grateful for the love, kindness, sensibility, and devotion she showed me from day one; and my sisters, May and Rabab, who throughout the years tolerated their younger brother, filled his life with fun and happiness, encouraged him, and stood by him through thick and thin. Finally, thanks goes to All Mighty God for giving me the ability, mindset, and perseverance to be where I am now.

Contents

List of Figures

List of Tables

Chapter 1

Introduction

1.1 Motivation

We investigate nonlinear modal interactions that may occur in externally excited cantilever beams. Airplane wings, helicopter blades, gun barrels, and high-rise buildings are just some of the mechanical and structural examples where vibration analysis of structures in general and beams in particular is essential for their design. Linear modeling of structures can be inaccurate, inadequate, and misleading. It is inaccurate when the amplitudes of oscillations are high and the natural frequencies become increasingly dependent on these amplitudes (e.g., Woinowski-Krieger, 1950; Burgreen, 1951). It is inadequate because it does not consider the effect of one mode's oscillations on another, and therefore it eliminates the possibilities of quasiperiodic and whirling motions (e.g., McDonald, 1955; Haight and King, 1970 and 1972). Finally, it is misleading because it might predict a certain solution to be stable when in fact it is unstable (e.g., Nayfeh and Mook, 1979,§7.3). Needless to say, certain response characteristics, such as jumps, bifurcations, saturation, and multiplicity of solutions, are all ignored by linear models, all of which can occur in a structure. Therefore, to fully grasp and anticipate the behavior of a structure, one needs to consider the influence of nonlinearities inherent in the system (von Kármán, 1940; Zavodney, 1987; Nayfeh, Mook, and Nayfeh, 1987; Hodges, Crespo da Silva, and Peters, 1988; and Nayfeh and Balachandran, 1989).

Nonlinearities may couple the different flexural, torsional, and longitudinal modes of a structure,

and hence the reaction to a simple harmonic excitation can be either a simple harmonic response or a very complex response consisting of many modes and exhibiting undesirable motions, such as chaotic oscillations. Therefore, unless these responses are fully understood and accounted for in designing a structure, unpredictable results that can be in some instances catastrophic may occur. To further illustrate this point, we present three examples.

Probably, the most notorious is the collapse of the Tacoma Narrows Bridge on November 7, 1940, just a few months after it was finished (Billah and Scanlan, 1990). From the beginning, motorists noticed that the bridge repeatedly and noticeably vibrated in pure bending, even when under good weather conditions, that it was labeled "Galloping Gertie." However inconvenient, such bending motions were believed to be safe because their amplitudes were small and limited, and so they would eventually be damped out. However, on the ill-fated day, the narrow I-section bridge was hit by a 42 mph wind gust that ever-so-slightly excited the fundamental torsional mode. This torsional motion, whose amplitude was not limited, induced a flutter wake. The flutter wake in turn fed energy back into the torsional motion, acting as a parametric excitation that produced negative damping in the system. This process continued for nearly 45 minutes with the torsional motion monotonically increasing until the bridge fell apart, as can be seen from Figures 1.1 and 1.2. Subsequent design modifications included a larger width-to-span ratio and framed sides. This stiffened the bridge in torsion and prevented the wind from getting trapped underneath it, thereby eliminating the possibility of introducing negative damping.

An equally disastrous event is that of the Lockheed L-188 Electra plane (Serling, 1963). In 1959, Lockheed introduced its first turboprop engine plane that was capable of carrying at least 65 passengers and cruising at a speed of more than 400 mph. The plane, which was propelled by four engines, was designed to be fail-safe and was extensively tested both for structural strength and for handling and performance under severe weather conditions. It also passed and exceeded all of the required Civil Aeronautics Administration (now the Federal Aviation Agency) safety specifications. However, on September 29, 1959, just ten days after it was delivered, Braniff flight 542 on its way from Houston to New York broke apart and crashed over Buffalo, Texas, killing all passengers. Investigators combed through the wreckage and found that parts of the left engines (numbers one and two) as well as a section of the left wing were the farthest distance away, indicating a structural

(a) (b)

Figure 1.1: The Tacoma Narrows bridge before failure exhibiting large twisting motions. (a) Side view and (b) end view. Obtained from the internet site: http://www.fen.bris.ac.uk/engmaths/research/nonlinear/tacoma/tacoma.html.

failure of the left wing. However, they were baffled as to the cause for such a failure, especially since the weather was calm and the wings had been put through torture without failing.

Less than six months later, on March 17, 1960, Northwest flight 710 from Minneapolis to Miami crashed over Tell City, Indiana as it encountered severe "clear-air" turbulence. Similar to the first accident, the right wing and parts of the right-most engine (number four) were located the farthest away from the crash site. It was later discovered that small whirling motions of the propeller caused the engine to wobble in its nacelle in the opposite direction. Such whirling motions were not uncommon and are usually resisted and quenched by the stiffness in the nacelle. However, in this case, the engine mounts were designed for strength but lacked the necessary stiffness. As the opposing whirlings of the propeller and turbine kept feeding each other, their gyroscopic motion caused the wing to vibrate. After some time, as the frequency of the whirling motion slowed down, its amplitude became very large, thereby inducing very violent forces on the wing. Eventually, the whirling frequency went down to about 3 Hz, which happened to be the flutter frequency of the wing. At that moment, the wing tore apart. It is estimated that the whole process took about thirty seconds.

Figure 1.2: A side view of the Tacoma Narrows bridge tearing apart. Obtained from the internet site: http://www.civeng.carleton.ca/Exhibits/Tacoma_Narrows/DSmith/photos.html.

Figure 1.3: A model of the Lockheed L-188 Electra plane (Braniff Airways).

The third case happened early last year as I was driving my 1988 Ford Escort in Blacksburg. For weeks, squeaking noises were coming from the engine hood because the alternator belt was slipping. The belt was replaced several times, but the slipping persisted. One day, the alternator mounting bracket all of a sudden snapped and broke into two pieces. The bracket was originally attached to the engine block by two bolts. Apparently, one bolt had sheared and the other one, while still able to hold the bracket to the block, could not keep it still. Excitations due to the tension forces in the belt and the inertia of the alternator caused the bracket to vibrate to the point that the bolt rimmed the block around it, creating a hole twice the diameter of the original one. Presumably, because of the bracket's increasing oscillations, the stresses became so large that it broke. The

cut was smooth and at an angle indicating that it might have been vibrating in torsion as well as bending. This is quite possible as the cast-aluminum part had an almost C-type cross-section which can be susceptible to twisting.

These incidents clearly demonstrate the importance of considering modal interactions, whether occurring within the structure itself or between the structure and its surroundings. The purpose of this work is to investigate such interactions in cantilever beams.

1.2 Background and Literature Review

The analytical investigations of the nonplanar responses of cantilever beams basically fall into two categories. In the first category, the influence of nonlinearities were either neglected or partially considered. Some included the effect of inertia nonlinearities but disregarded the effect of geometric ones (Haight and King, 1970, 1972; and Hyer, 1979); some considered just the effect of geometric nonlinearities (Tso, 1968); and then, others considered just the linear system (Dugundji and Mukhopadhyay, 1973; Cartmell and Roberts, 1987; and Kar and Sujata, 1990, 1992). In the second category, both geometric and inertia nonlinearities were considered (Crespo da Silva and Glynn, 1978b; Nayfeh and Pai, 1989; Pai and Nayfeh, 1990a, b and 1991a, b; Crespo da Silva, Zaretzky, and Hodges, 1991; Shyu, Mook, and Plaut, 1993a, b, and c; Crespo da Silva and Zaretzky, 1994; Zaretzky and Crespo da Silva, 1994b; and Lee, Lee, and Chang, 1997).

The second-category work clearly shows that including both geometric and inertia nonlinearities is very important for predicting the beam's response accurately. Therefore, we account for both geometric and inertia nonlinearities in our analysis. Furthermore, unlike most studies, we account for nonlinearities in the boundary conditions. This is important for ensuring that the obtained approximate solution without the damping terms is derivable from a Lagrangian and a virtual-work term, and hence the conservative nature of the beam in the absence of damping is not lost. Moreover, neglecting the effect of nonlinearities in the boundary conditions leads to inaccurate results, which may be more significant in the case of composite beams where the coupling is linear as well as nonlinear.

In general, two analytical approaches have been used to investigate the nonlinear vibrations of

distributed-parameter systems. In the first approach, the governing partial-differential equations and boundary conditions are first discretized using a variant of the method of weighted residuals. Then, a perturbation method is applied to a truncated set of the discretized nonlinear ordinary-differential equation. In the second approach, a perturbation method is directly applied to the partial-differential system. To third order, both of these approaches are equivalent for systems possessing cubic nonlinearities, as in the case of flexural-flexural vibrations of beams. On the other hand, for systems possessing quadratic and cubic nonlinearities, as in the case of flexural-flexural-torsional vibrations of beams, the first approach may lead to erroneous values for the coefficients of the modulation equations. This is because the influence of the spatial solution at second order is incorrectly accounted for (Nayfeh, 1997).

Therefore, throughout our investigation, we employ the direct approach and apply the method of multiple scales directly to the partial-differential equations of motion and nonlinear boundary conditions or apply the method of time-averaged Lagrangian along with Hamilton's extended principle directly to the Lagrangian and virtual-work term. This is in contrast to the work of Crespo da Silva and Zaretzky (1994), Zaretzky and Crespo da Silva (1994b), and Lee, Lee, and Chang (1997) who investigated flexural-flexural-torsional responses of cantilever beams by treating a truncated set of discretized equations and neglecting nonlinearities in the boundary conditions. We demonstrate such discrepancy between these two approaches for a metallic beam that experiences bending-torsional interactions due to combination parametric resonances.

Feng and Leal (1994) pointed out and analytically established symmetries in the modulation equations derived by Nayfeh and Pai (1989) for flexural-flexural vibrations of cantilever beams. Using the method of time-averaged Lagrangian, we show that, as long as a system is derivable from a Lagrangian and a virtual-work term, the corresponding modulation equations possess some symmetries. Next, we present a review of the relevant investigations in more detail.

1.2.1 Flexural-Flexural Oscillations of Inextensional Beams

Free Oscillations and Primary Resonance Responses

Haight and King (1972) theoretically and experimentally investigated the responses of circular and near-square cantilever beams to lateral base excitations. They neither accounted for the effect of torsional oscillations nor included geometric nonlinearities; they included only the inertia nonlinearities. They found that, in certain cases, planar motions can lose stability, thereby driving the nonplanar motions. In addition, they found that whirling motions existed in the instability zones in contrast to their experience with parametrically excited beams (Haight and King, 1970). Dowell, Traybar, and Hodges (1977) experimentally investigated the free responses of cantilever beam-mass systems taking into account the effect of static twist. The static deflections and natural frequencies were measured and compared to analytical results obtained using the equations of Hodges and Dowell (1974) for helicopter blades. They found good agreement for relatively small tip loads. However, the discrepancies widened for heavier tip loads.

Crespo da Silva and Glynn (1978b) used the equations they (1978a) had derived to investigate the flexural-flexural responses of near-square cantilever beams to primary resonances. They accounted for both geometric and inertia nonlinearities. They found that the response curves for the first mode are significantly different from the response curves for the higher ones. Furthermore, the influence of the nonlinear curvature terms on the response diminishes for higher modes. They (1979) also used their equations to investigate the free nonplanar responses of internally resonant cantilever beams.

Hyer (1979) investigated the whirling responses of compact cantilever beams to lateral base excitations. He used the equations of Haight and King (1972), neglected the effect of damping, and found that whirling motions exist when the beam is excited near resonance. Furthermore, he was unable to locate unstable whirling motions. Crespo da Silva (1980) also considered the whirling motions of base-excited cantilever beams by using the equations of Crespo da Silva and Glynn (1978b) and including viscous damping. He found that some whirling motions are unstable and that, in some ranges of frequency detuning, neither planar nor nonplanar stable steady-state motions existed.

Pai and Nayfeh (1990a) used the equations of Crespo da Silva and Glynn (1978b) to investigate

the nonplanar oscillations of square and rectangular cantilever beams to lateral base excitations. They located Hopf bifurcations and found that the system can exhibit quasiperiodic (beating) and chaotic motions. Furthermore, they found that the geometric nonlinearities dominate the inertia nonlinearities for the low-frequency modes, whereas the inertia nonlinearities dominate the geometric nonlinearities for the high-frequency modes. The geometric nonlinearities produce a hardening spring effect and the inertia nonlinearities produce a softening spring effect.

Crespo da Silva, Zaretzky, and Hodges (1991), in a work related to that of Dowell, Traybar, and Hodges (1977), analytically investigated the accuracy of approximate solutions for the free nonplanar response of cantilever beam-mass systems. They found excellent agreement with the results obtained by numerically integrating the exact equations, even for large tip loads.

Shyu, Mook, and Plaut (1993a, b, and c) investigated the nonlinear response of square cantilever beams to transverse harmonic and nonstationary excitations. In addition to the cubic geometric and inertia nonlinearities, they accounted for the effect of the static deflection due to the beam's weight, which introduced quadratic nonlinearities in the governing equations. They applied the method of multiple scales to the discretized system and studied primary, superharmonic, and subharmonic resonances. They found that whirling motions are possible and in some cases they are the only stable motions. Furthermore, they found that increasing the damping reduces the amplitudes of the whirling motions.

Zaretzky and Crespo da Silva (1994a) experimentally investigated the nonlinear flexural-flexural responses of cantilever beams to harmonic base excitations. They found excellent agreement between their experimental results and the analytical results obtained by Crespo da Silva and Glynn (1978b). Furthermore, they concluded that the effect of nonlinear damping can be quite significant for high-amplitude motions.

Principal Parametric Resonance

Very interesting phenomena that can occur in the vibrations of structures are parametric resonances. In such cases, the excitation appears as a time varying coefficient in the equations of motion. Principal parametric resonances occur when the excitation frequency is near twice one of

the natural frequencies of the system. Many studies investigated the responses of general single- and multi-degree-of freedom systems to parametric resonances (Krishnaiyar, 1922; Rayleigh, 1945, §68*b*; Bolotin, 1964; Mettler, 1967; Asmis and Tso, 1972; Tso and Asmis, 1974; Nayfeh and Mook, 1979; Tezak, Nayfeh, and Mook, 1982; Nayfeh, 1983a, b and 1987; Nayfeh and Zavodney, 1986; Nayfeh and Jebril, 1987; Streit, Bajaj, and Krousgrill, 1988; Cartmell, 1990; and Chin, Nayfeh, and Mook, 1995).

Evan-Iwanowski (1965) gave an excellent review of the parametric response of structures. He noted that although such a phenomenon was first observed by Faraday in 1833, Beliaev in 1924 was the first to investigate it in connection with the vibrations of structures. Beliaev considered the linear response of a pinned-pinned beam under a combined harmonic and constant axial load and found that the first resonant frequency of oscillation was one-half the forcing frequency. This was followed by the works of Kryloff and Bogolyubov in 1935, Mettler in 1940, Lubkin and Stoker in 1943, Gol'denblat in 1944, and Bolotin in 1950, just to name a few. More recently, a summary of the stability of parametrically excited structures was given by Ariaratnam (1986).

Haight and King (1970) theoretically and experimentally investigated the stability of cantilever beams, which are axially excited at principal parametric resonance and have a one-to-one internal resonance involving the in-plane and out-of-plane flexural modes. They included the nonlinear inertia effects, but neglected the effects of geometric nonlinearities and torsional oscillations. They found that, when the internal resonance was perfectly detuned, the in-plane motions were always stable and hence the out-of-plane modes would never be excited. If, on the other hand, the frequency ratio was slightly mistuned, then the in-plane motions could lose stability and the out-of-plane motions would be excited. Furthermore, they concluded that whirling motions cannot occur for all practical purposes. Comparing their analytical results to experimental ones, they found good qualitative agreement but significant quantitative differences.

Nayfeh and Pai (1989) used the equations of Crespo da Silva and Glynn (1978a, b) to investigate the nonlinear nonplanar responses of cantilever beams to parametric excitations in the presence of a one-to-one internal resonance involving two flexural modes. They applied the method of multiple scales directly to the integro-partial-differential equations and obtained the equations governing the modulation of the amplitudes and phases. They found that the geometric nonlinearities dominate

the inertia nonlinearities for the first mode, while the inertia nonlinearities dominate the geometric nonlinearities for the higher modes. The inertia nonlinearities have a softening effect, whereas the geometric nonlinearities have a hardening effect. They located Hopf bifurcations and showed that quasiperiodic (beating) oscillations can occur.

Kar and Sujata (1990) investigated the parametric instabilities that can occur in the response of a linear damped beam that is elastically restrained at one end and free at the other to a harmonic force. They assumed the force to be acting at the free end and considered the cases of uniaxial and follower-type forces. They found that the regions of instability for a uniaxial force are in general wider than those for a follower-type force. They (1992) also investigated the parametric instabilities of a rotating, pretwisted, and preconed cantilever beam, taking into consideration the Coriolis effects. They found that the Coriolis force reduces the instability zones of the principal parametric resonance.

High-to-Low Resonance

A nonresonant mechanism that is responsible for transferring energy from a high-frequency mode to a low-frequency mode was discovered experimentally by Anderson, Balachandran, and Nayfeh (1992). They considered a thin rectangular beam whose first four natural frequencies are 0.65, 5.65, 16.19, and 31.91 Hz. They excited the beam around 32.0 Hz so that the third and fourth modes were activated by principal and fundamental parametric resonances, respectively. As they varied the excitation frequency, the two-mode response lost stability and resulted in modulated oscillations that contained a significant contribution from the first mode. A characteristic of the response was the presence of sidebands in the spectrum around the peak corresponding to the third mode, which were separated by approximately 0.65 Hz ($\approx \omega_1$). In a second experiment, they excited the beam parametrically at 138 Hz and found that the second mode dominated the response even though no resonance relationship was apparent. Again, there were small peaks in the strain gage spectrum near the excitation frequency, which were separated by approximately 5.6 Hz ($\approx \omega_2$). Sidebands were also found in the acceleration spectrum, indicating that the base acceleration was modulated. Anderson, Balachandran, and Nayfeh (1994) excited the same beam parametrically near its third natural frequency. In some regions of the excitation frequency, they found that only

the fourth and the first modes were excited with the first mode dominating the response. Tabaddor and Nayfeh (1997) experimentally investigated the response of a cantilever beam whose first four natural frequencies are 0.70, 5.89, 16.75, and 33.10 Hz. They directly excited the fourth mode and found that, as they slowly varied the excitation frequency, a contribution from the first mode appeared in the response.

Nayfeh and Nayfeh (1992, 1994) investigated the response of a circular cross-section cantilever beam. They directly excited the fifth mode whose natural frequency is $\omega_5 = 83.1$ Hz. They found that the response was dominated by the first mode whose natural frequency is $\omega_1 = 1.3$ Hz. The spectrum showed that both the peaks corresponding to the fifth and first modes had sidebands. Nayfeh and Nayfeh (1993) theoretically investigated the mechanism that is responsible for transferring energy from high-frequency to low-frequency modes in directly excited systems. They used the method of averaging to study the behavior of the fixed-point and periodic solutions and found that the latter leads to chaotic attractors via a sequence of period-doubling bifurcations.

Nayfeh and Chin (1995) investigated the system of Nayfeh and Nayfeh (1993) when it is excited at principal parametric resonance and found that the response can be complex, including chaos, crises, and intermittency. Feng (1996) investigated the existence of Shilnikov homoclinic orbits in the system of Nayfeh and Chin (1995).

Nayfeh and Mook (1995) gave a comprehensive review of the investigations of the different mechanisms responsible for the transfer of energy from high- to low-frequency modes in structures.

1.2.2 Flexural-Flexural-Torsional Oscillations of Inextensional Beams

Primary Resonance

Crespo da Silva and Zaretzky (1994) investigated the nonlinear flexural-flexural-torsional responses of cantilever beams to primary resonances in the presence of a one-to-one internal resonance between the first torsional mode and the directly excited flexural mode. They accounted for the torsional motion explicitly and found that the system exhibits jumps and saturation.

Lee, Lee, and Chang (1997) used the equations of Crespo da Silva and Zaretzky (1994) to investi-

gate the nonlinear flexural-flexural-torsional responses of cantilever rectangular beams to harmonic torsional base excitations in the presence of a one-to-one internal resonance. They found that two-mode oscillations occur as a result of the torsional mode losing stability. Furthermore, the two-mode solutions of the modulation equations undergo Hopf bifurcations, resulting in periodically varying amplitudes and hence quasiperiodic beam motions.

Internal Combination Resonance

Internal combination resonances can occur when three or more of the system's natural frequencies are near commensurate. For systems with quadratic nonlinearities, they have the form $\omega_k \approx \omega_i \pm \omega_j$. For systems with cubic nonlinearities, they have the forms $\omega_l \approx \omega_k \pm \omega_i \pm \omega_j$ or $\omega_k \approx 2\omega_i + \omega_j$ (Nayfeh and Mook, 1978; Nayfeh and Mook, 1979).

Zaretzky and Crespo da Silva (1994b) investigated the nonlinear nonplanar response of cantilever beams having the internal combination resonance $\omega_\phi \approx \omega_v + \omega_w$, with the in-plane bending mode being excited at primary resonance (i.e., $\Omega \approx \omega_v$). They discretized the partial-differential equations and then used perturbation methods to analyze the motion. They found that, when the multimode solution is activated, the out-of-plane bending and torsional modes are related by a constant. In addition, the directly excited in-plane bending mode seems to saturate.

Combination Parametric Resonance

Combination parametric resonances occur when the excitation frequency is near the sum or difference of two of the system's natural frequencies. Dugundji and Mukhopadhyay (1973) theoretically and experimentally investigated the response of a thin cantilever beam to combination parametric resonances involving the first bending and torsional modes, $\Omega \approx \omega_{B1} + \omega_{T1}$, in one case, and the second bending and first torsional modes, $\Omega \approx \omega_{B2} + \omega_{T1}$, in another. They included only coupling due to the parametric force and nonlinearities caused by damping. However, they neglected geometric and inertia nonlinearities. They found that the beam exhibits significant oscillations both in bending and in torsion. In addition, at large excitation amplitudes they observed the beam snapping-through and whipping around.

Cartmell and Roberts (1987) theoretically and experimentally investigated the response of a cantilever beam-mass system excited by two simultaneous combination parametric resonances $\Omega \approx \omega_{B1} + \omega_{T1} \approx \omega_{B2} - \omega_{T1}$. They neglected the cubic nonlinear terms and used the method of multiple scales to determine periodic responses and their stability. They found good agreement between theory and experiment within certain ranges of the excitation frequency. However, in other regions where periodic modulations can occur, the correlation was not satisfactory because the theoretical solution could not predict nonstationary responses.

In addition to investigating principal parametric resonances, Kar and Sujata (1990, 1992) also investigated instabilities due to combination parametric resonances. For an elastically restrained beam, they (1990) found that, when the force is uniaxial or supertangential, only additive-type combination parametric resonances occur. In contrast, difference-type combination parametric resonances are dominant when the force is subtangential or tangential. For a rotating, pretwisted, and preconed beam, they (1992) found that including the Coriolis force increases the instability zones of the combination parametric resonances.

Ibrahim and Hijawi (1998) investigated the nonlinear responses of cantilever beam-mass systems near combination parametric resonances to deterministic and stochastic excitations. They took into account geometric and inertia nonlinearities; however they analyzed a discretized model of the beam using the method of multiple scales.

1.2.3 Longitudinal-Torsional Oscillations of Inextensional Beams

Tso (1968) investigated the torsional response of rectangular cantilever beams to parametric longitudinal excitations. He considered both the case where the longitudinal modes were not at primary resonance and the case where they were resonant. He included coupling between the longitudinal and torsional motions due to the "shortening effect" (Cullimore, 1949). In the first case, he ignored the longitudinal inertia and reduced the system to a single equation for the torsional oscillations. He found regions of instability when the forcing frequency is near twice the natural frequency of the excited torsional mode. The instability regions widen for higher torsional modes. In the second case, the effect of the longitudinal inertia is significant. He found two regions of instability: the first is when the forcing frequency is near twice the natural frequency of a torsional mode and the

second is when the forcing frequency is near the natural frequency of the excited longitudinal mode. Furthermore, he found the second region to be sensitive to longitudinal damping. He concluded that, in the presence of a two-to-one internal resonance, a single larger region of instability would result.

1.2.4 Nonplanar Oscillations of Composite Inextensional Beams

Bauchau and Hong (1988) developed a composite beam theory that includes the effects of shear deformations and torsional warping. They further generalized their theory to account for pretwist and initial curvature.

Pai and Nayfeh (1990b) used a Newtonian formulation to derive a system of partial-differential equations governing the nonplanar motions of extensional and inextensional composite beams. They neglected the effect of shear deformation and expanded their transcendental equations in terms of polynomials keeping up to third order. They noted that, for asymmetrically laminated composite beams, the assumption of inextensionality is not valid due to the extension-torsion and extension-bending linear couplings. They (1992) presented an improved and a more comprehensive beam theory that includes the effects of shear deformation to third order.

Zavodney and Nayfeh (1989) experimentally investigated the response of a composite beam-mass system to parametric excitations. The beam was made of $[0°/90°/90°/0°]_s$ 4-ply graphite-epoxy material. In addition to planar steady-state periodic oscillations, they observed the beam to undergo large chaotic motions, which involved out-of-plane bending and torsion.

Pai and Nayfeh (1991a, b) used their equations (1990b) to investigate the response of symmetrically laminated cantilever composite beams to flapwise (in-plane) and chordwise (out-of-plane) base excitations, respectively. In both cases, they considered the two-to-one internal resonance $\omega_w \approx 2\omega_v = \omega_\phi$, where ω_v, ω_w, and ω_ϕ are the fundamental flapwise-bending, chordwise-bending, and torsional natural frequencies. They applied the method of multiple scales directly to the partial-differential equations of motion to obtain the equations governing the modulations of the amplitudes and phases of the interacting modes. They found that the system can exhibit interesting dynamics, including periodic, quasiperiodic, and chaotic motions.

1.2.5 Theories for Rotating Beams and Blades

The nonlinear nonplanar equations of motion for inextensional beams may be considered as a specialized case of the equations of motion of rotating blades. In addition to the influence of centrifugal forces, other effects that are considered include pretwist and precone angles and asymmetric cross-sections. Therefore, we present here some of the theories for rotating blades that are germane to this work.

Hodges and Dowell (1974) developed a set of equations governing the motion of a rotor blade both by using Hamilton's principle and Newton's equations. They kept up to quadratic nonlinear terms and accounted for the effect of warping. Anderson (1975) formulated the nonlinear equations of motion for a rotating beam in terms of the longitudinal force, the shear force, and the bending moment. He then used the linearized form of these equations to show that the frequencies of the longitudinal modes increase as the angular velocity of rotation increases. Crespo da Silva (1981) extended the work of Hodges and Dowell (1974) and derived the equations describing the flap-lead/lag-torsional motions of rotor blades in hover and in forward flight, keeping up to cubic nonlinear terms and accounting for warping.

1.3 Dissertation Objectives and Organization

Because many systems may be idealized as inextensional beams, it is very important to gain good understanding of the responses of such beams. It is clear from the previous section that great strides have been accomplished in that respect. The works of Haight and King, Crespo da Silva et al., and Nayfeh and Pai may stand out as most closely related to this research. Therefore, the objectives of this dissertation are two-fold. First, we expand on some of the investigations already conducted. To do so, we use alternate approaches to those previously used to analyze the systems in greater detail. Second, we fill in some of the gaps by investigating newer cases that are of practical importance. Emphasis is placed on the concept of energy transfer from high-frequency modes to low-frequency modes via either a resonant or a nonresonant (zero-to-one) mechanism.

In Chapter 2, we use a combination of a 3-2-1 Euler-angle body rotation, a Lagrange multiplier, the

theory of mechanics of composites, and Hamilton's extended principle to derive the Lagrangian, and hence the governing nonlinear partial-differential equations of motion and associated boundary conditions, for monoclinic composite and metallic inextensional Euler-Bernoulli beams. In Chapters 3 and 4, we use the method of time-averaged Lagrangian to investigate in detail the nonlinear bending-bending responses of near-square metallic beams to parametric and direct excitations, respectively. In Chapter 5, we investigate the nonlinear bending-bending-twisting responses of metallic beams to combination parametric resonances. Results from the two approaches are compared. First, we directly attack the partial-differential system of equations and boundary conditions. Second, we attack a discretized set of ordinary-differential equations. In Chapter 6, we investigate the nonlinear bending-bending-twisting responses of metallic beams, accounting for the transfer of energy from high- to low-frequency modes through a zero-to-one resonance. In Chapter 7, we show that the modulation equations for symmetrically laminated composite beams do in fact exhibit symmetry properties, as in the case of metallic beams. In Chapter 8, we present our conclusions and recommendations for future work.

Chapter 2

Introduction to Beam Theory

2.1 Brief Historical Background

In what follows, a brief and by no means complete historical summary of the origins of the theory of beams is presented. According to Love (1944), the first to consider the elastic problem of thin beams was James (Jacob according to Timoshenko, 1983) Bernoulli in 1705 where he assumed that the moment resisting the deflection is the result of the elongation and contraction of the beam's filaments. His results amounted to the fact that the bending moment is proportional to the curvature after deflection. Following a suggestion by Daniel Bernoulli in 1742 that the differential equation describing the deflection of a beam can be obtained by minimizing the work done by the bending moment, Euler in 1744 was able to derive such equation and classify several cases. A detailed account of the works of the Bernoulli's and Euler, among others, is given by Cannon and Dostrovsky (1981).

Unlike Euler who in his theory assumed the beam to consist of a line of particles resistant to bending, Coulomb in 1776 was the first to apply the force and moment equilibrium equations to a finite section to obtain a more accurate differential equation. He was also the first to consider the idea that beams are also resistant to torsion. However, his results were not based on any elasticity theory. A more robust theory on the torsion of prismatic bars was presented by Saint-Venant in 1855 and 1856. Saint-Venant assumed that the extension and contraction of the beam's filaments

are proportional to their normal distance from the centroidal axis. Furthermore, as a simplification, Saint-Venant proposed that the effect of replacing distributed end loads by a statically equivalent resultant load system on a point that is relatively far away from the boundary is negligible (Shames and Dym, 1985). This later came to be known as *Saint-Venant's principle of the elastic equivalence of statically equipollent systems of loads* (Love, 1944).

In 1859, Kirchhoff derived an approximate measure of the strain in an element of a rod, and thus he was able to determine an expression for the potential energy in the element. Then, by varying this energy, he obtained the equilibrium and vibration equations. Furthermore, he showed that the equations of a thin rod subjected only to end forces have the same form as those of a rigid body oscillating about a fixed point. This is referred to as *Kirchhoff's kinetic analogue* (Love, 1944; Southwell, 1941)

In his book *The Theory of Sound*, first published in 1877, Rayleigh (1945) included the effects of rotary inertia in the equations describing the flexural and longitudinal vibrations of beams and showed that, at high-frequency oscillations, such corrections to the natural frequencies are important. The effect of shear deformation on the vibrations of beams was introduced by Timoshenko (1921, 1922). As an example, he considered free vibrations of a simply-supported beam and showed that the correction due to shear is four times more important than that due to rotary inertia. Furthermore, he showed that the Euler-Bernoulli and Rayleigh beam equations are special cases of his result.

2.2 Variational Mechanics

Crespo da Silva and Glynn (1978a, b) used a variational formulation to derive the equations governing nonlinear nonplanar vibrations of metallic beams. Pai (1990) used a Newtonian formulation to derive the equations governing nonlinear nonplanar vibrations of symmetrically laminated composite beams. Here, we will make use of both of their results and use a variational formulation to derive the equations governing nonlinear nonplanar vibrations of symmetrically laminated composite beams. We will then reduce our results to the equations of Crespo da Silva and Glynn (1978a, b) for metallic beams.

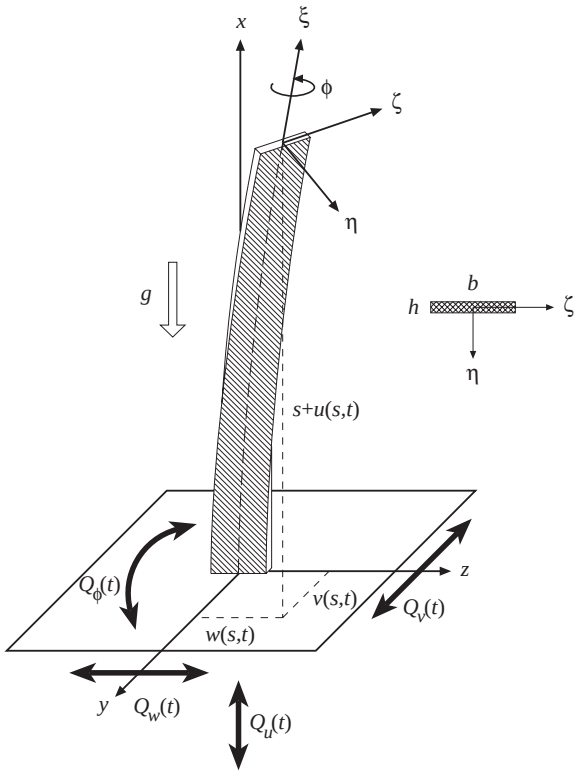

Figure 2.1: A schematic of a composite cantilever beam under direct and parametric excitations.

2.2.1 Stress-Strain Relationships

The dynamics of a beam are described through the longitudinal displacement $u(s,t)$, the transverse displacements $v(s,t)$ and $w(s,t)$ along the y- and z-axes, respectively, and the torsional angle $\phi(s,t)$, as shown in Figure 2.1. Here, $x-y-z$ is a global orthogonal coordinate system, while $\xi-\eta-\zeta$ is a local orthogonal coordinate system. When using index notation in our derivation, we assume that $u_1 = u$, $u_2 = v$, $u_3 = w$, $x_1 = x$, $x_2 = y$, and $x_3 = z$. Furthermore, the coordinates s and ξ are used interchangeably.

Two Cartesian coordinate systems x_i and x_i' can be related to each other through the transformation

$$\begin{Bmatrix} x_1' \\ x_2' \\ x_3' \end{Bmatrix} = \begin{bmatrix} a_{11} & a_{12} & a_{13} \\ a_{21} & a_{22} & a_{23} \\ a_{31} & a_{32} & a_{33} \end{bmatrix} \begin{Bmatrix} x_1 \\ x_2 \\ x_3 \end{Bmatrix} \tag{2.1}$$

where $a_{ij} = \cos(x'_i, x_j)$ is cosine of the angle between the ith primed and jth unprimed coordinate system. Then, using this transformation, one can relate the stresses, σ'_{ij}, acting on a body with respect to the primed coordinate system to the stresses, σ_{kl}, with respect to the unprimed coordinate system as (Whitney, 1987)

$$\sigma'_{ij} = a_{ik} a_{jl} \sigma_{kl} \equiv [T_\sigma]\, \sigma_{kl} \tag{2.2}$$

The Lagrangian (or Green) strain tensor is related to the displacements $u_i(x_j, t)$ as (Mase, 1970)

$$L_{ij} = \frac{1}{2}\left(\frac{\partial u_i}{\partial x_j} + \frac{\partial u_j}{\partial x_i}\right) + \frac{1}{2}\frac{\partial u_k}{\partial x_i}\frac{\partial u_k}{\partial x_j} \tag{2.3}$$

For infinitesimal strains, one can neglect the nonlinear terms and obtain the linearized Lagrangian strain tensor

$$l_{ij} = \frac{1}{2}\left(\frac{\partial u_i}{\partial x_j} + \frac{\partial u_j}{\partial x_i}\right) \tag{2.4}$$

However, it is more convenient here to consider the *engineering* strains ε_{ij}, which are defined as

$$\varepsilon_{ij} = \begin{cases} L_{ij} & \text{for } i = j \\ 2L_{ij} & \text{for } i \neq j \end{cases} \tag{2.5}$$

Then, similar to the stresses, the engineering strains with respect to the primed coordinate system can be related to the engineering strains with respect to the unprimed coordinate system as

$$\varepsilon'_{ij} = a_{ik} a_{jl} \varepsilon_{kl} \equiv [T_\varepsilon]\, \varepsilon_{kl} \tag{2.6}$$

For a rotation of angle θ about the x_2-axis, as shown in Figure 2.2, Eqs. (2.1), (2.2), and (2.6) become

$$\begin{Bmatrix} x'_1 \\ x'_2 \\ x'_3 \end{Bmatrix} = \begin{bmatrix} \cos\theta & 0 & -\sin\theta \\ 0 & 1 & 0 \\ \sin\theta & 0 & \cos\theta \end{bmatrix} \begin{Bmatrix} x_1 \\ x_2 \\ x_3 \end{Bmatrix} = \begin{bmatrix} m & 0 & -n \\ 0 & 1 & 0 \\ n & 0 & m \end{bmatrix} \begin{Bmatrix} x_1 \\ x_2 \\ x_3 \end{Bmatrix} \tag{2.7}$$

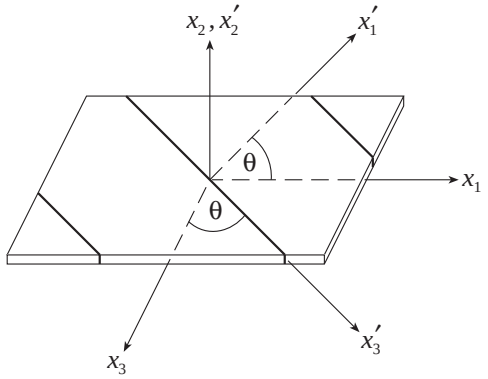

Figure 2.2: The coordinate system x_i' as a result of rotating the coordinate system x_i with angle θ about the x_2-axis.

$$\begin{Bmatrix} \sigma'_{11} \\ \sigma'_{22} \\ \sigma'_{33} \\ \sigma'_{23} \\ \sigma'_{31} \\ \sigma'_{12} \end{Bmatrix} = \begin{bmatrix} m^2 & 0 & n^2 & 0 & -2mn & 0 \\ 0 & 1 & 0 & 0 & 0 & 0 \\ n^2 & 0 & m^2 & 0 & 2mn & 0 \\ 0 & 0 & 0 & m & 0 & n \\ mn & 0 & -mn & 0 & m^2 - n^2 & 0 \\ 0 & 0 & 0 & -n & 0 & m \end{bmatrix} \begin{Bmatrix} \sigma_{11} \\ \sigma_{22} \\ \sigma_{33} \\ \sigma_{23} \\ \sigma_{31} \\ \sigma_{12} \end{Bmatrix} \tag{2.8}$$

$$\begin{Bmatrix} \varepsilon'_{11} \\ \varepsilon'_{22} \\ \varepsilon'_{33} \\ \varepsilon'_{23} \\ \varepsilon'_{31} \\ \varepsilon'_{12} \end{Bmatrix} = \begin{bmatrix} m^2 & 0 & n^2 & 0 & -mn & 0 \\ 0 & 1 & 0 & 0 & 0 & 0 \\ n^2 & 0 & m^2 & 0 & mn & 0 \\ 0 & 0 & 0 & m & 0 & n \\ 2mn & 0 & -2mn & 0 & m^2 - n^2 & 0 \\ 0 & 0 & 0 & -n & 0 & m \end{bmatrix} \begin{Bmatrix} \varepsilon_{11} \\ \varepsilon_{22} \\ \varepsilon_{33} \\ \varepsilon_{23} \\ \varepsilon_{31} \\ \varepsilon_{12} \end{Bmatrix} \tag{2.9}$$

where $m = \cos\theta$ and $n = \sin\theta$.

The stress-strain relationship (or generalized Hooke's law) for the mth lamina with respect to the x_i' coordinate system is given by

$$\sigma_{ij}'^{(m)} = C_{ijkl}^{(m)} \varepsilon_{kl}'^{(m)} \tag{2.10}$$

Substituting Eqs. (2.2) and (2.6) into Eq. (2.10) and premultiplying the result by $[T_\sigma]^{-1}$, we obtain the stress-strain relationship for the mth lamina with respect to the x_i coordinate system as

$$\sigma_{ij}^{(m)} = [T_\sigma]^{-1} C_{ijkl}^{(m)} [T_\varepsilon] \varepsilon_{kl}^{(m)} = Q_{ijkl}^{(m)} \varepsilon_{kl}^{(m)} \tag{2.11}$$

In Eqs. (2.10) and (2.11), $C_{ijkl}^{(m)}$ and $Q_{ijkl}^{(m)}$ are fourth-order tensors that denote the material properties of the mth lamina with respect to the x_i' and x_i coordinate systems, respectively. For a general *anisotropic* material, Q_{ijkl} (or C_{ijkl}) is given by

$$[Q] = \begin{bmatrix} Q_{1111} & Q_{1122} & Q_{1133} & Q_{1123} & Q_{1113} & Q_{1112} \\ Q_{1122} & Q_{2222} & Q_{2233} & Q_{2223} & Q_{2213} & Q_{2212} \\ Q_{1133} & Q_{2233} & Q_{3333} & Q_{3323} & Q_{3313} & Q_{3312} \\ Q_{1123} & Q_{2223} & Q_{3323} & Q_{2323} & Q_{2313} & Q_{2312} \\ Q_{1113} & Q_{2213} & Q_{3313} & Q_{2313} & Q_{1313} & Q_{1312} \\ Q_{1112} & Q_{2212} & Q_{3312} & Q_{2312} & Q_{1312} & Q_{1212} \end{bmatrix} \tag{2.12}$$

which has 21 independent constants.

If there is one plane of symmetry, then the material is called *monoclinic*. Assuming x_2 is the axis perpendicular to the plane of symmetry, then one has

$$Q_{1123} = Q_{1112} = Q_{2223} = Q_{2212} = Q_{3323} = Q_{3312} = Q_{2313} = Q_{1312} = 0 \tag{2.13}$$

and the fourth-order tensor becomes

$$[Q] = \begin{bmatrix} Q_{1111} & Q_{1122} & Q_{1133} & 0 & Q_{1113} & 0 \\ Q_{1122} & Q_{2222} & Q_{2233} & 0 & Q_{2213} & 0 \\ Q_{1133} & Q_{2233} & Q_{3333} & 0 & Q_{3313} & 0 \\ 0 & 0 & 0 & Q_{2323} & 0 & Q_{2312} \\ Q_{1113} & Q_{2213} & Q_{3313} & 0 & Q_{1313} & 0 \\ 0 & 0 & 0 & Q_{2312} & 0 & Q_{1212} \end{bmatrix} \tag{2.14}$$

which has 13 independent constants. If a second plane of symmetry is present, then the material

is called *orthotropic* and, in addition to Eq. (2.13), we have

$$Q_{1113} = Q_{2213} = Q_{3313} = Q_{2312} = 0 \tag{2.15}$$

Hence, the fourth-order tensor becomes

$$[Q] = \begin{bmatrix} Q_{1111} & Q_{1122} & Q_{1133} & 0 & 0 & 0 \\ Q_{1122} & Q_{2222} & Q_{2233} & 0 & 0 & 0 \\ Q_{1133} & Q_{2233} & Q_{3333} & 0 & 0 & 0 \\ 0 & 0 & 0 & Q_{2323} & 0 & 0 \\ 0 & 0 & 0 & 0 & Q_{1313} & 0 \\ 0 & 0 & 0 & 0 & 0 & Q_{1212} \end{bmatrix} \tag{2.16}$$

which has 9 independent constants. Furthermore, if in addition to two planes of symmetry, one of the planes is isotropic and hence its material properties are independent of direction, then the composite is called *transversely isotropic* and the fourth-order tensor, $[Q]$, is given in terms of 5 independent constants. Lastly, if the material properties are independent of direction in two planes of symmetry, then the material is called *isotropic* and, in addition to Eqs. (2.13) and (2.15), we have

$$Q_{1111} = Q_{2222} = Q_{3333} = \hat{\lambda} + 2\hat{\mu},\ Q_{1122} = Q_{1133} = Q_{2233} = \hat{\lambda},\ \text{and}\ Q_{2323} = Q_{1313} = Q_{1212} = \hat{\mu} \tag{2.17}$$

where $\hat{\lambda}$ and $\hat{\mu}$ are called the Lamé constants. Hence, the fourth-order tensor in terms of 2 independent constants becomes

$$[Q] = \begin{bmatrix} \hat{\lambda} + 2\hat{\mu} & \hat{\lambda} & \hat{\lambda} & 0 & 0 & 0 \\ \hat{\lambda} & \hat{\lambda} + 2\hat{\mu} & \hat{\lambda} & 0 & 0 & 0 \\ \hat{\lambda} & \hat{\lambda} & \hat{\lambda} + 2\hat{\mu} & 0 & 0 & 0 \\ 0 & 0 & 0 & \hat{\mu} & 0 & 0 \\ 0 & 0 & 0 & 0 & \hat{\mu} & 0 \\ 0 & 0 & 0 & 0 & 0 & \hat{\mu} \end{bmatrix} \tag{2.18}$$

The Lamé constants in terms of Young's modulus E, Poisson's ratio ν, and the shear modulus G, are given by

$$\hat{\mu} = G = \frac{E}{2(1+\nu)} \qquad \text{and} \qquad \hat{\lambda} = \frac{E\nu}{1-\nu-2\nu^2} \tag{2.19}$$

Because for most materials $0 \leq \nu \leq 0.5$, it is popular to assume that $\nu^2 \ll 1$ and neglect it in Eq. (2.19).

The analysis presented from here on will assume that the beam has at least one plane of symmetry (i.e., monoclinic). Furthermore, we choose $x_1 - x_3$ to be the plane of symmetry. Then, substituting Eq. (2.14) into Eq. (2.11), one obtains the following constitutive equations for a monoclinic material:

$$\sigma_{11} = Q_{1111}\varepsilon_{11} + Q_{1113}\varepsilon_{13} + Q_{1122}\varepsilon_{22} + Q_{1133}\varepsilon_{33} \tag{2.20}$$

$$\sigma_{22} = Q_{1122}\varepsilon_{11} + Q_{2213}\varepsilon_{13} + Q_{2222}\varepsilon_{22} + Q_{2233}\varepsilon_{33} \tag{2.21}$$

$$\sigma_{33} = Q_{1133}\varepsilon_{11} + Q_{3313}\varepsilon_{13} + Q_{2233}\varepsilon_{22} + Q_{3333}\varepsilon_{33} \tag{2.22}$$

$$\sigma_{23} = Q_{2312}\varepsilon_{12} + Q_{2323}\varepsilon_{23} \tag{2.23}$$

$$\sigma_{31} = Q_{1113}\varepsilon_{11} + Q_{1313}\varepsilon_{13} + Q_{2213}\varepsilon_{22} + Q_{3313}\varepsilon_{33} \tag{2.24}$$

$$\sigma_{12} = Q_{1212}\varepsilon_{12} + Q_{2312}\varepsilon_{23} \tag{2.25}$$

For long thin beams having no traction, one can assume that the normal stresses σ_{22} and σ_{33} as well as the shear stress σ_{23} are equal to zero (Pai, 1990). Then, from Eqs. (2.21)-(2.23), one can solve for the strains ε_{22}, ε_{33}, and ε_{23} as

$$\varepsilon_{22} = -\frac{(Q_{1133}Q_{2233} - Q_{1122}Q_{3333})}{Q_{2233}^2 - Q_{2222}Q_{3333}}\varepsilon_{11} - \frac{(Q_{2233}Q_{3313} - Q_{2213}Q_{3333})}{Q_{2233}^2 - Q_{2222}Q_{3333}}\varepsilon_{13} \tag{2.26}$$

$$\varepsilon_{22} = -\frac{(Q_{1122}Q_{2233} - Q_{1133}Q_{2222})}{Q_{2233}^2 - Q_{2222}Q_{3333}}\varepsilon_{11} - \frac{(Q_{2213}Q_{2233} - Q_{2222}Q_{3313})}{Q_{2233}^2 - Q_{2222}Q_{3333}}\varepsilon_{13} \tag{2.27}$$

$$\varepsilon_{23} = -\frac{Q_{2312}}{Q_{2323}}\varepsilon_{12} \tag{2.28}$$

Substituting Eqs. (2.26)-(2.28) into Eqs. (2.20), (2.24), and (2.25), we obtain

$$\begin{Bmatrix} \sigma_{11} \\ \sigma_{31} \\ \sigma_{12} \end{Bmatrix} = \begin{bmatrix} \bar{Q}_{11} & \bar{Q}_{15} & 0 \\ \bar{Q}_{15} & \bar{Q}_{55} & 0 \\ 0 & 0 & \bar{Q}_{66} \end{bmatrix} \begin{Bmatrix} \varepsilon_{11} \\ \varepsilon_{31} \\ \varepsilon_{12} \end{Bmatrix} \tag{2.29}$$

where

$$\bar{Q}_{11} = Q_{1111} + \frac{Q_{2222}Q_{1133}^2 - 2Q_{1122}Q_{1133}Q_{2233} + Q_{3333}Q_{1122}^2}{Q_{2233}^2 - Q_{2222}Q_{3333}} \tag{2.30}$$

$$\bar{Q}_{15} = Q_{1113} + \frac{Q_{1133}\left(Q_{2222}Q_{3313} - Q_{2213}Q_{2233}\right) + Q_{1122}\left(Q_{2213}Q_{3333} - Q_{2233}Q_{3313}\right)}{Q_{2233}^2 - Q_{2222}Q_{3333}} \tag{2.31}$$

$$\bar{Q}_{55} = Q_{1313} + \frac{Q_{2222}Q_{3313}^2 - 2Q_{2213}Q_{2233}Q_{3313} + Q_{2213}^2Q_{3333}}{Q_{2233}^2 - Q_{2222}Q_{3333}} \tag{2.32}$$

$$\bar{Q}_{66} = Q_{1212} - \frac{Q_{2312}^2}{Q_{2323}} \tag{2.33}$$

The strains ε_{11}, ε_{31}, and ε_{12} at a point having the coordinates (ξ, η, ζ) can be expressed as

$$\varepsilon_{11} = e(\xi, t) - \eta\rho_\zeta(\xi, t) + \zeta\rho_\eta(\xi, t) \tag{2.34}$$

$$\varepsilon_{31} = \varepsilon_{\zeta\xi}(\xi, t) + \eta\rho_\xi(\xi, t) \tag{2.35}$$

$$\varepsilon_{12} = \varepsilon_{\xi\eta}(\xi, t) - \zeta\rho_\xi(\xi, t) \tag{2.36}$$

where e, $\varepsilon_{\zeta\xi}$, and $\varepsilon_{\xi\eta}$ are the axial and shear strains at the point $(\xi, 0, 0)$ along the elastic axis and ρ_ξ, ρ_η, and ρ_ζ are the curvatures. The variation of Eqs. (2.34)-(2.36) is given by

$$\delta\varepsilon_{11} = \delta e(\xi, t) - \eta\delta\rho_\zeta(\xi, t) + \zeta\delta\rho_\eta(\xi, t) \tag{2.37}$$

$$\delta\varepsilon_{31} = \delta\varepsilon_{\zeta\xi}(\xi, t) + \eta\delta\rho_\xi(\xi, t) \tag{2.38}$$

$$\delta\varepsilon_{12} = \delta\varepsilon_{\xi\eta}(\xi, t) - \zeta\delta\rho_\xi(\xi, t) \tag{2.39}$$

2.2.2 Strain Energy

The strain energy is given by

$$\begin{aligned}\mathcal{U} &= \frac{1}{2}\int_0^L \int_{-\frac{h}{2}}^{\frac{h}{2}} \int_{-\frac{b}{2}}^{\frac{b}{2}} \left(\sigma_{11}\varepsilon_{11} + \sigma_{31}\varepsilon_{31} + \sigma_{12}\varepsilon_{12}\right) d\zeta d\eta d\xi \\ &= \frac{1}{2}\int_0^L \int_{-\frac{h}{2}}^{\frac{h}{2}} \int_{-\frac{b}{2}}^{\frac{b}{2}} \left(\bar{Q}_{11}\varepsilon_{11}^2 + 2\bar{Q}_{15}\varepsilon_{11}\varepsilon_{31} + \bar{Q}_{55}\varepsilon_{31}^2 + \bar{Q}_{66}\varepsilon_{12}^2\right) d\zeta d\eta d\xi \end{aligned} \tag{2.40}$$

Taking the variation of Eq. (2.40) and using Eqs. (2.37)-(2.39), we obtain

$$\begin{aligned}\delta\mathcal{U} &= \int_0^L \int_{-\frac{h}{2}}^{\frac{h}{2}} \int_{-\frac{b}{2}}^{\frac{b}{2}} \left[\left(\bar{Q}_{11}\varepsilon_{11} + \bar{Q}_{15}\varepsilon_{31}\right)\delta\varepsilon_{11} + \left(\bar{Q}_{15}\varepsilon_{11} + \bar{Q}_{55}\varepsilon_{31}\right)\delta\varepsilon_{31} + \bar{Q}_{66}\varepsilon_{12}\delta\varepsilon_{12}\right] d\zeta d\eta d\xi \\ &= \int_0^L \Bigg[\left(A_{11}e + A_{13}\varepsilon_{\zeta\xi} + B_{11}\rho_\xi + B_{13}\rho_\zeta\right)\delta e + \left(A_{22}\varepsilon_{\xi\eta}\right)\delta\varepsilon_{\xi\eta} + \left(A_{13}e + A_{33}\varepsilon_{\zeta\xi} + B_{31}\rho_\xi \right. \\ &\quad \left. + B_{33}\rho_\zeta\right)\delta\varepsilon_{\zeta\xi} + \left(B_{11}e + B_{31}\varepsilon_{\zeta\xi} + D_{11}\rho_\xi + D_{13}\rho_\zeta\right)\delta\rho_\xi + \left(D_{22}\rho_\eta\right)\delta\rho_\eta + \left(B_{13}e + B_{33}\varepsilon_{\zeta\xi}\right. \\ &\quad \left. + D_{13}\rho_\xi + D_{33}\rho_\zeta\right)\delta\rho_\zeta \Bigg] d\xi \end{aligned} \tag{2.41}$$

where

$$\begin{Bmatrix} A_{11} \\ A_{13} \\ A_{22} \\ A_{33} \end{Bmatrix} = \int_{-\frac{h}{2}}^{\frac{h}{2}} \int_{-\frac{b}{2}}^{\frac{b}{2}} \begin{Bmatrix} \bar{Q}_{11} \\ \bar{Q}_{15} \\ \bar{Q}_{66} \\ \bar{Q}_{55} \end{Bmatrix} d\eta d\zeta = b\sum_{m=1}^{M} \begin{Bmatrix} \bar{Q}_{11}^{(m)} \\ \bar{Q}_{15}^{(m)} \\ \bar{Q}_{66}^{(m)} \\ \bar{Q}_{55}^{(m)} \end{Bmatrix} \left[h_{(m)} - h_{(m-1)}\right] \tag{2.42}$$

$$\begin{Bmatrix} B_{11} \\ B_{13} \\ B_{31} \\ B_{33} \end{Bmatrix} = \int_{-\frac{h}{2}}^{\frac{h}{2}} \int_{-\frac{b}{2}}^{\frac{b}{2}} \begin{Bmatrix} \eta\bar{Q}_{15} \\ -\eta\bar{Q}_{11} \\ \eta\bar{Q}_{55} \\ -\eta\bar{Q}_{15} \end{Bmatrix} d\eta d\zeta = \frac{b}{2}\sum_{m=1}^{M} \begin{Bmatrix} \bar{Q}_{15}^{(m)} \\ -\bar{Q}_{11}^{(m)} \\ \bar{Q}_{55}^{(m)} \\ -\bar{Q}_{15}^{(m)} \end{Bmatrix} \left[h_{(m)}^2 - h_{(m-1)}^2\right] \tag{2.43}$$

$$\begin{Bmatrix} D_{11} \\ D_{13} \\ D_{22} \\ D_{33} \end{Bmatrix} = \int_{-\frac{h}{2}}^{\frac{h}{2}} \int_{-\frac{b}{2}}^{\frac{b}{2}} \begin{Bmatrix} \eta^2\bar{Q}_{55} + \zeta^2\bar{Q}_{66} \\ -\eta^2\bar{Q}_{15} \\ \zeta^2\bar{Q}_{11} \\ \eta^2\bar{Q}_{11} \end{Bmatrix} d\eta d\zeta$$

$$= \frac{b}{3}\sum_{m=1}^{M}\begin{Bmatrix} \bar{Q}_{55}^{(m)} \\ -\bar{Q}_{15}^{(m)} \\ 0 \\ \bar{Q}_{11}^{(m)} \end{Bmatrix}\left[h_{(m)}^3 - h_{(m-1)}^3\right] + \frac{b^3}{12}\sum_{m=1}^{M}\begin{Bmatrix} \bar{Q}_{66}^{(m)} \\ 0 \\ \bar{Q}_{11}^{(m)} \\ 0 \end{Bmatrix}\left[h_{(m)} - h_{(m-1)}\right] \tag{2.44}$$

and $h_{(m)}$ is defined in Figure 2.3. Using the results from Eqs. (2.42)-(2.44), we rewrite the strain energy (i.e., Eq. (2.40)) as

$$\mathcal{U} = \frac{1}{2}\int_0^L \boldsymbol{\varepsilon}^T [K]\,\boldsymbol{\varepsilon} d\xi \tag{2.45}$$

where

$$\boldsymbol{\varepsilon} = \begin{Bmatrix} e \\ \varepsilon_{\xi\eta} \\ \varepsilon_{\zeta\xi} \\ \rho_\xi \\ \rho_\eta \\ \rho_\zeta \end{Bmatrix} \quad \text{and} \quad [K] = \begin{bmatrix} [A] & [B] \\ [B]^T & [D] \end{bmatrix} = \begin{bmatrix} A_{11} & 0 & A_{13} & B_{11} & 0 & B_{13} \\ 0 & A_{22} & 0 & 0 & 0 & 0 \\ A_{13} & 0 & A_{33} & B_{31} & 0 & B_{33} \\ B_{11} & 0 & B_{31} & D_{11} & 0 & D_{13} \\ 0 & 0 & 0 & 0 & D_{22} & 0 \\ B_{13} & 0 & B_{33} & D_{13} & 0 & D_{33} \end{bmatrix} \tag{2.46}$$

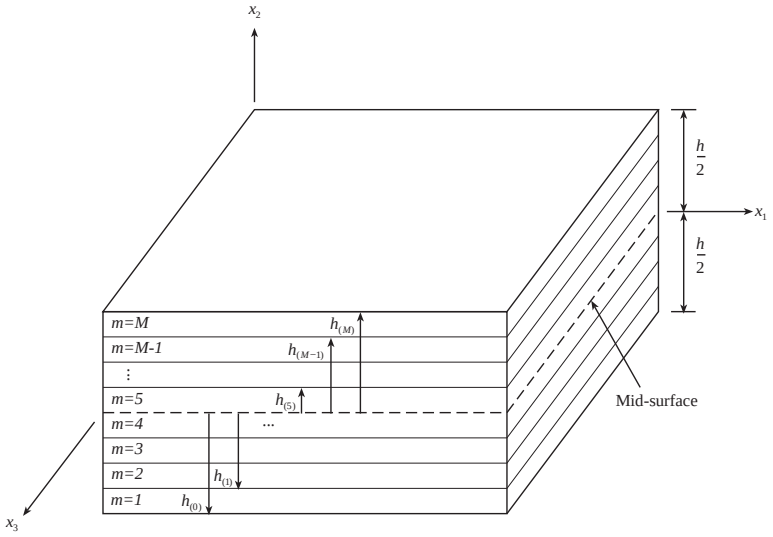

Figure 2.3: A schematic of a composite beam element showing how $h_{(m)}$ is defined.

Note that, although $A_{ij} = A_{ji}$ and $D_{ij} = D_{ji}$, $B_{ij} \neq B_{ji}$. In fact, it is clear from Eq. (2.43) that $B_{13} \neq B_{31}$.

The strain energy and its variation given by Eqs. (2.40) and (2.41) include the effects of first-order shear deformation. However, warping and Poisson effects were neglected. In our analysis, we consider beams that follow the Euler-Bernoulli theory, which assumes that the normal to the mid-surface before deformation remains normal to it after deformation. Therefore, we let the shear strains and their variation be

$$\varepsilon_{\zeta\xi}(\xi,t) = \varepsilon_{\eta\xi}(\xi,t) = \delta\varepsilon_{\zeta\xi}(\xi,t) = \delta\varepsilon_{\eta\xi}(\xi,t) = 0 \tag{2.47}$$

Then, Eqs. (2.40) and (2.41) become

$$\begin{aligned}\mathcal{U} = \frac{1}{2}\int_0^L \Big(& A_{11}e^2 + D_{11}\rho_\xi^2 + D_{22}\rho_\eta^2 + D_{33}\rho_\zeta^2 + 2D_{13}\rho_\zeta\rho_\xi + 2B_{11}\rho_\xi e \\ & + 2B_{13}\rho_\zeta e\Big) d\xi \end{aligned} \tag{2.48}$$

$$\begin{aligned}\delta\mathcal{U} = \int_0^L \Big[& \left(A_{11}e + B_{11}\rho_\xi + B_{13}\rho_\zeta\right)\delta e + \left(B_{11}e + D_{11}\rho_\xi + D_{13}\rho_\zeta\right)\delta\rho_\xi \\ & + \left(D_{22}\rho_\eta\right)\delta\rho_\eta + \left(B_{13}e + D_{13}\rho_\xi + D_{33}\rho_\zeta\right)\delta\rho_\zeta\Big] d\xi \end{aligned} \tag{2.49}$$

Note that, in Eqs. (2.48) and (2.49), the terms multiplying D_{13} produce linear coupling between the in-plane bending and twist deflections, while those multiplying B_{11} and B_{13} produce linear couplings between the stretching and twisting and stretching and in-plane bending deflections, respectively. Because of our choice of the plane of symmetry, the out-of-plane bending deflection is linearly uncoupled.

2.2.3 Strain-Displacement Relationships

Before deformation, the position of a point on the elastic axis is given by $\mathbf{r}_0 = s\mathbf{e}_x$. After deformation, its position is given by

$$\mathbf{r} = (s+u)\mathbf{e}_\xi + v\mathbf{e}_\eta + w\mathbf{e}_\zeta \tag{2.50}$$

Then, the strain along the elastic axis of a differential element ds is defined by

$$e = \left(\frac{\partial \mathbf{r}}{\partial s} \cdot \frac{\partial \mathbf{r}}{\partial s}\right)^{\frac{1}{2}} - \left(\frac{\partial \mathbf{r}_0}{\partial s} \cdot \frac{\partial \mathbf{r}_0}{\partial s}\right)^{\frac{1}{2}} = \sqrt{(1+u')^2 + v'^2 + w'^2} - 1 \tag{2.51}$$

If the beam is assumed to be *inextensional*, then the elongation eds is assumed to be zero, yielding the condition

$$\left(1+u'\right)^2 + v'^2 + w'^2 = 1 \tag{2.52}$$

Solving for u' and expanding the result in a Taylor expansion, we have

$$u' = \sqrt{1 - v'^2 - w'^2} - 1 \approx -\frac{1}{2}\left(v'^2 + w'^2\right) + \cdots \tag{2.53}$$

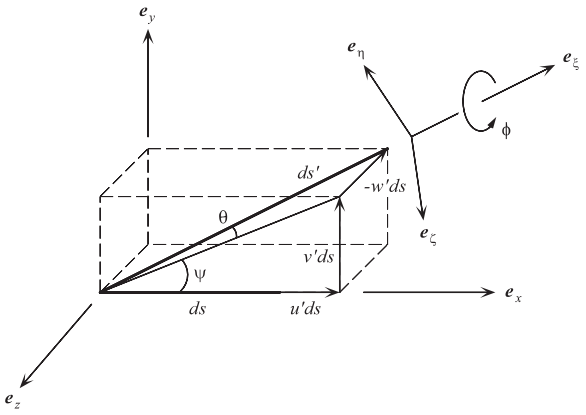

Figure 2.4: Deformation of a beam element.

Therefore, if v and w are of order $O(\epsilon)$, $\epsilon \ll 1$, then $u = O(\epsilon^2)$. Such an assumption is reasonable when the boundary conditions are geometric at one end only, such as in cantilever or pin-free beams. However, when there are geometric boundary conditions at both ends, such as in simply-supported beams, the effect of midplane stretching is significant and cannot be neglected. In addition, for anisotropic composite beams (i.e., asymmetrically laminated), linear bending-stretching and twisting-stretching couplings exist, and hence one cannot assume the beam to be inextensional regardless of the boundary conditions (Pai, 1990). On the other hand, assuming inextensionality for monoclinic composite beams is valid because, upon substituting Eq. (2.53), the terms multiplying

B_{11} and B_{13} in Eqs. (2.48) and (2.49) vanish. In this work, we concentrate only on symmetrically laminated and isotropic cantilever beams.

We consider a differential element initially of length ds along the $\mathbf{e}_x$ direction. After deformation, its length is given by $ds' = (1+e)ds$ along the $\mathbf{e}_\xi$ direction. The relationship between the original and deformed coordinate systems can be described by three successive Euler-angle rotations (Crespo da Silva and Glynn, 1978a). In this case, we use a 3-2-1 body rotation with the angles of rotation being $\psi(s,t)$, $\theta(s,t)$, and $\phi(s,t)$, respectively. This yields the transformation

$$\begin{Bmatrix} \mathbf{e}_x \\ \mathbf{e}_y \\ \mathbf{e}_z \end{Bmatrix} = \begin{bmatrix} \cos\psi & \sin\psi & 0 \\ -\sin\psi & \cos\psi & 0 \\ 0 & 0 & 1 \end{bmatrix} \begin{bmatrix} \cos\theta & 0 & \sin\theta \\ 0 & 1 & 0 \\ -\sin\theta & 0 & \cos\theta \end{bmatrix} \begin{bmatrix} 1 & 0 & 0 \\ 0 & \cos\phi & -\sin\phi \\ 0 & \sin\phi & \cos\phi \end{bmatrix} \begin{Bmatrix} \mathbf{e}_\xi \\ \mathbf{e}_\eta \\ \mathbf{e}_\zeta \end{Bmatrix} \tag{2.54}$$

$$= \begin{bmatrix} \cos\psi\cos\theta & \sin\psi\cos\phi + \cos\psi\sin\theta\sin\phi & -\sin\psi\sin\phi + \cos\psi\sin\theta\cos\phi \\ -\sin\psi\cos\theta & \cos\psi\cos\phi - \sin\psi\sin\theta\sin\phi & -\cos\psi\sin\phi - \sin\psi\sin\theta\cos\phi \\ -\sin\theta & \cos\theta\sin\phi & \cos\theta\cos\phi \end{bmatrix} \begin{Bmatrix} \mathbf{e}_\xi \\ \mathbf{e}_\eta \\ \mathbf{e}_\zeta \end{Bmatrix}$$

The rotation angles can be related to the deflections from geometry. Referring to Figure 2.4, one can see that

$$\sin\psi = \frac{v'}{\sqrt{(1+u')^2 + v'^2}} \qquad \cos\psi = \frac{(1+u')}{\sqrt{(1+u')^2 + v'^2}} \qquad \tan\psi = \frac{v'}{1+u'} \tag{2.55}$$

$$\sin\theta = \frac{-w'}{\sqrt{(1+u')^2 + v'^2 + w'^2}} \qquad \cos\theta = \frac{\sqrt{(1+u')^2 + v'^2}}{\sqrt{(1+u')^2 + v'^2 + w'^2}} \qquad \tan\theta = \frac{-w'}{\sqrt{(1+u')^2 + v'^2}}$$

The angular velocity of the element for the 3-2-1 body rotation used above can be defined by

$$\begin{aligned} \boldsymbol{\omega} &= \dot{\psi}\mathbf{e}_z + \dot{\theta}\mathbf{e}_{y'} + \dot{\phi}\mathbf{e}_{x''} \\ &= \left(\dot{\phi} - \dot{\psi}\sin\theta\right)\mathbf{e}_\xi + \left(\dot{\psi}\cos\theta\sin\phi + \dot{\theta}\cos\phi\right)\mathbf{e}_\eta + \left(\dot{\psi}\cos\theta\cos\phi - \dot{\theta}\sin\phi\right)\mathbf{e}_\zeta \\ \boldsymbol{\omega} &\equiv \omega_\xi\mathbf{e}_\xi + \omega_\eta\mathbf{e}_\eta + \omega_\zeta\mathbf{e}_\zeta \end{aligned} \tag{2.56}$$

By virtue of Kirchhoff's kinetic analogue (Love, 1944), we can obtain the beam's curvatures ρ_ξ, ρ_η, and ρ_ζ by replacing the time derivatives $\frac{\partial}{\partial t}$ with the spatial derivatives $\frac{\partial}{\partial s}$ in the angular velocity expressions. Therefore, the curvatures are given by

$$\begin{aligned}\boldsymbol{\rho} &= \left(\phi' - \psi'\sin\theta\right)\mathbf{e}_\xi + \left(\psi'\cos\theta\sin\phi + \theta'\cos\phi\right)\mathbf{e}_\eta + \left(\psi'\cos\theta\cos\phi - \theta'\sin\phi\right)\mathbf{e}_\zeta \\ &\equiv \rho_\xi\mathbf{e}_\xi + \rho_\eta\mathbf{e}_\eta + \rho_\zeta\mathbf{e}_\zeta \end{aligned} \tag{2.57}$$

Using the definitions in Eq. (2.55), we obtain exact expressions for $\dot{\psi}$, $\dot{\theta}$, ψ', and θ' by differentiating $\tan\psi$ and $\tan\theta$. The result is

$$\begin{aligned}\dot{\psi} &= \frac{\dot{v}'\left(1+u'\right) - v'\dot{u}'}{\left(1+u'\right)^2 + v'^2} \\ \dot{\theta} &= \frac{1}{\left[\left(1+u'\right)^2 + v'^2 + w'^2\right]}\left\{\frac{w'\left[\left(1+u'\right)\dot{u}' + v'\dot{v}'\right]}{\sqrt{\left(1+u'\right)^2 + v'^2}} - \dot{w}'\sqrt{\left(1+u'\right)^2 + v'^2}\right\} \\ \psi' &= \frac{v''\left(1+u'\right) - v'u''}{\left(1+u'\right)^2 + v'^2} \\ \theta' &= \frac{1}{\left[\left(1+u'\right)^2 + v'^2 + w'^2\right]}\left\{\frac{w'\left[\left(1+u'\right)u'' + v'v''\right]}{\sqrt{\left(1+u'\right)^2 + v'^2}} - w''\sqrt{\left(1+u'\right)^2 + v'^2}\right\}\end{aligned} \tag{2.58}$$

Assuming v, w, and $\phi = O(\epsilon)$ and $u = O\left(\epsilon^2\right)$, substituting Eqs. (2.55) and (2.58) into Eqs. (2.56) and (2.57), and expanding the outcomes in Taylor series, we find that the angular velocities and curvatures, up to $O\left(\epsilon^3\right)$, are

$$\omega_\xi = \dot{\phi} + w'\dot{v}' + \cdots \tag{2.59}$$

$$\omega_\eta = -\dot{w}' + \phi\dot{v}' + w'\dot{u}' + v'w'\dot{v}' + \frac{1}{2}\phi^2\dot{w}' + u'\dot{w}' + \frac{1}{2}v'^2\dot{w}' + w'^2\dot{w}' + \cdots \tag{2.60}$$

$$\omega_\zeta = \dot{v}' + \phi\dot{w}' - v'\dot{u}' - \frac{1}{2}\phi^2\dot{v}' - u'\dot{v}' - v'^2\dot{v}' - \frac{1}{2}w'^2\dot{v}' + \cdots \tag{2.61}$$

$$\rho_\xi = \phi' + w'v'' + \cdots \tag{2.62}$$

$$\rho_\eta = -w'' + \phi v'' + w'u'' + v'w'v'' + \frac{1}{2}\phi^2 w'' + u'w'' + \frac{1}{2}v'^2 w'' + w'^2 w'' + \cdots \tag{2.63}$$

$$\rho_\zeta = v'' + \phi w'' - v'u'' - \frac{1}{2}\phi^2 v'' - u'v'' - v'^2 v'' - \frac{1}{2}w'^2 v'' + \cdots \tag{2.64}$$

2.2.4 Kinetic Energy

The kinetic energy for a beam consists of two parts: one accounts for the motion due to displacement and the other accounts for the motion due to rotation. For beams having symmetric cross sections, the product mass moments of inertia J_{ij}, $i \neq j$, are zero because a principal coordinate system is being used. Therefore, using the notation $J_{11} = J_\xi$, $J_{22} = J_\eta$, and $J_{33} = J_\zeta$, one can express the inertia tensor for a beam with a rectangular cross section as

$$[J] = \begin{bmatrix} J_\xi & 0 & 0 \\ 0 & J_\eta & 0 \\ 0 & 0 & J_\zeta \end{bmatrix} = \frac{1}{12} m \begin{bmatrix} (b^2 + h^2) & 0 & 0 \\ 0 & b^2 & 0 \\ 0 & 0 & h^2 \end{bmatrix} \tag{2.65}$$

The kinetic energy is then defined as

$$\mathcal{T} = \frac{1}{2} \int_0^L \left\{ m \left(\dot{u}^2 + \dot{v}^2 + \dot{w}^2 \right) + \boldsymbol{\omega}^T [J] \boldsymbol{\omega} \right\} ds \tag{2.66}$$

2.3 Lagrangian and Virtual-Work Term

The Lagrangian is defined as $\mathcal{L} \equiv \mathcal{T} - \mathcal{U}$. Using Eqs. (2.45) and (2.66) and introducing the Lagrange multiplier $\lambda(s,t)$ to enforce the inextensionality conditions, we have

$$\mathcal{L} = \frac{1}{2} \int_0^L \left\{ m \left(\dot{u}^2 + \dot{v}^2 + \dot{w}^2 \right) + \boldsymbol{\omega}^T [J] \boldsymbol{\omega} - \boldsymbol{\varepsilon}^T [K] \boldsymbol{\varepsilon} + \lambda \left[1 - \left(1 + u' \right)^2 + v'^2 + w'^2 \right] \right\} ds \tag{2.67}$$

Then, substituting Eqs. (2.46), (2.56), and (2.65) into Eq. (2.67), we express the Lagrangian for monoclinic composite beams as

$$\begin{aligned} \mathcal{L} = \frac{1}{2} \int_0^L \Big\{ & m \left(\dot{u}^2 + \dot{v}^2 + \dot{w}^2 \right) + \left(J_\xi \omega_\xi^2 + J_\eta \omega_\eta^2 + J_\zeta \omega_\zeta^2 \right) - \left(A_{11} e^2 + D_{11} \rho_\xi^2 + D_{22} \rho_\eta^2 \right. \\ & \left. + D_{33} \rho_\zeta^2 + 2 D_{13} \rho_\zeta \rho_\xi + 2 B_{11} \rho_\xi e + 2 B_{13} \rho_\zeta e \right) + \lambda \left[1 - \left(1 + u' \right)^2 + v'^2 + w'^2 \right] \Big\} ds \end{aligned} \tag{2.68}$$

For isotropic beams, linear couplings among the bending, stretching, and twisting terms no longer exist. Therefore, we set

$$A_{11} = EA, \quad D_{11} = D_\xi, \quad D_{22} = D_\eta, \quad D_{33} = D_\zeta, \quad \text{and} \quad D_{13} = B_{11} = B_{13} = 0 \tag{2.69}$$

For beams with rectangular cross sections (Timoshenko, 1970),

$$D_\xi = Gbh^3\kappa_\xi \tag{2.70}$$

$$D_\eta = \frac{1}{12}Ehb^3 \tag{2.71}$$

$$D_\zeta = \frac{1}{12}Ebh^3 \tag{2.72}$$

where

$$\kappa_\xi = \frac{1}{3}\left\{1 - \left[\frac{192}{\pi^5}\left(\frac{h}{b}\right)\right]\sum_{n=1,3,\cdots}^{\infty}\frac{1}{n^5}\tanh\left[\frac{n\pi}{2}\left(\frac{b}{h}\right)\right]\right\} \tag{2.73}$$

Then, from Eqs. (2.68) and (2.69), the Lagrangian for isotropic beams is

$$\begin{aligned}\mathcal{L} = \frac{1}{2}\int_0^L \Big\{ & m\left(\dot{u}^2 + \dot{v}^2 + \dot{w}^2\right) + \left(J_\xi\omega_\xi^2 + J_\eta\omega_\eta^2 + J_\zeta\omega_\zeta^2\right) - \big(EAe^2 \\ & + D_\xi\rho_\xi^2 + D_\eta\rho_\eta^2 + D_\zeta\rho_\zeta^2\big) + \lambda\left[1 - \left(1+u'\right)^2 + v'^2 + w'^2\right]\Big\}ds\end{aligned} \tag{2.74}$$

To account for nonconservative forces, such as damping and external excitations, we introduce the virtual-work term

$$\begin{aligned}\delta\mathcal{W} &= \int_0^L \left(Q_u^*\delta u + Q_v^*\delta v + Q_w^*\delta w + Q_\phi^*\delta\phi + Q_\lambda^*\delta\lambda\right)ds \\ &= \int_0^L \left[\left(Q_u - c_u\dot{u}\right)\delta u + \left(Q_v - c_v\dot{v}\right)\delta v + \left(Q_w - c_w\dot{w}\right)\delta w + \left(Q_\phi - c_\phi\dot{\phi}\right)\delta\phi\right]ds\end{aligned} \tag{2.75}$$

where $Q_\lambda^* = 0$.

2.3.1 Symmetrically Laminated Composite Beams

Substituting Eqs. (2.59)-(2.64) into Eq. (2.68), we obtain the Lagrangian up to quartic terms for monoclinic composite beams as

$$\begin{aligned}\mathcal{L} = \frac{1}{2}\int_0^L \Bigg\{ & m\left(\dot{u}^2+\dot{v}^2+\dot{w}^2\right) + J_\xi\left(\dot{\phi}^2+2\dot{\phi}\dot{v}'w'+\dot{v}'^2w'^2\right) + J_\eta\Big(\dot{w}'^2-2\phi\dot{v}'\dot{w}'+\phi^2\dot{v}'^2 \\ & -2v'\dot{v}'w'\dot{w}'-2\dot{u}'w'\dot{w}'-\phi^2\dot{w}'^2-2u'\dot{w}'^2-v'^2\dot{w}'^2-2w'^2\dot{w}'^2\Big) + J_\zeta\Big(\dot{v}'^2+2\phi\dot{v}'\dot{w}' \\ & -2\dot{u}'v'\dot{v}'-\phi^2\dot{v}'^2-2u'\dot{v}'^2-2v'^2\dot{v}'^2-\dot{v}'^2w'^2+\phi^2\dot{w}'^2\Big) - D_{11}\left(\phi'^2+2\phi'v''w'+v''^2w'^2\right) \\ & -D_{22}\Big(w''^2-2\phi v''w''+\phi^2v''^2-\phi^2w''^2-2u''w'w''-2v'v''w'w''-2u'w''^2-v'^2w''^2 \\ & -2w'^2w''^2\Big) - D_{33}\Big(v''^2+2\phi v''w''-2u''v'v''-2u'v''^2+\phi^2w''^2-\phi^2v''^2-2v'^2v''^2 \\ & -v''^2w'^2\Big) + D_{13}\Big(2v'\phi'u''-2\phi'v''+\phi^2\phi'v''+2u'\phi'v''+2v'^2\phi'v''+w'^2\phi'v''-2w'v''^2 \\ & -2\phi\phi'w''-2\phi w'v''w''\Big) - B_{11}\Big(2u'\phi'+v'^2\phi'+w'^2\phi'+2u'w'v''+v'^2w'v''+w'^3v''\Big) \\ & -B_{13}\left(2u'v''+v'^2v''+w'^2v''+2\phi u'w''+\phi v'^2w''+\phi w'^2w''\right) - A_{11}\Big(u'^2+u'v'^2 \\ & +u'w'^2+\frac{1}{4}v'^4+\frac{1}{2}v'^2w'^2+\frac{1}{4}w'^4\Big) + \lambda\left[1-\left(1+u'\right)^2-v'^2-w'^2\right]\Bigg\}ds \end{aligned} \tag{2.76}$$

Then, substituting the inextensionality condition, given by Eq. (2.53), and applying the boundary condition $u(0,t)=0$, and hence

$$u(s,t) = -\frac{1}{2}\int_0^s \left(v'^2+w'^2\right)ds + \cdots, \tag{2.77}$$

we rewrite the Lagrangian for monoclinic composite beams in terms of v, w, and ϕ as

$$\begin{aligned}\mathcal{L} = \frac{1}{2}\int_0^L \Bigg\{ & m\left[\frac{\partial}{\partial t}\int_0^s \frac{1}{2}\left(v'^2+w'^2\right)ds\right]^2 + m\left(\dot{v}^2+\dot{w}^2\right) + J_\xi\Big(\dot{\phi}^2+2\dot{\phi}\dot{v}'w'+\dot{v}'^2w'^2\Big) \\ & + J_\eta\Big(\dot{w}'^2+\phi^2\dot{v}'^2-2\phi\dot{v}'\dot{w}'-\phi^2\dot{w}'^2+w'^2\dot{w}'^2\Big) + J_\zeta\Big(\dot{v}'^2-\phi^2\dot{v}'^2+v'^2\dot{v}'^2+2\phi\dot{v}'\dot{w}' \\ & +2v'w'\dot{v}'\dot{w}'+\phi^2\dot{w}'^2\Big) - D_{11}\left(\phi'^2+2\phi'v''w'+v''^2w'^2\right) - D_{22}\Big(w''^2+\phi^2v''^2-2\phi v''w'' \\ & -\phi^2w''^2+w'^2w''^2\Big) - D_{33}\Big(v''^2-\phi^2v''^2+v'^2v''^2+2\phi v''w''+2v'w'v''w''+\phi^2w''^2\Big)\end{aligned}$$

$$- D_{13}\Big(2\phi' v'' - \phi^2\phi' v'' + v'^2\phi' v'' + 2w' v''^2 + 2\phi\phi' w'' + 2v' w'\phi' w'' + 2\phi w' v'' w''\Big)\Big\} ds \quad (2.78)$$

We note that the first term multiplying D_{13} is the only one left that produces linear coupling in the governing equations and associated boundary conditions. It couples the in-plane bending and twisting equations.

2.3.2 Isotropic Metallic Beams

Substituting Eqs. (2.59)-(2.64) into Eq. (2.74) yields the following Lagrangian up to quartic terms for isotropic beams:

$$\begin{aligned}\mathcal{L} = \frac{1}{2}\int_0^L \Big\{ & m\left(\dot{u}^2 + \dot{v}^2 + \dot{w}^2\right) + J_\xi\left(\dot{\phi}^2 + 2\dot{\phi}\dot{v}' w' + \dot{v}'^2 w'^2\right) + J_\eta\Big(\dot{w}'^2 - 2\phi\dot{v}'\dot{w}' + \phi^2\dot{v}'^2 \\ & - 2v'\dot{v}' w'\dot{w}' - 2\dot{u}' w'\dot{w}' - \phi^2\dot{w}'^2 - 2u'\dot{w}'^2 - v'^2\dot{w}'^2 - 2w'^2\dot{w}'^2\Big) + J_\zeta\Big(\dot{v}'^2 + 2\phi\dot{v}'\dot{w}' \\ & - 2\dot{u}' v'\dot{v}' - \phi^2\dot{v}'^2 - 2u'\dot{v}'^2 - 2v'^2\dot{v}'^2 - \dot{v}'^2 w'^2 + \phi^2\dot{w}'^2\Big) - D_\xi\left(\phi'^2 + 2\phi' v'' w' + v''^2 w'^2\right) \\ & - D_\eta\Big(w''^2 - 2\phi v'' w'' + \phi^2 v''^2 - \phi^2 w''^2 - 2u'' w' w'' - 2v' v'' w' w'' - 2u' w''^2 - v'^2 w''^2 \\ & - 2w'^2 w''^2\Big) - D_\zeta\left(v''^2 + 2\phi v'' w'' - 2u'' v' v'' - 2u' v''^2 + \phi^2 w''^2 - \phi^2 v''^2 - 2v'^2 v''^2 - v''^2 w'^2\right) \\ & - EA\left(u'^2 + u' v'^2 + u' w'^2 + \frac{1}{4}v'^4 + \frac{1}{2}v'^2 w'^2 + \frac{1}{4}w'^4\right) + \lambda\left[1 - \left(1 + u'\right)^2 - v'^2 - w'^2\right]\Big\} ds\end{aligned} \quad (2.79)$$

Then, substituting Eqs. (2.53) and (2.77) into Eq. (2.79), we rewrite the Lagrangian for isotropic beams in terms of v, w, and ϕ as

$$\begin{aligned}\mathcal{L} = \frac{1}{2}\int_0^L \Bigg\{ & m\left[\frac{\partial}{\partial t}\int_0^s \frac{1}{2}\left(v'^2 + w'^2\right) ds\right]^2 + m\left(\dot{v}^2 + \dot{w}^2\right) + J_\xi\Big(\dot{\phi}^2 + 2\dot{\phi}\dot{v}' w' + \dot{v}'^2 w'^2\Big) \\ & + J_\eta\Big(\dot{w}'^2 + \phi^2\dot{v}'^2 - 2\phi\dot{v}'\dot{w}' - \phi^2\dot{w}'^2 + w'^2\dot{w}'^2\Big) + J_\zeta\Big(\dot{v}'^2 - \phi^2\dot{v}'^2 + v'^2\dot{v}'^2 + 2\phi\dot{v}'\dot{w}' \\ & + 2v' w'\dot{v}'\dot{w}' + \phi^2\dot{w}'^2\Big) - D_\xi\left(\phi'^2 + 2\phi' v'' w' + v''^2 w'^2\right) - D_\eta\Big(w''^2 + \phi^2 v''^2 - 2\phi v'' w'' \\ & - \phi^2 w''^2 + w'^2 w''^2\Big) - D_\zeta\Big(v''^2 - \phi^2 v''^2 + v'^2 v''^2 + 2\phi v'' w'' + 2v' w' v'' w'' + \phi^2 w''^2\Big)\Bigg\} ds\end{aligned} \quad (2.80)$$

2.4 Equations of Motion and Boundary Conditions

The governing equations of motion and boundary conditions can be determined using Hamilton's extended principle

$$\delta\mathcal{I} = \int_{t_1}^{t_2} (\delta\mathcal{L} + \delta\mathcal{W})\, dt = 0 \tag{2.81}$$

Defining $\ell(s,t)$ as the Lagrangian density (i.e., $\mathcal{L}(t) = \int_0^L \ell(s,t)ds$), we have

$$\delta\mathcal{I} = \int_{t_1}^{t_2}\int_0^L \left(\delta\ell + Q_u^*\delta u + Q_v^*\delta v + Q_w^*\delta w + Q_\phi^*\delta\phi + Q_\lambda^*\delta\lambda\right) dsdt = 0 \tag{2.82}$$

where δu, δv, δw, $\delta\phi$, and $\delta\lambda = 0$ at $t = t_1$ and t_2. Because the Lagrangian density for beam systems is $\ell = \ell(q_i, \dot{q}_i, q_i', q_i'', \dot{q}_i', s, t)$, Eq. (2.82) yields the following equations of motion (Meirovitch, 1997):

$$\frac{\partial\ell}{\partial q_i} - \frac{\partial}{\partial s}\left(\frac{\partial\ell}{\partial q_i'}\right) + \frac{\partial^2}{\partial s^2}\left(\frac{\partial\ell}{\partial q_i''}\right) - \frac{\partial}{\partial t}\left(\frac{\partial\ell}{\partial\dot{q}_i}\right) + \frac{\partial^2}{\partial s\partial t}\left(\frac{\partial\ell}{\partial\dot{q}_i'}\right) = -Q_i^*, \qquad 0 < s < L \tag{2.83}$$

and associated boundary conditions:

$$B1_i = \left\{\left[\frac{\partial\ell}{\partial q_i'} - \frac{\partial}{\partial s}\left(\frac{\partial\ell}{\partial q_i''}\right) - \frac{\partial}{\partial t}\left(\frac{\partial\ell}{\partial\dot{q}_i'}\right)\right]\delta q_i\right\}_{s=0}^{s=L} = 0 \tag{2.84}$$

$$B2_i = \left\{\left[\frac{\partial\ell}{\partial q_i''}\right]\delta q_i'\right\}_{s=0}^{s=L} = 0 \tag{2.85}$$

where $q_i(s,t)$ represents the variables $u(s,t)$, $v(s,t)$, $w(s,t)$, $\phi(s,t)$, and $\lambda(s,t)$.

2.4.1 Symmetrically Laminated Composite Beams

Setting $q_i = u(s,t)$ and applying Eqs. (2.83)-(2.85) to Eq. (2.76), we obtain the following equation of motion governing the longitudinal vibrations:

$$\begin{aligned} m\ddot{u} - Q_u^* = {} & \left[\lambda\left(1+u'\right)\right]' + A_{11}\left(u' + \frac{v'^2}{2} + \frac{w'^2}{2}\right)' + B_{11}\left(\phi' + v''w'\right)' + B_{13}\left(v'' + \phi w''\right)' \\ & + D_{22}\left(w'w'''\right)' + D_{33}\left(v'v'''\right)' + D_{13}\left(v'\phi''\right)' - J_\eta\left(w'\ddot{w}'\right)' - J_\zeta\left(v'\ddot{v}'\right)' \end{aligned} \tag{2.86}$$

The associated boundary conditions are

$$u = 0 \quad \text{at the fixed end } s = 0, \tag{2.87}$$

and

$$\begin{aligned}\lambda\left(1+u'\right) = &-A_{11}\left(u' + \frac{v'^2}{2} + \frac{w'^2}{2}\right) - B_{11}\left(\phi' + v''w'\right) - B_{13}\left(v'' + \phi w''\right) \\ &- D_{22}\left(w'w'''\right) - D_{33}\left(v'v'''\right) - D_{13}\left(v'\phi''\right) + J_\eta\left(w'\ddot{w}'\right) + J_\zeta\left(v'\ddot{v}'\right)\end{aligned} \tag{2.88}$$

at the free end $s = L$. Then, using Eqs. (2.53) and (2.77) and keeping terms up to $O(\epsilon^2)$, we solve Eqs. (2.86) and (2.88) for the Lagrange multiplier $\lambda(s,t)$. The result is

$$\begin{aligned}\lambda = &J_\eta\left(w'\ddot{w}'\right) + J_\zeta\left(v'\ddot{v}'\right) - D_{22}\left(w'w'''\right) - D_{33}\left(v'v'''\right) - D_{13}\left(v'\phi''\right) - B_{11}\left(\phi' + v''w'\right) \\ &- B_{13}\left(v'' + \phi w''\right) - \frac{m}{2}\int_L^s\left[\frac{\partial^2}{\partial t^2}\int_0^s\left(v'^2 + w'^2\right)ds\right]ds - \int_L^s Q_u^* ds + \cdots\end{aligned} \tag{2.89}$$

Setting $q_i = v(s,t)$, applying Eqs. (2.83)-(2.85) to Eq. (2.76), and then substituting Eqs. (2.53), (2.77), and (2.89), we obtain the following equation of motion governing the in-plane bending vibrations:

$$\begin{aligned}m\ddot{v} + c_v\dot{v} + D_{33}v^{iv} + D_{13}\phi''' - J_\zeta\ddot{v}'' = &Q_v - D_{11}\left(\phi'w' + v''w'^2\right)'' - \left(D_{22} - D_{33}\right)\left(\phi^2 v'' - \phi w''\right)'' \\ &- D_{33}\left[v'\left(v'v''\right)' + v'\left(w'w''\right)'\right]' + D_{13}\left[\frac{1}{2}\left(\phi'\phi^2\right)'\right. \\ &\left. - \left(2v''w'\right)' - \frac{1}{2}v'^2\phi'' - \left(w'w''\right)'\phi\right]' + J_\xi\frac{\partial}{\partial t}\left(\dot{\phi}w' + \dot{v}'w'^2\right)' \\ &- \left(J_\eta - J_\zeta\right)\left[\left(v'w'\ddot{w}'\right) - \frac{\partial}{\partial t}\left(\dot{v}'\phi^2 - \dot{w}'\phi\right)\right]' + J_\zeta\Big(v'\dot{v}'^2 \\ &+ v'\dot{w}'^2\Big)' - \frac{m}{2}\left\{v'\int_L^s\left[\frac{\partial^2}{\partial t^2}\int_0^s\left(v'^2 + w'^2\right)ds\right]ds\right\}' \\ &- \left(v'\int_L^s Q_u^* ds\right)'\end{aligned} \tag{2.90}$$

The boundary conditions are

$$v = 0 \quad \text{and} \quad v' = 0 \quad \text{at the fixed end } s = 0, \tag{2.91}$$

and

$$\begin{aligned} D_{33}v'' + D_{13}\phi' = &-D_{11}\left(v''w'^2 + \phi'w'\right) - \left(D_{22} - D_{33}\right)\left(\phi^2 v'' - \phi w'' - v'w'w''\right) \\ &+ D_{13}\left(\frac{1}{2}\phi^2\phi' - \frac{1}{2}v'^2\phi' - \phi w'w'' - 2v''w'\right) \end{aligned} \tag{2.92}$$

$$\begin{aligned} D_{33}v''' + D_{13}\phi'' - J_\zeta\ddot{v}' = &-D_{11}\left(\phi'w' + w'^2v''\right)' - \left(D_{22} - D_{33}\right)\left(\phi^2 v'' - \phi w''\right)' \\ &- D_{33}\left[v'\left(v'v''\right)' + v'\left(w'w''\right)'\right] + D_{13}\left[\frac{1}{2}\left(\phi^2\phi'\right)' - \frac{1}{2}v'^2\phi'' \right. \\ &\left. - \phi\left(w'w''\right)' - 2\left(v''w'\right)'\right] + J_\xi\frac{\partial}{\partial t}\left(\dot{\phi}w' + w'^2\dot{v}'\right) \\ &+ \left(J_\eta - J_\zeta\right)\frac{\partial}{\partial t}\left(\phi^2\dot{v}' - \phi\dot{w}'\right) + J_\zeta\left[v'\frac{\partial}{\partial t}\left(v'\dot{v}'\right) + v'\frac{\partial}{\partial t}\left(w'\dot{w}'\right)\right] \end{aligned} \tag{2.93}$$

at the free end $s = L$.

Setting $q_i = w(s,t)$, applying Eqs. (2.83)-(2.85) to Eq. (2.76), and then substituting Eqs. (2.53), (2.77), and (2.89), we obtain the following equation of motion governing the out-of-plane bending vibrations:

$$\begin{aligned} m\ddot{w} + c_w\dot{w} + D_{22}w^{iv} - J_\eta\ddot{w}'' = &\, Q_w + D_{11}\left(\phi'v'' + v''^2w'\right)' + \left(D_{22} - D_{33}\right)\left(\phi^2 w'' + \phi v''\right)'' \\ &- D_{22}\left[w'\left(w'w''\right)'\right]' - D_{33}\left[w'\left(v'v''\right)'\right]' + D_{13}\left[v''^2 - \left(\phi\phi'\right)'\right. \\ &\left. - w'\left(\phi v'\right)''\right]' - J_\xi\left(\dot{\phi}\dot{v}' + \dot{v}'^2w'\right)' + J_\eta\left(w'\dot{w}'^2\right)' + J_\zeta\left(w'\dot{v}'^2\right)' \\ &- \left(J_\eta - J_\zeta\right)\frac{\partial}{\partial t}\left[\left(\dot{w}'\phi^2\right) + \left(\dot{v}'\phi\right)\right]' - \left(w'\int_L^s Q_u^* ds\right)' \\ &- \frac{m}{2}\left\{w'\int_L^s\left[\frac{\partial^2}{\partial t^2}\int_0^s\left(v'^2 + w'^2\right)ds\right]ds\right\}' \end{aligned} \tag{2.94}$$

The boundary conditions are

$$w = 0 \quad \text{and} \quad w' = 0 \quad \text{at the fixed end } s = 0, \tag{2.95}$$

and

$$D_{22}w'' = (D_{22} - D_{33})\left(\phi^2 w'' + \phi v''\right) - D_{13}\left[\phi\phi' + \left(\phi v'\right)' w'\right] \tag{2.96}$$

$$\begin{aligned} D_{22}w''' - J_\eta \ddot{w}' = {} & D_{11}\left(w'v''^2 + v''\phi'\right) - D_{22}\left[w'\left(w'w''\right)'\right] - D_{33}\left[w'\left(v'v''\right)'\right] \\ & + (D_{22} - D_{33})\left(\phi^2 w'' + \phi v''\right)' - D_{13}\left[w'\left(\phi v'\right)'' + \left(\phi\phi'\right)' - v''^2\right] \\ & - J_\xi\left(w'\dot{v}'^2 + \dot{\phi}\dot{v}'\right) + J_\eta\left[w'\frac{\partial}{\partial t}\left(w'\dot{w}'\right)\right] + J_\zeta\left[w'\frac{\partial}{\partial t}\left(v'\dot{v}'\right)\right] \\ & - (J_\eta - J_\zeta)\frac{\partial}{\partial t}\left(\phi^2\dot{w}' + \phi\dot{v}'\right) \end{aligned} \tag{2.97}$$

at the free end $s = L$.

Setting $q_i = \phi(s,t)$, applying Eqs. (2.83)-(2.85) to Eq. (2.76), and then substituting Eqs. (2.53), (2.77), and (2.89), we obtain the following equation of motion governing the torsional vibrations:

$$\begin{aligned} J_\xi\ddot{\phi} + c_\phi\dot{\phi} - D_{11}\phi'' - D_{13}v''' = {} & Q_\phi + D_{11}\left(v''w'\right)' + (D_{22} - D_{33})\left(v''w'' - \phi v''^2 + \phi w''^2\right) \\ & + D_{13}\left[\frac{1}{2}\left(v'^2 v''\right)' - \frac{1}{2}\phi^2 v''' + v'\left(w'w''\right)' + \phi w'''\right] \\ & - J_\xi\frac{\partial}{\partial t}\left(\dot{v}'w'\right) + (J_\eta - J_\zeta)\left(\phi\dot{v}'^2 - \phi\dot{w}'^2 - \dot{v}'\dot{w}'\right) \end{aligned} \tag{2.98}$$

The boundary conditions are

$$\phi = 0 \quad \text{at the fixed end } s = 0, \tag{2.99}$$

and

$$D_{11}\phi' + D_{13}v'' = -D_{11}\left(v''w'\right) + D_{13}\left(\frac{1}{2}\phi^2 v'' - \frac{1}{2}v'^2 v'' - \phi w'' - v'w'w''\right) \tag{2.100}$$

at the free end $s = L$.

In addition to the linear coupling terms, Eqs. (2.90)-(2.100) also contain quadratic and cubic nonlinearities coupling the bending-bending and bending-twisting motions. We should also note that, because $\phi(s,t)$ is actually an Euler-rotation angle, the angle of twist $\gamma(s,t)$, which the beam

physically experiences, can be obtained from integrating the twisting curvature, Eq. (2.62), and using Eq. (2.99). The result is

$$\gamma = \int_0^s \rho_\xi ds = \phi + \int_0^s v''w'ds + \cdots = \phi + v'w' - \int_0^s v'w''ds + \cdots \tag{2.101}$$

Although the governing equations of motion and associated boundary conditions are independent of the terms multiplying B_{11} and B_{13}, the Lagrange multiplier λ is not. One can interpret λ as an axial force acting at the beam's tip to prevent it from stretching. We see from Eq. (2.89) that λ is $O(\epsilon)$. However, if we apply Eq. (2.69) to Eq. (2.89), we find for isotropic beams that

$$\begin{aligned}\lambda = {} & J_\eta\left(w'\ddot{w}'\right) + J_\zeta\left(v'\ddot{v}'\right) - D_\eta\left(w'w'''\right) - D_\zeta\left(v'v'''\right) \\ & - \frac{m}{2}\int_L^s\left[\frac{\partial^2}{\partial t^2}\int_0^s\left(v'^2 + w'^2\right)ds\right]ds - \int_L^s Q_u^* ds + \cdots\end{aligned} \tag{2.102}$$

which is $O(\epsilon^2)$. Therefore, a larger axial force may be needed to enforce the inextensionality of a composite beam.

2.4.2 Isotropic Metallic Beams

Whether repeating the same process as in Section (2.4.1) but with Eq. (2.79) or applying Eq. (2.69) to Eqs. (2.86)-(2.100), one obtains the following equations of motion governing the *bending-bending-torsional* vibrations of inextensional metallic beams:

$$\begin{aligned}m\ddot{v} + c_v\dot{v} + D_\zeta v^{iv} - J_\zeta\ddot{v}'' = {} & Q_v - D_\xi\left(\phi'w' + v''w'^2\right)'' - \left(D_\eta - D_\zeta\right)\left(\phi^2 v'' - \phi w''\right)'' \\ & - D_\zeta\left[v'\left(v'v''\right)' + v'\left(w'w''\right)'\right]' + J_\xi\frac{\partial}{\partial t}\left(\dot{\phi}w' + \dot{v}'w'^2\right)' \\ & - \left(J_\eta - J_\zeta\right)\left[\left(v'w'\ddot{w}'\right) - \frac{\partial}{\partial t}\left(\dot{v}'\phi^2 - \dot{w}'\phi\right)\right]' + J_\zeta\left[v'\left(\dot{v}'^2 + \dot{w}'^2\right)\right]' \\ & - \frac{m}{2}\left\{v'\int_L^s\left[\frac{\partial^2}{\partial t^2}\int_0^s\left(v'^2 + w'^2\right)ds\right]ds\right\}' - \left(v'\int_L^s Q_u^* ds\right)'\end{aligned} \tag{2.103}$$

$$\begin{aligned}m\ddot{w} + c_w\dot{w} + D_\eta w^{iv} - J_\eta\ddot{w}'' = {} & Q_w + D_\xi\left(\phi'v'' + v''^2 w'\right)' + \left(D_\eta - D_\zeta\right)\left(\phi^2 w'' + \phi v''\right)'' \\ & - D_\eta\left[w'\left(w'w''\right)'\right]' - D_\zeta\left[w'\left(v'v''\right)'\right]' - J_\xi\left(\dot{\phi}\dot{v}' + \dot{v}'^2 w'\right)'\end{aligned}$$

$$
\begin{aligned}
&- (J_\eta - J_\zeta) \frac{\partial}{\partial t} \left[\left(\dot{w}' \phi^2 \right) + \left(\dot{v}' \phi \right) \right]' + J_\eta \left(w' \dot{w}'^2 \right)' + J_\zeta \left(w' \dot{v}'^2 \right)' \\
&- \frac{m}{2} \left\{ w' \int_L^s \left[\frac{\partial^2}{\partial t^2} \int_0^s \left(v'^2 + w'^2 \right) ds \right] ds \right\}' - \left(w' \int_L^s Q_u^* ds \right)'
\end{aligned} \tag{2.104}
$$

$$
\begin{aligned}
J_\xi \ddot{\phi} + c_\phi \dot{\phi} - D_\xi \phi'' = Q_\phi &+ D_\xi \left(v'' w' \right)' + (D_\eta - D_\zeta) \left(v'' w'' - \phi v''^2 + \phi w''^2 \right) \\
&- J_\xi \frac{\partial}{\partial t} \left(\dot{v}' w' \right) + (J_\eta - J_\zeta) \left(\phi \dot{v}'^2 - \phi \dot{w}'^2 - \dot{v}' \dot{w}' \right)
\end{aligned} \tag{2.105}
$$

The associated boundary conditions are:

$$
v = 0, \quad v' = 0, \quad w = 0, \quad w' = 0, \quad \text{and} \quad \phi = 0 \quad \text{at the fixed end } s = 0, \tag{2.106}
$$

and

$$
D_\zeta v'' = -D_\xi \left(v'' w'^2 + \phi' w' \right) - (D_\eta - D_\zeta) \left(\phi^2 v'' - \phi w'' - v' w' w'' \right) \tag{2.107}
$$

$$
\begin{aligned}
D_\zeta v''' - J_\zeta \ddot{v}' = &- D_\xi \left(\phi' w' + w'^2 v'' \right)' - (D_\eta - D_\zeta) \left(\phi^2 v'' - \phi w'' \right)' \\
&- D_\zeta \left[v' \left(v' v'' \right)' + v' \left(w' w'' \right)' \right] + J_\xi \frac{\partial}{\partial t} \left(\dot{\phi} w' + w'^2 \dot{v}' \right) \\
&+ (J_\eta - J_\zeta) \frac{\partial}{\partial t} \left(\phi^2 \dot{v}' - \phi \dot{w}' \right) + J_\zeta \left[v' \frac{\partial}{\partial t} \left(v' \dot{v}' \right) + v' \frac{\partial}{\partial t} \left(w' \dot{w}' \right) \right]
\end{aligned} \tag{2.108}
$$

$$
D_\eta w'' = (D_\eta - D_\zeta) \left(\phi^2 w'' + \phi v'' \right) \tag{2.109}
$$

$$
\begin{aligned}
D_\eta w''' - J_\eta \ddot{w}' = &D_\xi \left(w' v''^2 + v'' \phi' \right) - D_\eta \left[w' \left(w' w'' \right)' \right] - D_\zeta \left[w' \left(v' v'' \right)' \right] \\
&+ (D_\eta - D_\zeta) \left(\phi^2 w'' + \phi v'' \right)' - (J_\eta - J_\zeta) \frac{\partial}{\partial t} \left(\phi^2 \dot{w}' + \phi \dot{v}' \right) \\
&- J_\xi \left(w' \dot{v}'^2 + \dot{\phi} \dot{v}' \right) + J_\eta \left[w' \frac{\partial}{\partial t} \left(w' \dot{w}' \right) \right] + J_\zeta \left[w' \frac{\partial}{\partial t} \left(v' \dot{v}' \right) \right]
\end{aligned} \tag{2.110}
$$

$$
D_\xi \phi' = -D_\xi \left(v'' w' \right) \tag{2.111}
$$

at the fixed end $s = L$.

We note that Eqs. (2.103)-(2.111) are linearly uncoupled. Furthermore, although the nonlinearities coupling the bending-twisting motions are quadratic and cubic, the nonlinearities coupling the bending-bending motions are only cubic. In deriving the governing system of equations and associated boundary conditions, we neglected the effect of shear deformation. Hence, they are applicable

to long thin beams. Furthermore, because the effect of the rotatory inertia terms (i.e., J_η and J_ζ terms) is the same order as the effect of the shear deformation terms (Timoshenko, 1921), we will neglect them in what follows.

A special case of practical importance may be considered for beams whose fundamental torsional frequency is much higher than the frequencies of the directly excited flexural modes. This is true, for example, in beams that have near-square or near-circular cross-sections and hence, they are very rigid in torsion. Then, the torsional inertia terms can be neglected in comparison with the flexural inertia and stiffness terms (Crespo da Silva, 1978b). Consequently, integrating Eq. (2.105) twice, using Eqs. (2.106e) and (2.111), and keeping terms of $O(\epsilon^2)$, we obtain

$$D_\xi \phi = -D_\xi \int_0^s v'' w' ds - \int_0^s \int_L^s \left[Q_\phi^* + (D_\eta - D_\zeta)\, v'' w'' \right] ds ds + \cdots \tag{2.112}$$

Therefore, for such beams, if v and $w = O(\epsilon)$, then from Eq. (2.112), $\phi = O(\epsilon^2)$.

Substituting Eq. (2.112) into Eqs. (2.103) and (2.104), we obtain the following equations of motion governing the nonlinear *bending-bending* vibrations of inextensional metallic beams:

$$\begin{aligned} m\ddot{v} + c_v \dot{v} + D_\zeta v^{iv} = Q_v &+ \underline{(D_\eta - D_\zeta) \left[w'' \int_L^s v'' w'' ds - w''' \int_0^s v'' w' ds \right]'} \\ &- \underline{\frac{(D_\eta - D_\zeta)^2}{D_\xi} \left[w'' \int_0^s \int_L^s v'' w'' ds ds \right]''} - \underline{\underline{D_\zeta \left[v' \left(v' v'' + w' w'' \right)' \right]'}} \\ &- \underline{\underline{\frac{m}{2} \left\{ v' \int_L^s \left[\frac{\partial^2}{\partial t^2} \int_0^s \left(v'^2 + w'^2 \right) ds \right] ds \right\}'}} - \left(v' \int_L^s Q_u^* ds \right)' \\ &+ \left(w' \int_L^s Q_\phi^* ds \right)'' - \frac{(D_\eta - D_\zeta)}{D_\xi} \left(w'' \int_0^s \int_L^s Q_\phi^* ds ds \right)'' \end{aligned} \tag{2.113}$$

$$\begin{aligned} m\ddot{w} + c_w \dot{w} + D_\eta w^{iv} = Q_w &- \underline{(D_\eta - D_\zeta) \left[v'' \int_L^s v'' w'' ds - v''' \int_0^s v' w'' ds \right]'} \\ &- \underline{\frac{(D_\eta - D_\zeta)^2}{D_\xi} \left[v'' \int_0^s \int_L^s v'' w'' ds ds \right]''} - \underline{\underline{D_\eta \left[w' \left(v' v'' + w' w'' \right)' \right]'}} \\ &- \underline{\underline{\frac{m}{2} \left\{ w' \int_L^s \left[\frac{\partial^2}{\partial t^2} \int_0^s \left(v'^2 + w'^2 \right) ds \right] ds \right\}'}} - \left(w' \int_L^s Q_u ds \right)' \\ &- \left(v'' \int_L^s Q_\phi^* ds \right)' - \frac{(D_\eta - D_\zeta)}{D_\xi} \left(v'' \int_0^s \int_L^s Q_\phi^* ds ds \right)'' \end{aligned} \tag{2.114}$$

The boundary conditions reduce to

$$v = 0, \quad v' = 0, \quad w = 0, \quad \text{and} \quad w' = 0, \quad \text{at} \quad s = 0 \tag{2.115}$$

$$v'' = 0, \quad v''' = 0, \quad w'' = 0, \quad \text{and} \quad w'''= 0, \quad \text{at} \quad s = L \tag{2.116}$$

and the corresponding Lagrangian is given by

$$\begin{aligned}\mathcal{L} = \frac{1}{2}\int_0^L \Bigg\{ & m\left[\frac{\partial}{\partial t}\int_0^s \frac{1}{2}\left(v'^2 + w'^2\right) ds\right]^2 + m\left(\dot{v}^2 + \dot{w}^2\right) - \left(D_\eta - D_\zeta\right)\left(2v''w''\int_0^s v''w'ds\right) \\ & - D_\eta\left(w''^2 + w'^2 w''^2\right) - D_\zeta\left(v''^2 + v'^2 v''^2 + 2v'v''w'w''\right) \\ & - \frac{\left(D_\eta - D_\zeta\right)^2}{D_\xi}\left[\left(\int_L^s v''w''ds\right)^2 + \left(2v''w''\int_0^s\int_L^s v''w''dsds\right)\right]\Bigg\}ds\end{aligned} \tag{2.117}$$

The nonlinearities coupling the bending-bending motions in Eqs. (2.113) and (2.114) are only cubic. This is unlike the case when we directly accounted for the torsional vibrations. The terms underlined once represent the bending-twisting geometric nonlinearities; the terms underlined twice represent the bending-bending inertia nonlinearities; and the terms underlined three times represent the bending-bending geometric nonlinearities.

We note that for near-square or near-circular cross-section beams, the coefficient $(D_\eta - D_\zeta) = O(\epsilon)$. Therefore, the important nonlinearities in the responses of such beams are the bending-bending geometric and inertia nonlinearities. Crespo da Silva and Glynn (1978b) showed that the geometric nonlinearities are as important as the inertia nonlinearities and hence should not be neglected. Nayfeh and Pai (1989) and Pai and Nayfeh (1990) showed that the geometric nonlinearities, having a hardening influence, are dominant when the modes excited are low, whereas the inertia nonlinearities, having a softening influence, are dominant when the modes excited are high. Therefore, the overall effective nonlinearity may either be hardening or softening, depending on the mode being excited.

Setting $w(s,t) = 0$, one obtains the following equation of motion governing the nonlinear *planar*

bending vibrations of inextensional beams:

$$m\ddot{v} + c_v\dot{v} + D_\zeta v^{iv} = -D_\zeta \left[v' \left(v'v''\right)'\right]' - \frac{m}{2}\left\{v' \int_L^s \left[\frac{\partial^2}{\partial t^2}\int_0^s v'^2 ds\right] ds\right\}' - \left(v' \int_L^s Q_u^* ds\right)' + Q_v \tag{2.118}$$

The corresponding Lagrangian is

$$\mathcal{L} = \frac{1}{2}\int_0^L \left\{m\left[\frac{\partial}{\partial t}\int_0^s \frac{1}{2}v'^2 ds\right]^2 + m\dot{v}^2 - D_\zeta\left(v''^2 + v'^2 v''^2\right)\right\} ds \tag{2.119}$$

Chapter 3

Bending-Bending Dynamics of Parametrically Excited Cantilever Beams

The nonlinear nonplanar response of a cantilever inextensional metallic beam to a principal parametric excitation of two of its flexural modes, one in each plane, is investigated. The lowest torsional frequencies of the beams considered are much larger than the frequencies of the excited modes so that the torsional inertia can be neglected. The method of time-averaged Lagrangian is used to derive four first-order nonlinear ordinary-differential equations governing the modulation of the amplitudes and phases of the two interacting modes. These modulation equations are shown to exhibit the symmetry conditions found by Feng and Leal (1994). A pseudo-arclength scheme is used to trace the branches of the equilibrium solutions and the eigenvalues of the Jacobian matrix are used to assess their stability. The effect of the cross-section and forcing frequency detunings on the static and dynamic bifurcations is investigated. The equilibrium solutions experience pitchfork, saddle-node, Hopf, and codimension-2 bifurcations. Five branches of dynamic (periodic and chaotic) solutions of the modulation equations are found. Two of these branches emerge from two Hopf bifurcations and the other three are isolated. The limit cycles undergo symmetry-breaking, cyclic-fold, and period-doubling bifurcations, whereas the chaotic attractors undergo attractor-merging

and boundary crises. Other interesting phenomena found include bubble structures, phase-locked limit cycles, and explosive bifurcations.

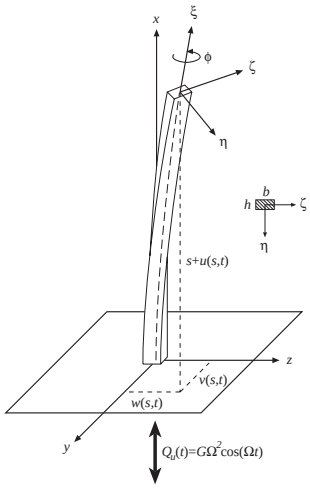

Figure 3.1: A schematic of a near-square cantilever beam under parametric excitation.

3.1 Problem Formulation

Using the nondimensional quantities

$$s^* = \frac{s}{L}, \qquad t^* = \sqrt{\frac{D_\eta}{mL^4}}t, \qquad v^* = \frac{v}{L}, \qquad w^* = \frac{w}{L}, \qquad \beta_y = \frac{D_\zeta}{D_\eta}, \qquad \beta_\gamma = \frac{D_\xi}{D_\eta} \tag{3.1}$$

in Eq. (2.117), we express the nondimensional Lagrangian $\mathcal{L}^* = (L/D_\eta)\,\mathcal{L}$ as

$$\begin{aligned}\mathcal{L} = \int_0^1 \Bigg(& \frac{1}{2}\Bigg\{ \left[\frac{\partial}{\partial t}\int_0^s \frac{1}{2}\left(v'^2 + w'^2\right) ds\right]^2 + \dot{v}^2 + \dot{w}^2 \Bigg\} - (1-\beta_y)\left\{ v''w'' \int_0^s v''w' ds \right\} \\ & - \frac{1}{2}\Bigg\{ w''^2 + w'^2 w''^2 \Bigg\} - \frac{1}{2}\beta_y \Bigg\{ v''^2 + v'^2 v''^2 + 2v'v''w'w'' \Bigg\} \\ & - \frac{(1-\beta_y)^2}{2\beta_\gamma}\Bigg\{ \left[\int_1^s v''w'' ds\right]^2 + \left[2v''w'' \int_0^s \int_1^s v''w'' ds ds\right] \Bigg\} \Bigg) ds \end{aligned} \tag{3.2}$$

where the asterisk has been dropped for convenience. To account for the damping and parametric excitation, we set $Q_u(t) = G\Omega^2 \cos(\Omega t)$ and introduce the nondimensional virtual-work term

$$\begin{aligned}\delta W &= \int_0^1 \Big(Q_v^* \delta v + Q_w^* \delta w \Big) ds \\ &= -\int_0^1 \Big(\big[v''(s-1) + v' \big] G\Omega^2 \cos(\Omega t) + c_v \dot{v} \Big) \delta v ds \\ &\quad - \int_0^1 \Big(\big[w''(s-1) + w' \big] G\Omega^2 \cos(\Omega t) + c_w \dot{w} \Big) \delta w ds \end{aligned} \tag{3.3}$$

The corresponding nondimensional governing equations of motion are obtained by applying Eq. (3.1) to Eqs. (2.113) and (2.114). The result is

$$\begin{aligned}\ddot{v} + c_v \dot{v} + \beta_y v'''' &= (1-\beta_y) \left[w'' \int_1^s v'' w'' ds - w''' \int_0^s v'' w' ds \right]' \\ &\quad - \frac{(1-\beta_y)^2}{\beta_\gamma} \left[w'' \int_0^s \int_1^s v'' w'' ds ds \right]'' - \beta_y \left[v' \left(v' v'' + w' w'' \right)' \right]' \\ &\quad - \frac{1}{2} \left\{ v' \int_1^s \frac{\partial^2}{\partial t^2} \left[\int_0^s \left(v'^2 + w'^2 \right) ds \right] ds \right\}' - \left[v'' (s-1) + v' \right] G\Omega^2 \cos(\Omega t) \end{aligned} \tag{3.4}$$

$$\begin{aligned}\ddot{w} + c_w \dot{w} + w'''' &= -(1-\beta_y) \left[v'' \int_1^s v'' w'' ds - v''' \int_0^s v' w'' ds \right]' \\ &\quad - \frac{(1-\beta_y)^2}{\beta_\gamma} \left[v'' \int_0^s \int_1^s v'' w'' ds ds \right]'' - \left[w' \left(v' v'' + w' w'' \right)' \right]' \\ &\quad - \frac{1}{2} \left\{ w' \int_1^s \frac{\partial^2}{\partial t^2} \left[\int_0^s \left(v'^2 + w'^2 \right) ds \right] ds \right\}' - \left[w'' (s-1) + w' \right] G\Omega^2 \cos(\Omega t) \end{aligned} \tag{3.5}$$

The associated boundary conditions are given by Eqs. (2.115) and (2.116).

3.2 Perturbation Analysis

To determine the modulation equations governing the amplitudes and phases, we apply the method of multiple scales (Nayfeh, 1973, 1981) directly to the Lagrangian and virtual-work term. We introduce $\epsilon \ll 1$ as a bookkeeping parameter such that the kth time scale $T_k = \epsilon^k t$ for $k = 0, 1, 2, \cdots$.

Then, using the chain rule, we transform the first and second time derivatives according to

$$\begin{aligned}\frac{\partial}{\partial t} &= \frac{\partial}{\partial T_0} + \epsilon\frac{\partial}{\partial T_1} + \epsilon^2\frac{\partial}{\partial T_2} + \cdots \\ &\equiv D_0 + \epsilon D_1 + \epsilon^2 D_2 + \cdots \qquad (3.6)\\ \frac{\partial^2}{\partial t^2} &= \frac{\partial^2}{\partial T_0^2} + 2\epsilon\frac{\partial^2}{\partial T_0 \partial T_1} + \epsilon^2\left(\frac{\partial^2}{\partial T_1^2} + 2\frac{\partial^2}{\partial T_0 \partial T_2}\right) + \cdots \\ &\equiv D_0^2 + 2\epsilon D_0 D_1 + \epsilon^2\left(D_1^2 + 2D_0 D_2\right) + \cdots \qquad (3.7)\end{aligned}$$

Because Eqs. (3.4) and (3.5) contain only cubic nonlinearities, the solution is independent of the time scale T_1. Then, we seek a uniform expansion for $v(s,t)$ and $w(s,t)$ as

$$v(s,t) = v(s,T_0,T_2) = \epsilon v_1(s,T_0,T_2) + \epsilon^3 v_3(s,T_0,T_2) + \cdots \qquad (3.8)$$

$$w(s,t) = w(s,T_0,T_2) = \epsilon w_1(s,T_0,T_2) + \epsilon^3 w_3(s,T_0,T_2) + \cdots \qquad (3.9)$$

It follows from Eqs. (2.115), (2.116), (3.4), and (3.5) that the linear undamped natural frequencies and their corresponding mode shapes are given by

$$\hat{\omega}_{1m} = z_m^2\sqrt{\beta_y}, \quad \omega_{2n} = z_n^2 \qquad (3.10)$$

$$\Phi_i(s) = \cosh z_i s - \cos z_i s + \frac{\cos z_i + \cosh z_i}{\sin z_i + \sinh z_i}\left(\sin z_i s - \sinh z_i s\right), \quad i = m, n \qquad (3.11)$$

where $\hat{\omega}_{1m}$ and ω_{2n} are the natural frequencies in the y and z directions and the z_i are the roots of

$$1 + \cos z \cosh z = 0 \qquad (3.12)$$

The lowest five roots are 1.8751, 4.6941, 7.8548, 10.9955, and 14.1372.

Following Nayfeh and Pai (1989), we consider the case of one-to-one internal resonance between the mth mode in the y direction and the nth mode in the z direction; that is, $\hat{\omega}_{1m} \approx \omega_{2n}$. To express

the nearness of these frequencies quantitatively, we let

$$\beta_y = 1 + \delta_0 + \epsilon^2 \delta_2 \tag{3.13}$$

so that when $\delta_2 = 0$, the internal resonance is perfectly tuned and we have

$$\omega_{1m} = z_m^2 \sqrt{1 + \delta_0} = z_n^2 = \omega_{2n} \tag{3.14}$$

We note that $\delta_0 = 0$ for a near-square cross-section. For the case of principal parametric resonance of the nth mode in the z direction, we put

$$\Omega = 2\omega_{2n}\left(1 + \epsilon^2 \sigma\right) = 2\omega_{1m}\left(1 + \epsilon^2 \sigma\right) \tag{3.15}$$

where σ is a detuning parameter. We also set $G = \epsilon^2 g$.

Nayfeh and Pai (1989) directly attacked Equations (3.4) and (3.5) by using the method of multiple scales and obtained the following second-order uniform expansion of the response of the beam:

$$v(s, T_0, T_2) = \epsilon \Phi_m(s) A_1(T_2) e^{i\omega_{1m} T_0} + \text{cc} + \cdots \tag{3.16}$$

$$w(s, T_0, T_2) = \epsilon \Phi_n(s) A_2(T_2) e^{i\omega_{2n} T_0} + \text{cc} + \cdots \tag{3.17}$$

where the complex-valued functions A_1 and A_2 are governed by

$$\begin{aligned} i\omega_{1m}\left(2A_1' + 2\mu_1 A_1\right) = &-\delta_2 z_m^4 A_1 - \left[\delta_0 \alpha_1 + \frac{\delta_0^2}{\beta_\gamma}\alpha_2 + (1 + \delta_0)\,\alpha_3\right]\left(2A_1 A_2 \bar{A}_2 + \bar{A}_1 A_2^2\right) \\ &- 3(1 + \delta_0)\alpha_4 A_1^2 \bar{A}_1 + 2\alpha_5 \omega_{1m}^2 \bar{A}_1 A_1^2 + 2\alpha_6 \omega_{2n}^2 \bar{A}_1 A_2^2 \\ &- 2\alpha_7 g \omega_{2n}^2 \bar{A}_1 e^{2i\omega_{2n}\sigma T_2} \end{aligned} \tag{3.18}$$

$$\begin{aligned} i\omega_{2n}\left(2A_2' + 2\mu_2 A_2\right) = &\left(\delta_0 \beta_1 - \frac{\delta_0^2}{\beta_\gamma}\beta_2 - \beta_3\right)\left(2A_2 A_1 \bar{A}_1 + \bar{A}_2 A_1^2\right) \\ &- 3\beta_4 A_2^2 \bar{A}_2 + 2\beta_5 \omega_{2n}^2 \bar{A}_2 A_2^2 + 2\beta_6 \omega_{1m}^2 \bar{A}_2 A_1^2 \\ &- 2\beta_7 g \omega_{2n}^2 \bar{A}_2 e^{2i\omega_{2n}\sigma T_2} \end{aligned} \tag{3.19}$$

and μ_1 and μ_2 are defined by

$$\epsilon^2\mu_1 = \frac{1}{2}\int_0^1 c_v\Phi_m^2 ds \qquad \text{and} \qquad \epsilon^2\mu_2 = \frac{1}{2}\int_0^1 c_w\Phi_n^2 ds \tag{3.20}$$

The α_i are given by

$$\alpha_1 = \int_0^1 \Phi_m\left[\Phi_n''\int_1^s \Phi_m''\Phi_n'' ds - \Phi_n'''\int_0^s \Phi_m''\Phi_n' ds\right]' ds \tag{3.21}$$

$$\alpha_2 = \int_0^1 \Phi_m\left[\Phi_n''\int_0^s\int_1^s \Phi_m''\Phi_n'' ds ds\right]'' ds \tag{3.22}$$

$$\alpha_3 = \int_0^1 \Phi_m\left[\Phi_m'\left(\Phi_n'\Phi_n''\right)'\right]' ds \tag{3.23}$$

$$\alpha_4 = \int_0^1 \Phi_m\left[\Phi_m'\left(\Phi_m'\Phi_m''\right)'\right]' ds \tag{3.24}$$

$$\alpha_5 = \int_0^1 \Phi_m\left[\Phi_m'\int_1^s\int_0^s \Phi_m'^2 ds ds\right]' ds \tag{3.25}$$

$$\alpha_6 = \int_0^1 \Phi_m\left[\Phi_m'\int_1^s\int_0^s \Phi_n'^2 ds ds\right]' ds \tag{3.26}$$

$$\alpha_7 = \int_0^1 \Big[(s-1)\Phi_m\Phi_m'' + \Phi_m\Phi_m'\Big] ds \tag{3.27}$$

The β_i can be obtained from the α_i by interchanging the subscripts m and n.

By analytically manipulating the integrals in Eqs. (3.21)-(3.27), Feng and Leal (1994) proved that

$$\alpha_1 + \alpha_3 = -\beta_1, \;\; \alpha_2 = \beta_2, \;\; \alpha_3 = \beta_3, \;\; \text{and} \;\; \alpha_6 = \beta_6 \tag{3.28}$$

for a beam with rectangular cross-section. For near-square beams, $\Phi_m = \Phi_n$ and hence

$$\mu_1 = \mu_2, \;\; \alpha_3 = \alpha_4, \;\; \alpha_5 = \alpha_6, \;\; \text{and} \;\; \alpha_i = \beta_i \;\; \text{for} \;\; i = 1, 2, \cdots, 6 \tag{3.29}$$

Next, we show that beams exhibit these symmetry conditions by deriving the modulation equations using the method of time-averaged Lagrangian.

To apply the method of time-averaged Lagrangian, we substitute Eqs. (3.16) and (3.17) into the Lagrangian and virtual-work term, perform the spatial integrations, keep the slowly varying terms

only, and obtain

$$\begin{aligned}\frac{<\mathcal{L}>}{\epsilon^4} &= -\delta_2 z_m^4 A_1\bar{A}_1 - i\omega_{1m}\left(A_1'\bar{A}_1 - A_1\bar{A}_1'\right) - i\omega_{2n}\left(A_2'\bar{A}_2 - A_2\bar{A}_2'\right)\\ &+ \left[\omega_{1m}^2\Gamma_5 - \frac{3}{2}\left(1+\delta_0\right)\Gamma_4\right]A_1^2\bar{A}_1^2 + \left(\omega_{2n}^2\Lambda_5 - \frac{3}{2}\Lambda_4\right)A_2^2\bar{A}_2^2\\ &+ \omega_{1m}\omega_{2n}\Gamma_6\left(A_1^2\bar{A}_2^2 + \bar{A}_1^2A_2^2\right) - \left[\frac{1}{2}\left(1+\delta_0\right)\Gamma_3 + \frac{1}{2}\delta_0\Gamma_1 + \frac{\delta_0^2}{2\beta_\gamma}\Gamma_2\right]\\ &\times\left(A_1^2\bar{A}_2^2 + 4A_1\bar{A}_1A_2\bar{A}_2 + \bar{A}_1^2A_2^2\right) + \cdots \qquad (3.30)\\ \frac{\delta W}{\epsilon^4} &= Q_1^*\delta A_1 + Q_2^*\delta A_2 + \bar{Q}_1^*\delta\bar{A}_1 + \bar{Q}_2^*\delta\bar{A}_2\\ &= -\left[2g\omega_{1m}^2\Gamma_7A_1e^{-2i\omega_{1m}\sigma T_2} - 2i\omega_{1m}\mu_1\bar{A}_1\right]\delta A_1 - \left[2g\omega_{1m}^2\Gamma_7\bar{A}_1e^{2i\omega_{1m}\sigma T_2}\right.\\ &\left.+ 2i\omega_{1m}\mu_1A_1\right]\delta\bar{A}_1 - \left[2g\omega_{2n}^2\Lambda_7A_2e^{-2i\omega_{2n}\sigma T_2} - 2i\omega_{2n}\mu_2\bar{A}_2\right]\delta A_2\\ &- \left[2g\omega_{2n}^2\Lambda_7\bar{A}_2e^{2i\omega_{2n}\sigma T_2} + 2i\omega_{2n}\mu_2A_2\right]\delta\bar{A}_2 + \cdots \qquad (3.31)\end{aligned}$$

where

$$\Gamma_1 = -2\int_0^1 \Phi_m''\Phi_n''\left(\int_0^s \Phi_m''\Phi_n' ds\right)ds \qquad (3.32)$$

$$\Gamma_2 = \int_0^1\left[\left(\int_0^s \Phi_m''\Phi_n'' ds\right)^2 + 2\Phi_m''\Phi_n''\int_0^s\int_1^s \Phi_m''\Phi_n'' ds ds\right]ds \qquad (3.33)$$

$$\Gamma_3 = 2\int_0^1 \Phi_m'\Phi_m''\Phi_n'\Phi_n'' ds \qquad (3.34)$$

$$\Gamma_4 = 2\int_0^1 \Phi_m'^2\Phi_m''^2 ds \qquad (3.35)$$

$$\Lambda_4 = 2\int_0^1 \Phi_n'^2\Phi_n''^2 ds \qquad (3.36)$$

$$\Gamma_5 = \int_0^1\left(\int_0^s \Phi_m'^2 ds\right)^2 ds \qquad (3.37)$$

$$\Lambda_5 = \int_0^1\left(\int_0^s \Phi_n'^2 ds\right)^2 ds \qquad (3.38)$$

$$\Gamma_6 = \int_0^1\left(\int_0^s \Phi_m'^2 ds\right)\left(\int_0^s \Phi_n'^2 ds\right)ds \qquad (3.39)$$

$$\Gamma_7 = \int_0^1\left[\Phi_m\Phi_m''(s-1) + \Phi_m\Phi_m'\right]ds \qquad (3.40)$$

$$\Lambda_7 = \int_0^1 \left[\Phi_n \Phi_n''(s-1) + \Phi_n \Phi_n'\right] ds \tag{3.41}$$

Table 3.1: Values of the Γ_i and Λ_i for different mode combinations.

Term	Modes (1,1)	Modes (1,2)	Modes (1,3)
Γ_1	-20.220	334.259	996.978
Γ_2	-16.608	-263.080	-585.081
Γ_3	40.440	172.740	321.098
Γ_4	40.440	40.440	40.440
Λ_4	40.440	13418.226	264372.686
Γ_5	4.597	4.597	4.597
Λ_5	4.597	144.728	999.865
Γ_6	4.597	25.174	66.898
Γ_7	1.571	1.571	1.571
Λ_7	1.571	8.647	24.953
Term	Modes (2,1)	Modes (2,2)	Modes (2,3)
Γ_1	-507.000	-6709.113	86993.521
Γ_2	-263.080	-63028.330	-98696.589
Γ_3	172.740	13418.226	6829.742
Γ_4	13418.226	13418.226	13418.226
Λ_4	40.440	13418.226	264372.686
Γ_5	144.728	144.728	144.728
Λ_5	4.597	144.728	999.865
Γ_6	25.174	144.728	369.714
Γ_7	8.647	8.647	8.647
Λ_7	1.571	8.647	24.953
Term	Modes (3,1)	Modes (3,2)	Modes (3,3)
Γ_1	-1318.077	-93823.263	-132186.326
Γ_2	-585.081	-98696.589	-4503896.355
Γ_3	321.098	6829.742	264372.686
Γ_4	264372.686	264372.686	264372.686
Λ_4	40.440	13418.226	264372.686
Γ_5	999.865	999.865	999.865
Λ_5	4.597	144.728	999.865
Γ_6	66.898	369.714	999.865
Γ_7	24.953	24.953	24.953
Λ_7	1.571	8.647	24.953

The numerical values of the coefficients Γ_i and Λ_i are given in Table 3.1 for combinations of the

first three modes. Using Hamilton's extended principle

$$\frac{d}{dT_2}\left(\frac{\partial < \mathcal{L} >}{\partial \bar{A}_1'}\right) - \frac{\partial < \mathcal{L} >}{\partial \bar{A}_1} = \bar{Q}_1^* \tag{3.42}$$

$$\frac{d}{dT_2}\left(\frac{\partial < \mathcal{L} >}{\partial \bar{A}_2'}\right) - \frac{\partial < \mathcal{L} >}{\partial \bar{A}_2} = \bar{Q}_2^* \tag{3.43}$$

and Eqs. (3.30) and (3.31), we obtain the modulation equations

$$\begin{aligned} 2i\omega_{1m}\frac{dA_1}{dT_2} &= \left[2\omega_{1m}^2\Gamma_5 - 3\left(1+\delta_0\right)\Gamma_4\right]A_1^2\bar{A}_1 + 2\omega_{1m}\omega_{2n}\Gamma_6\bar{A}_1A_2^2 - \left(2i\omega_{1m}\mu_1 + \delta_2 z_m^4\right)A_1 \\ &\quad - \left[\left(1+\delta_0\right)\Gamma_3 + \frac{\delta_0^2}{\beta_\gamma}\Gamma_2 + \delta_0\Gamma_1\right]\left(\bar{A}_1A_2^2 + 2A_1A_2\bar{A}_2\right) - 2g\omega_{1m}^2\Gamma_7\bar{A}_1e^{2i\omega_{1m}\sigma T_2} \end{aligned} \tag{3.44}$$

$$\begin{aligned} 2i\omega_{2n}\frac{dA_2}{dT_2} &= \left(2\omega_{2n}^2\Lambda_5 - 3\Lambda_4\right)A_2^2\bar{A}_2 + 2\omega_{1m}\omega_{2n}\Gamma_6A_1^2\bar{A}_2 - 2i\omega_{2n}\mu_2A_2 \\ &\quad - \left[\left(1+\delta_0\right)\Gamma_3 + \frac{\delta_0^2}{\beta_\gamma}\Gamma_2 + \delta_0\Gamma_1\right]\left(A_1^2\bar{A}_2 + 2A_1\bar{A}_1A_2\right) - 2g\omega_{2n}^2\Lambda_7\bar{A}_2e^{2i\omega_{2n}\sigma T_2} \end{aligned} \tag{3.45}$$

Comparing Equations (3.44) and (3.45) obtained with the time-averaged Lagrangian with Equations (3.18) and (3.19) obtained by directly attacking the integro-partial-differential equations, we conclude that

$$\begin{array}{llll} \Gamma_1 = \alpha_1 & \Gamma_2 = \alpha_2 = \beta_2 & \Gamma_3 = \alpha_3 = \beta_3 & \Gamma_1 + \Gamma_3 = -\beta_1 \\ \Gamma_4 = \alpha_4 & \Lambda_4 = \beta_4 & \Gamma_5 = \alpha_5 & \Lambda_5 = \beta_5 \\ \Gamma_6 = \alpha_6 = \beta_6 & \Gamma_7 = \alpha_7 & \Lambda_7 = \beta_7 & \end{array} \tag{3.46}$$

For a near-square cross-section, $\Phi_m(s) = \Phi_n(s)$ and hence

$$\begin{aligned} \Gamma_4 = \Lambda_4 = \alpha_4 = \beta_4 \\ \Gamma_5 = \Lambda_5 = \alpha_5 = \beta_5 \\ \Gamma_7 = \Lambda_7 = \alpha_7 = \beta_7 \\ \Gamma_5 = \Gamma_6 = \alpha_5 = \alpha_6 \\ \Gamma_3 = \Gamma_4 = \alpha_3 = \alpha_4 \end{aligned} \tag{3.47}$$

These symmetry conditions are the same as those obtained by Feng and Leal (1994).

To analyze solutions of the modulation equations, we express A_1 and A_2 in the polar form

$$A_1(T_2) = \frac{1}{2}a_1(T_2)e^{i\theta_1(T_2)} \qquad \text{and} \qquad A_2(T_2) = \frac{1}{2}a_2(T_2)e^{i\theta_2(T_2)} \tag{3.48}$$

separate Eqs. (3.44) and (3.45) into real and imaginary parts, and obtain

$$2\omega_{1m}a_1' = -\Big[R_1 + R_2 a_2^2 \sin[2(\gamma_1 - \gamma_2)] + R_3 \sin(2\gamma_1)\Big]a_1 \tag{3.49}$$

$$2\omega_{1m}a_1\gamma_1' = \Big[R_4 + R_5 a_1^2 - R_6 a_2^2 - R_2 a_2^2 \cos[2(\gamma_1 - \gamma_2)] - R_3 \cos(2\gamma_1)\Big]a_1 \tag{3.50}$$

$$2\omega_{2n}a_2' = -\Big[E_1 - R_2 a_1^2 \sin[2(\gamma_1 - \gamma_2)] + E_3 \sin(2\gamma_2)\Big]a_2 \tag{3.51}$$

$$2\omega_{2n}a_2\gamma_2' = \Big[E_4 + E_5 a_2^2 - R_6 a_1^2 - R_2 a_1^2 \cos[2(\gamma_1 - \gamma_2)] - E_3 \cos(2\gamma_2)\Big]a_2 \tag{3.52}$$

where

$$\gamma_1 = \omega_{1m}\sigma T_2 - \theta_1 \tag{3.53}$$

$$\gamma_2 = \omega_{2n}\sigma T_2 - \theta_2 \tag{3.54}$$

and the R_i and E_i are defined in Appendix A. Alternatively, one can express A_1 and A_2 in the Cartesian form

$$A_1 = \frac{1}{2}(p_1 - iq_1)e^{i\omega_{1m}\sigma T_2} \qquad \text{and} \qquad A_2 = \frac{1}{2}(p_2 - iq_2)e^{i\omega_{2n}\sigma T_2} \tag{3.55}$$

separate real and imaginary parts in Eqs. (3.44) and (3.45), and obtain

$$\begin{aligned} p_1' = -\frac{1}{2\omega_{1m}}\Big\{ & R_4 q_1 + R_5\left(p_1^2 + q_1^2\right)q_1 - R_6\left(p_2^2 + q_2^2\right)q_1 \\ & + R_1 p_1 + R_2\Big[\left(p_2^2 - q_2^2\right)q_1 - 2p_1 p_2 q_2\Big] + R_3 q_1\Big\} \end{aligned} \tag{3.56}$$

$$\begin{aligned} q_1' = -\frac{1}{2\omega_{1m}}\Big\{ & - R_4 p_1 - R_5\left(p_1^2 + q_1^2\right)p_1 + R_6\left(p_2^2 + q_2^2\right)p_1 \\ & + R_1 q_1 + R_2\Big[\left(p_2^2 - q_2^2\right)p_1 + 2q_1 p_2 q_2\Big] + R_3 p_1\Big\} \end{aligned} \tag{3.57}$$

$$p_2' = -\frac{1}{2\omega_{2n}}\Big\{ E_4 q_2 + E_5\left(p_2^2+q_2^2\right)q_2 - R_6\left(p_1^2+q_1^2\right)q_2 + E_1 p_2 + R_2\Big[\left(p_1^2-q_1^2\right)q_2 - 2p_1q_1p_2\Big] + E_3 q_2\Big\} \tag{3.58}$$

$$q_2' = -\frac{1}{2\omega_{2n}}\Big\{ -E_4 p_2 - E_5\left(p_2^2+q_2^2\right)p_2 + R_6\left(p_1^2+q_1^2\right)p_2 + E_1 q_2 + R_2\Big[\left(p_1^2-q_1^2\right)p_2 + 2p_1q_1q_2\Big] + E_3 p_2\Big\} \tag{3.59}$$

We note that the system (3.56)-(3.59) is invariant under the transformations $(p_1, q_1, p_2, q_2) \Longleftrightarrow (-p_1, -q_1, p_2, q_2) \Longleftrightarrow (p_1, q_1, -p_2, -q_2) \Longleftrightarrow (-p_1, -q_1, -p_2, -q_2)$. Therefore, for any asymmetric solution found, three other solutions can be obtained using the above transformations (Nayfeh and Balachandran, 1995).

In the next section, we describe bifurcations of solutions of the modulation equations in the case of beams with near-square cross-sections in detail. For such beams, $\delta_0 = 0$, $E_1 = R_1$, $E_3 = R_3$, and $E_5 = R_5$.

3.3 Bifurcation Analysis

3.3.1 Equilibrium Solutions

First, we determine the equilibrium solutions and their stability. To this end, we set the time derivatives in Eqs. (3.56)-(3.59) equal to zero and solve the resulting system of algebraic equations for p_1, q_1, p_2, and q_2 for a specified value of the parameter σ, which is a measure of the detuning of the principal parametric resonance. Then, the amplitudes a_1 and a_2 are calculated from $a_i = \sqrt{p_i^2+q_i^2}$. The stability of a fixed point is determined by investigating the eigenvalues of the Jacobian matrix of the right-hand sides of Eqs. (3.56)-(3.59). A pseudo-arclength scheme is used to trace branches of the equilibrium solutions (Nayfeh and Balachandran, 1995; Seydel, 1994).

When $\delta_2 = -0.05$, we show in Figure 3.2 typical frequency-response curves for modes (1,1) and (2,2). For modes (1,1), the planar response curves are bent to the right and hence the effective nonlinearity is of the hardening type. Therefore, the nonlinear geometric terms are dominant for these modes. In part (b), the planar response curves are bent to the left and hence the effective

nonlinearity is of the softening type for modes (2,2). Therefore, the nonlinear inertia terms are dominant for these modes. These results agree with those of Nayfeh and Pai (1989). In part (a), the nonplanar response undergoes a Hopf bifurcation at $\sigma = 0.0566242$, resulting in the creation of limit cycles for the amplitudes and phases. The corresponding fixed point at the Hopf point is $(p_1, q_1, p_2, q_2) = (0.241107, 0.0240642, -0.0929129, 0.131068)$. On the other hand, the nonplanar response of modes (2,2) do not undergo Hopf bifurcations for the parameters used.

Changing the detuning parameter δ_2 from -0.05 to -0.5, we obtained the frequency-response curves shown in Figure 3.3 for modes (1,1). For the most part, the general characteristics of these curves are qualitatively similar to those in Figure 3.2(a).

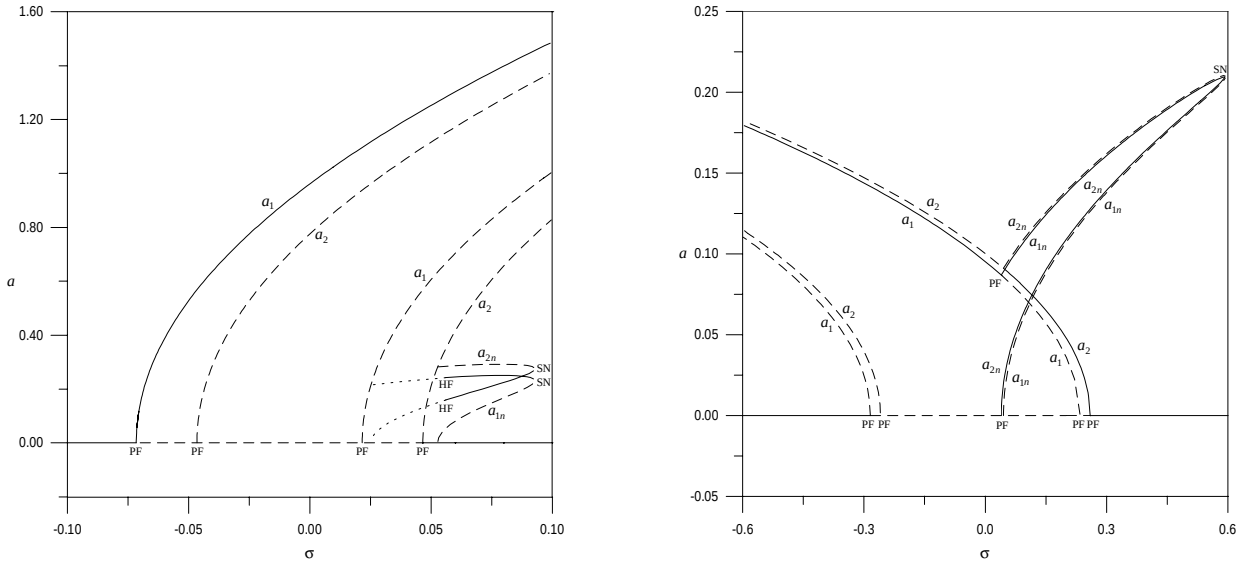

(a) (b)

Figure 3.2: Frequency-response curves when $\delta_2 = -0.05$, $\mu_1 = \mu_2 = 0.025$, $g = 0.03$, and $\beta_\gamma = 0.6489$: (a) modes (1,1) and (b) modes (2,2). The planar response amplitudes are denoted by a_1 and a_2 and the nonplanar response amplitudes are denoted by a_{1n} and a_{2n}. (——) Stable solution, (– – –) saddles, and ($\cdots$) unstable foci, PF = pitchfork bifurcation, SN = saddle-node bifurcation, and HF = Hopf bifurcation.

The normal form of any autonomous system near a generic Hopf bifurcation point is (Nayfeh and

Balachandran, 1995)

$$\dot{r} = \epsilon_1(\sigma - \sigma_c)r + \alpha_r r^3 \tag{3.60}$$

$$\dot{\theta} = \epsilon_2(\sigma - \sigma_c) + \alpha_i r^2 \tag{3.61}$$

where r is a measure of the amplitude of the created limit cycle. The bifurcation is generic if $\epsilon_1 \neq 0$ and subcritical if $\alpha_r > 0$ and supercritical if $\alpha_r < 0$. The created limit cycle is stable if the bifurcation is supercritical and unstable if the bifurcation is subcritical. The amplitudes of the created limit cycle are given by $r = \sqrt{-\epsilon_1(\sigma - \sigma_c)/\alpha_r}$.

A *Mathematica* code was used to calculate the coefficients in the normal form of the Hopf bifurcations. For the Hopf bifurcation at $\sigma = 0.0694703$, the corresponding fixed point is $(p_1, q_1, p_2, q_2) = (0.254868, 0.0200404, -0.0560086, 0.411458)$. For this point, $\epsilon_1 = -39.1347$ and $\alpha_r = 1.41995$, indicating that the bifurcation is generic and subcritical. Hence, the created limit cycles are unstable. The two-mode solutions occur over a longer range of values for σ because increasing the magnitude of the detuning δ_2 creates stronger coupling between the in-plane and out-of-plane modes. An important difference in this case is the occurrence of a second Hopf bifurcation point at $\sigma = -0.0383338$ and $(p_1, q_1, p_2, q_2) = (0.005642228, 0.0001068165, -0.02463237, 0.324553)$. The corresponding values for ϵ_1 and α_r are 1049.01 and -2844.36, respectively, indicating a generic supercritical Hopf bifurcation with the unstable foci to its right. In Figure 3.4, we show a clearer view of this Hopf bifurcation point, which is very close to the pitchfork bifurcation that occurs at $\sigma = -0.0383862$.

The characteristic equation of the matrix $[J - \lambda I]$ is given by

$$\lambda^4 + r_1\lambda^3 + r_2\lambda^2 + r_3\lambda + r_4 = 0 \tag{3.62}$$

where $[J]$ is the Jacobian matrix evaluated at a fixed point $FP(\sigma, \delta_2) = (p_1, q_1, p_2, q_2)$ and the $r_i = r_i(\sigma, \delta_2; FP)$. Applying the Routh-Hurwitz criterion yields the following conditions for stability:

$$r_1 > 0,\ r_1 r_2 - r_3 > 0,\ r_3\,(r_1 r_2 - r_3) - r_1^2 r_4 > 0,\ \text{and } r_4 > 0 \tag{3.63}$$

A static bifurcation occurs when a real eigenvalue crosses transversely the imaginary axis. The locus of such a bifurcation is given by $r_4 = 0$. On the other hand, a Hopf bifurcation occurs when a pair of complex conjugate eigenvalues cross transversely the imaginary axis. In this case, the locus of the Hopf bifurcation is determined from $r_3\,(r_1 r_2 - r_3) - r_1^2 r_4 = 0$. A codimension-2 bifurcation occurs when two real eigenvalues or one real and two complex conjugate eigenvalues cross transversely the imaginary axis at the same time. In this case two parameters are needed to analyze the system.

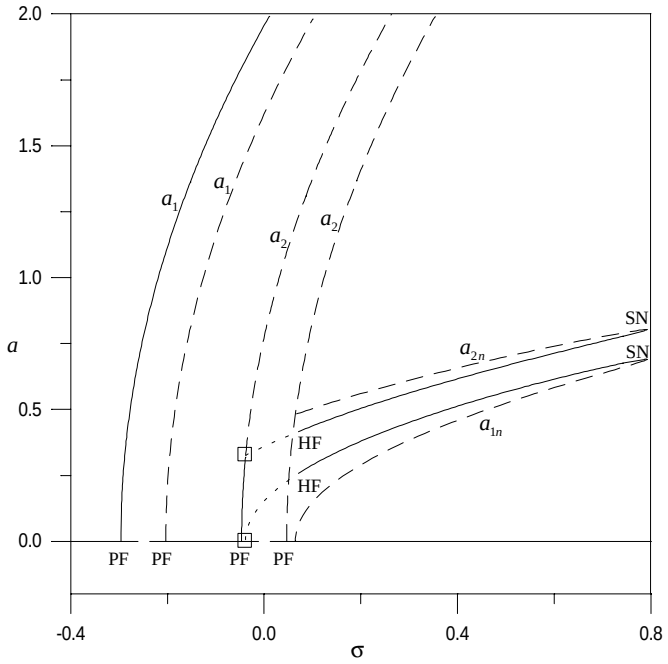

Figure 3.3: Frequency-response curves for modes (1,1) when $\delta_2 = -0.5$, $\mu_1 = \mu_2 = 0.025$, $g = 0.03$, and $\beta_\gamma = 0.6489$. The planar response amplitudes are denoted by a_1 and a_2 and the nonplanar response amplitudes are denoted by a_{1n} and a_{2n}. (——) Stable solution, (– – –) saddles, and $(\cdots)$ unstable foci, PF = pitchfork bifurcation, SN = saddle-node bifurcation, and HF = Hopf bifurcation.

The loci of the bifurcations, in terms of the frequency detuning parameter σ and the bending stiffness ratio (or cross-section ratio) detuning parameter δ_2, are presented in Figure 3.5 for modes (1,1). The lines denoted by PF1 and PF2 are the loci of pitchfork bifurcations of the trivial solution, resulting in single-mode solutions for a_1. The lines denoted by PF3 and PF4 are the loci of pitchfork bifurcations of the trivial solution, resulting in single-mode solutions for a_2. The lines denoted by

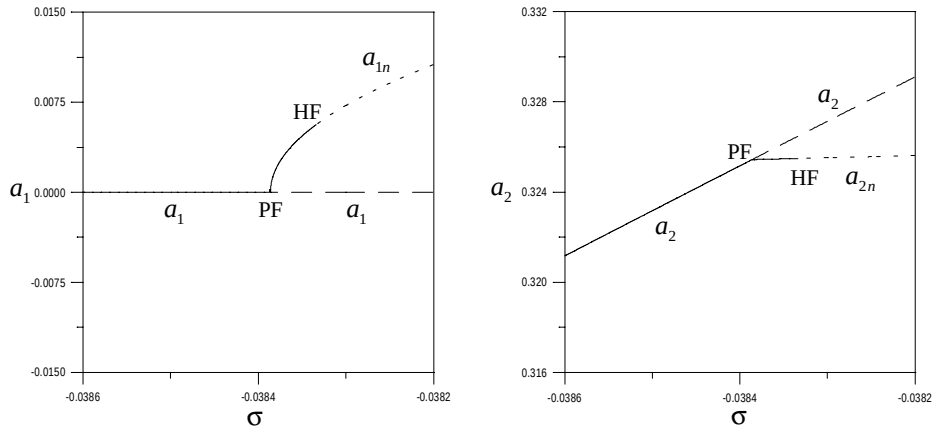

Figure 3.4: Enlargements of the blocked areas shown in Figure 3.3. The planar response amplitudes are denoted by a_1 and a_2 and the nonplanar response amplitudes are denoted by a_{1n} and a_{2n}. (——) Stable solution, (– – –) saddles, and $(\cdots)$ unstable foci, PF = pitchfork bifurcation, and HF = Hopf bifurcation.

PF5 and PF6 are the loci of pitchfork bifurcations of the single-mode solutions, resulting in two-mode solutions. The lines denoted by HF1 and HF2 are the loci of supercritical and subcritical Hopf bifurcations, respectively. Lastly, the line denoted by SN is the locus of saddle-node bifurcations.

We note that the loci of the pitchfork bifurcations PF3 and PF4 are unaffected by δ_2 whereas those of PF1 and PF2 do vary with δ_2. Therefore, as δ_2 is increased beyond point A, where A is given by $(\sigma, \delta_2, p_1, q_1, p_2, q_2) = (-0.0465906, -0.186362218, 0, 0, 0, 0)$, the order of the single-mode branches changes. This is evident from comparing Figures 3.2(a) and 3.3. As δ_2 approaches point A, the supercritical Hopf bifurcation HF1 and the pitchfork bifurcations PF2, PF3, and PF5 merge with each other, resulting in a codimension-2 bifurcation, as shown in Figure 3.6(a). Increasing δ_2 beyond point A, only the pitchfork bifurcations survive so that the codimension-2 bifurcation results in the creation (or destruction) of the supercritical Hopf bifurcation. A second codimension-2 bifurcation occurs at point B where the loci of the subcritical Hopf bifurcation HF2 and the saddle-node bifurcation SN merge together, as shown in Figure 3.6(b). This codimension-2 bifurcation is given by $(\sigma, \delta_2, p_1, q_1, p_2, q_2) = (0.0527954, -0.0103, -0.135242, -0.0237346, 0.217697, -0.0382052)$. As we increase δ_2 past point B, only the saddle-node bifurcation survives and then vanishes at point C. However, point C is not a codimension-2 bifurcation as the corresponding fixed points for the saddle-node SN and pitchfork PF6 are different from each other. Further increasing δ_2, we

have only the pitchfork bifurcations PF1-PF6.

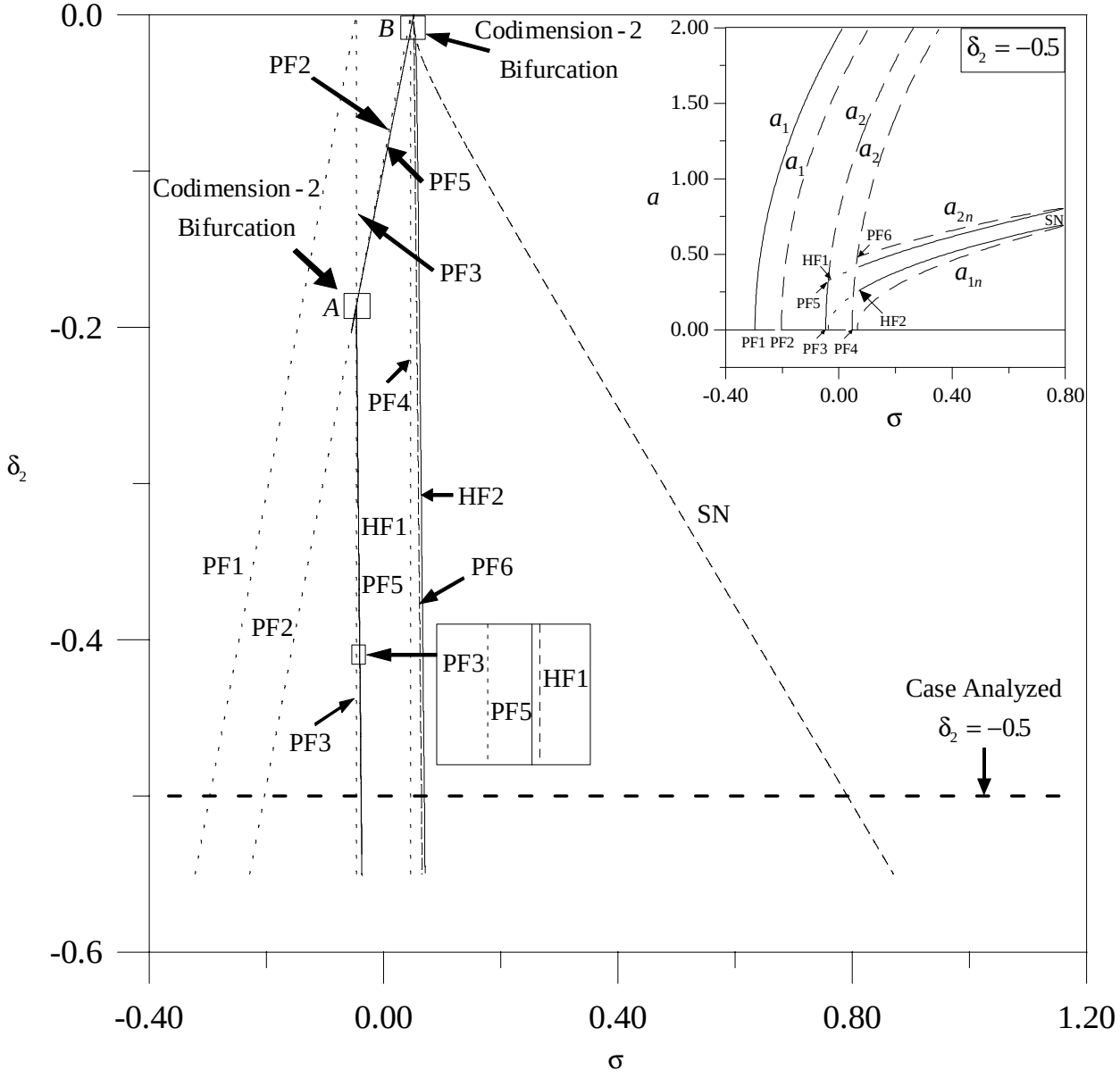

Figure 3.5: Bifurcation diagram showing the loci of the static and dynamic bifurcation points, which the equilibrium solutions (trivial and nontrivial) undergo, in terms of the frequency detuning parameter σ and the bending stiffness ratio detuning parameter δ_2 for modes (1,1) when $\mu_1 = \mu_2 = 0.025$, $g = 0.03$, and $\beta_\gamma = 0.6489$. SN = saddle-node bifurcation, PFi = pitchfork bifurcation, HF1 = supercritical Hopf bifurcation, and HF2 = subcritical Hopf bifurcation.

3.3.2 Dynamic Solutions

The dynamic behavior of the modulation equations was studied for modes (1,1) for the case $\delta_2 = -0.5$, corresponding to Figures 3.3 and 3.4. A long-time integration, a combination of a two-point boundary-value program and Newton's scheme, and Floquet theory (Nayfeh and Balachandran, 1995) were used to generate five branches of dynamic solutions and assess their stability. The two Hopf bifurcation points, one supercritical and the other subcritical, produce two branches of dynamic solutions. Branch I corresponds to dynamic solutions that emerge from the supercritical Hopf bifurcation, whereas branch IV corresponds to dynamic solutions that emerge from the subcritical Hopf bifurcation. Branches II and V are isolated branches found near branch I, whereas branch III spans the region between the two Hopf points. In Figure 3.7, we show a schematic of the regions where dynamic solutions occur; in Figure 3.8(a), we give a clearer view of branches I, II, and V; and in Figure 3.8(b) we show a close-up of the period-doubling sequence on branch III.

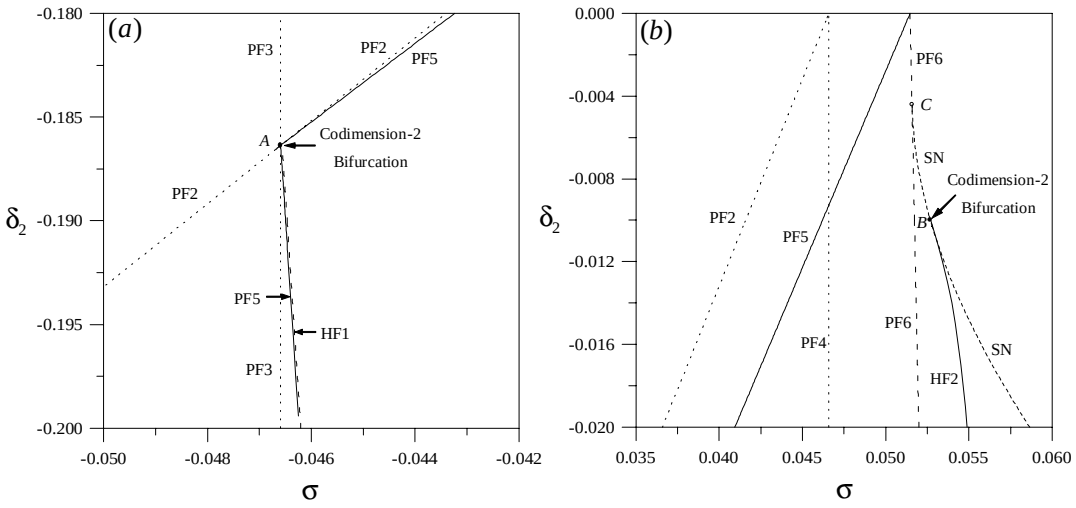

Figure 3.6: Enlargements of the blocked area in Figure 3.5 showing a clearer view of the codimension-2 bifurcations. In part (a) the supercritical Hopf and three pitchfork bifurcation points merge and in part (b) the subcritical Hopf and saddle-node bifurcation points merge. SN = saddle-node bifurcation, PFi = pitchfork bifurcation, HF1 = supercritical Hopf bifurcation, and HF2 = subcritical Hopf bifurcation.

In Figure 3.9, we show a schematic of the dynamic solutions on branch I. The asymmetric limit cycle that emerges from the supercritical Hopf bifurcation at $\sigma = -0.0383338$ grows and deforms

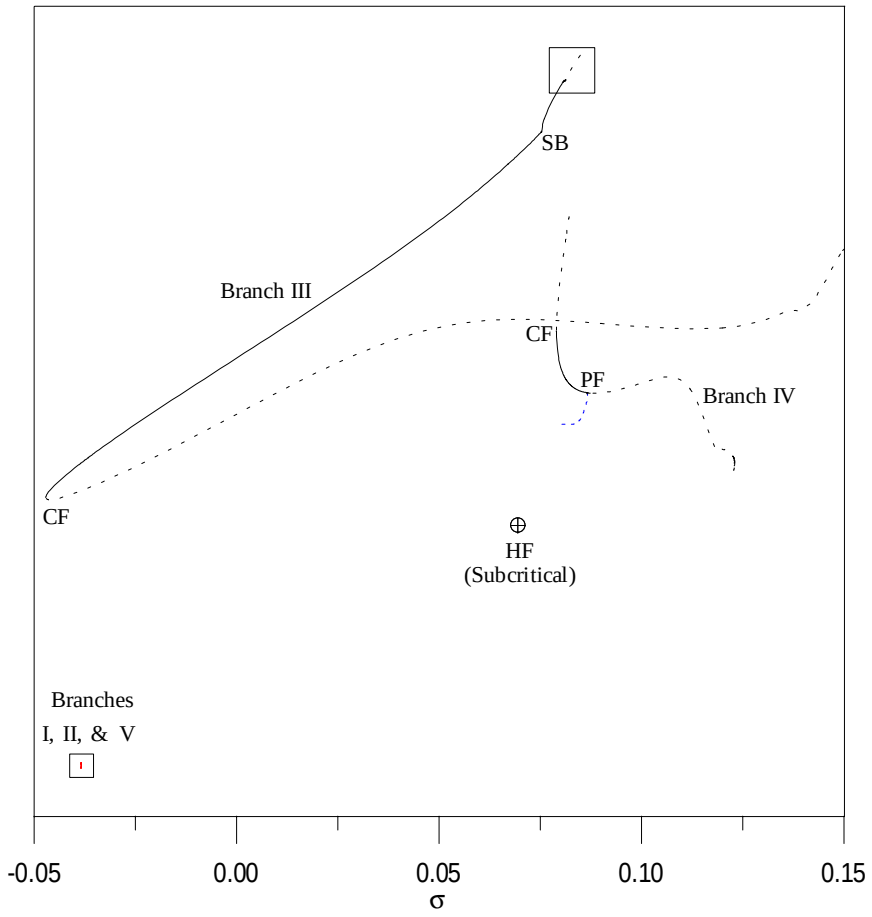

Figure 3.7: A schematic of the dynamic solutions found for modes (1,1) when $\delta_2 = -0.5$, $\mu_1 = \mu_2 = 0.025$, $g = 0.03$, and $\beta_\gamma = 0.6489$. (——) Stable limit cycle, $(\cdots)$ unstable limit cycle, CF = cyclic-fold bifurcation, SB = symmetry-breaking bifurcation, PF = pitchfork bifurcation, and HF = Hopf bifurcation.

as σ increases, as shown in Figures 3.10(a)-(c). Then it undergoes a sequence of period-doubling bifurcations, culminating in a chaotic attractor, as shown in Figures 3.10(d)-(i). The attractor and its three clowns continue to grow and deform as σ is increased further, as shown in Figure 3.11(a). When σ is increased to -0.03831015, the four clown chaotic attractors merge in pairs, forming two larger asymmetric chaotic attractors. The time histories in Figures 3.11(b)-(c) demonstrate the irregular switching of the motion on one of these attractors between its two ghost attractors. Increasing $\sigma = -0.03830689$, the two large asymmetric chaotic attractors undergo an explosive bifurcation (Nayfeh and Balachandran, 1996; Nayfeh and Chin, 1996), resulting in their merger

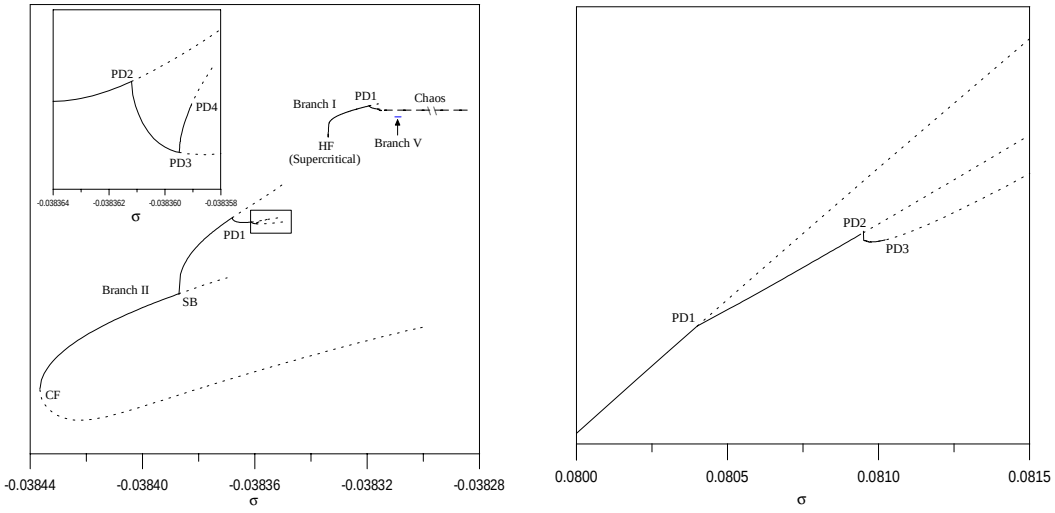

(a) (b)

Figure 3.8: Enlargements of the blocked areas in Figure 3.7. (a) Branches I, II, and V (b) branch III. (——) Stable limit cycle, $(\cdots)$ unstable limit cycle, CF = cyclic-fold bifurcation, SB = symmetry-breaking bifurcation, PDn = nth period-doubling bifurcation, and HF = Hopf bifurcation.

and the creation of a much larger single symmetric chaotic attractor. In Figure 3.12(a), we show one of the asymmetric chaotic attractors before the explosive bifurcation, and in Figure 3.12(b), we show the large symmetric chaotic attractor after the explosive bifurcation. As σ is further increased, the large symmetric chaotic attractor continues to grow and deform until it undergoes a boundary crisis, resulting in a large limit cycle on the isolated branch III, as shown in Figure 3.13.

On branch III, we followed the symmetric limit cycle, shown in Figure 3.14(a), that resulted from the chaotic attractor on branch I having experienced a boundary crisis. In Figure 3.14(a), we also show the corresponding FFT for this limit cycle. As σ is decreased, this limit cycle undergoes a cyclic-fold bifurcation at $\sigma = -0.047110$ and tends to the single-mode equilibrium solution. As σ is increased, the symmetric limit cycle grows and deforms, as seen in Figures 3.14(b)-(c). It then undergoes a symmetry-breaking bifurcation at $\sigma = 0.079000$ as is demonstrated by the FFT in Figure 3.14(d). The asymmetric limit cycle then undergoes a sequence of period-doubling bifurcations, culminating in a chaotic attractor, as shown in Figures 3.14(e)-(h). This chaotic attractor continues to grow until it undergoes a boundary crisis at $\sigma = 0.081070$, resulting in a jump to a smaller symmetric

limit cycle on branch IV, as shown in Figure 3.15.

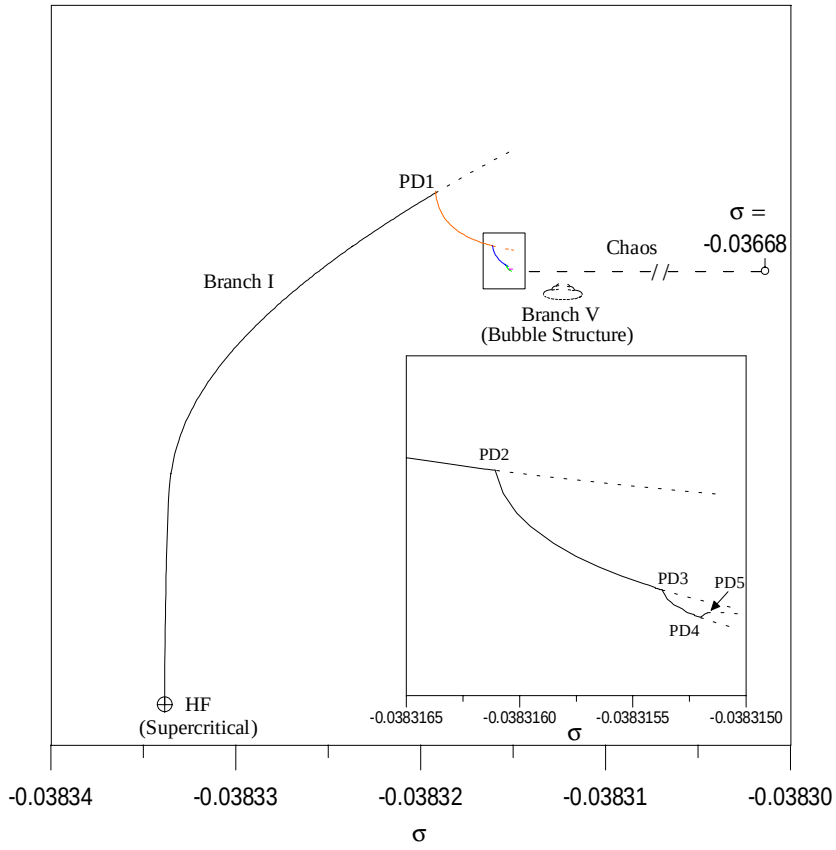

Figure 3.9: A schematic of the dynamic solutions found on branches I and V for modes (1,1) when $\delta_2 = -0.5$, $\mu_1 = \mu_2 = 0.025$, $g = 0.03$, and $\beta_\gamma = 0.6489$. (——) Stable limit cycle, $(\cdots)$ unstable limit cycle, PDn = nth period-doubling bifurcation, and HF = Hopf bifurcation.

A schematic of the dynamic solutions on branch IV is shown in Figure 3.16. We followed the symmetric limit cycle, shown in Figure 3.15(b), that resulted from the boundary crisis on branch III. As σ is decreased, the limit cycle goes through a cyclic-fold bifurcation at $\sigma = 0.0790294$, causing it to jump to the two-mode equilibrium solution. As σ is increased, it undergoes a subcritical pitchfork bifurcation, creating unstable limit cycles that eventually tend to the two-mode equilibrium solution. Tracing the unstable limit cycle as σ is increased by using a combination of a shooting technique and Floquet theory led us to another stable symmetric limit cycle. An example is shown in Figure 3.17(a) for $\sigma = 0.1229000$. As σ is increased further, the limit cycle undergoes a cyclic-fold bifurcation, causing it to jump to the two-mode equilibrium solution. The corresponding unstable

limit cycle is traced back towards the subcritical Hopf bifurcation point, as is shown in Figure 3.16. On the other hand, if σ is decreased, the limit cycle undergoes a symmetry-breaking bifurcation at $\sigma = 0.1227400$, as shown in Figure 3.17(b). As σ is decreased further, the asymmetric limit cycle undergoes repeated period-doubling bifurcations resulting in a chaotic attractor, as shown in Figures 3.17(c)-(e). Then, the chaotic attractor undergoes a boundary crisis and tends to the two-mode equilibrium solution.

A small isolated branch, labeled V in Figure 3.8(a), was found. In Figure 3.18(a), we show a limit cycle found on this branch at $\sigma = -0.038310125$. As σ is decreased, this limit cycle encounters a cyclic-fold bifurcation at $\sigma = -0.038310132$, and a chaotic attractor similar to the one shown in Figure 3.10(i) emerges. As σ is increased, the limit cycle undergoes a sequence of period-doubling bifurcations, culminating in a chaotic attractor, as shown in Figure 3.18(d). When $\sigma = -0.038310115$, the chaotic attractor undergoes an attractor-merging crisis and a larger attractor that is similar to that shown in Figure 3.11(b) emerges. As σ is increased further, this chaotic attractor deforms and then splits into two smaller attractors, as shown in Figure 3.19a. Consequently, it undergoes a sequence of reverse period-doubling bifurcations, resulting in a limit cycle, as shown in Figure 3.19. The dynamics on this branch is an example of a bubble structure (Nayfeh and Balachandran, 1995). The limit cycle then encounters a cyclic-fold bifurcation at $\sigma = -0.038307990$, causing the response to jump to the chaotic attractor on branch I.

In Figure 3.20, we show a phase-locked limit cycle (Nayfeh and Balachandran, 1995; Thompson and Stewart, 1988) found just to the left of Branch V at $\sigma = -0.0383106$. The one-sided Poincaré section in part (c) showing seven points is a clear indication of the long-period limit cycle.

On the isolated branch II, a symmetric limit cycle was found at $\sigma = -0.03842000$ through simulation of the modulation equations. As σ is decreased, the limit cycle encounters a cyclic-fold bifurcation at $\sigma = -0.03843652$, causing the response to jump to the single-mode equilibrium solution. As σ is increased, the symmetric limit cycle grows, as seen in Figures 3.21(a)-(c). It then goes through a symmetry-breaking bifurcation at $\sigma = -0.03838650$, as shown in Figures 3.21(d)-(e). The asymmetric limit cycle then undergoes successive period-doubling bifurcations until the motion becomes chaotic, as shown in Figures 3.21(f)-(i). This chaotic attractor continues to grow until it experiences an attractor-merging crisis at $\sigma = -0.03835000$, resulting in a symmetric attractor,

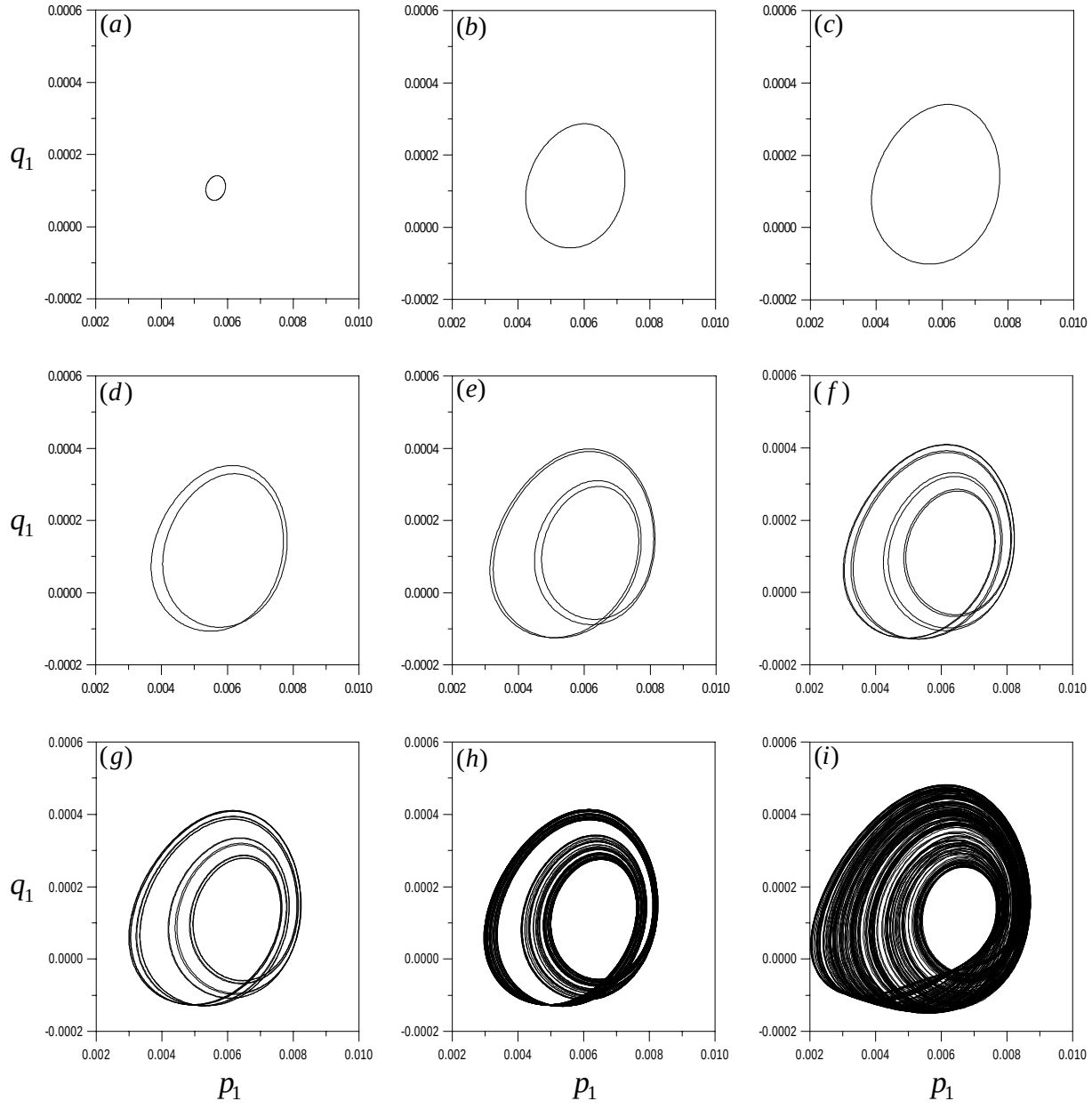

Figure 3.10: Two-dimensional projections of the phase portraits onto the p_1q_1-plane, showing bifurcations of the created limit cycle on branch I resulting from the supercritical Hopf bifurcation. As σ is increased, the limit cycle grows, deforms, and undergoes repeated period-doubling bifurcations that culminate in chaos, as shown in part (i). The corresponding values of σ are $\sigma_a = -0.03833350$, $\sigma_b = -0.03832500$, $\sigma_c = -0.03831920$, $\sigma_d = -0.03831900$, $\sigma_e = -0.03831600$, $\sigma_f = -0.03831530$, $\sigma_g = -0.03831519$, $\sigma_h = -0.03831500$, and $\sigma_i = -0.03831100$.

as shown in Figure 3.22(a). As σ is increased to -0.03834964, the symmetric chaotic attractor goes through an exterior crisis (Nayfeh and Balachandran, 1995; Nayfeh and Chin, 1996), causing it to jump to the two-mode equilibrium solution, as shown in Figure 3.22(b).

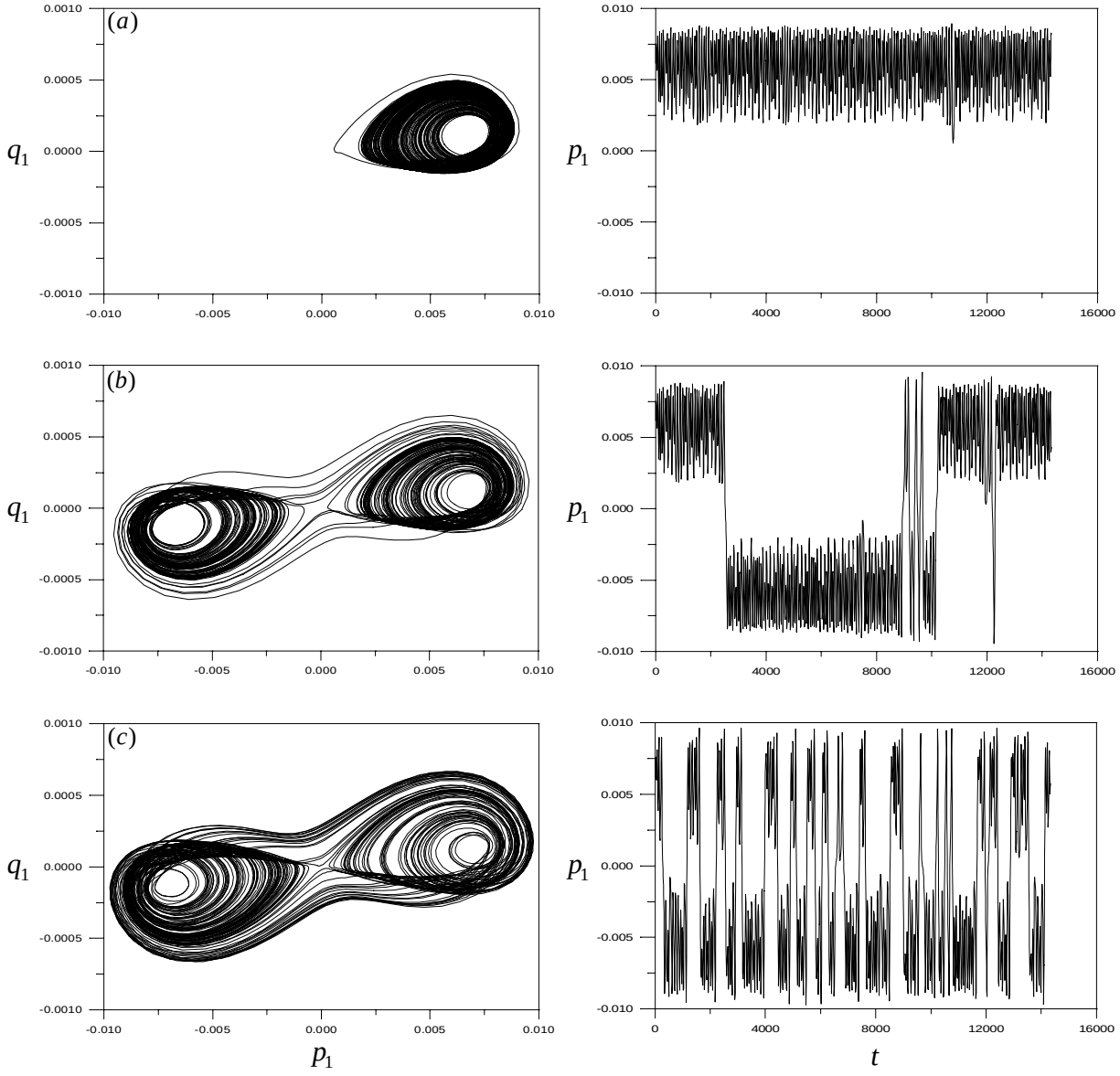

Figure 3.11: Two-dimensional projections of the phase portraits onto the p_1q_1-plane and long-time histories showing an attractor-merging crisis. The corresponding values of σ are $\sigma_a = -0.03831016$, $\sigma_b = -0.03831015$, and $\sigma_c = -0.03830690$.

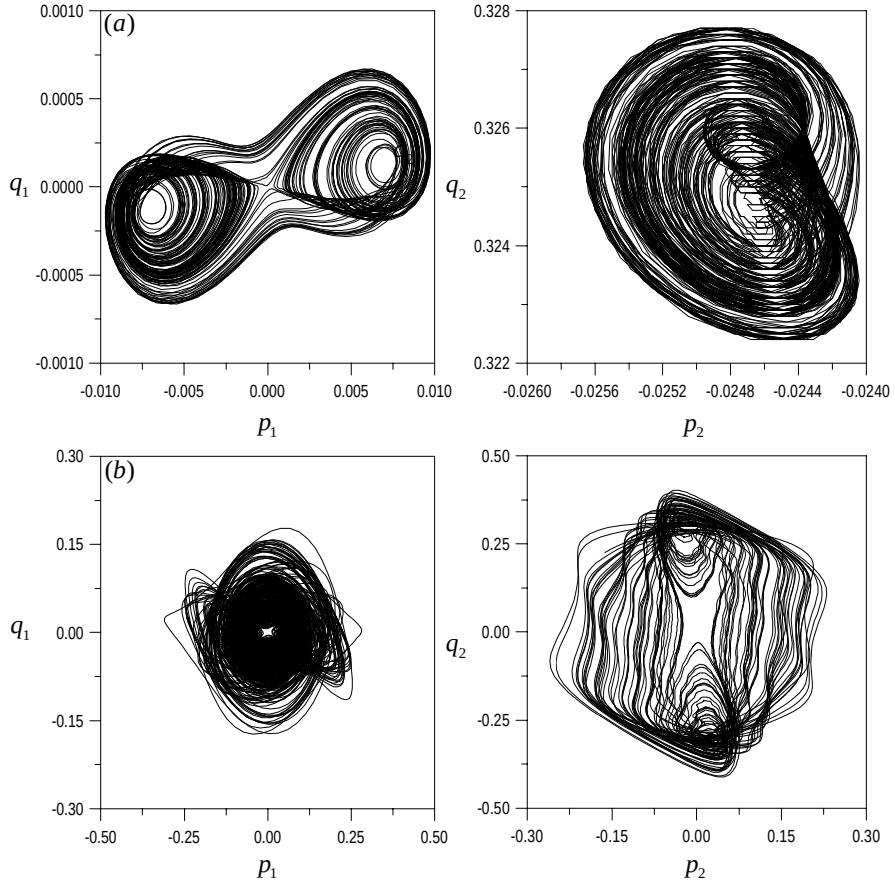

Figure 3.12: Two-dimensional projections of the phase portraits onto the p_1q_1- and p_2q_2-planes showing the chaotic attractor before and after the explosive bifurcation. The values of σ are $\sigma_a = -0.03830690$ and $\sigma_b = -0.03669000$.

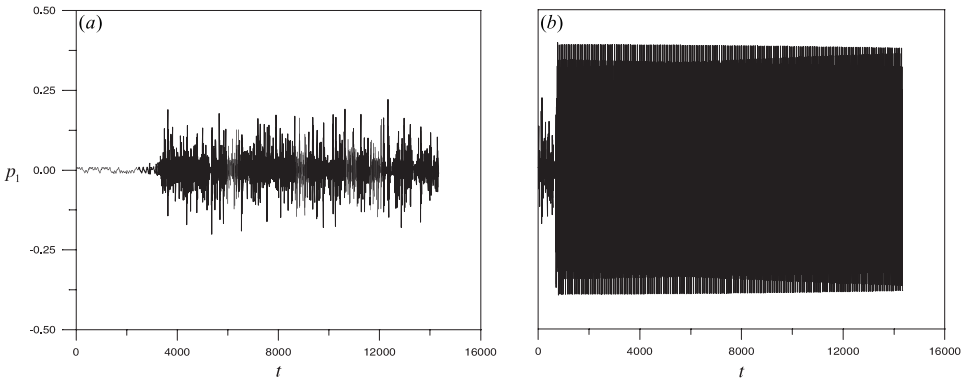

Figure 3.13: Long-time histories showing the chaotic attractor undergoing an explosive bifurcation followed by a boundary crisis. The values of σ are $\sigma_a = -0.03830689$ and $\sigma_b = -0.03668000$.

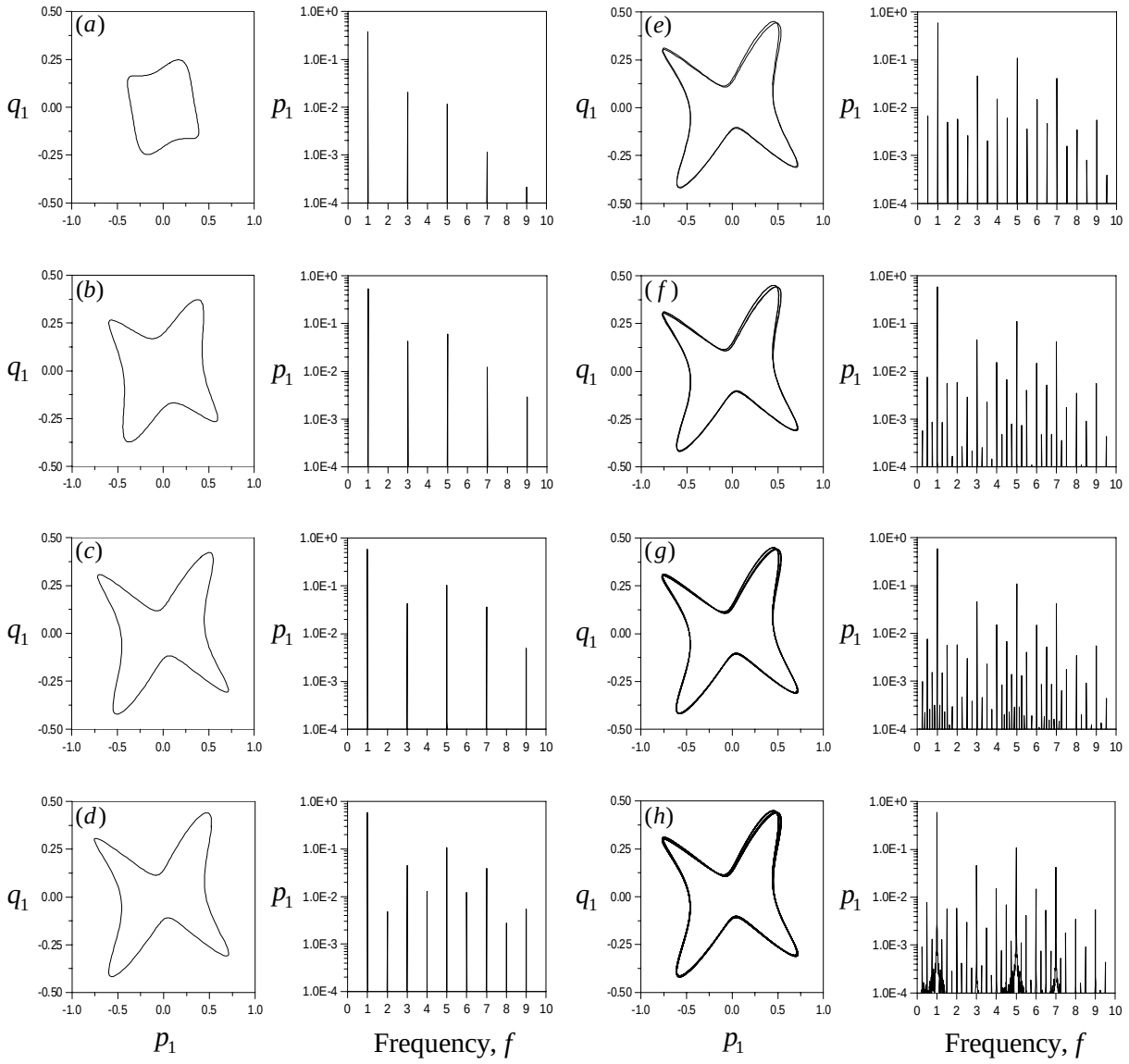

Figure 3.14: Two-dimensional projections of the phase portraits onto the p_1q_1-plane and FFT's of p_1 showing bifurcations of the limit cycle on the isolated branch III. As σ is increased, the limit cycle grows, deforms, and undergoes repeated period-doubling bifurcations that culminate in chaos, as shown in part (h). The corresponding values for σ are $\sigma_a = -0.036680$, $\sigma_b = 0.040000$, $\sigma_c = 0.075000$, $\sigma_d = 0.079000$, $\sigma_e = 0.080850$, $\sigma_f = 0.080970$, $\sigma_g = 0.081034$, and $\sigma_h = 0.081060$.

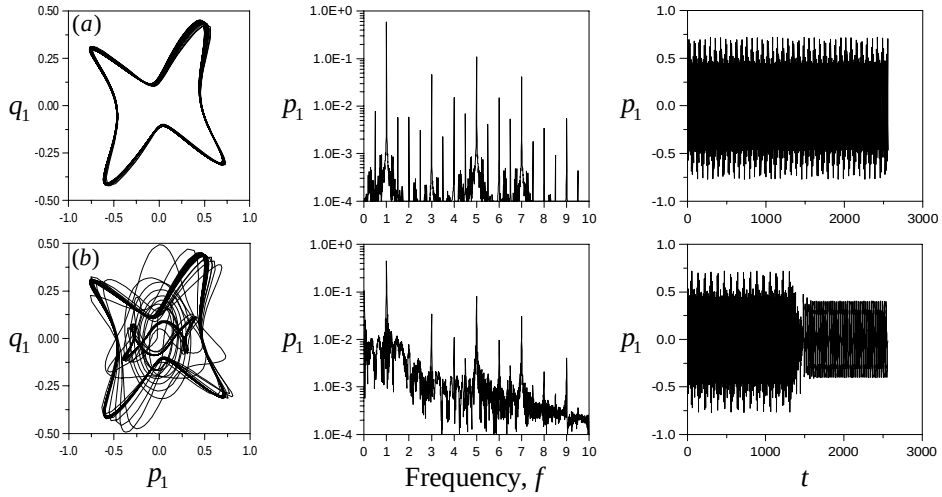

Figure 3.15: Two-dimensional projections of the phase portraits onto the p_1q_1-plane, FFT's of p_1, and time histories showing the chaotic attractor in Figure 3.14(h) as it goes through a boundary crisis and tends to a periodic limit cycle on branch IV as shown in part (b). The corresponding values of σ are $\sigma_a = 0.081069$ and $\sigma_b = 0.081070$.

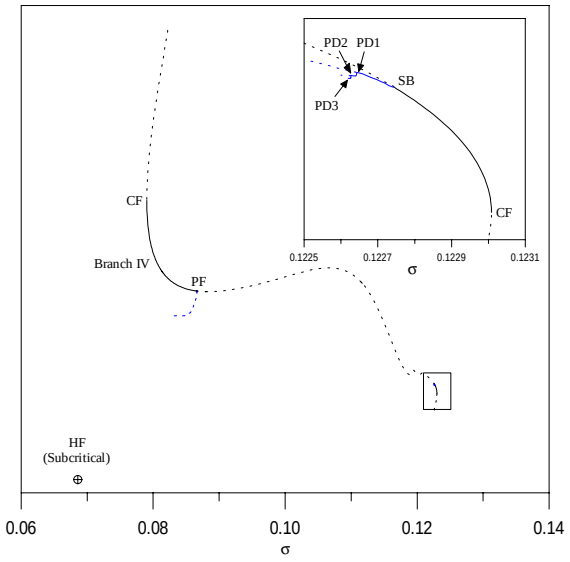

Figure 3.16: A schematic of the dynamic solutions found on branch IV for modes (1,1) when $\delta_2 = -0.5, \mu_1 = \mu_2 = 0.025, g = 0.03$, and $\beta_\gamma = 0.6484$. (——) Stable limit cycle, $(\cdots)$ unstable limit cycle, CF = cyclic-fold bifurcation, SB = symmetry-breaking bifurcation, PF = pitchfork bifurcation, PDn = nth period-doubling bifurcation, and HF = Hopf bifurcation.

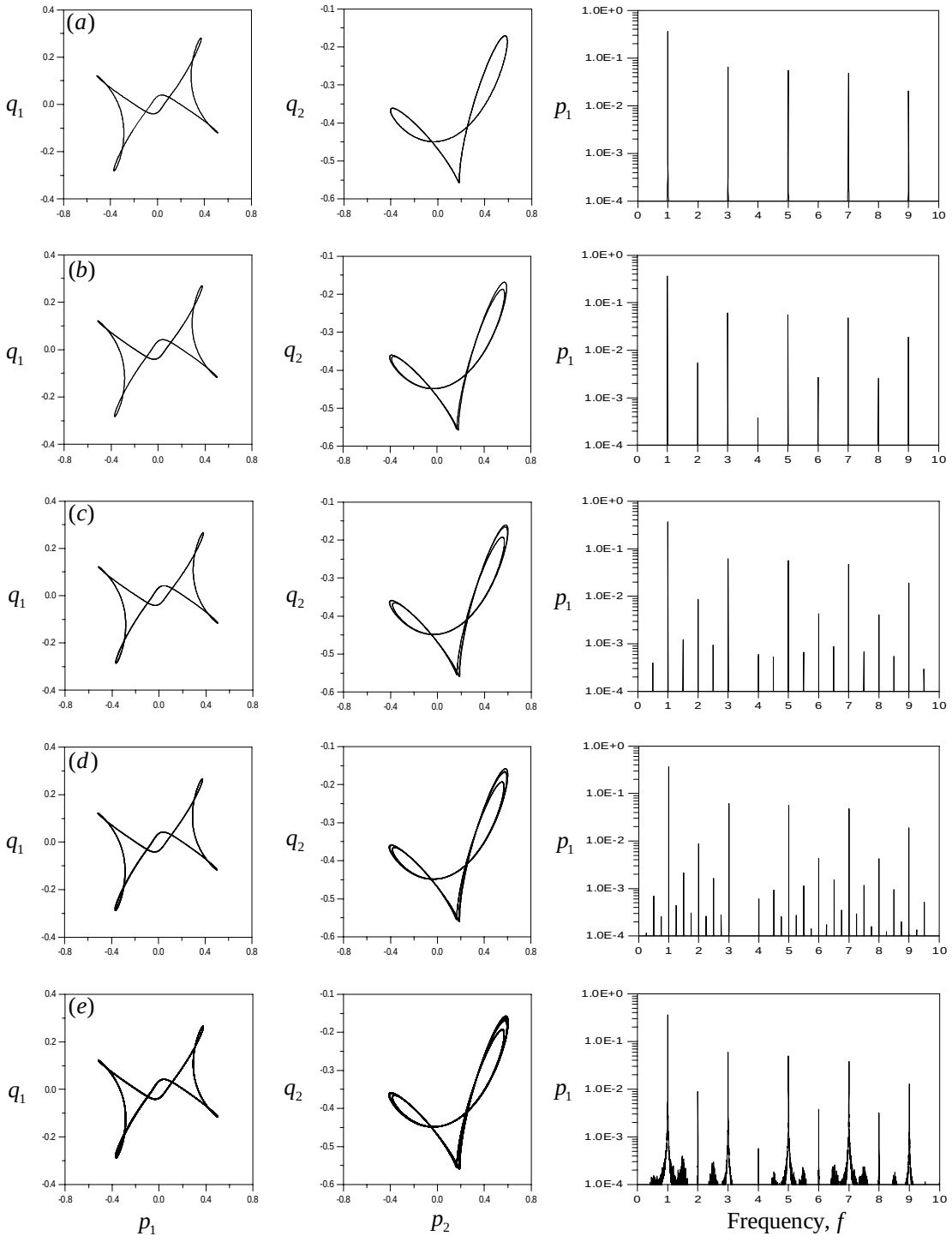

Figure 3.17: Two-dimensional projections of the phase portraits onto the p_1q_1- and p_2q_2-planes and FFT's of q_2 showing the symmetric limit cycle on branch IV breaking its symmetry, undergoing repeated period-doubling bifurcations, and eventually becoming chaotic. The corresponding values for σ are $\sigma_a = 0.1229000$, and $\sigma_b = 0.1227000$, $\sigma_c = 0.1226368$, $\sigma_d = 0.1226250$, and $\sigma_e = 0.1226230$.

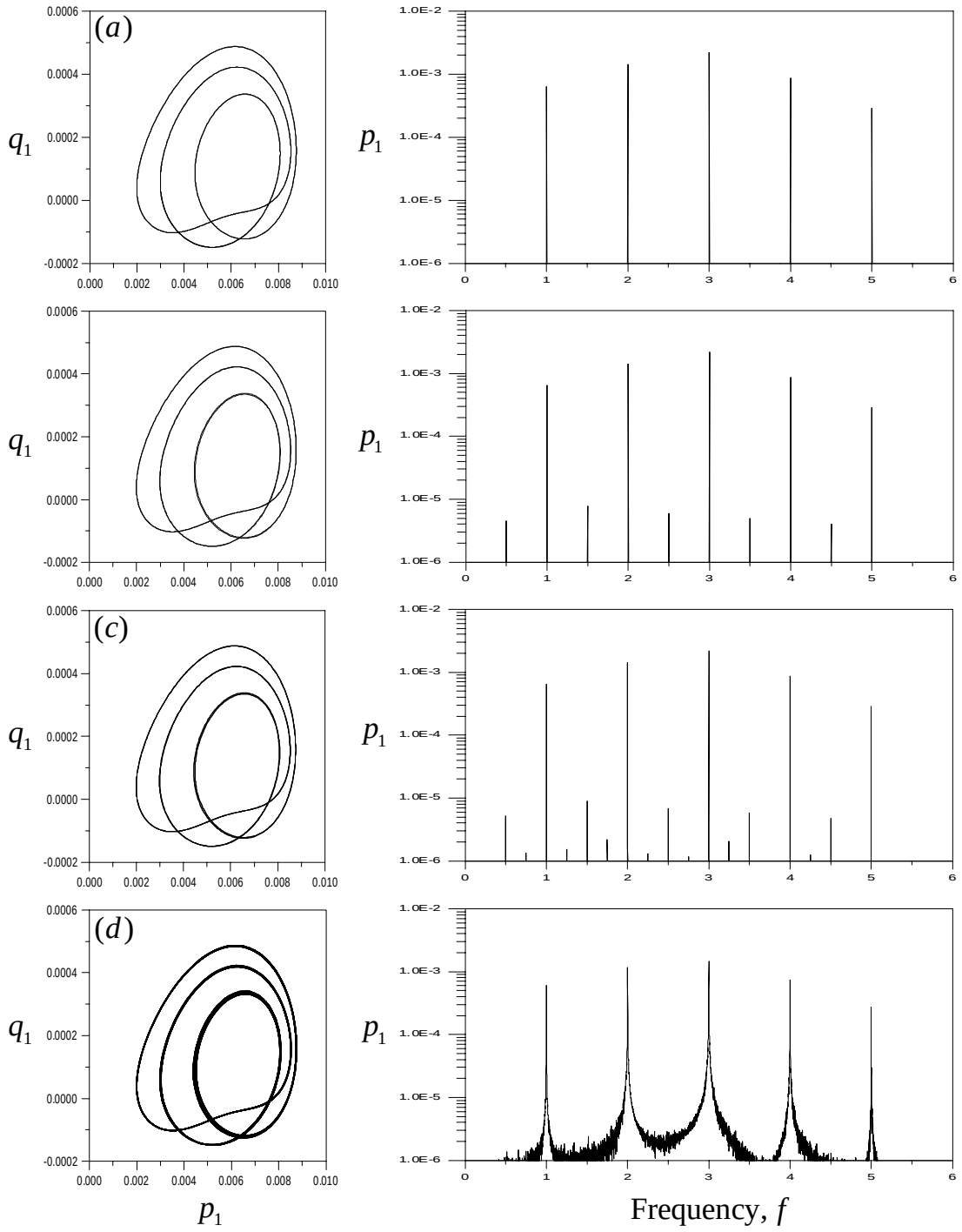

Figure 3.18: Two-dimensional projections of the phase portraits onto the p_1q_1-plane and FFT's of p_1 showing the left part of the bubble structure found on branch V. As σ is increased, the limit cycle in part (a) undergoes a sequence of period-doubling bifurcations that culminates in a chaotic attractor, as shown in part (d). The corresponding values of σ are $\sigma_a = -0.038310125$, $\sigma_b = -0.038310122$, $\sigma_c = -0.038310121$, and $\sigma_d = -0.038310116$.

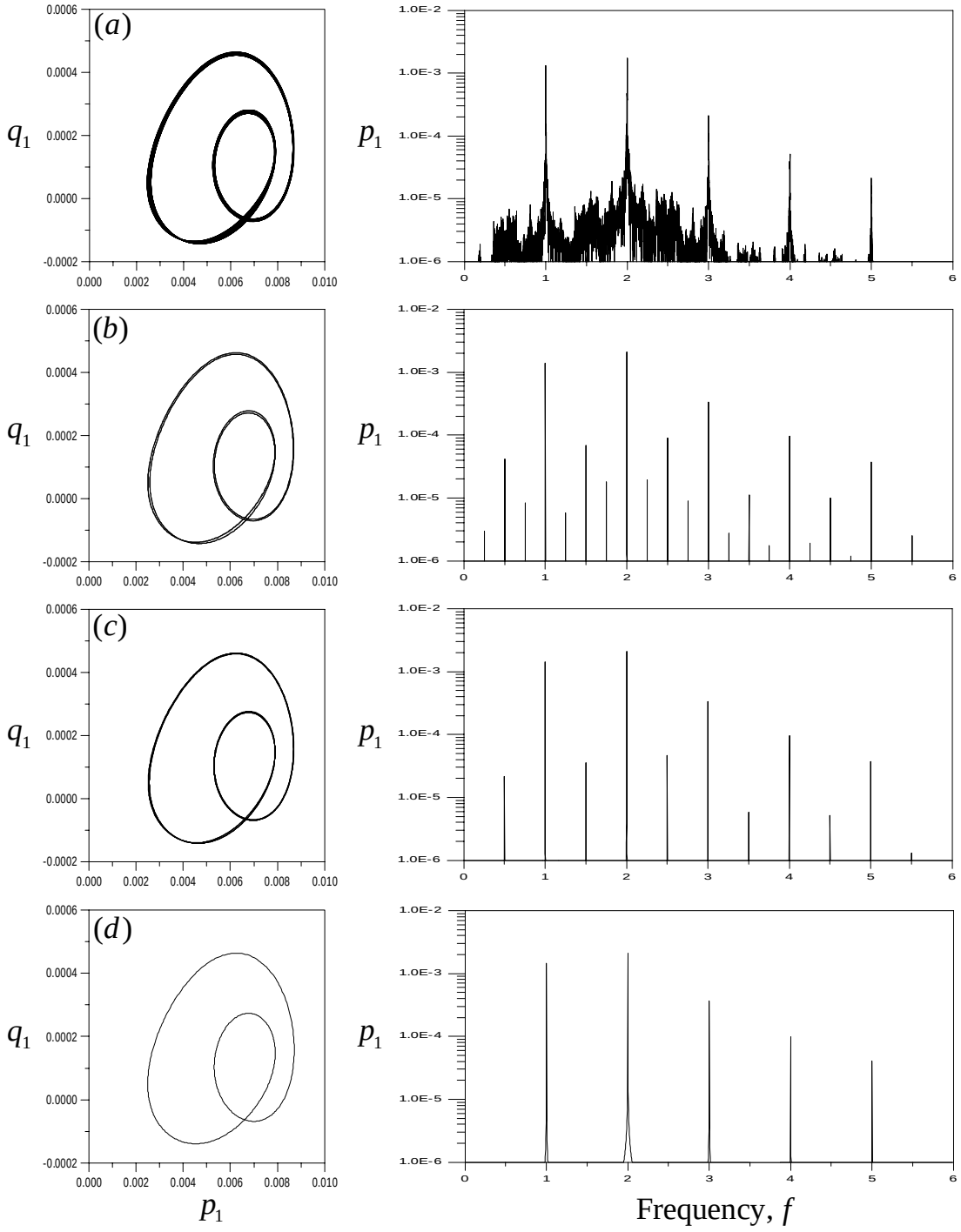

Figure 3.19: Two-dimensional projections of the phase portraits onto the p_1q_1-plane and FFT's of p_1 showing the right part of the bubble structure on branch V. As σ is increased, the chaotic attractor in Figure 3.18(d) undergoes a sequence of reverse period-doubling bifurcations that results in a limit cycle, as shown in part (d). The corresponding values of σ are $\sigma_a = -0.03830840$, $\sigma_b = -0.03830831$, $\sigma_c = -0.03830822$, and $\sigma_d = -0.03830800$.

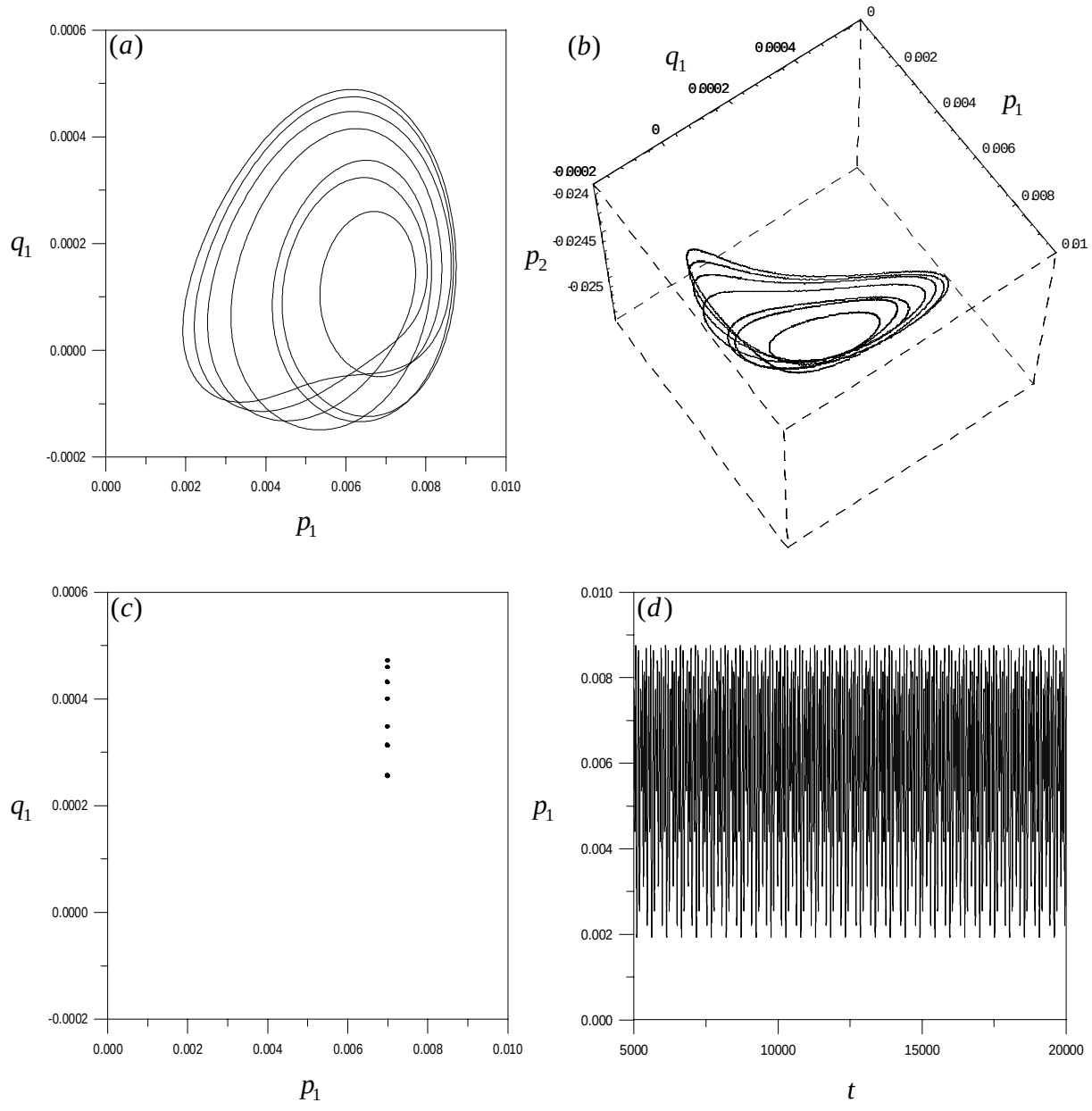

Figure 3.20: A phase-locked limit cycle found at $\sigma_i = -0.0383106$. (a) Two-dimensional projection of the phase portrait onto the p_1q_1-plane, (b) three-dimensional projection of the phase portrait onto the $p_1q_1p_2$-space, (c) Poincaré section, and (d) time history.

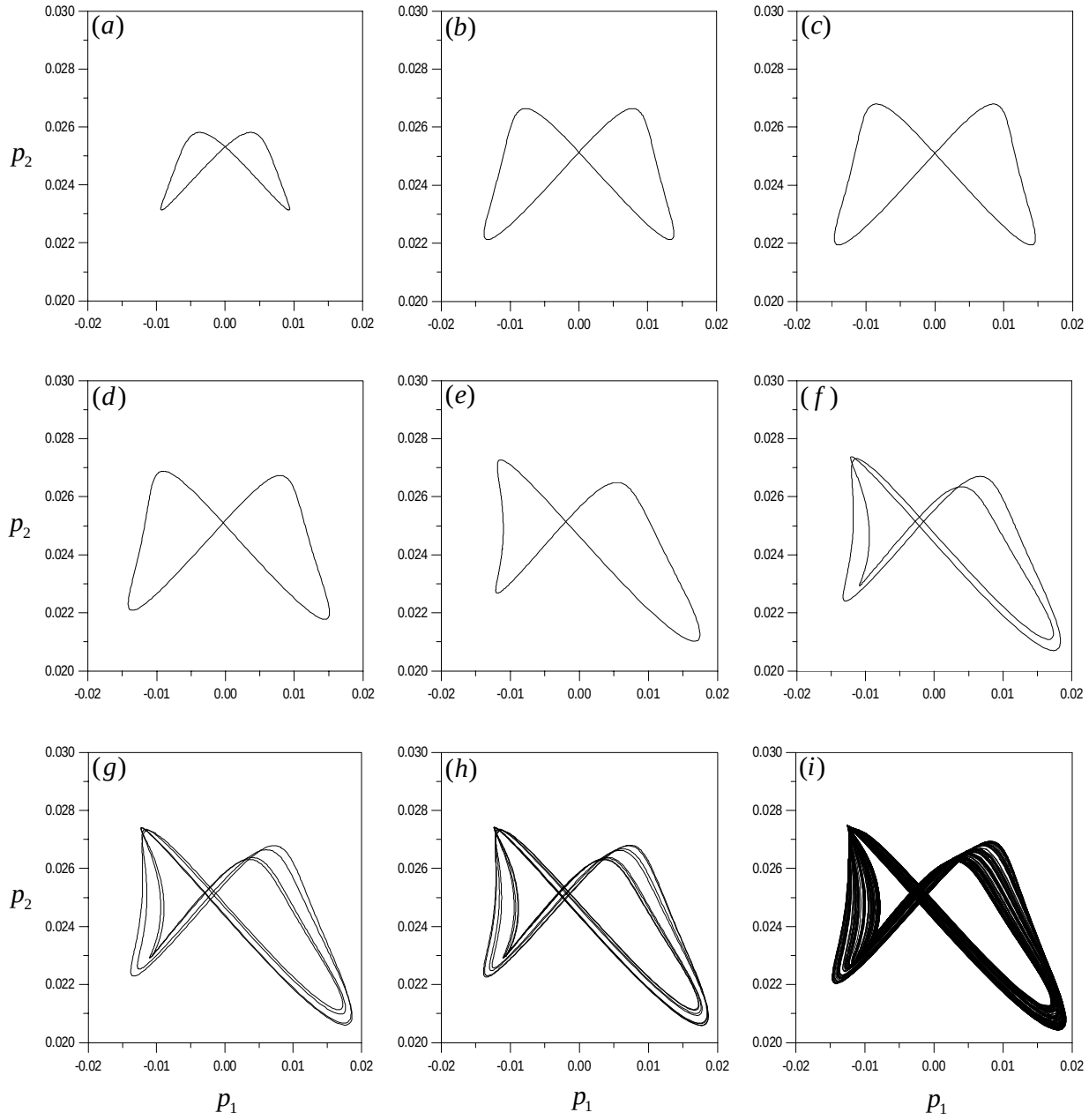

Figure 3.21: Two-dimensional projections of the phase portraits onto the p_1p_2-plane showing the symmetric limit cycle located on the isolated branch II. As σ is increased, the limit cycle grows, deforms, and undergoes repeated period-doubling bifurcations that culminate in chaos, as shown in part (i). The corresponding values for the σ are $\sigma_a = -0.038436515$, $\sigma_b = -0.03840000$, $\sigma_c = -0.03838750$, $\sigma_d = -0.03838650$, $\sigma_e = -0.03836810$, $\sigma_f = -0.03836150$, $\sigma_g = -0.03835950$, $\sigma_h = -0.03835907$, and $\sigma_i = -0.03835550$.

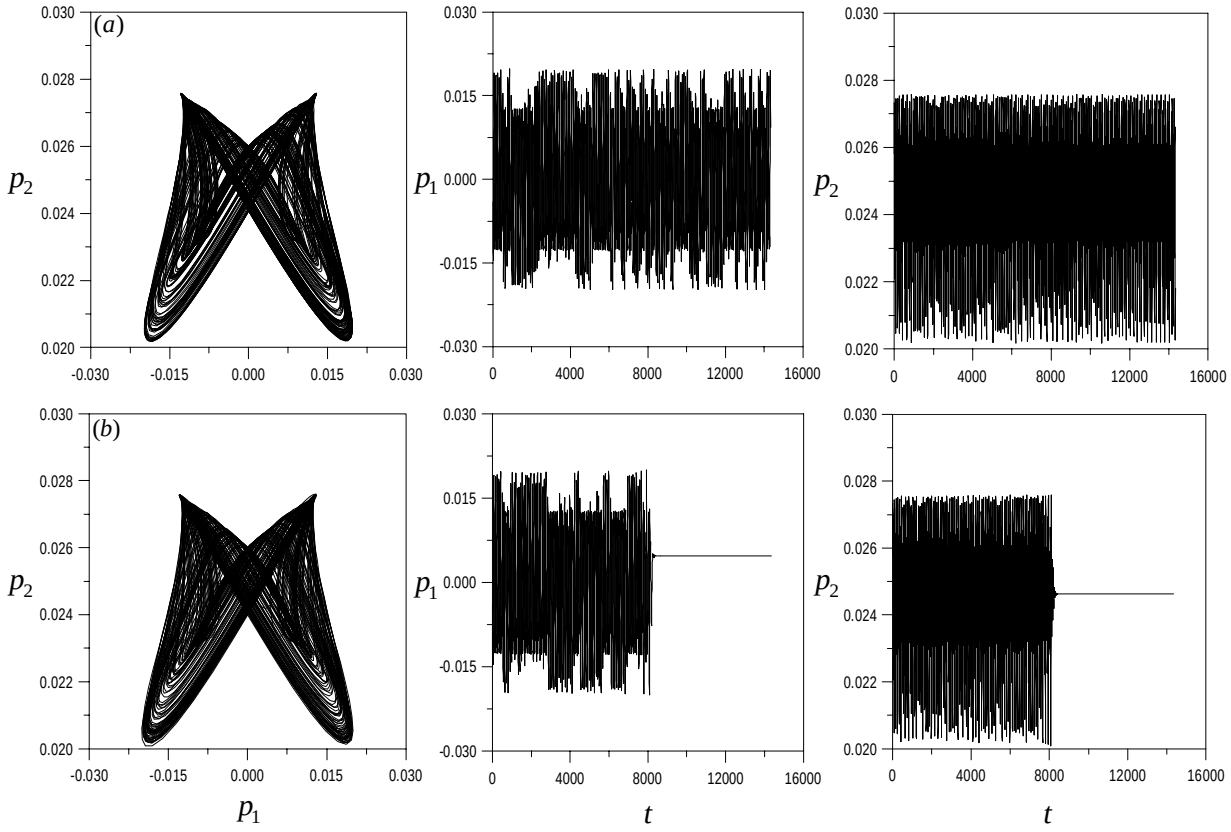

Figure 3.22: Two-dimensional projections of the phase portraits onto the p_1p_2-plane and long-time histories showing the chaotic attractor in Figure 3.21(i) undergoing an attractor-merging crisis when increasing the parameter σ. Further increasing σ, this new attractor goes through a boundary crisis and reverts to the two-mode equilibrium solution. The corresponding values for σ are $\sigma_a = -0.03835000$ and $\sigma_b = -0.03834964$.

Chapter 4

Nonlinear Nonplanar Dynamics of Directly Excited Cantilever Beams

The nonlinear nonplanar response of a cantilever inextensional metallic beam to a transverse base excitation of one of its flexural modes is investigated. The lowest torsional frequencies of the beams considered are much larger than the frequencies of the excited modes so that the torsional inertia can be neglected. In Chapter 3, when the beam was parametrically excited, we used the method of time-averaged Lagrangian to derive a set of four first-order nonlinear ordinary-differential equations governing the modulation of the amplitude and phases of the two interacting modes. Modifying the virtual-work term to account instead for the transverse excitation, we obtain a similar set of modulation equations when the beam is excited at primary resonance. A pseudo-arclength scheme is used to trace the branches of the equilibrium solutions and the eigenvalues of the Jacobian matrix are used to assess their stability. The effects of the cross-section detuning, forcing-frequency detuning, and forcing amplitude on the static and dynamic bifurcations are investigated. The equilibrium solutions experience pitchfork, saddle-node, and Hopf bifurcations. Eleven branches of dynamic (periodic and chaotic) solutions of the modulation equations are found. Two of these branches emerge from two Hopf bifurcations and the rest are isolated. The limit cycles undergo symmetry-breaking, cyclic-fold, and period-doubling bifurcations, whereas the chaotic attractors undergo attractor-merging and boundary crises. Other interesting phenomena found include bubble

structures and homoclinic bifurcations.

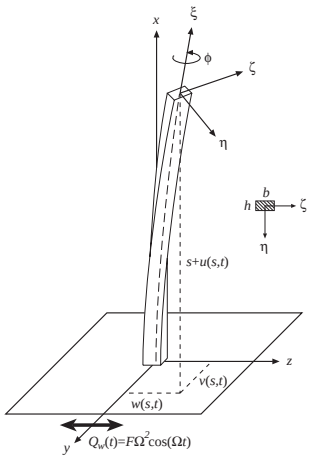

Figure 4.1: A schematic of a near-square cantilever beam under transverse base excitation.

4.1 Problem Formulation

The nondimensional bending-bending equations of motions for a base excited cantilever beam are obtained by setting $Q_u(t) = 0$, $Q_v(t) = 0$, $Q_\phi(t) = 0$, and $Q_w(t) = F\Omega^2 \cos(\Omega t)$ in Eqs. (2.113) and (2.114) and then applying Eq. (3.1). The result is

$$\begin{aligned}
\ddot{v} + c_v\dot{v} + \beta_y v'''' &= (1-\beta_y)\left[w''\int_1^s v''w''ds - w'''\int_0^s v''w'ds\right]' \\
&\quad - \frac{(1-\beta_y)^2}{\beta_\gamma}\left[w''\int_0^s\int_1^s v''w''dsds\right]'' - \beta_y\left[v'\left(v'v''+w'w''\right)'\right]' \\
&\quad - \frac{1}{2}\left\{v'\int_1^s \frac{\partial^2}{\partial t^2}\left[\int_0^s \left(v'^2+w'^2\right)ds\right]ds\right\}' \qquad (4.1)\\
\ddot{w} + c_w\dot{w} + w'''' &= -(1-\beta_y)\left[v''\int_1^s v''w''ds - v'''\int_0^s v'w''ds\right]' \\
&\quad - \frac{(1-\beta_y)^2}{\beta_\gamma}\left[v''\int_0^s\int_1^s v''w''dsds\right]'' - \left[w'\left(v'v''+w'w''\right)'\right]' \\
&\quad - \frac{1}{2}\left\{w'\int_1^s \frac{\partial^2}{\partial t^2}\left[\int_0^s \left(v'^2+w'^2\right)ds\right]ds\right\}' + F\Omega^2\cos(\Omega t) \qquad (4.2)
\end{aligned}$$

The nondimensional Lagrangian corresponding to Eqs. (4.1) and (4.2) is given by Eq. (3.2). The corresponding nondimensional virtual-work term is

$$\delta W = \int_0^1 \left(Q_v^* \delta v + Q_w^* \delta w\right) ds = -\int_0^1 \left\{c_v \dot{v}\delta v + \left[c_w \dot{w} - F\Omega^2 \cos\left(\Omega t\right)\right] \delta w\right\} ds \tag{4.3}$$

The one-to-one internal resonance between the mth in-plane bending mode and nth out-of-plane bending mode is defined by Eq. (3.14) and is repeated here for convenience

$$\hat{\omega}_{1m} = z_m^2 \sqrt{\beta_y} = z_m^2 \sqrt{1 + \delta_0 + \epsilon^2 \delta_2} + \cdots \tag{4.4}$$

$$\omega_{1m} = z_m^2 \sqrt{1 + \delta_0} = z_n^2 = \omega_{2n} \tag{4.5}$$

To relate the nearness of the forcing frequency Ω to the natural frequency of the nth out-of-plane bending mode ω_{2n}, we introduce the detuning parameter σ defined according to

$$\Omega = \omega_{2n} + \epsilon^2 \sigma \tag{4.6}$$

Furthermore, we scale the damping and forcing terms so that their effects balance the effect of the nonlinearities. Therefore, we replace c_v and c_w by $\epsilon^2 c_v$ and $\epsilon^2 c_w$ and F by $\epsilon^3 f$.

Because, except for the forcing terms, the perturbation analysis is the same as that used in the case of parametric excitation (Section 3.2), we present only the final solution. The modulation equations that govern the interaction between the in-plane and out-of-plane bending modes in complex-valued form are

$$\begin{aligned} 2i\omega_{1m}\frac{dA_1}{dT_2} = {} & \left[2\omega_{1m}^2 \Gamma_5 - 3\left(1+\delta_0\right)\Gamma_4\right] A_1^2 \bar{A}_1 + 2\omega_{1m}\omega_{2n}\Gamma_6 \bar{A}_1 A_2^2 - \left(2i\omega_{1m}\mu_1 + \delta_2 z_m^4\right) A_1 \\ & - \left[\left(1+\delta_0\right)\Gamma_3 + \frac{\delta_0^2}{\beta_\gamma}\Gamma_2 + \delta_0\Gamma_1\right]\left(\bar{A}_1 A_2^2 + 2A_1 A_2 \bar{A}_2\right) \end{aligned} \tag{4.7}$$

$$\begin{aligned} 2i\omega_{2n}\frac{dA_2}{dT_2} = {} & \left(2\omega_{2n}^2 \Lambda_5 - 3\Lambda_4\right) A_2^2 \bar{A}_2 + 2\omega_{1m}\omega_{2n}\Gamma_6 A_1^2 \bar{A}_2 - 2i\omega_{2n}\mu_2 A_2 \\ & - \left[\left(1+\delta_0\right)\Gamma_3 + \frac{\delta_0^2}{\beta_\gamma}\Gamma_2 + \delta_0\Gamma_1\right]\left(A_1^2 \bar{A}_2 + 2A_1 \bar{A}_1 A_2\right) + \frac{\Omega^2}{2}\Lambda_8 f e^{i\omega_{2n}\sigma T_2} \end{aligned} \tag{4.8}$$

where the Γ_i and Λ_i are defined by Eqs. (3.32)-(3.40) and

$$\Lambda_8 = \int_0^1 \Phi_n ds \tag{4.9}$$

Using Eq. (3.48), we express the modulation equations in the polar form

$$2\omega_{1m}a_1' = -\Big\{R_1 + R_2 a_2^2 \sin[2(\gamma_1 - \gamma_2)]\Big\}a_1 \tag{4.10}$$

$$2\omega_{1m}a_1\gamma_1' = \Big\{R_4 + R_5 a_1^2 - R_6 a_2^2 - R_2 a_2^2 \cos[2(\gamma_1 - \gamma_2)]\Big\}a_1 \tag{4.11}$$

$$2\omega_{2n}a_2' = -\Big\{E_1 - R_2 a_1^2 \sin[2(\gamma_1 - \gamma_2)]\Big\}a_2 + E_8 \sin\gamma_2 \tag{4.12}$$

$$2\omega_{2n}a_2\gamma_2' = \Big\{E_4 + E_5 a_2^2 - R_6 a_1^2 - R_2 a_1^2 \cos[2(\gamma_1 - \gamma_2)]\Big\}a_2 + E_8 \cos\gamma_2 \tag{4.13}$$

where

$$\gamma_1 = \omega_{1m}\sigma T_2 - \theta_1 \tag{4.14}$$

$$\gamma_2 = \omega_{2n}\sigma T_2 - \theta_2 \tag{4.15}$$

and the R_i and E_i are defined in Appendix A. Alternatively, using Eq. (3.55), we express the modulation equations in the Cartesian form

$$\begin{aligned} p_1' = -\frac{1}{2\omega_{1m}}\Big\{ & R_4 q_1 + R_5\left(p_1^2 + q_1^2\right)q_1 - R_6\left(p_2^2 + q_2^2\right)q_1 \\ & + R_1 p_1 + R_2\Big[\left(p_2^2 - q_2^2\right)q_1 - 2p_1 p_2 q_2\Big]\Big\} \end{aligned} \tag{4.16}$$

$$\begin{aligned} q_1' = -\frac{1}{2\omega_{1m}}\Big\{ & - R_4 p_1 - R_5\left(p_1^2 + q_1^2\right)p_1 + R_6\left(p_2^2 + q_2^2\right)p_1 \\ & + R_1 q_1 + R_2\Big[\left(p_2^2 - q_2^2\right)p_1 + 2q_1 p_2 q_2\Big]\Big\} \end{aligned} \tag{4.17}$$

$$\begin{aligned} p_2' = -\frac{1}{2\omega_{2n}}\Big\{ & E_4 q_2 + E_5\left(p_2^2 + q_2^2\right)q_2 - R_6\left(p_1^2 + q_1^2\right)q_2 \\ & + E_1 p_2 + R_2\Big[\left(p_1^2 - q_1^2\right)q_2 - 2p_1 q_1 p_2\Big]\Big\} \end{aligned} \tag{4.18}$$

$$q_2' = -\frac{1}{2\omega_{2n}}\Big\{ - E_4 p_2 - E_5\left(p_2^2 + q_2^2\right)p_2 + R_6\left(p_1^2 + q_1^2\right)p_2$$

$$+ E_1 q_2 + R_2\Big[\left(p_1^2 - q_1^2\right) p_2 + 2 p_1 q_1 q_2\Big] - E_8\Big\} \tag{4.19}$$

We note that the system (4.16)-(4.19) is invariant under the transformation $(p_1, q_1, p_2, q_2) \Longleftrightarrow (-p_1, -q_1, p_2, q_2)$. That is, for any asymmetric solution found, a second solution can be obtained using the above transformation. This is unlike the case of parametric excitation, where for any asymmetric solution, three other solutions can be found.

In the next section, we investigate bifurcations of the solutions of the modulation equations for a near-square beam (i.e., $\delta_0 = 0$ and $m = n$). The influence of the forcing-frequency detuning σ on the fixed points was investigated by Pai and Nayfeh (1990a). Therefore, we concentrate on the influence of the forcing amplitude f and cross-section detuning δ_2 on the fixed points of Eqs. (4.16)-(4.19). Then, a detailed bifurcation analysis of limit-cycle solutions of Eqs. (4.16)-(4.19) in terms of the forcing-frequency detuning is presented.

4.2 Bifurcation Analysis

4.2.1 Equilibrium Solutions

To determine the fixed points, we set $\dot{a}_1$, $\dot{\gamma}_1$, $\dot{a}_2$, and $\dot{\gamma}_2$ equal to zero in Eqs. (4.10)-(4.13) or $\dot{p}_1$, $\dot{q}_1$, $\dot{p}_2$, and $\dot{q}_2$ equal to zero in Eqs. (4.16)-(4.19) and solve for roots of the resulting algebraic system. Because the system is directly excited, a trivial solution is not possible. There are two possible solutions: (i) single-mode solutions where $a_1 = 0$ and $a_2 \neq 0$, and (ii) two-mode solutions where $a_1 \neq 0$ and $a_2 \neq 0$. In the first case, only the directly excited mode is activated and the motion is planar. In the second case, both the in-plane and out-of-plane modes are activated and the motion of the beam is nonplanar (i.e., whirling motion).

For the case of planar motion, one can obtain a solution for a_2 in closed form. Setting $a_1 = 0$ in Eqs. (4.12) and (4.13) and then squaring and adding the results, we obtain

$$E_5^2 a_2^6 + 2E_4 E_5 a_2^4 + \left(E_1^2 + E_4^2\right) a_2^2 - E_8^2 = 0 \tag{4.20}$$

which is cubic in a_2^2. Therefore, either one or three branches of single-mode solutions exist, de-

pending the values of the parameters used. On the other hand, for the case of nonplanar motion, a closed-form solution is not readily available, and therefore the fixed points are determined numerically using a pseudo-arclength scheme (Nayfeh and Balachandran, 1995; Seydel, 1994). In this case, it was more convenient to use Eqs. (4.16)-(4.19).

Crespo da Silva and Glynn (1978b) and Pai and Nayfeh (1990a) investigated the effect of slowly varying the forcing frequency on the fixed points. They found that the effect of the geometric nonlinearities, which have a hardening-spring behavior, is as important as the effect of the inertia nonlinearities, which have a softening-spring behavior. For the first bending modes, the geometric nonlinearities dominate the response, whereas for the higher modes, the inertia nonlinearities dominate the response.

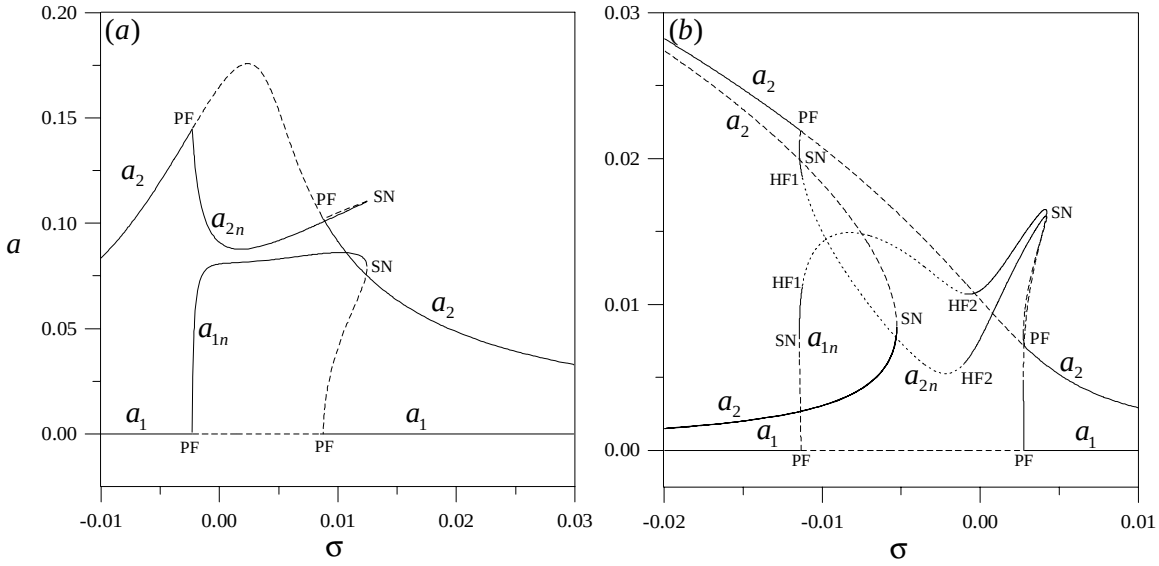

Figure 4.2: Frequency-response curves for (a) modes (1,1) and (b) modes (2,2) when $\mu_1 = \mu_2 = 0.02$. In (a), $\delta_2 = -0.01$ and $\Lambda_8 f = 0.002$ and in (b), $\delta_2 = 0.002$ and $\Lambda_8 f = 0.00006$. The planar response amplitudes are denoted by a_1 and a_2 and the nonplanar response amplitudes are denoted by a_{1n} and a_{2n}. (——) Stable solution, (– – –) saddles, $(\cdots)$ unstable foci, PF = pitchfork bifurcation, SN = saddle-node bifurcation, and HF = Hopf bifurcation.

In Figure 4.2, we present frequency-response curves that were initially calculated by Pai and Nayfeh (1990a). In Figure 4.2a, modes (1,1) are considered when $\Lambda_8 f = 0.002$ and $\delta_2 = -0.01$, whereas in Figure 4.2b, modes (2,2) are considered when $\Lambda_8 f = 0.00006$ and $\delta_2 = 0.002$. The curves for single-mode solutions are bent to the right in Figure 4.2a, indicating that the effective nonlinearity

is of the hardening type for modes (1,1). On the other hand, the curves for single-mode solutions are bent to the left in Figure 4.2b, indicating that the effective nonlinearity is of the softening type for modes (2,2). Furthermore, the fixed points in the case of modes (2,2) undergo two Hopf bifurcations that lead to limit cycles, whereas, in the case of modes (1,1), the fixed points do not undergo any Hopf bifurcations. This is in contrast to the case of principal parametric resonance where the fixed points for modes (1,1) undergo Hopf bifurcations, while those for modes (2,2) do not (see Figures 3.2 and 3.3). Furthermore, it follows from Figure 4.2b that, there is a region where no stable fixed points (either single-mode or two-mode solutions) exist. Hence, the response of the beam in this region is expected to be either quasiperiodic or chaotic. We study this region in greater detail in Section 4.3.2.

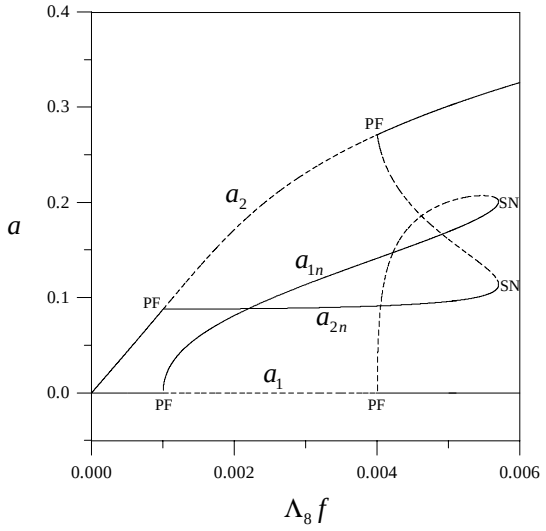

Figure 4.3: Amplitude-response curves for modes (1,1) when $\delta_2 = -0.01$, $\sigma = 0.001$, and $\mu_1 = \mu_2 = 0.02$. The planar response amplitudes are denoted by a_1 and a_2 and the nonplanar response amplitudes are denoted by a_{1n} and a_{2n}. (——) Stable solution, (– – –) saddles, PF = pitchfork bifurcation, SN = saddle-node bifurcation.

In Figure 4.3, we present amplitude-response curves for modes (1,1) when $\delta_2 = -0.01$ and $\sigma = 0.001$. Because the beam is directly excited, planar oscillations occur as soon as the excitation amplitude is increased from zero. As the excitation level exceeds a certain threshold, two-mode solutions occur as a result of the single-mode solution losing stability through a supercritical pitchfork bifurcation. As the forcing amplitude increases further, the amplitude a_{2n} of the directly excited mode remains almost constant while the amplitude a_{1n} of the indirectly excited mode increases monotonously,

which is reminiscent of the saturation phenomenon (Nayfeh and Mook, 1978). Further increasing $\Lambda_8 f$, we find that the two-mode solution loses stability through a saddle-node bifurcation and a jump to the stable branch of single-mode fixed points occurs.

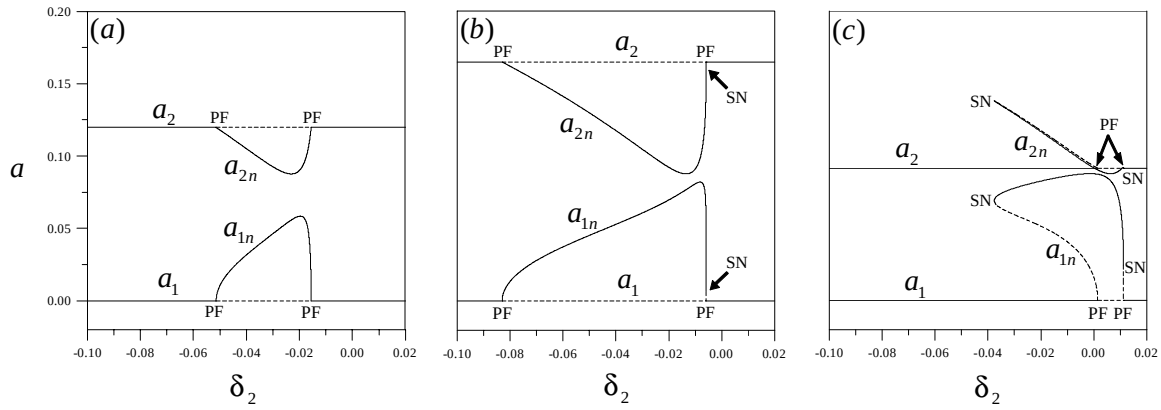

Figure 4.4: Response curves for modes (1,1) in terms of the cross-section detuning δ_2 when $\Lambda_8 f = 0.002$ and $\mu_1 = \mu_2 = 0.02$. The corresponding values of σ are $\sigma_a = -0.005$, $\sigma_b = 0.0$, and $\sigma_c = 0.01$. The planar response amplitudes are denoted by a_1 and a_2 and the nonplanar response amplitudes are denoted by a_{1n} and a_{2n}. (——) Stable solution, (– – –) saddles, PF = pitchfork bifurcation, and SN = saddle-node bifurcation.

In Figure 4.4, we present response curves for modes (1,1) in terms of the cross-section detuning parameter δ_2 when $\Lambda_8 f = 0.002$. In part (a) $\sigma = -0.005$, in part (b) $\sigma = 0.0$, and in part (c) $\sigma = 0.01$. From Appendix A, we note that none of the E_i coefficients depends on δ_2. Therefore, it follows from Eq. (4.20) that the amplitude a_2 of the single-mode response is independent of δ_2, as shown Figures 4.4a, b, and c. This is because the governing equations of motion were nondimensionalized with respect to the out-of-plane bending rigidity D_η. In other words, if the base excitation was instead along the y-axis in Eqs. (4.1) and (4.2), the amplitude a_1 of the single-mode response would be dependent on δ_2. In either case, the influence of δ_2 on the response cannot be ignored because it affects the stability of both planar and nonplanar oscillations, as can be seen from Figures 4.4.

When $\delta_2 < 0$, the beam is less rigid in bending in the plane normal to the base excitation, whereas when $\delta_2 > 0$, the beam is less rigid in the plane along the base excitation. Therefore, activating nonplanar oscillations through the internal resonance is easier when $\delta_2 < 0$. Figures 4.4a, b, and c clearly illustrate this point. In part (a), when $\sigma = -0.005$, the single-mode response loses

stability through two supercritical pitchfork bifurcations, thereby transitioning smoothly to two-mode solutions. When $\sigma = 0.0$, one of the pitchfork bifurcations is supercritical and the other is subcritical, as shown in part (b). When $\sigma = 0.01$, both pitchfork bifurcations are subcritical, resulting in sudden jumps to the branches of two-mode solutions.

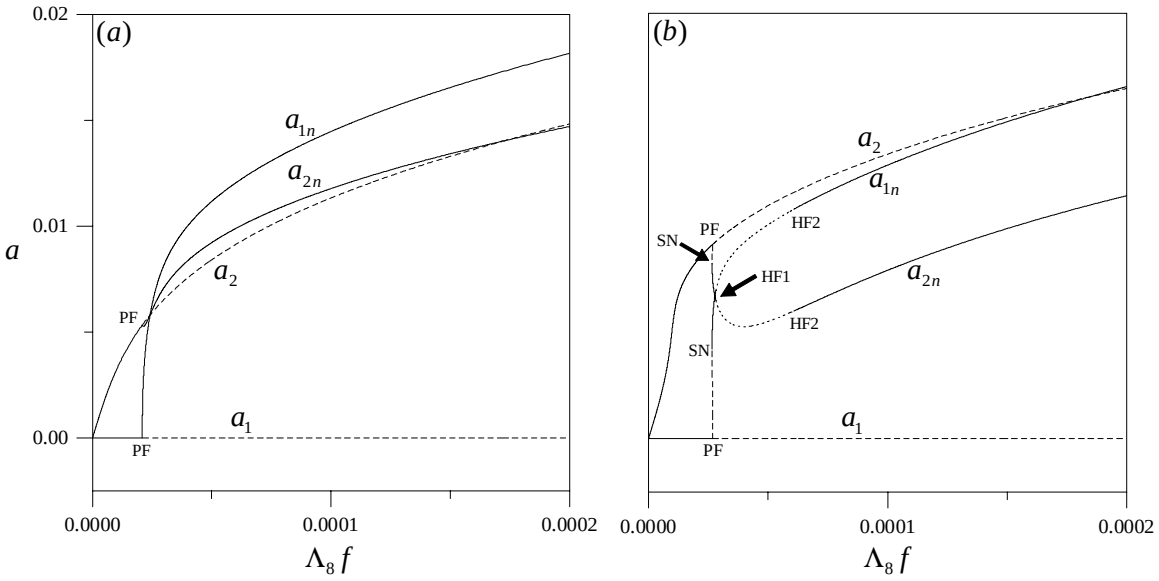

Figure 4.5: Amplitude-response curves for modes (2,2) when $\delta_2 = 0.002$ and $\mu_1 = \mu_2 = 0.02$. The corresponding values of σ are $\sigma_a = 0.001$ and $\sigma_b = -0.001$. The planar response amplitudes are denoted by a_1 and a_2 and the nonplanar response amplitudes are denoted by a_{1n} and a_{2n}. (——) Stable solution, (– – –) saddles, ($\cdots$) unstable foci, PF = pitchfork bifurcation, SN = saddle-node bifurcation, and HF = Hopf bifurcation.

In Figure 4.5, we present amplitude-response curves for modes (2,2) when $\delta_2 = 0.002$. In part (a), $\sigma = 0.001$ and in part (b), $\sigma = -0.001$. Because the beam is directly excited, planar oscillations occur as soon as the excitation amplitude is increased from zero, as shown in Figures 4.5a and b. As the level of excitation increases beyond a threshold, two-mode solutions occur as a result of the single-mode solution losing stability through a pitchfork bifurcation. In part (a), the pitchfork bifurcation is supercritical and the transition is gradual, whereas in part (b), the pitchfork bifurcation is subcritical and a jump occurs. The two-mode solutions in part (a) remain stable and their amplitudes monotonously increase as f increases, whereas in part (b), they undergo two Hopf bifurcations that result in limit cycles. In the region between the two Hopf bifurcations, there are no stable solutions, and hence aperiodic, including chaotic, oscillations may occur.

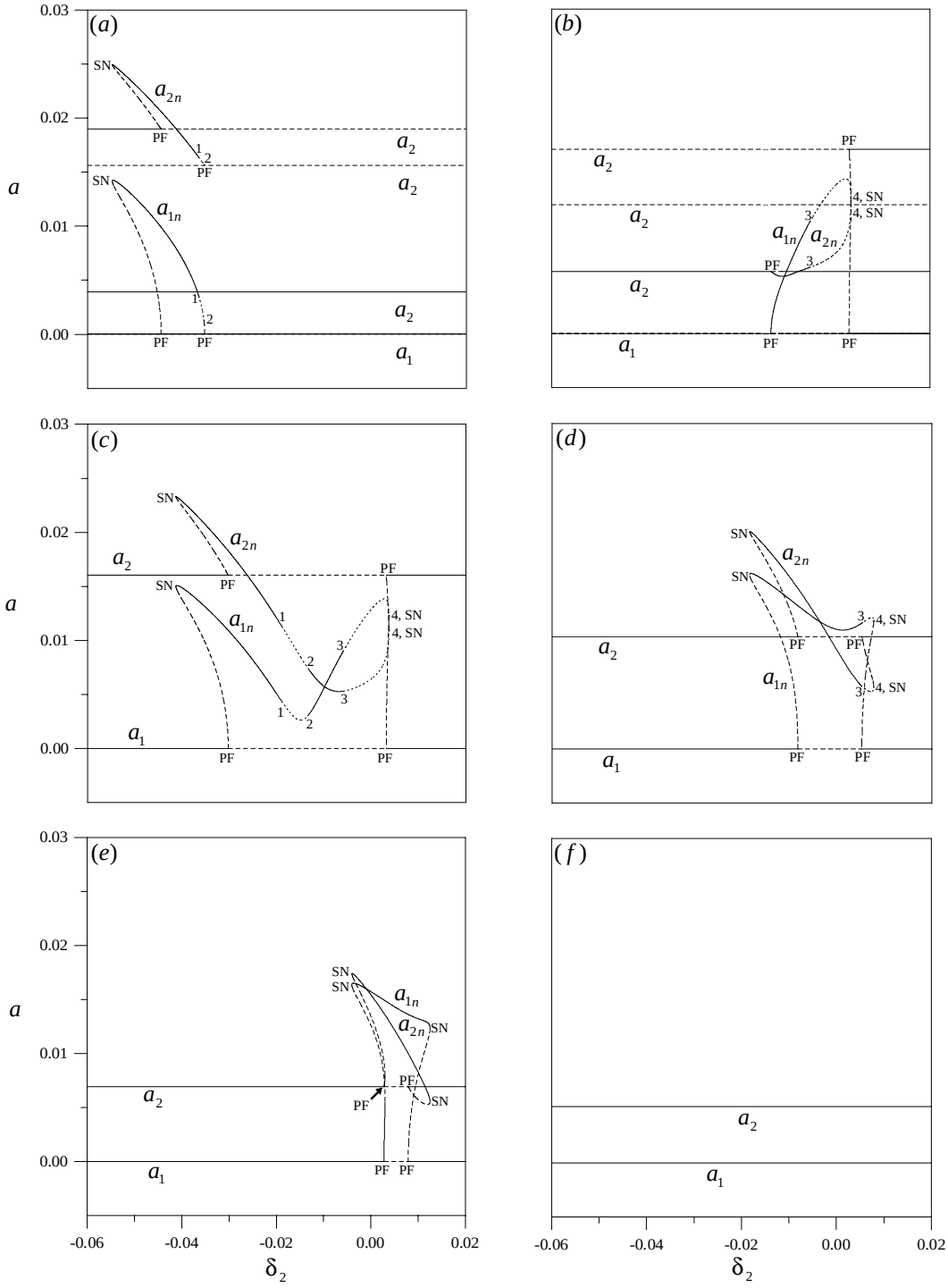

Figure 4.6: Response curves for modes (2,2) in terms of the cross-section detuning δ_2 when $\Lambda_8 f = 0.00006$ and $\mu_1 = \mu_2 = 0.02$. The corresponding values of σ are $\sigma_a = -0.008$, $\sigma_b = -0.006$, $\sigma_c = -0.005$, $\sigma_d = 0.0$, $\sigma_e = 0.003$, and $\sigma_f = 0.005$. The planar response amplitudes are denoted by a_1 and a_2 and the nonplanar response amplitudes are denoted by a_{1n} and a_{2n}. (——) Stable solution, (– – –) saddles, ($\cdots$) unstable foci, PF = pitchfork bifurcation, SN = saddle-node bifurcation, and the numbers 1, 2, 3, and 4 denote the Hopf bifurcations HF1, HF2, HF3, and HF4.

In Figure 4.6, we present response curves for modes (2,2) in terms of the cross-section detuning parameter δ_2 when $\Lambda_8 f = 0.00006$. In part (a) $\sigma = -0.008$, in part (b) $\sigma = -0.006$, in part (c) $\sigma = -0.005$, in part (d) $\sigma = 0.0$, in part (e) $\sigma = 0.003$, and in part (f) $\sigma = 0.005$. In parts (a)-(e), nonplanar motions occur as the single-mode solution loses stability through either a supercritical or a subcritical pitchfork bifurcation. In part (f), the single-modes solution is always stable and hence the motion remains planar.

In Figures 4.6a and b, three branches of single-mode solutions exist. In both parts, the nonplanar fixed points undergo two Hopf bifurcations, resulting in limit cycles. It is interesting to note, from Figures 4.6a and b, that the branches of two-mode solutions start from one branch of single-mode solutions and end at a different branch of single-mode solutions as δ_2 is varied. When $\sigma = -0.005$, only one branch of single-mode solutions exists, as shown in Figure 4.6c. Furthermore, the branches of two-mode solutions from parts (a) and (b) seem to have coalesced in part (c), creating a larger branch of nonplanar fixed points that undergoes four Hopf bifurcations. As σ is increased to 0.0, the regions of unstable single-mode and stable two-mode solutions decrease and only one region of unstable foci exists, as shown in Figure 4.6d. When $\sigma = 0.003$, the unstable region between the two pitchfork bifurcations further decreases and the nonplanar solutions no longer undergo any Hopf bifurcations, as shown in Figure 4.6e. Finally, for values of $\sigma \geq 0.005$, the two pitchfork bifurcation points coalesce and only stable single-mode solutions exist, as shown in Figure 4.6f.

4.2.2 Dynamic Solutions

We investigated the dynamic solutions of the modulation equations for modes (2,2) when $\delta_2 = 0.002$ and $\Lambda_8 f = 0.00006$, corresponding to Figure 4.2b. Using long-time integration, a combination of a two-point boundary-value program and Newton's scheme, and Floquet theory, we were able to determine eleven branches $(A - K)$ of dynamic solutions, as shown in Figure 4.7. Two of these branches result from the equilibrium solutions undergoing two Hopf bifurcations, branch A from the point HF1 and branch K from the point HF2. The remaining branches are isolated. Calculating the normal forms for the Hopf bifurcations, defined by Eqs. (3.60) and (3.61), we found that both HF1 at $\sigma = -0.011259$ and HF2 at $\sigma = -0.000988$ are supercritical.

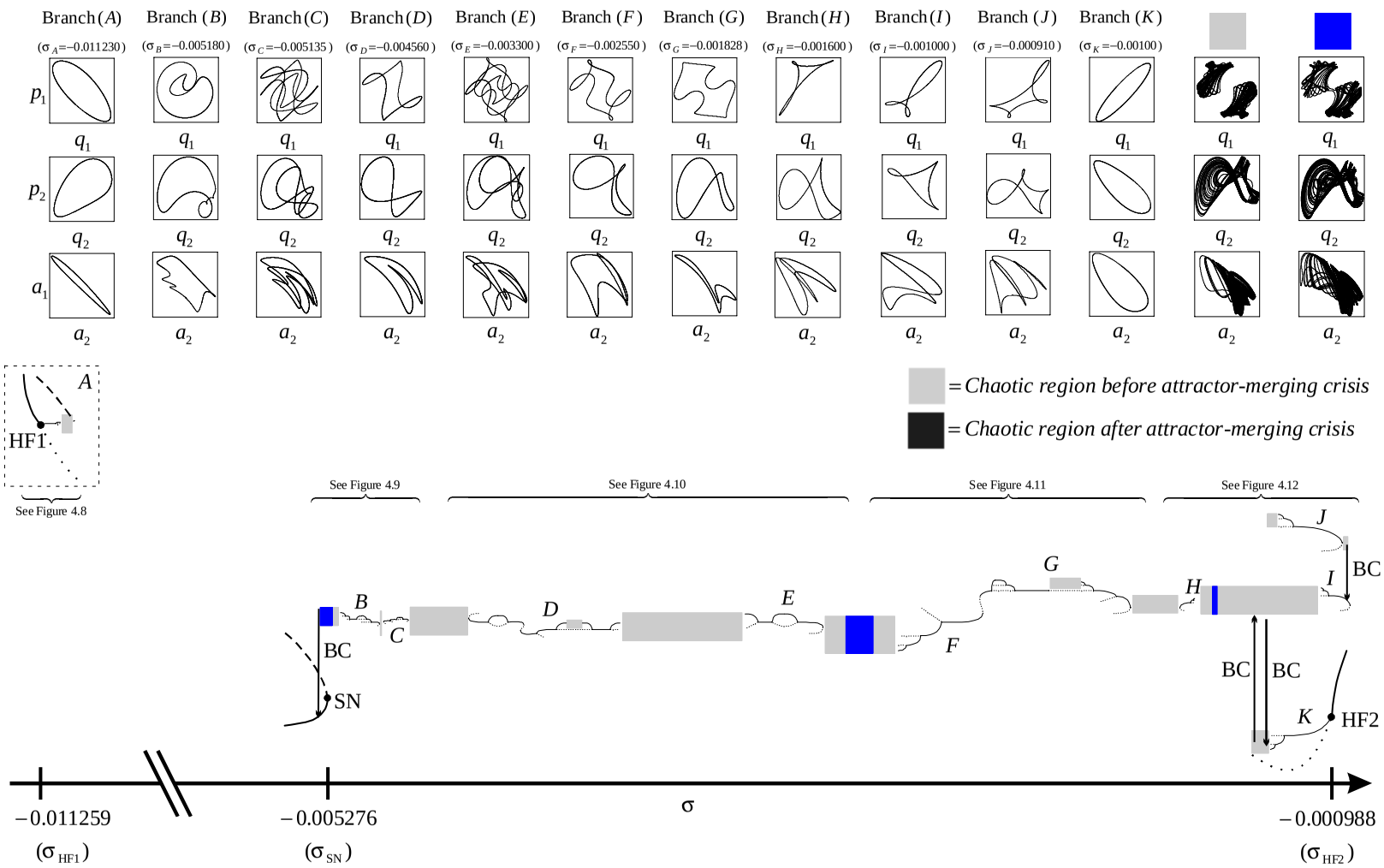

Figure 4.7: A schematic of the dynamic solutions found for modes (2,2) when $\delta_2 = 0.002$, $\Lambda_8 f = 0.00006$, and $\mu_1 = \mu_2 = 0.02$. Thick solid lines denote stable fixed points, thick dashed lines denote saddles, thick dotted lines denote unstable foci, (——) stable limit cycles, $(\cdots)$ unstable limit cycles, BC = boundary crisis, SN = saddle-node bifurcation, and HF1 and HF2 = Hopf bifurcations.

In Figure 4.7, we present a schematic diagram showing the regions where periodic and chaotic solutions occur in terms of σ. Thick solid and dashed lines denote branches of stable and saddle fixed points, thick dotted lines denote branches of unstable foci, and thin solid and dotted lines denote branches of stable and unstable limit cycles. The light-shaded areas are regions of chaotic attractors that result from limit cycles undergoing either cyclic-fold bifurcations or sequences of period-doubling bifurcations. On the other hand, the dark-shaded areas are regions of chaotic attractors that result from the smaller attractors undergoing attractor-merging crises. In addition, we present in Figure 4.7 phase portraits in the p_1q_1-, p_2q_2-, and a_1a_2-, planes characterizing the period-one limit cycles found on each branch.

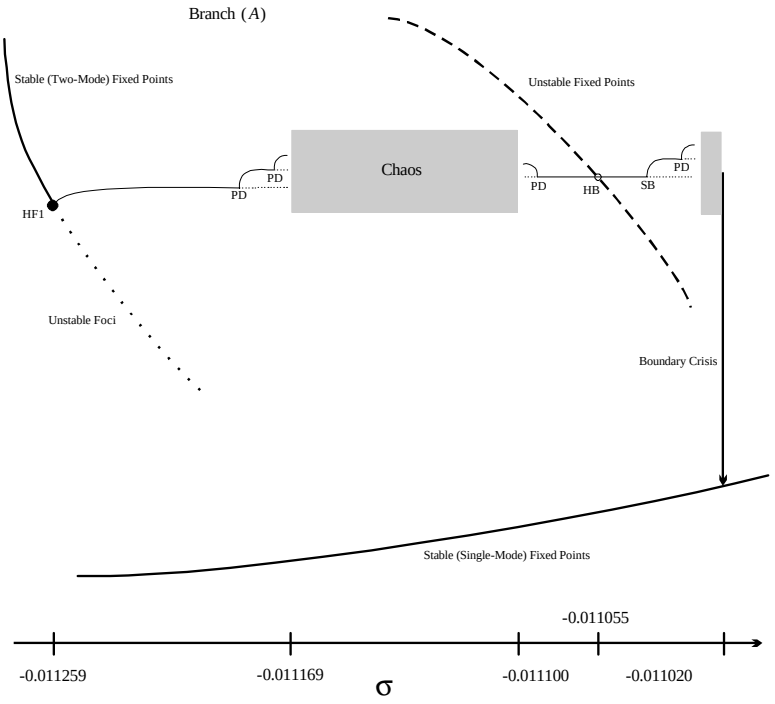

Figure 4.8: A schematic of the dynamic solutions found on branch A for modes (2,2) when $\delta_2 = 0.002$, $\Lambda_8 f = 0.00006$, and $\mu_1 = \mu_2 = 0.02$. (——) Stable limit cycles, $(\cdots)$ unstable limit cycle, PD = period-doubling bifurcation, CF = cyclic-fold bifurcation, HF1 = Hopf bifurcations, and HB = homoclinic bifurcation.

It is interesting to note from Figure 4.7 that most branches of dynamic solutions are located in the region between the saddle-node bifurcation SN and the right Hopf bifurcation HF2. In contrast, only branch A, which emanates from the left Hopf bifurcation HF1, was found in the region to the

left of SN. This is most likely due to the fact that no stable fixed points exist in the region between SN and HF2, whereas single- and two-mode fixed points exist in the region between HF1 and SN, as shown in Figure 4.2b. Therefore, the response of the beam in the region to the left of SN and the region to the right of HF2 is likely to be periodic in one plane or a simple whirling motion in two planes. On the other hand, the response of the beam in the region between SN and HF2 is likely to be aperiodic (beating-type whirling) and chaotic.

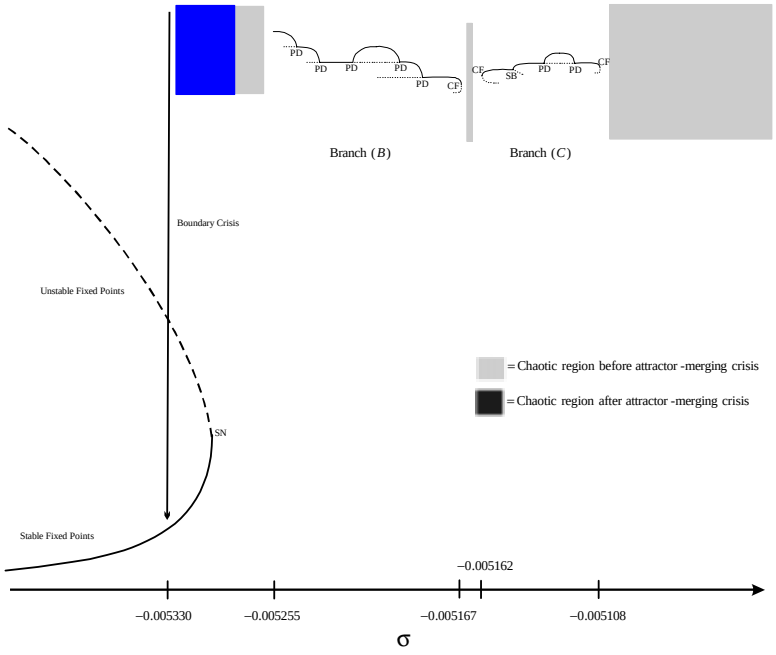

Figure 4.9: A schematic of the dynamic solutions found on branches B and C for modes (2,2) when $\delta_2 = 0.002$, $\Lambda_8 f = 0.00006$, and $\mu_1 = \mu_2 = 0.02$. (——) Stable limit cycles, $(\cdots)$ unstable limit cycles, SN = saddle-node bifurcation, PD = period-doubling bifurcation, CF = cyclic-fold bifurcation, and SB = symmetry-breaking bifurcation.

More detailed schematic diagrams of the dynamic solutions and their bifurcations are presented in Figures 4.8-4.12. In Figure 4.8, we consider branch A; in Figure 4.9, we consider branches B and C; in Figure 4.10, we consider branches D and E; in Figure 4.11, we consider branches F and G; and in Figure 4.12, we consider branches H, I, J, and K.

In Figure 4.13a, we present two-dimensional projections of the phase portraits onto the p_1q_1- and p_2q_2-planes of a small limit cycle on branch A that resulted from the supercritical Hopf bifurcation HF1 at $\sigma_{HF1} = -0.011259$. As we increase σ, the limit cycle grows, as shown in Figures 4.13b and

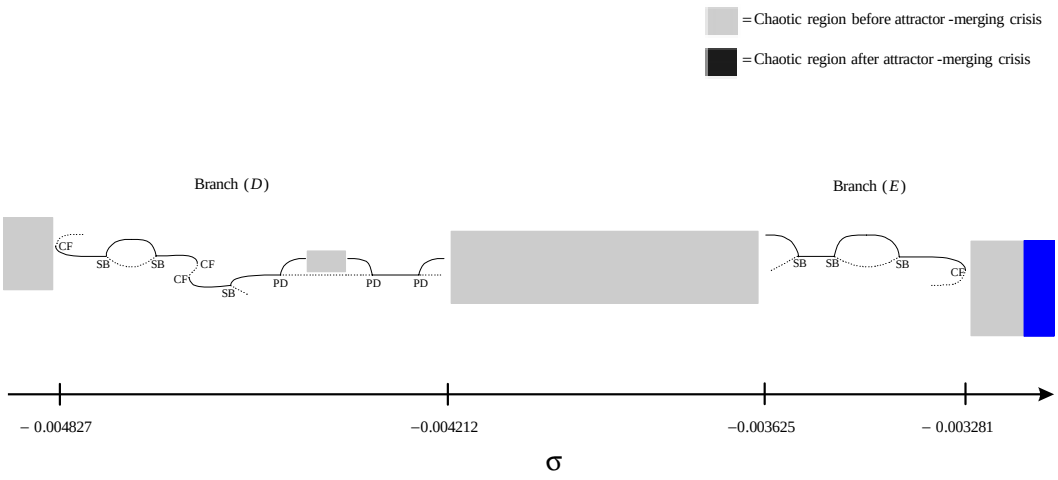

Figure 4.10: A schematic of the dynamic solutions found on branches D and E for modes (2,2) when $\delta_2 = 0.002$, $\Lambda_8 f = 0.00006$, and $\mu_1 = \mu_2 = 0.02$. (——) Stable limit cycles, $(\cdots)$ unstable limit cycles, PD = period-doubling bifurcation, CF = cyclic-fold bifurcation, and SB = symmetry-breaking bifurcation.

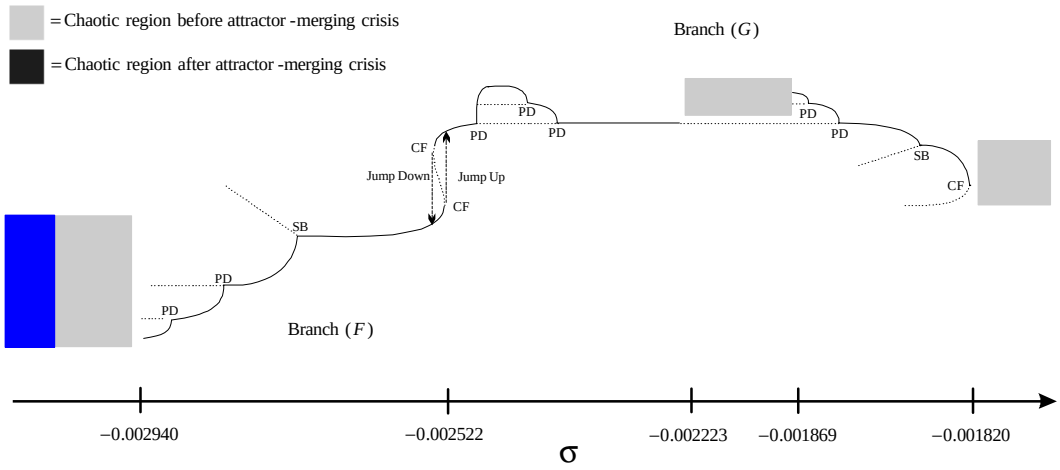

Figure 4.11: A schematic of the dynamic solutions found on branches F and G for modes (2,2) when $\delta_2 = 0.002$, $\Lambda_8 f = 0.00006$, and $\mu_1 = \mu_2 = 0.02$. (——) Stable limit cycles, $(\cdots)$ unstable limit cycles, PD = period-doubling bifurcation, CF = cyclic-fold bifurcation, and SB = symmetry-breaking bifurcation.

c. It then goes through a sequence of period-doubling bifurcations resulting in a chaotic attractor, as shown in Figures 4.13d-f. Increasing σ further, the chaotic attractor grows and deforms, as shown in parts g and h, then goes through a sequence of reverse period-doubling bifurcations, resulting in a larger limit cycle, as shown in Figure 4.13j.

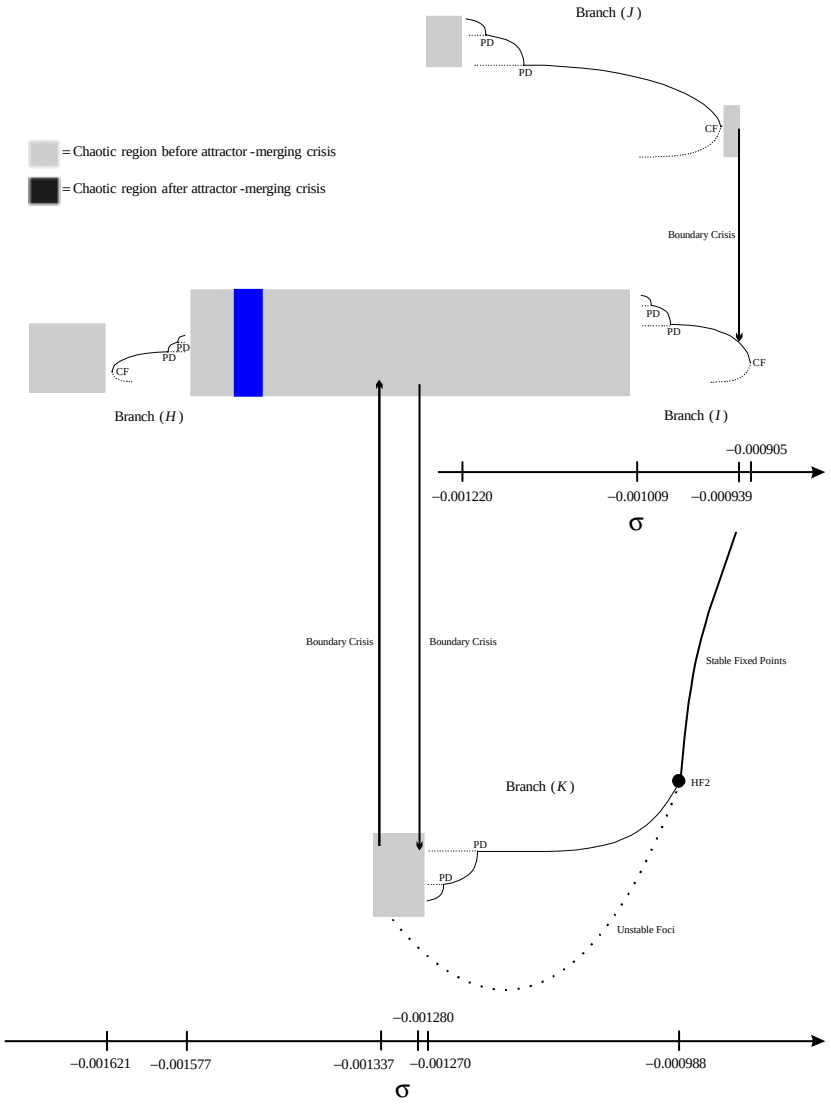

Figure 4.12: A schematic of the dynamic solutions found on branches I, J, K, and L for modes (2,2) when $\delta_2 = 0.002$, $\Lambda_8 f = 0.00006$, and $\mu_1 = \mu_2 = 0.02$. (——) Stable limit cycles, $(\cdots)$ unstable limit cycle, PD = period-doubling bifurcation, CF = cyclic-fold bifurcation, and HF2 = Hopf bifurcations.

As σ is increased further, the asymmetric limit cycle in Figure 4.13j and its clone approach a saddle-focus, as shown in Figures 4.14a and b. When $\sigma = -0.011056$ (σ_{HB}), the orbits become homoclinic to the saddle-focus located at $(p_1, q_1, p_2, q_2) = (0, 0, -0.0163588, 0.0141822)$. This is confirmed by the fact that the period of the limit cycle approaches infinity as $\sigma \longrightarrow \sigma_{HB}$, as shown in Figure 4.15.

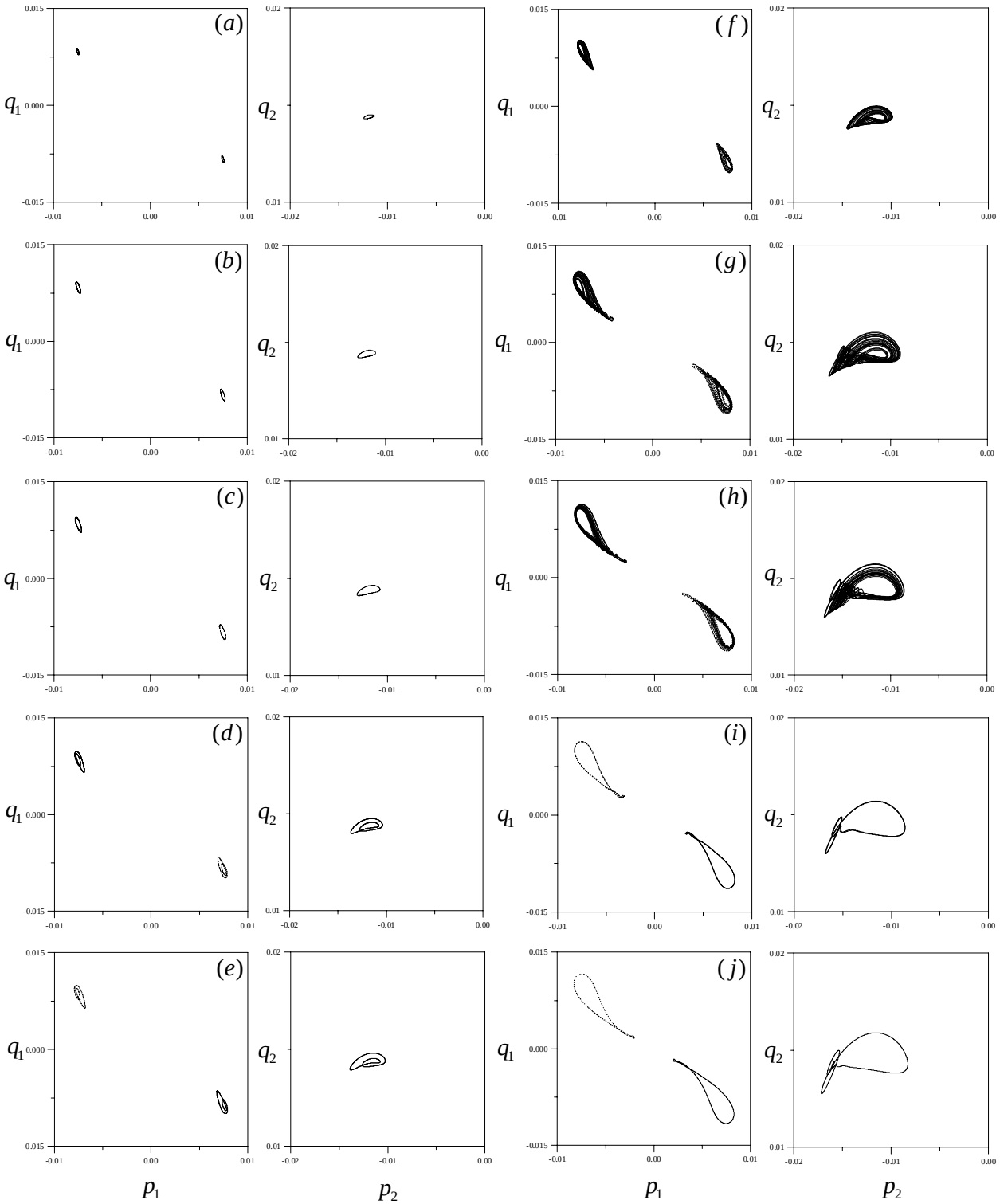

Figure 4.13: Two-dimensional projections of the phase portraits on the p_1q_1- and p_2q_2-planes showing bifurcations of the limit cycle on branch A. $\sigma_a = -0.011250$ (P1), $\sigma_b = -0.011230$ (P1), $\sigma_c = -0.011210$ (P1), $\sigma_d = -0.011190$ (P2), $\sigma_e = -0.011180$ (P4), $\sigma_f = -0.011160$ (Chaos), $\sigma_g = -0.011140$, $\sigma_h = -0.011120$, $\sigma_i = -0.011100$ (P2), and $\sigma_j = -0.011075$ (P1).

Following Shilnikov (1965, 1968, and 1970), we consider the three-dimensional system

$$\dot{x} = -\rho x - \omega y + f_1(x, y, z; \epsilon) \tag{4.21}$$

$$\dot{y} = -\rho y + \omega x + f_2(x, y, z; \epsilon) \tag{4.22}$$

$$\dot{z} = \mu z + f_3(x, y, z; \epsilon) \tag{4.23}$$

where ρ, ω, and μ are positive constants and the origin $(x, y, z, \epsilon) = (0, 0, 0, 0)$ is a saddle-focus. The eigenvalues of Eqs. (4.21)-(4.23) corresponding to the saddle-focus are given by $\lambda_{1,2} = -\rho \pm i\omega$ and $\lambda_3 = \mu$. Defining $\delta \equiv \frac{\rho}{\mu}$, then when there is an orbit homoclinic to a saddle-focus, Shilnikov proved the following result. If $\delta > 1$, the system has a periodic orbit on one side of the homoclinicity and no recurrent behavior on the other. As the orbit approaches the saddle-focus (i.e., $\epsilon \to 0$), its period tends to infinity. On the other hand, if $\delta < 1$, the system has an infinite number of unstable periodic orbits near the homoclinic orbit and hence the response is chaotic. Furthermore, Glendinning (1994) showed that if Eqs. (4.21)-(4.23) possess the symmetry $(x, y, z) \Longleftrightarrow (-x, -y, -z)$, then for $\delta > 1$, two asymmetric periodic orbits exist on one side of the homoclinicity, while one symmetric orbit exists on the other side.

Although, this theory is presented for three-dimensional systems, it applies to higher-dimensional systems provided that the eigenvalues of the Jacobian at the saddle-focus are as follows. First, of all the eigenvalues on the right-half of the complex plane, the closest to the imaginary axis must be real. Second, of all the eigenvalues on the left-half of the complex plane, the closest to the imaginary axis must be a pair of complex conjugates. The reverse is also true. That is, if the eigenvalue on the right-half of the complex plane closest to the imaginary axis is a complex pair, then the eigenvalue on the left-half of the complex plane closest to the imaginary axis must be real for application of the Shilnikov theory.

For the four-dimensional system analyzed here, these conditions are met as the eigenvalues of the Jacobian corresponding to the saddle-focus at $\sigma_{HB} = -0.011056$ are $\lambda_{1,2} = -0.02 \pm 0.113295i$, $\lambda_3 = 0.00643158$, and $\lambda_4 = -0.0464316$. Since the corresponding value of $\delta = 3.118 > 1$ and Eqs. (4.16)-(4.19) exhibit the symmetry $(p_1, q_1, p_2, q_2) \Longleftrightarrow (-p_1, -q_1, p_2, q_2)$, we expect to have two periodic orbits on one side of the homoclinicity and a single symmetric orbit on the other

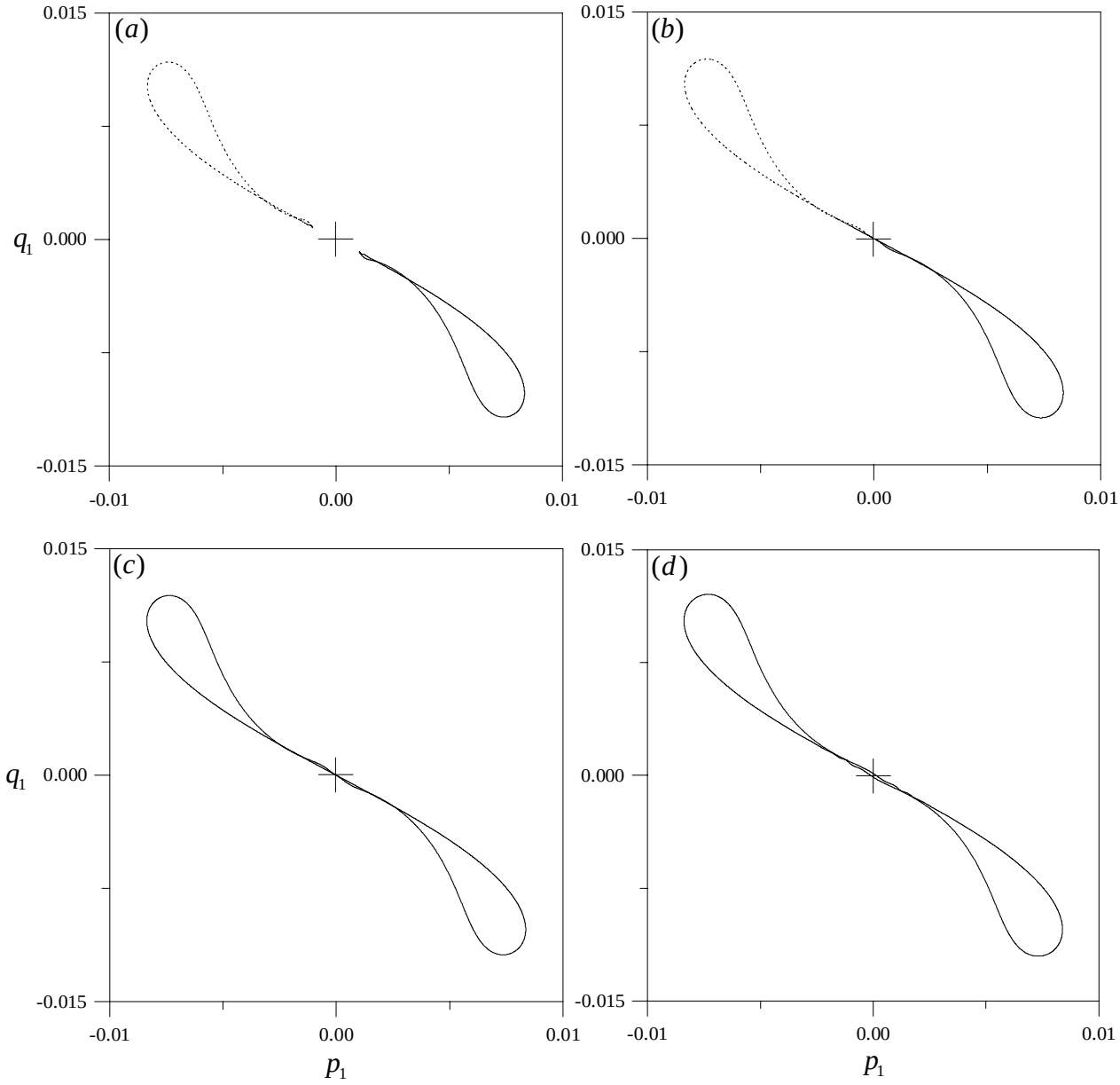

Figure 4.14: Two-dimensional projections of the phase portraits on the p_1q_1-plane of the limit cycle on branch A, before and after homoclinicity to the saddle-focus. $\sigma_a = -0.011060$, $\sigma_b = -0.011056$, $\sigma_c = -0.011055$, and $\sigma_d = -0.011045$

side, as shown in Figure 4.14. In Figure 4.16, we present the time histories of p_1 and p_2 before the homoclinicity at $\sigma = -0.011056$ and after the homoclinicity at $\sigma = -0.011055$. The period of the asymmetric limit cycle at $\sigma = -0.011056$ is approximately 990.6 whereas, the period of the symmetric limit at $\sigma = -0.011055$ is approximately 1729.3. As σ increases further, the symmetric

limit cycle loses symmetry and goes through a period-doubling route to chaos. The chaotic attractor then undergoes a boundary crisis, resulting in a jump to the branch of single-mode fixed points, as shown in Figure 4.8.

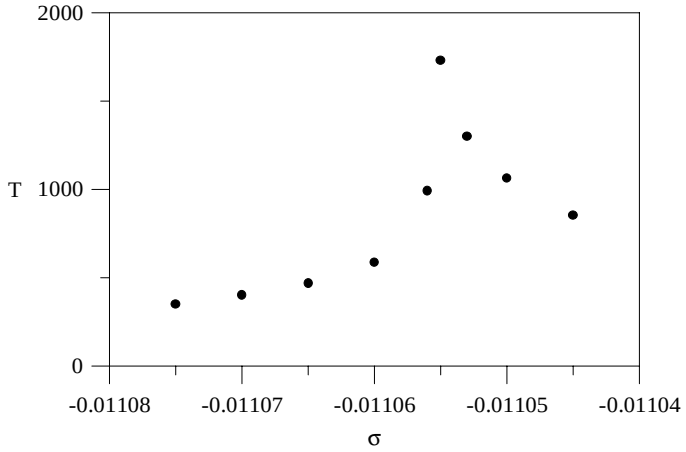

Figure 4.15: Variation of the period of the period-one limit cycle on branch A with changes in σ.

If follows from Figures 4.8-4.12 that period-doubling routes to chaos and bubble structures are very common. In a representative manner, we concentrate on the dynamics occurring on branch D, shown in Figure 4.10. In Figure 4.17a, we present two-dimensional phase portraits onto the p_1q_1-plane and FFTs of p_1 of a symmetric limit cycle on branch D at $\sigma = -0.0048$. As σ decreases beyond -0.004827, the limit cycle experiences a cyclic-fold bifurcation and the response becomes chaotic. As σ increases, the limit cycle goes through a symmetry-breaking bifurcation, as shown in part (b), followed soon by a reverse symmetry-breaking bifurcation, as shown in part (c). In parts (a) and (c), the FFT contains only odd harmonics, indicating that the limit cycle is symmetric, whereas in part (b), the FFT contains even and odd harmonics, indicating that the limit cycle is asymmetric. As σ increases further, the limit cycle experiences a cyclic-fold bifurcation and the response jumps to another subbranch. The symmetric limit cycle on this subbranch is shown in Figure 4.17d for $\sigma = -0.0045$. As σ decreases slightly, the limit cycle shown in part (d) experiences a cyclic-fold bifurcation and the response jumps back to the limit cycle shown in part (c).

The limit cycle in part (d) undergoes a symmetry-breaking bifurcation as σ increases, as shown in Figure 4.17e for $\sigma = -0.0044$. It then undergoes a sequence of period-doubling bifurcations, culminating in a single-band chaotic attractor, as shown in parts (f)-(i). The presence of subharmonics

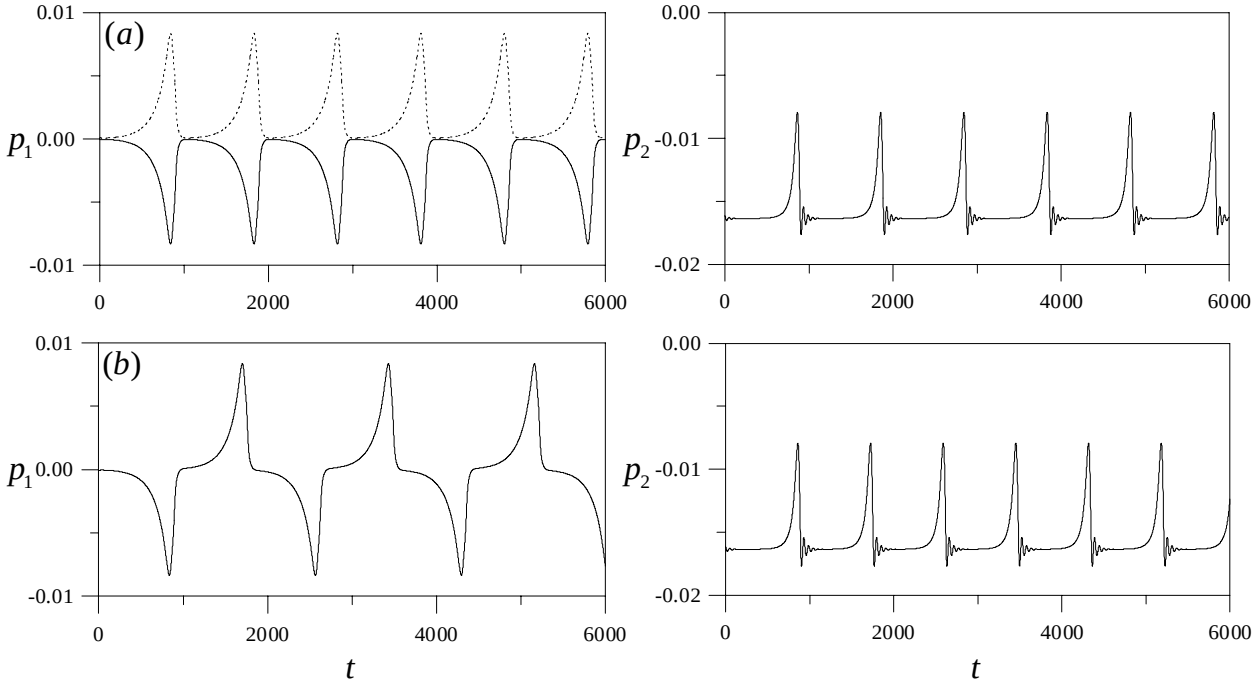

Figure 4.16: Time histories for p_1 and p_2 of the limit cycle on branch A, before and after homoclinicity to the saddle-focus. $\sigma_a = -0.011260$ and $\sigma_b = -0.011255$

of order $\frac{1}{k}$, $k = 2, 4, 8$, in the FFTs in parts (f)-(h) is a characteristic of period-k limit cycles. In addition, the broad-band nature of the FFT in part (i) is a characteristic of a chaotic attractor.

As σ is increased further, a small periodic window emerges, as shown in Figure 4.17(j) for $\sigma = -0.00432$. The FFT in part (j) contains harmonics of order $\frac{1}{3}$, indicating a window of a period-three limit cycle. Soon after, the periodic window closes and the response reverts to a two-band (Thompson and Stewart, 1988) chaotic attractor, as shown in part (k) for $\sigma = -0.00431$. The chaotic attractor then undergoes a sequence of reverse period-doubling bifurcations, parts (l) and (m), resulting in an asymmetric limit cycle, as shown in part (n) for $\sigma = -0.00423$. Soon after, this limit cycle experiences another sequence of period-doubling bifurcations, culminating in a chaotic attractor. The chaotic region separates branches D and E.

The dynamics in Figures 4.13c-j on branch A and Figures 4.17e-n on branch D are examples of bubble structures. Bubble structures where chaos does not ensue are also possible and were found on branches B, C, and G, as shown in Figures 4.9 and 4.11.

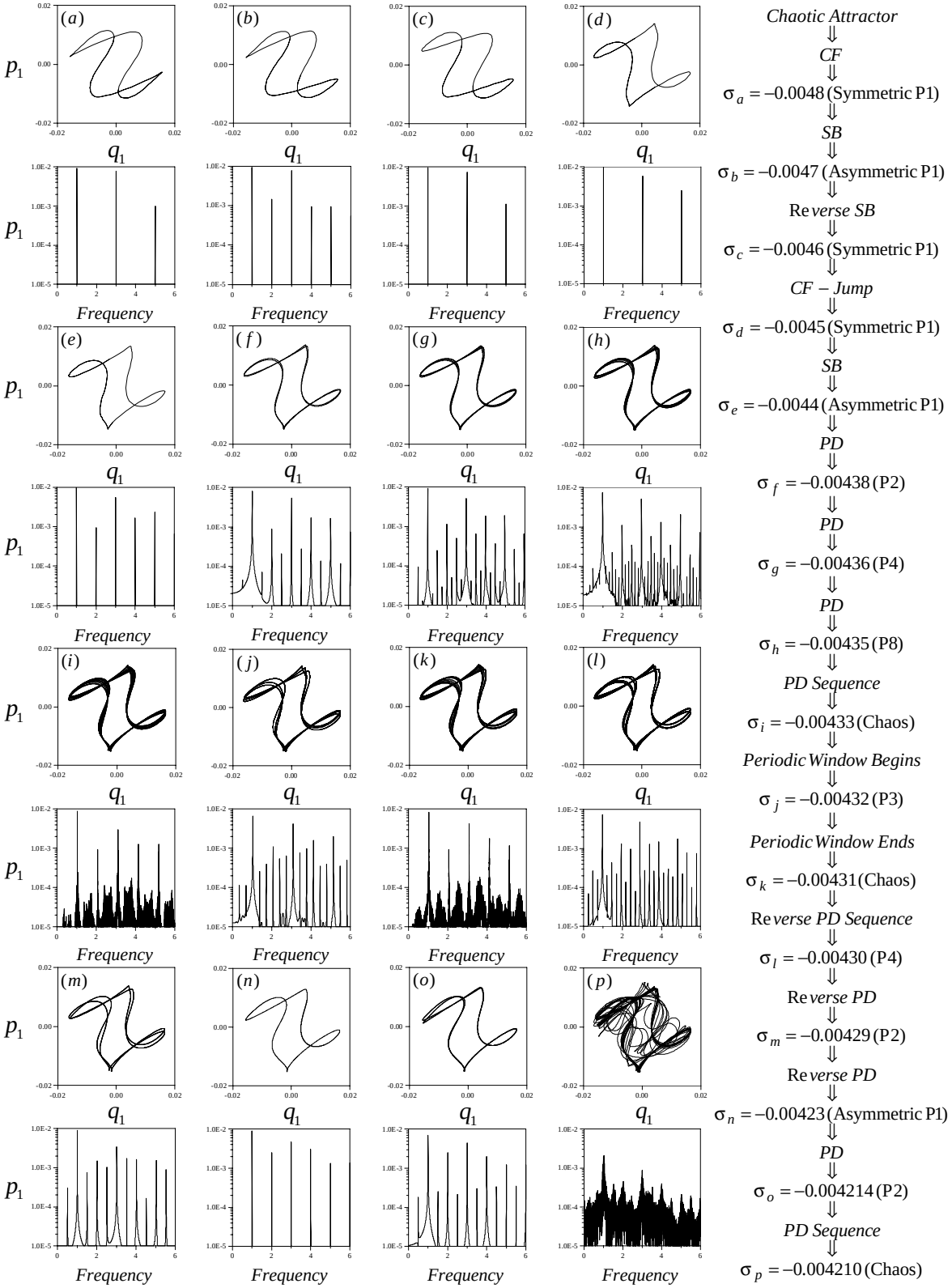

Figure 4.17: Two-dimensional projections of the phase portraits onto the p_1q_1-plane and FFT's of p_1 showing the dynamics that occur on Branch D as σ is slowly increased. CF = cyclic-fold bifurcation, SB = symmetry-breaking bifurcation, and PD = period-doubling bifurcation.

Other interesting dynamics the system exhibits include attractor-merging and boundary crises. In the case of attractor-merging crises, two asymmetric chaotic attractors merge together and form a single larger symmetric chaotic attractor. The reverse is also possible. Attractor merging crises were observed in the chaotic regions between the saddle-node SN and branch B, branches E and F, and branches H and I, as shown in Figure 4.7. Three different types of boundary crises were observed. In the first, a jump from a chaotic attractor to a fixed point (single-mode) occurred, as shown in Figure 4.9. In the second, a jump from a chaotic attractor to a limit cycle (on branch I) occurred. In the third, jumps between two chaotic attractors in both directions occurred. The last two types are illustrated in Figure 4.12.

Chapter 5

Nonlinear Bending-Bending-Torsional Oscillations of Cantilever Beams to Combination Parametric Excitations

The nonlinear nonplanar oscillations of cantilever beams to combination parametric resonances of the form $\Omega \approx \omega_v + \omega_\phi$ are investigated. Two approaches to determine uniform expansions of the solutions are presented. In the first, the method of multiple scales is directly applied to the partial-differential equations of motion and associated boundary conditions to derive the equations governing the modulations of the amplitudes and phases of the interacting modes. In the second, a set of three ordinary-differential equations is obtained using the Galerkin procedure. Then, the method of multiple scales is applied to determine the modulation equations. The influence of the forcing frequency and amplitude on the responses is analyzed and both solutions are compared. The results show that, through this mechanism, a small-amplitude high-frequency excitation can produce a large-amplitude low-frequency response, which cannot be predicted by linear theory.

5.1 Introduction

Using Eq. (3.1) in Eqs. (2.103)-(2.111) and neglecting rotatory inertia terms, we obtain the following nondimensional equations of motion and boundary conditions:

$$\begin{aligned}\ddot{v}+c_v\dot{v}+\beta_y v^{iv} &= (1-\beta_y)\left(\phi w''\right)'' - \Big\{ (1-\beta_y)\left(\phi^2 v''\right)'' + \beta_\gamma\left(\phi' w' + v'' w'^2\right)'' \\ &\quad - J_\xi \frac{\partial}{\partial t}\left(\dot{\phi} w' + \dot{v}' w'^2\right)' + \beta_y\left[v'\left(v'v''\right)' + v'\left(w'w''\right)'\right]' \\ &\quad + \frac{1}{2}\left[v'\int_1^s \frac{\partial^2}{\partial t^2}\int_0^s \left(v'^2+w'^2\right) ds ds\right]'\Big\} \qquad (5.1)\\ \ddot{w}+c_w\dot{w}+w^{iv} &= Q_w(t) + \Big\{\beta_\gamma\left(\phi' v'' + v''^2 w'\right)' + (1-\beta_y)\left(\phi^2 w'' + \phi v''\right)'' \\ &\quad - J_\xi\left(\dot{\phi}\dot{v}' + \dot{v}'^2 w'\right)' - \left[w'\left(w'w''\right)'\right]' - \beta_y\left[w'\left(v'v''\right)'\right]' \\ &\quad - \frac{1}{2}\left[w'\int_1^s \frac{\partial^2}{\partial t^2}\int_0^s \left(v'^2+w'^2\right) ds ds\right]'\Big\} \qquad (5.2)\\ J_\xi\ddot{\phi}+c_\phi\dot{\phi}-\beta_\gamma\phi'' &= (1-\beta_y)\left(v''w''\right) + \Big\{\beta_\gamma\left(v''w'\right)' - (1-\beta_y)\left(\phi v''^2 - \phi w''^2\right) \\ &\quad - J_\xi\frac{\partial}{\partial t}\left(\dot{v}' w'\right)\Big\} \qquad (5.3)\end{aligned}$$

At the fixed end $s=0$,

$$v=0, \quad v'=0, \quad w=0, \quad w'=0, \quad \text{and} \quad \phi=0. \qquad (5.4)$$

At the free end $s=1$,

$$\begin{aligned}\beta_y v'' &= -\beta_\gamma\left(v''w'^2+\phi' w'\right) - (1-\beta_y)\left(\phi^2 v'' - \phi w'' - v' w' w''\right) \qquad (5.5)\\ \beta_y v''' &= -\beta_\gamma\left(\phi' w' + v'' w'^2\right)' - (1-\beta_y)\left(\phi^2 v'' - \phi w''\right)' \\ &\quad - \beta_y\left[v'\left(v'v''\right)' + v'\left(w'w''\right)'\right] + J_\xi\frac{\partial}{\partial t}\left(\dot{\phi}w' + \dot{v}'w'^2\right) \qquad (5.6)\\ w'' &= (1-\beta_y)\left(\phi^2 w'' + \phi v''\right) \qquad (5.7)\\ w''' &= \beta_\gamma\left(v''^2 w' + \phi' v''\right) + (1-\beta_y)\left(\phi^2 w'' + \phi v''\right)' \\ &\quad - \left[w'\left(w'w''\right)'\right] - \beta_y\left[w'\left(v'v''\right)'\right] - J_\xi\left(\dot{\phi}\dot{v}' + \dot{v}'^2 w'\right) \qquad (5.8)\end{aligned}$$

$$\beta_\gamma \phi' = -\beta_\gamma \left(v'' w' \right) \tag{5.9}$$

The beams considered here are assumed to have a large width-to-thickness ratio, and hence the

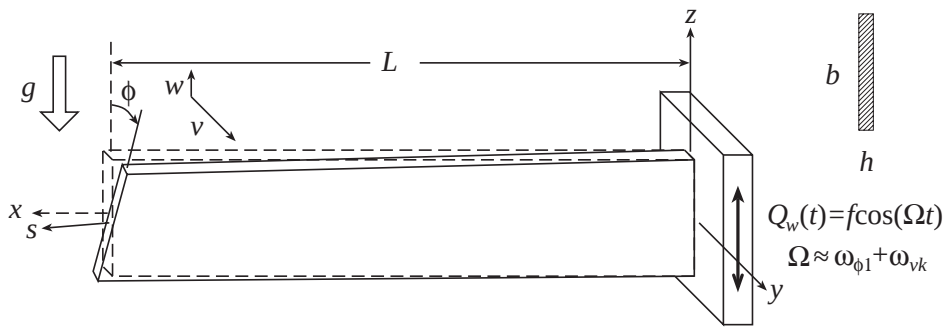

Figure 5.1: A schematic of a thin rectangular cantilever beam under combination parametric excitation.

out-of-plane bending rigidity is much higher than the in-plane bending and torsional rigidities. Equations (5.1)-(5.9) can be simplified to two partial-differential equations for $v(s,t)$ and $\phi(s,t)$ as follows. First, we neglect the nonlinear terms in the boundary conditions and those between the parenthesis in Eqs. (5.1)-(5.3). Second, because the beams are much more rigid in the out-of-plane bending direction, we assume that the out-of-plane oscillations are quasi-static; that is, $\dot{w}$ and $\ddot{w} \approx 0$. Then, it follows from Eq. (5.2) that $w'' = \frac{1}{2}(s-1)^2 Q_w(t)$. As a result, Eqs. (5.1) and (5.3) reduce to

$$\ddot{v} + c_v \dot{v} + \beta_y v^{iv} = \frac{1}{2}\left(1-\beta_y\right)\left[\phi(s-1)^2\right]'' Q_w(t) \tag{5.10}$$

$$J_\xi \ddot{\phi} + c_\phi \dot{\phi} - \beta_\gamma \phi'' = \frac{1}{2}\left(1-\beta_y\right)\left[v''(s-1)^2\right] Q_w(t) \tag{5.11}$$

Bolotin (1964) used Eqs. (5.10) and (5.11) to discuss the parametric stability of beam structures. Dugundji and Mukhopadhyay (1973) and Dokumaci (1978) analytically and experimentally investigated the stability of the linear responses of cantilever beams to the combination parametric resonances $\Omega \approx \omega_v + \omega_\phi$. Dugundji and Mukhopadhyay (1973) discretized Eqs. (5.10) and (5.11) using the Galerkin procedure and then applied the method of harmonic balance to calculate the boundaries of instabilities. On the other hand, Dokumaci (1978) applied the Rayleigh-Ritz method

and a perturbation technique to determine general expressions for the boundaries of instabilities.

Of particular interest here, are the results of the experiments of Dugundji and Mukhopadhyay (1973) conducted on an aluminum beam having the natural frequencies $f_{v1} = 1.08$ Hz, $f_{v2} = 7.0$ Hz, and $f_{\phi 1} = 17.0$ Hz. When they excited the beam near $\Omega = \omega_{v1} + \omega_{\phi 1}$, they observed it oscillating significantly both in bending and in torsion. Furthermore, at large excitation amplitudes, they observed the beam snapping-through and whipping around. This is despite the fact that the ratio of Ω to ω_{v1} is approximately $18:1$, demystifying the myth that high-frequency excitations only cause safe high-frequency low-amplitude vibrations.

5.2 Direct Perturbation Analysis of the Partial-Differential Equations of Motion and Boundary Conditions

We use the method of multiple scales to determine a second-order uniform expansion of the solution of Eqs. (5.1)-(5.9). To this end, we introduce the nondimensional parameter $\epsilon \ll 1$ as a measure of smallness and seek uniform expansions for v, w, and ϕ in the form

$$v(s,t) = \epsilon v_1(s,T_0,T_1,T_2) + \epsilon^2 v_2(s,T_0,T_1,T_2) + \epsilon^3 v_3(s,T_0,T_1,T_2) + \cdots \tag{5.12}$$

$$w(s,t) = \epsilon w_1(s,T_0,T_1,T_2) + \epsilon^2 w_2(s,T_0,T_1,T_2) + \epsilon^3 w_3(s,T_0,T_1,T_2) + \cdots \tag{5.13}$$

$$\phi(s,t) = \epsilon \phi_1(s,T_0,T_1,T_2) + \epsilon^2 \phi_2(s,T_0,T_1,T_2) + \epsilon^3 \phi_3(s,T_0,T_1,T_2) + \cdots \tag{5.14}$$

Furthermore, we scale the damping and forcing terms so that their effects balance the effect of the nonlinearities. So we replace c_v, c_w, and c_ϕ by $\epsilon^2 c_v$, $\epsilon^2 c_w$, and $\epsilon^2 c_\phi$ and set the forcing $Q_w(t) = \epsilon^2 f \cos(\Omega t)$, where $\Omega \approx \omega_v + \omega_\phi$. Next, we substitute Eqs. (5.12)-(5.14) into Eqs. (5.1)-(5.9), equate coefficients of like powers of ϵ, and obtain

Order ϵ

$$D_0^2 v_1 + \beta_y v_1^{iv} = 0 \tag{5.15}$$

$$J_\xi D_0^2 \phi_1 - \beta_\gamma \phi_1'' = 0 \tag{5.16}$$

$$D_0^2 w_1 + w_1^{iv} = 0 \tag{5.17}$$

$$v_1 = 0, \quad v_1' = 0, \quad \phi_1 = 0, \quad w_1 = 0, \quad \text{and} \quad w_1' = 0 \quad \text{at } s = 0 \tag{5.18}$$

$$v_1'' = 0, \quad v_1''' = 0, \quad \phi_1' = 0, \quad w_1'' = 0, \quad \text{and} \quad w_1''' = 0 \quad \text{at } s = 1 \tag{5.19}$$

Order ϵ^2

$$D_0^2 v_2 + \beta_y v_2^{iv} = -2D_0 D_1 v_1 + (1-\beta_y)\left(\phi_1 w_1''\right)'' + J_\xi D_0\left[(D_0\phi_1) w_1'\right]' - \beta_\gamma\left(\phi_1' w_1'\right)'' \tag{5.20}$$

$$J_\xi D_0^2 \phi_2 - \beta_\gamma \phi_2'' = -2J_\xi D_0 D_1 \phi_1 + (1-\beta_y)\left(v_1'' w_1''\right) - J_\xi D_0\left[\left(D_0 v_1'\right) w_1'\right] + \beta_\gamma\left(v_1'' w_1'\right)' \tag{5.21}$$

$$\begin{aligned} D_0^2 w_2 + w_2^{iv} = &-2D_0 D_1 w_1 - J_\xi\left[(D_0\phi_1)(D_0 v_1')\right]' + (1-\beta_y)(\phi_1 v_1'')'' + \beta_\gamma(\phi_1' v_1'')' \\ &+ f\cos(\Omega T_0) \end{aligned} \tag{5.22}$$

$$v_2 = 0, \quad v_2' = 0, \quad \phi_2 = 0, \quad w_2 = 0, \quad \text{and} \quad w_2' = 0 \quad \text{at } s = 0 \tag{5.23}$$

$$\begin{aligned} &v_2'' = 0, \quad \phi_2' = 0, \quad w_2'' = 0, \quad w_2''' = -J_\xi\left[(D_0\phi_1)(D_0 v_1')\right], \\ &\text{and} \quad \beta_y v_2''' = -\beta_\gamma\left(\phi_1' w_1'\right)' + J_\xi D_0\left[(D_0\phi_1) w_1'\right] \quad \text{at } s = 1 \end{aligned} \tag{5.24}$$

Order ϵ^3

$$\begin{aligned} D_0^2 v_3 + \beta_y v_3^{iv} = &-D_1^2 v_1 - 2D_0 D_2 v_1 - 2D_0 D_1 v_2 - c_v D_0 v_1 + J_\xi D_1\left[(D_0\phi_1) w_1'\right]' \\ &- \beta_\gamma\left(\phi_1' w_2' + \phi_2' w_1' + v_1'' w_1'^2\right)'' - \beta_y\left[v_1'\left(v_1' v_1''\right)' + v_1'\left(w_1' w_1''\right)'\right]' \\ &- (1-\beta_y)\left(\phi_1^2 v_1'' - \phi_1 w_2'' - \phi_2 w_1''\right)'' + J_\xi D_0\left[(D_0\phi_2) w_1' + (D_1\phi_1) w_1'\right. \\ &\left. + (D_0\phi_1) w_2' + \left(D_0 v_1'\right) w_1'^2\right]' - \frac{1}{2}\left[v_1'\int_1^s\int_0^s D_0^2(v_1'^2 + w_1'^2) ds ds\right]' \end{aligned} \tag{5.25}$$

$$\begin{aligned} J_\xi D_0^2\phi_3 - \beta_\gamma\phi_3'' = &-2J_\xi D_0 D_1\phi_2 - 2J_\xi D_0 D_2\phi_1 - J_\xi D_1^2\phi_1 - c_\phi D_0\phi_1 - J_\xi D_0\left[\left(D_0 v_1'\right) w_2'\right. \\ &\left. + \left(D_0 v_2'\right) w_1' + \left(D_1 v_1'\right) w_1'\right] - J_\xi D_1\left[\left(D_0 v_1'\right) w_1'\right] + \beta_\gamma\left(v_1'' w_2' + v_2'' w_1'\right)' \\ &- (1-\beta_y)\left(\phi_1 v_1''^2 - \phi_1 w_1''^2 - v_1'' w_2'' - v_2'' w_1''\right) \end{aligned} \tag{5.26}$$

$$v_3 = 0, \quad v_3' = 0, \quad \text{and} \quad \phi_3 = 0 \quad \text{at } s = 0 \tag{5.27}$$

$$\begin{aligned} v_3'' = 0, \quad \phi_3' = 0, \quad & \text{and} \\ \beta_y v_3''' = -\beta_\gamma \left(\phi_1' w_2' + \phi_2' w_1'\right)' + (1-\beta_y)\left(\phi_1 w_2''\right)' + J_\xi D_1 \left[(D_0\phi_1)\, w_1'\right] & \\ + J_\xi D_0 \Big[(D_0\phi_1) w_2' + (D_0\phi_2) w_1' + (D_1\phi_1) w_1' + \left(D_0 v_1'\right) w_1'^2\Big] \quad \text{at } s = 1 & \end{aligned} \tag{5.28}$$

5.2.1 First-Order Problem

Because of the presence of damping and the absence of internal resonances, the steady-state response of the beam will consist of only the modes that are directly excited by the forcing. Hence, we take $w_1 = 0$ because none of the associated modes is directly or indirectly excited. Furthermore, we assume that v_1 and ϕ_1 consist of the modes excited by the combination resonance; that is,

$$v_1(s, T_0, T_1, T_2) = \Phi_v(s)\left[A_v(T_1, T_2) e^{i\omega_v T_0} + \text{cc}\right] \tag{5.29}$$

$$\phi_1(s, T_0, T_1, T_2) = \Phi_\phi(s)\left[A_\phi(T_1, T_2) e^{i\omega_\phi T_0} + \text{cc}\right] \tag{5.30}$$

where cc stands for the complex conjugate of the preceding terms and A_v and A_ϕ are complex-valued functions, which will be determined at higher-order levels of approximation. The functions $\Phi_v(s)$ and $\Phi_\phi(s)$ are the linear undamped mode shapes for a cantilever beam. They are given by

$$\Phi_v(s) = \kappa_v \left\{\cosh zs - \cos zs + \frac{\cos(z) + \cosh(z)}{\sin(z) + \sinh(z)}\left[\sin zs - \sinh zs\right]\right\} \tag{5.31}$$

$$\Phi_\phi(s) = \kappa_\phi \sin\left[\frac{1}{2}(2n-1)\,\pi s\right] \tag{5.32}$$

where z is a root of $1 + \cos(z)\cosh(z) = 0$. The mode shape $\Phi_w(s)$ can be obtained from Eq. (5.31) by replacing the subscript v by w. The first five roots are 1.8751, 4.6941, 7.8548, 10.9955, and

14.1372. The constants κ_v and κ_ϕ are chosen so that

$$\int_0^1 \Phi_v^2 ds = 1 \qquad \text{and} \qquad \int_0^1 \Phi_\phi^2 ds = 1 \tag{5.33}$$

which yield 1 and $\sqrt{2}$, respectively. The nondimensional natural frequencies are given by

$$\omega_v = z^2\sqrt{\beta_y}, \quad \omega_w = z^2, \quad \text{and} \quad \omega_\phi = \frac{1}{2}(2n-1)\,\pi\sqrt{\frac{\beta_\gamma}{J_\xi}} \tag{5.34}$$

5.2.2 Second-Order Problem

Substituting Eqs. (5.29) and (5.30) into Eqs. (5.20)-(5.22), we obtain

$$D_0^2 v_2 + \beta_y v_2^{iv} = -2i\omega_v \Phi_v \frac{\partial A_v}{\partial T_1} e^{i\omega_v T_0} + cc \tag{5.35}$$

$$J_\xi D_0^2 \phi_2 - \beta_\gamma \phi_2'' = -2i\omega_\phi J_\xi \Phi_\phi \frac{\partial A_\phi}{\partial T_1} e^{i\omega_\phi T_0} + cc \tag{5.36}$$

$$\begin{aligned} D_0^2 w_2 + w_2^{iv} = {} & \Big[\beta_\gamma(\Phi_\phi'\Phi_v'')' + (1-\beta_y)(\Phi_\phi\Phi_v'')'' + J_\xi\omega_v\omega_\phi(\Phi_\phi\Phi_v')'\Big] A_\phi A_v e^{i(\omega_\phi+\omega_v)T_0} \\ & + \Big[\beta_\gamma(\Phi_\phi'\Phi_v'')' + (1-\beta_y)(\Phi_\phi\Phi_v'')'' - J_\xi\omega_v\omega_\phi(\Phi_\phi\Phi_v')'\Big] A_\phi \bar{A}_v e^{i(\omega_\phi-\omega_v)T_0} \\ & + \frac{1}{2} f e^{i\Omega T_0} + \text{cc} \end{aligned} \tag{5.37}$$

The boundary conditions at $s = 0$ are given by Eq. (5.23), whereas at $s = 1$, Eqs. (5.24) become

$$\begin{aligned} & v_2'' = 0, \quad v_2''' = 0, \quad \phi_2' = 0, \quad w_2'' = 0, \quad \text{and} \\ & w_2''' = J_\xi\omega_\phi\omega_v \left(\Phi_\phi\Phi_v'\right)_{s=1} \left[A_\phi A_v e^{i(\omega_\phi+\omega_v)T_0} - A_\phi \bar{A}_v e^{i(\omega_\phi-\omega_v)T_0} + \text{cc}\right] \end{aligned} \tag{5.38}$$

Eliminating the terms that produce secular terms from Eqs. (5.35) and (5.36), we obtain

$$\frac{\partial A_v}{\partial T_1} = 0 \quad \text{and} \quad \frac{\partial A_\phi}{\partial T_1} = 0 \tag{5.39}$$

Therefore, both A_v and A_ϕ are independent of the time scale T_1. Then, the solutions of Eqs. (5.23) and (5.35)-(5.38) can be expressed as

$$v_2 = 0 \tag{5.40}$$

$$\phi_2 = 0 \tag{5.41}$$

$$w_2 = \Phi_w(s)A_w e^{i\omega_w T_0} + \Phi_1(s)A_\phi A_v e^{i(\omega_\phi+\omega_v)T_0} + \Phi_2(s)A_\phi \bar{A}_v e^{i(\omega_\phi-\omega_v)T_0} + \Phi_3(s)e^{i\Omega T_0} + \text{cc} \tag{5.42}$$

The function $\Phi_1(s)$ is determined from the boundary-value problem

$$\Phi_1^{iv} - (\omega_\phi + \omega_v)^2\Phi_1 = \beta_\gamma(\Phi'_\phi\Phi''_v)' + (1-\beta_y)(\Phi_\phi\Phi''_v)'' + J_\xi\omega_v\omega_\phi(\Phi_\phi\Phi'_v)' \tag{5.43}$$

$$\Phi_1 = 0 \quad \text{and} \quad \Phi'_1 = 0 \qquad \text{at} \quad s = 0 \tag{5.44}$$

$$\Phi''_1 = 0 \quad \text{and} \quad \Phi'''_1 = J_\xi\omega_\phi\omega_v\left(\Phi_\phi\Phi'_v\right) \qquad \text{at} \quad s = 1 \tag{5.45}$$

The function $\Phi_2(s)$ is determined from the boundary-value problem

$$\Phi_2^{iv} - (\omega_\phi - \omega_v)^2\Phi_2 = \beta_\gamma(\Phi'_\phi\Phi''_v)' + (1-\beta_y)(\Phi_\phi\Phi''_v)'' - J_\xi\omega_v\omega_\phi(\Phi_\phi\Phi'_v)' \tag{5.46}$$

$$\Phi_2 = 0 \quad \text{and} \quad \Phi'_2 = 0 \qquad \text{at} \quad s = 0 \tag{5.47}$$

$$\Phi''_2 = 0 \quad \text{and} \quad \Phi'''_2 = -J_\xi\omega_\phi\omega_v\left(\Phi_\phi\Phi'_v\right) \qquad \text{at} \quad s = 1 \tag{5.48}$$

The function $\Phi_3(s)$ is determined from the boundary-value problem

$$\Phi_3^{iv} - \Omega^2\Phi_3 = \frac{1}{2}f \tag{5.49}$$

$$\Phi_3 = 0 \quad \text{and} \quad \Phi'_3 = 0 \qquad \text{at} \quad s = 0 \tag{5.50}$$

$$\Phi''_3 = 0 \quad \text{and} \quad \Phi'''_3 = 0 \qquad \text{at} \quad s = 1 \tag{5.51}$$

The general form of the functions $\Phi_1(s)$ and $\Phi_2(s)$ can be expressed as

$$\begin{aligned}\Phi_i(s) = &\sin\left[\frac{1}{2}(2n-1)\pi s\right][B_{i1}\sin zs + B_{i2}\cos zs + B_{i3}\sinh zs + B_{i4}\cosh zs] \\ &+ \cos\left[\frac{1}{2}(2n-1)\pi s\right][B_{i5}\sin zs + B_{i6}\cos zs + B_{i7}\sinh zs + B_{i8}\cosh zs] \\ &+ B_{i9}\sin r_i s + B_{i10}\cos r_i s + B_{i11}\sinh r_i s + B_{i12}\cosh r_i s \end{aligned} \tag{5.52}$$

where $r_i = \sqrt{\omega_\phi + \omega_v}$ when $i = 1$ and $\sqrt{\omega_\phi - \omega_v}$ when $i = 2$. On the other hand, the function $\Phi_3(s)$ is given by

$$\Phi_3(s) = C_1\sin r_3 s + C_2\cos r_3 s + C_3\sinh r_3 s + C_4\cosh r_3 s - \frac{f}{2\Omega^2} \tag{5.53}$$

where $r_3 = \sqrt{\Omega}$.

5.2.3 Third-Order Problem

To relate quantitatively the nearness of Ω to $\omega_v + \omega_\phi$, we introduce the detuning parameter σ so that

$$\Omega = \omega_v + \omega_\phi + \epsilon^2\sigma \tag{5.54}$$

Substituting Eqs. (5.29), (5.30), and (5.40)-(5.42) into Eqs. (5.25)-(5.28) and using Eq. (5.54), we obtain

$$D_0^2 v_3 + \beta_y v_3^{iv} = g(s, T_2)e^{i\omega_v T_0} + \text{cc} + \text{NST} \tag{5.55}$$

$$J_\xi D_0^2\phi_3 - \beta_\gamma \phi_3'' = h(s, T_2)e^{i\omega_\phi T_0} + \text{cc} + \text{NST} \tag{5.56}$$

$$v_3 = 0, \quad v_3' = 0, \quad \text{and} \quad \phi_3 = 0 \quad \text{at } s = 0 \tag{5.57}$$

$$v_3'' = 0, \quad \phi_3' = 0, \quad \text{and} \quad \beta_y v_3''' = g_0(T_2)e^{i\omega_v T_0} + \text{cc} + \text{NST} \quad \text{at } s = 1 \tag{5.58}$$

where NST stands for terms that do not produce secular terms and the functions g, h, and g_0 are defined in Appendix B.

Next, to determine the equation governing A_v, we seek a solution to Eqs. (5.55), (5.57), and (5.58) in the form

$$v_3(s, T_0, T_2) = \psi(s, T_2)e^{i\omega_v T_0} + \text{cc} + \text{NST} \tag{5.59}$$

Hence, ψ is given by the boundary-value problem

$$\beta_y \psi^{iv} - \omega_v^2 \psi = g \tag{5.60}$$

$$\psi(0) = 0, \quad \psi'(0) = 0, \quad \psi''(1) = 0, \quad \text{and} \quad \beta_y \psi'''(1) = g_0 \tag{5.61}$$

Because the homogeneous problem corresponding to Eqs. (5.60) and (5.61) has a nontrivial solution, the inhomogeneous problem has a solution only if a solvability condition is satisfied (Nayfeh, 1981). To determine this solvability condition, we multiply Eq. (5.60) by the adjoint $\psi^*(s)$, integrate over the spatial domain, transfer the derivatives from ψ to ψ^* using repeated integrations by parts, and obtain

$$\beta_y \left[\psi^* \psi''' - \psi^{*\prime} \psi'' + \psi^{*\prime\prime} \psi' - \psi^{*\prime\prime\prime} \psi \right]_{s=0}^{s=1} + \int_0^1 \left(\beta_y \psi^{*iv} - \omega_v^2 \psi^* \right) \psi ds = \int_0^1 g \psi^* ds \tag{5.62}$$

To determine the adjoint, we consider the homogeneous problem (i.e., $g = 0$ and $g_0 = 0$). For this case, it turns out that the resulting boundary-value problem for the adjoint is the same as the homogeneous problem, and therefore the system is self-adjoint and $\psi^* = \Phi_v$. Then, Eq. (5.62) reduces to the solvability condition

$$\int_0^1 \Phi_v g ds - \Phi_v(1) g_0 = 0 \tag{5.63}$$

Similarly, to determine the equation governing A_ϕ, we seek a solution to Eqs. (5.56)-(5.58) in the

form

$$\phi_3(s, T_0, T_2) = \chi(s, T_2)e^{i\omega_\phi T_0} + \text{cc} + \text{NST} \tag{5.64}$$

where χ is given by the boundary-value problem

$$\beta_\gamma \chi'' + \omega_\phi^2 J_\xi \chi = -h \tag{5.65}$$

$$\chi(0) = 0 \quad \text{and} \quad \chi'(1) = 0 \tag{5.66}$$

Repeating the same process as before, we find that this problem is also self-adjoint, and hence the adjoint $\chi^*(s) = \Phi_\phi(s)$ and the solvability condition is given by

$$\int_0^1 \Phi_\phi h ds = 0 \tag{5.67}$$

Substituting for the functions g, h, and g_0 from Appendix B in Eqs. (5.63) and (5.67), we obtain the following modulation equations governing the behavior of A_v and A_ϕ:

$$2i\omega_v \frac{dA_v}{dT_2} = -2i\omega_v \mu_v A_v + \Gamma_1 A_v^2 \bar{A}_v + \Gamma_2 A_v A_\phi \bar{A}_\phi + \Gamma_3 \bar{A}_\phi e^{i\sigma T_2} \tag{5.68}$$

$$2i\omega_\phi J_\xi \frac{dA_\phi}{dT_2} = -2i\omega_\phi \mu_\phi A_\phi + \Gamma_4 A_\phi A_v \bar{A}_v + \Gamma_5 \bar{A}_v e^{i\sigma T_2} \tag{5.69}$$

where

$$\Gamma_1 = \omega_v^2 \alpha_7 - \beta_y \alpha_8 \tag{5.70}$$

$$\Gamma_2 = -\left[\beta_\gamma \alpha_1 + (1 - \beta_y)\alpha_2 + \omega_v \omega_\phi J_\xi \alpha_3\right] \tag{5.71}$$

$$\Gamma_3 = -\left[\beta_\gamma \alpha_4 + (1 - \beta_y)\alpha_5 + \omega_v \omega_\phi J_\xi \alpha_6\right] \tag{5.72}$$

$$\Gamma_4 = -\left[\beta_\gamma \alpha_9 + (1 - \beta_y)\alpha_{10} + \omega_v \omega_\phi J_\xi \alpha_{11}\right] \tag{5.73}$$

$$\Gamma_5 = -\left[\beta_\gamma \alpha_{12} + (1 - \beta_y)\alpha_{13} + \omega_v \omega_\phi J_\xi \alpha_{14}\right] \tag{5.74}$$

and α_i, μ_v, and μ_ϕ are defined in the Appendix B. Because in the absence of damping, the original

system is Hamiltonian, we expect that the coefficients in the modulation equations exhibit the symmetries

$$\Gamma_2 = \Gamma_4 \qquad \text{and} \qquad \Gamma_3 = \Gamma_5 \tag{5.75}$$

5.3 Perturbation Analysis of the Discretized System

Another approach that is popular in solving such problems is to treat a discretized model of the partial-differential equations of motion and boundary conditions. Using single-mode discretization, we let

$$v(s,t) = \Phi_v(s)V(t) \tag{5.76}$$

$$w(s,t) = \Phi_w(s)W(t) \tag{5.77}$$

$$\phi(s,t) = \Phi_\phi(s)\eta(t) \tag{5.78}$$

in Eqs. (5.1)-(5.3), take the inner product of each equation with its corresponding mode shape, and obtain one ordinary-differential equation for each of V, W, and η as

$$\ddot{V} + c_v\dot{V} + \omega_v^2 V = \delta_1\eta W + \delta_2\left(\dot{\eta}W\right)^{\cdot} + \delta_3 V^3 + \delta_4 V\left(V^2\right)^{\cdot\cdot} + \delta_5\eta^2 V \tag{5.79}$$

$$\ddot{W} + c_w\dot{W} + \omega_w^2 W = \delta_6\eta V + \delta_7\dot{\eta}\dot{V} + \delta_8 f\cos(\Omega t) \tag{5.80}$$

$$J_\xi\ddot{\eta} + c_\phi\dot{\eta} + J_\xi\omega_\phi^2\eta = \delta_9 VW + \delta_{10}\left(\dot{V}W\right)^{\cdot} + \delta_{11}\eta V^2 \tag{5.81}$$

where the δ_i are constants defined in Appendix B.

Next, we use the method of multiple scales to seek a uniform expansion of the solutions of Eqs. (5.79)-(5.81) in the form

$$V(t) = \epsilon V_1(T_1,T_2) + \epsilon^2 V_2(T_1,T_2) + \epsilon^3 V_3(T_1,T_2) + \cdots \tag{5.82}$$

$$W(t) = \epsilon W_1(T_1,T_2) + \epsilon^2 W_2(T_1,T_2) + \epsilon^3 W_3(T_1,T_2) + \cdots \tag{5.83}$$

$$\eta(t) = \epsilon\eta_1(T_1,T_2) + \epsilon^2\eta_2(T_1,T_2) + \epsilon^3\eta_3(T_1,T_2) + \cdots \tag{5.84}$$

Substituting Eqs. (5.82)-(5.84) into Eqs. (5.79)-(5.81) and equating coefficients of like power of ϵ, we obtain

Order ϵ

$$D_0^2 V_1 + \omega_v^2 V_1 = 0 \tag{5.85}$$

$$D_0^2 W_1 + \omega_w^2 W_1 = 0 \tag{5.86}$$

$$J_\xi D_0^2 \eta_1 + J_\xi \omega_\phi^2 \eta_1 = 0 \tag{5.87}$$

Order ϵ^2

$$D_0^2 V_2 + \omega_v^2 V_2 = -2D_0 D_1 V_1 + \delta_1 \eta_1 W_1 + \delta_2 D_0 \left[\left(D_0 \eta_1 \right) W_1 \right] \tag{5.88}$$

$$D_0^2 W_2 + \omega_w^2 W_2 = -2D_0 D_1 W_1 + \delta_6 \eta_1 V_1 + \delta_7 \left(D_0 \eta_1 \right) \left(D_0 V_1 \right) + \delta_8 f \cos\left(\Omega T_0 \right) \tag{5.89}$$

$$J_\xi D_0^2 \eta_2 + J_\xi \omega_\phi^2 \eta_2 = -2J_\xi D_0 D_1 \eta_1 + \delta_9 V_1 W_1 + \delta_{10} D_0 \left[\left(D_0 V_1 \right) W_1 \right] \tag{5.90}$$

Order ϵ^3

$$\begin{aligned} D_0^2 V_3 + \omega_v^2 V_3 = & -2D_0 D_1 V_2 - 2D_0 D_2 V_1 - D_1^2 V_1 - c_v D_0 V_1 + \delta_1 \left(\eta_1 W_2 + \eta_2 W_1 \right) \\ & + \delta_2 \Big\{ D_0 \left[\left(D_0 \eta_1 \right) W_2 \right] + D_0 \left[\left(D_0 \eta_2 \right) W_1 \right] + D_0 \left[\left(D_1 \eta_1 \right) W_1 \right] \\ & + D_1 \left[\left(D_0 \eta_1 \right) W_1 \right] \Big\} + \delta_3 V_1^3 + \delta_4 V_1 D_0^2 \left(V_1^2 \right) + \delta_5 \eta_1^2 V_1 \end{aligned} \tag{5.91}$$

$$\begin{aligned} D_0^2 W_3 + \omega_w^2 W_3 = & -2D_0 D_1 W_2 - 2D_0 D_2 W_1 - D_1^2 W_1 - c_w D_0 W_1 + \delta_6 \left(\eta_2 V_1 + \eta_1 V_2 \right) \\ & + \delta_7 \Big[\left(D_0 \eta_1 \right) \left(D_0 V_2 \right) + \left(D_0 \eta_2 \right) \left(D_0 V_1 \right) + \left(D_1 \eta_1 \right) \left(D_0 V_1 \right) \\ & + \left(D_0 \eta_1 \right) \left(D_1 V_1 \right) \Big] \end{aligned} \tag{5.92}$$

$$\begin{aligned} J_\xi D_0^2 \eta_3 + J_\xi \omega_\phi^2 \eta_3 = & -2J_\xi D_0 D_1 \eta_2 - 2J_\xi D_0 D_2 \eta_1 - J_\xi D_1^2 \eta_1 - c_\phi D_0 \eta_1 + \delta_9 \left(V_1 W_2 + V_2 W_1 \right) \\ & + \delta_{10} \Big\{ D_0 \left[\left(D_0 V_2 \right) W_1 \right] + D_0 \left[\left(D_1 V_1 \right) W_1 \right] + D_0 \left[\left(D_0 V_1 \right) W_2 \right] \\ & + D_1 \left[\left(D_0 V_1 \right) W_1 \right] \Big\} + \delta_{11} \eta_1 V_1^2 \end{aligned} \tag{5.93}$$

Carrying out the analysis at $O(\epsilon)$ and $O(\epsilon^2)$, we find that

$$V_1 = A_v(T_2) e^{i\omega_v T_0} + \bar{A}_v(T_2) e^{-i\omega_v T_0} \tag{5.94}$$

$$W_1 = A_w(T_2)e^{i\omega_w T_0} + \bar{A}_w(T_2)e^{-i\omega_w T_0} \tag{5.95}$$

$$\eta_1 = A_\phi(T_2)e^{i\omega_\phi T_0} + \bar{A}_\phi(T_2)e^{-i\omega_\phi T_0} \tag{5.96}$$

$$V_2 = 0 \tag{5.97}$$

$$W_2 = \Delta_1 A_v A_\phi e^{i(\omega_\phi+\omega_v)T_0} + \Delta_2 \bar{A}_v A_\phi e^{i(\omega_\phi-\omega_v)T_0} + \Delta_3 e^{i\Omega T_0} + \text{cc} \tag{5.98}$$

$$\eta_2 = 0 \tag{5.99}$$

where

$$\Delta_1 = \frac{(\delta_6 - \omega_v\omega_\phi\delta_7)}{\omega_w^2 - (\omega_\phi+\omega_v)^2}, \quad \Delta_2 = \frac{(\delta_6 + \omega_v\omega_\phi\delta_7)}{\omega_w^2 - (\omega_\phi-\omega_v)^2}, \quad \text{and} \quad \Delta_3 = \frac{\delta_8}{2\left(\omega_w^2 - \Omega^2\right)}f. \tag{5.100}$$

Then, substituting Eqs. (5.94)-(5.99) into Eqs. (5.91) and (5.93) and eliminating secular terms, we obtain the modulation equations in complex-valued form. They have the same form as Eqs. (5.68) and (5.69) except that the Γ_i are now defined as

$$\Gamma_1 = 3\delta_3 - 4\omega_v^2\delta_4 \tag{5.101}$$

$$\Gamma_2 = \delta_1\left(\Delta_1 + \Delta_2\right) + \delta_2\omega_v\omega_\phi\left(\Delta_1 - \Delta_2\right) + 2\delta_5 \tag{5.102}$$

$$\Gamma_3 = \left(\delta_1 + \delta_2\omega_v\omega_\phi\right)\Delta_3 \tag{5.103}$$

$$\Gamma_4 = \delta_9\left(\Delta_1 + \Delta_2\right) + \delta_{10}\omega_v\omega_\phi\left(\Delta_1 - \Delta_2\right) + 2\delta_{11} \tag{5.104}$$

$$\Gamma_5 = \left(\delta_9 + \delta_{10}\omega_v\omega_\phi\right)\Delta_3 \tag{5.105}$$

5.4 Response Analysis

We introduce the polar transformation

$$A_v = \frac{1}{2}a_v(T_2)e^{i\theta_v(T_2)} \quad \text{and} \quad A_\phi = \frac{1}{2}a_\phi(T_2)e^{i\theta_\phi(T_2)} \tag{5.106}$$

into Eqs. (5.68) and (5.69), separate real and imaginary parts, and obtain

$$a_v' = -\mu_v a_v + \frac{\Gamma_3}{2\omega_v}a_\phi\sin\gamma \tag{5.107}$$

$$a_v\theta_v' = -\frac{\Gamma_1}{8\omega_v}a_v^3 - \frac{\Gamma_2}{8\omega_v}a_v a_\phi^2 - \frac{\Gamma_3}{2\omega_v}a_\phi\cos\gamma \tag{5.108}$$

$$a_\phi' = -\mu_\phi a_\phi + \frac{\Gamma_5}{2\omega_\phi J_\xi}a_v\sin\gamma \tag{5.109}$$

$$a_\phi\theta_\phi' = -\frac{\Gamma_4}{8\omega_\phi J_\xi}a_\phi a_v^2 - \frac{\Gamma_5}{2\omega_\phi J_\xi}a_v\cos\gamma \tag{5.110}$$

$$\gamma = \sigma T_2 - \theta_v - \theta_\phi \tag{5.111}$$

Equations (5.107)-(5.111) admit two possible equilibrium (fixed-point) solutions: (a) $a_v = 0$ and $a_\phi = 0$ and the beam is not excited and (b) $a_v \neq 0$ and $a_\phi \neq 0$ and the beam's response is quasiperiodic. In the second case, Eqs. (5.108), (5.110), and (5.111) can be combined into a single equation governing γ:

$$\gamma' = \sigma + \left(\frac{\Gamma_1}{8\omega_v} + \frac{\Gamma_4}{8\omega_\phi J_\xi}\right)a_v^2 + \frac{\Gamma_2}{8\omega_v}a_\phi^2 + \left[\left(\frac{\Gamma_3}{2\omega_v}\right)\frac{a_\phi}{a_v} + \left(\frac{\Gamma_5}{2\omega_\phi J_\xi}\right)\frac{a_v}{a_\phi}\right]\cos\gamma \tag{5.112}$$

Setting the time derivatives equal to zero in Eqs. (5.107), (5.109), and (5.112) and solving the resulting equations, we obtain the equilibrium solutions

$$\Gamma_{eff}a_v^2 = -\sigma \pm (\mu_v + \mu_\phi)\sqrt{\frac{\Gamma_3\Gamma_5}{4\mu_v\mu_\phi\omega_v\omega_\phi J_\xi} - 1} \tag{5.113}$$

$$a_\phi^2 = \frac{\Gamma_5\mu_v\omega_v}{\Gamma_3\mu_\phi\omega_\phi J_\xi}a_v^2 \tag{5.114}$$

$$\sin\gamma = \pm\sqrt{\frac{4\mu_v\mu_\phi\omega_v\omega_\phi J_\xi}{\Gamma_3\Gamma_5}} \tag{5.115}$$

where the effective nonlinearity Γ_{eff} is

$$\Gamma_{eff} = \left[\left(\frac{\Gamma_1}{8\omega_v} + \frac{\Gamma_4}{8\omega_\phi J_\xi}\right) + \frac{\Gamma_2}{8\omega_v}\left(\frac{\Gamma_5\mu_v\omega_v}{\Gamma_3\mu_\phi\omega_\phi J_\xi}\right)\right] \tag{5.116}$$

The stability of the nontrivial equilibrium solutions can then be studied by calculating the eigenvalues of the Jacobian matrix of the modulations equations. Substituting Eqs. (5.29), (5.30), and (5.106) back into Eqs. (5.12) and (5.14), we find that to second order the in-plane bending

deflection and angle of torsion of the beam are given by

$$v(s,t) = \epsilon\Phi_v(s)a_v\cos(\omega_v t + \theta_v) + \cdots \tag{5.117}$$

$$\phi(s,t) = \epsilon\Phi_\phi(s)a_\phi\cos\left[\left(\omega_\phi + \epsilon^2\sigma\right)t - \gamma - \theta_v\right] + \cdots \tag{5.118}$$

As an example, we consider an aluminum beam having the following properties: $E = 10.1$Mpsi, $G = 3.7$Mpsi, $L = 13\,in$, $b = 0.992\,in$, and $h = 0.03\,in$. The corresponding nondimensional quantities are $J_\xi = 0.000486$, $\beta_y = 0.000915$, $\beta_\gamma = 0.001315$, $\omega_{v1} = 0.106$, $\omega_{v2} = 0.666$, $\omega_{\phi 1} = 2.584$, and $\omega_{w1} = 3.516$. We let $\mu_{v1} = 0.000242$, $\mu_{v2} = 0.001521$, and $\mu_{\phi 1} = 0.003659$. Values for the coefficients Γ_i and Γ_{eff} are presented in Table 5.1 for both the direct and discretization approaches.

Table 5.1: Values of Γ_i and Γ_{eff} for the cases $\Omega \approx \omega_{vk} + \omega_{\phi 1}$, $k = 1, 2$. In the discretization approach, ω_{w1} was used.

$\Omega \approx$ $\omega_{v1} + \omega_{\phi 1}$	Direct Approach	Discretization Approach
Γ_1	-0.0070	-0.0070
Γ_2	4.918	2.615
Γ_3	$0.373f$	$0.386f$
Γ_4	4.918	2.569
Γ_5	$0.373f$	$0.384f$
Γ_{eff}	522.160	273.001
$\Omega \approx$ $\omega_{v2} + \omega_{\phi 1}$	Direct Approach	Discretization Approach
Γ_1	91.713	91.713
Γ_2	278.930	-432.882
Γ_3	$-4.867f$	$-5.032f$
Γ_4	278.930	-433.340
Γ_5	$-4.867f$	$-5.025f$
Γ_{eff}	39342.719	-61034.424

We note from Table 5.1 that the symmetries given by Eq. (5.75) are satisfied when using the direct approach. However, this is not the case when using the discretization approach. This is because the discretization was done using the linear undamped mode shapes, and hence the nonlinearities in the boundary conditions were neglected, rendering the system non-Hamiltonian. Because the Lagrangian inherently contains the effect of nonlinearities in the boundary conditions, one can

remedy this inconsistency by first discretizing the Lagrangian and then obtaining the discretized equations of motion using Hamilton's principle.

Also, important to note from Table 5.1 are the significant discrepancies in the values of the Γ_i for both approaches. This is because, in the discretization approach, the influence of the spatial solution at order $O(\epsilon^2)$ is incorrectly accounted for in the modulation equations (Nayfeh, 1997).

In Figures 5.2 and 5.3 we present typical frequency-response curves when $f = 0.1$ and amplitude-response curves when $\sigma = 10$ for the case $\Omega \approx \omega_{v1} + \omega_{\phi 1}$. In Figures 5.4 and 5.5 we present typical frequency-response curves when $f = 0.1$ and amplitude-response curves when $\sigma = 10$ for the case $\Omega \approx \omega_{v2} + \omega_{\phi 1}$. For all figures, the curves in part (a) were obtained by using the direct approach and the curves in part (b) were obtained by using the discretization approach.

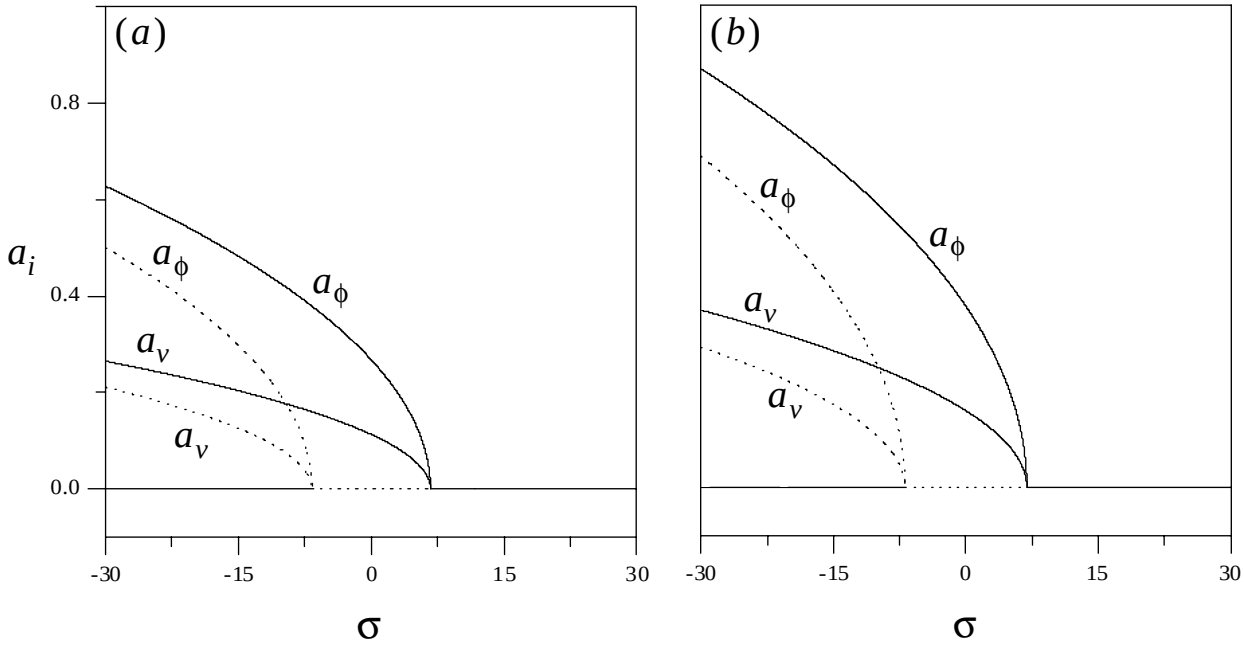

Figure 5.2: Frequency-response curves for the case $\Omega \approx \omega_{v1} + \omega_{\phi 1}$ when $f = 0.1$: (a) Direct approach and (b) discretization approach. (—) denote stable fixed points and $(\cdots)$ denote saddles.

In the case $\Omega \approx \omega_{v1} + \omega_{\phi 1}$, it can be concluded from Figures 5.2a and 5.2b and Figures 5.3a and 5.3b that the difference between analyzing the original partial-differential system and the discretized model is mainly quantitative. However, in the case $\Omega \approx \omega_{v2} + \omega_{\phi 1}$, the difference between the two approaches is qualitative as well as quantitative. It follows from Figures 5.4a and 5.4b

that the direct approach predicts a softening-spring behavior whereas the discretization approach predicts a hardening-spring behavior. Furthermore, in the direct approach, the modal interaction is activated as the trivial solution loses stability through a supercritical pitchfork bifurcation, whereas in the discretization approach, the trivial solution undergoes a subcritical pitchfork bifurcation, as shown in Figures 5.5a and 5.5b. Therefore, discretizing the system in this case leads to erroneous conclusions about the behavior.

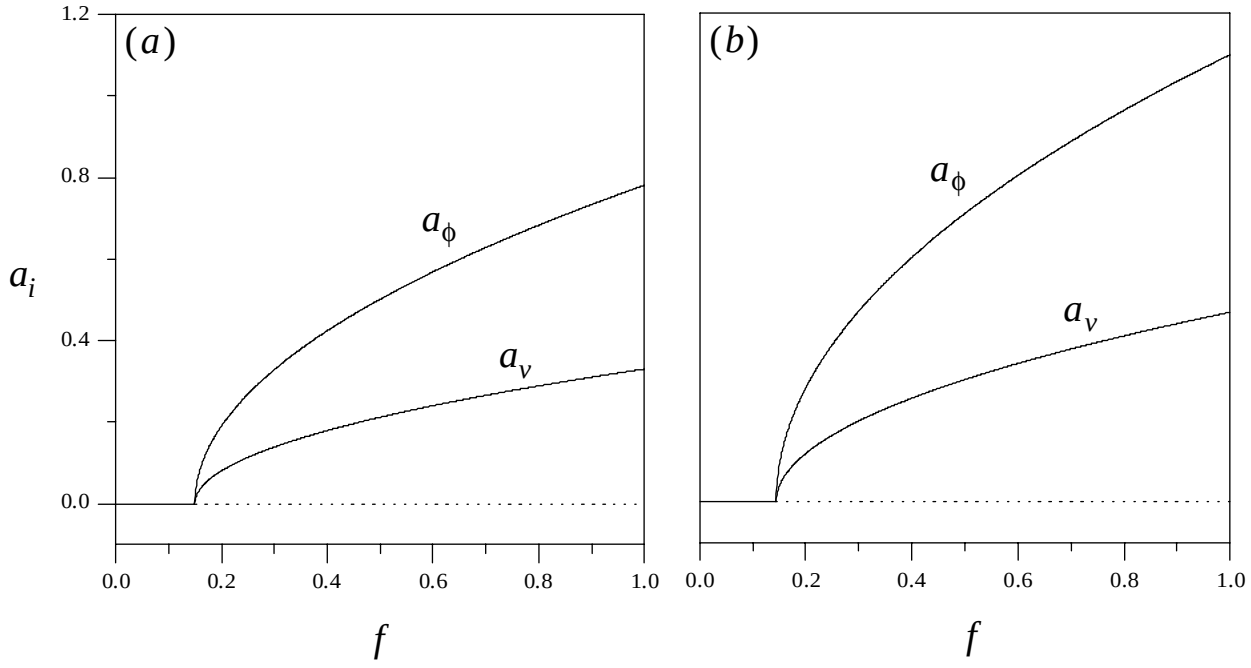

Figure 5.3: Amplitude-response curves for the case $\Omega \approx \omega_{v1}+\omega_{\phi 1}$ when $\sigma = 10$: (a) Direct approach and (b) discretization approach. (—) denote stable fixed points and $(\cdots)$ denote saddles.

Looking at Figures 5.2, 5.3, 5.4, and 5.5, one gets the impression that the amplitude of the torsional oscillations is much larger than the amplitude of the in-plane bending oscillations. This is misleading because a_ϕ is the amplitude of an angle, whereas a_v is the amplitude of a displacement. A more accurate representation would be to compare the maximum tip deflection due to twisting with the tip deflection due to bending. Therefore, we let

$$\rho_{Tip}(t) \equiv \frac{b}{2h}\phi(1,t) = \epsilon\frac{b}{2h}\Phi_\phi(1)a_\phi \cos\left[\left(\omega_\phi + \epsilon^2\sigma\right)t - \gamma - \theta_v\right] + \cdots \tag{5.119}$$

$$v_{Tip}(t) \equiv v(1,t) = \epsilon\Phi_v(1)a_v \cos\left[\omega_v t + \theta_v\right] + \cdots \tag{5.120}$$

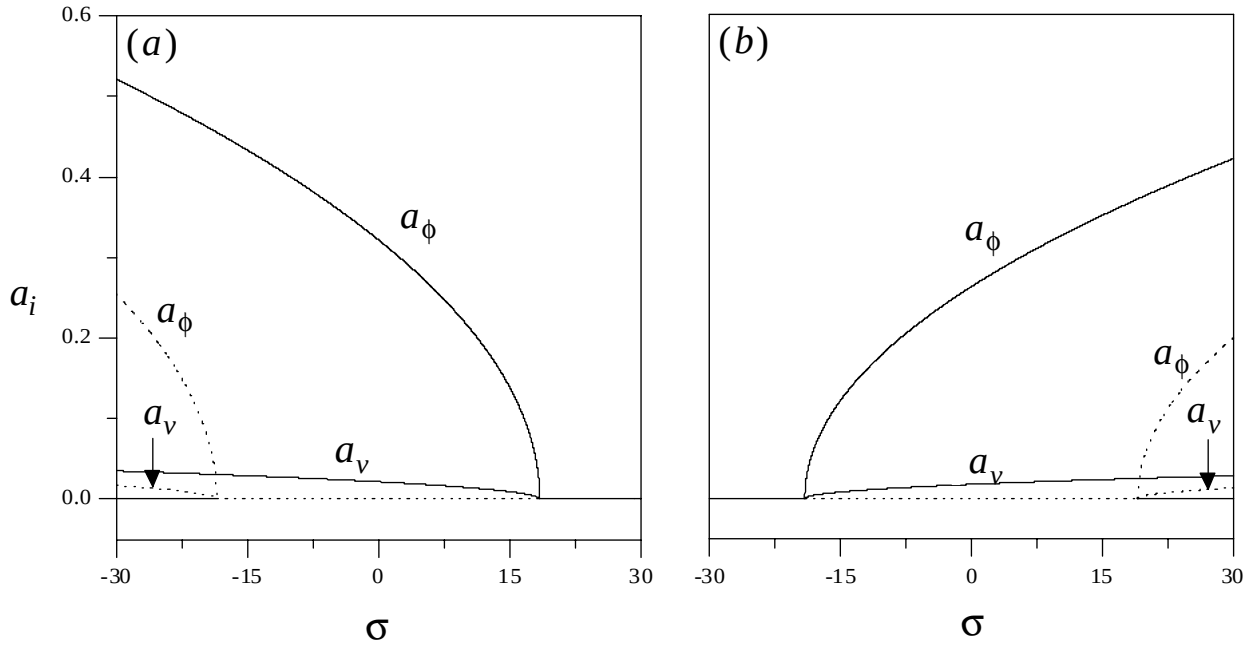

Figure 5.4: Frequency-response curves for the case $\Omega \approx \omega_{v2}+\omega_{\phi 1}$ when $f = 0.1$: (a) Direct approach and (b) discretization approach. (—) denote stable fixed points and $(\cdots)$ denote saddles.

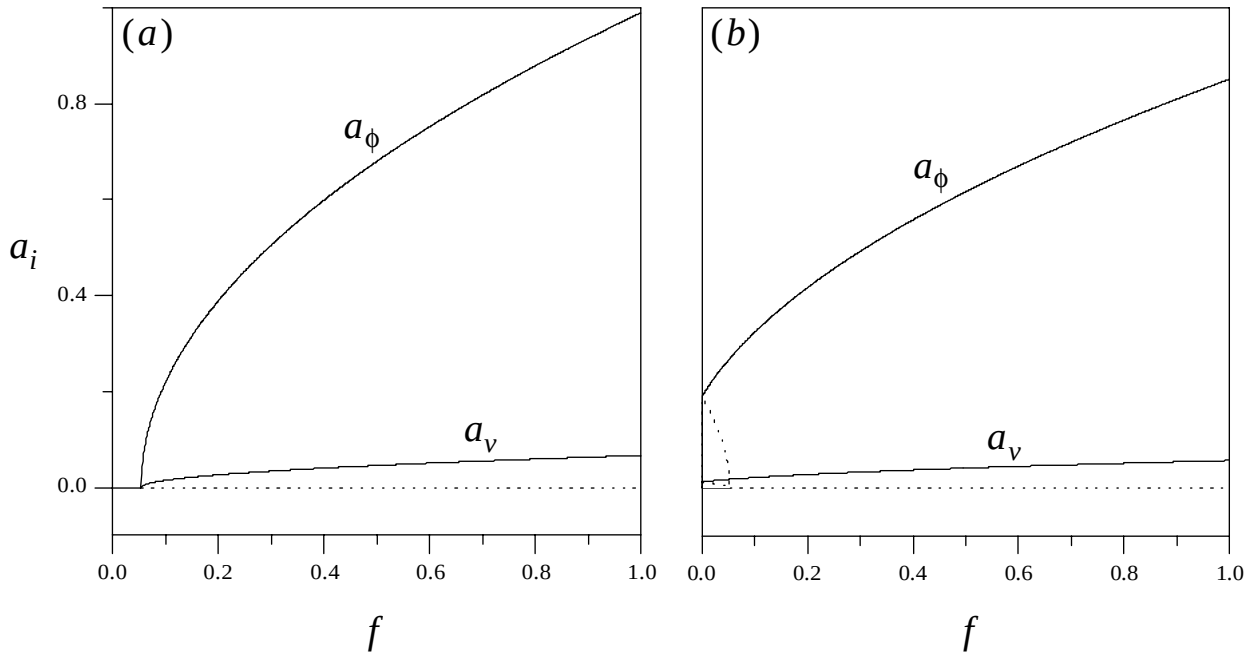

Figure 5.5: Amplitude-response curves for the case $\Omega \approx \omega_{v2}+\omega_{\phi 1}$ when $\sigma = 10$: (a) Direct approach and (b) discretization approach. (—) denote stable fixed points and $(\cdots)$ denote saddles.

In Figures 5.6 and 5.7 we present time histories of the beam's tip deflection v_{Tip} due to bending and the maximum tip deflection ρ_{Tip} due to twisting for the cases $\Omega \approx \omega_{v1} + \omega_{\phi 1}$ and $\Omega \approx \omega_{v2} + \omega_{\phi 1}$, respectively. Both figures reflect results using the direct approach and the parameters used are $f = 0.5$, $\sigma = 10$, and $\epsilon = 0.1$. Comparing Figures 5.6a and 5.6b and Figures 5.7a and 5.7b, one can see that the amplitude of the low-frequency vibrations due to bending are higher than the amplitude of the high-frequency vibrations due to torsion. Hence, the overall motion of the beam, although under a high-frequency excitation, may be dominated by a low-frequency high-amplitude component that, if ignored, may be disastrous.

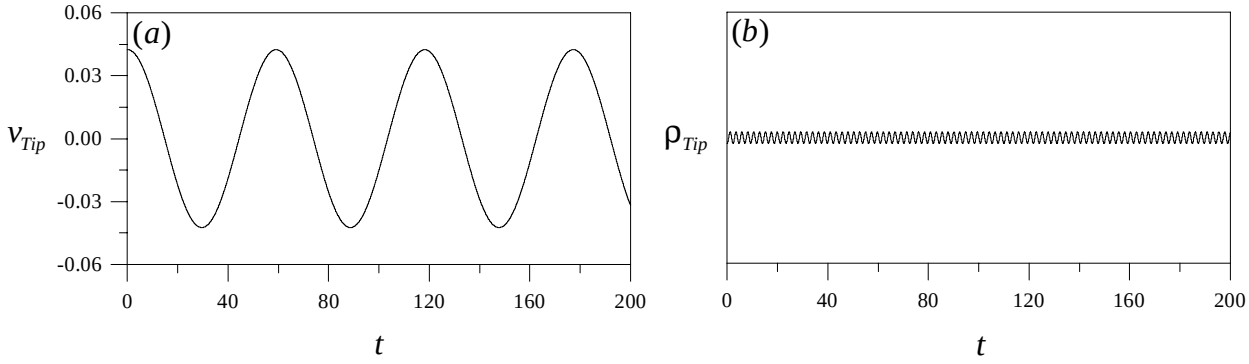

Figure 5.6: Time histories of the beam's tip for the case $\Omega \approx \omega_{v1} + \omega_{\phi 1}$ when $f = 0.5$, $\sigma = 10$, and $\epsilon = 0.1$: (a) Vibrations due to bending and (b) maximum vibrations due to twisting.

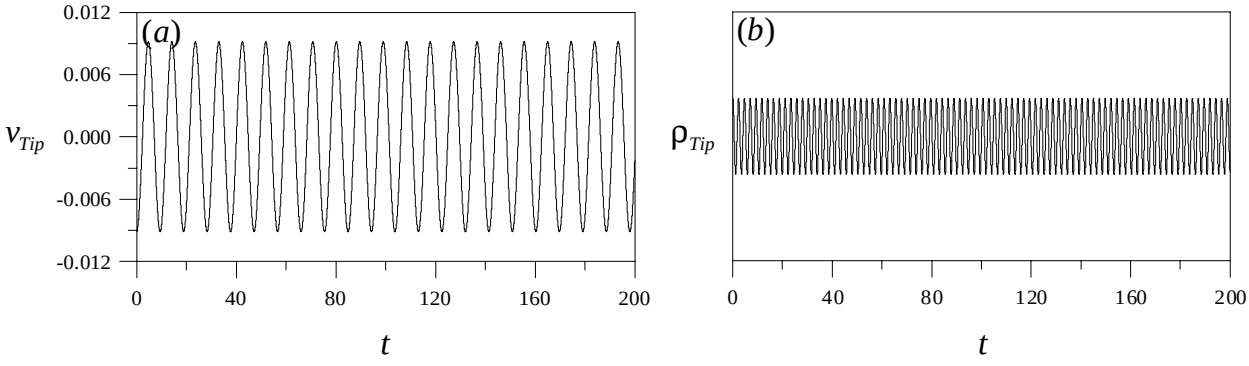

Figure 5.7: Time histories of the beam's tip for the case $\Omega \approx \omega_{v2} + \omega_{\phi 1}$ when $f = 0.5$, $\sigma = 10$, and $\epsilon = 0.1$: (a) Vibrations due to bending and (b) maximum vibrations due to twisting.

Chapter 6

Transfer of Energy from High- to Low-Frequency Modes in the Bending-Torsion Oscillations of Cantilever Beams

We investigate the nonlinear bending-torsion response of a cantilever beam to a transverse harmonic excitation, where the forcing frequency is near the natural frequency of the first torsional mode. Using perturbation techniques, we analyze the case where the first in-plane bending mode is activated by a non-resonant mechanism. Two approaches to analyze the system are presented. In the first, the method of multiple scales is directly applied to the governing nonlinear partial-differential equations and associated boundary conditions. In the second, the method of time-averaged Lagrangian and virtual-work term is used. In both cases, the modulation equations obtained are the same. These equations are then used to investigate the behavior of limit-cycle oscillations of the beam as the excitation amplitude is slowly varied. As an example, we consider the response of an aluminum beam for which the natural frequency of the first in-plane bending mode is $f_{v1} \approx 5.7$ Hz and the natural frequency of the first torsional mode is $f_{\phi 1} \approx 138.9$ Hz.

6.1 Introduction

Several recent experiments have demonstrated the transfer of energy from high-frequency modes to low-frequency modes of a system, resulting in overall large-amplitude oscillations. In most cases, the low-frequency modes are activated through a resonant mechanism, be it internal or external. Examples include two-to-one, three-to-one, combination, and subcombination resonances. In Chapter 5, we considered one such mechanism, namely the activation of low-frequency modes by a high-frequency excitation due to combination parametric resonances.

In some cases, however, low-frequency modes are activated even though they are not involved in a resonance relationship. This case is sometimes labeled *zero-to-one* resonance. A review of the works regarding this mechanism is presented in Section 1.3. Of importance are the experimental results of Anderson, Balachandran, and Nayfeh (1992, 1994), which dealt with the planar response of a cantilever beam, and Nayfeh and Nayfeh (1992, 1994), which dealt with the bending-bending response of a circular cross-section cantilever beam.

In experiments conducted on an aluminum beam with the same configuration shown in Figure 6.1 and having the natural frequencies $f_{v1} = 5.719$ Hz, $f_{\phi 1} = 138.938$ Hz, and $f_{w1} = 189.730$ Hz, we observed that, as the forcing amplitude is increased, the first in-plane bending mode was activated. As the forcing amplitude was increased further, the bending mode began to dominate the response, resulting in the beam oscillating at a large amplitude. In the frequency spectrum, we noticed the appearance of sidebands around $f_{\phi 1}$ that are approximately separated by f_{v1}. This is characteristic of the zero-to-one resonance. Increasing the excitation amplitude some more resulted in chaotic motions.

In this chapter, we investigate the nonlinear bending-torsion interactions of a cantilever beam due to nonresonant mechanisms. The beam considered is metallic and is assumed to be relatively long and to have a thin rectangular cross section. We excite the beam by a base harmonic forcing at a frequency near the natural frequency of the first torsional mode (i.e., fundamental parametric resonance). We apply the method of multiple scales directly to the governing partial-differential equations and associated boundary conditions to determine the modulation equations. We also show that one can obtain the same modulation equations by using the method of time-averaged

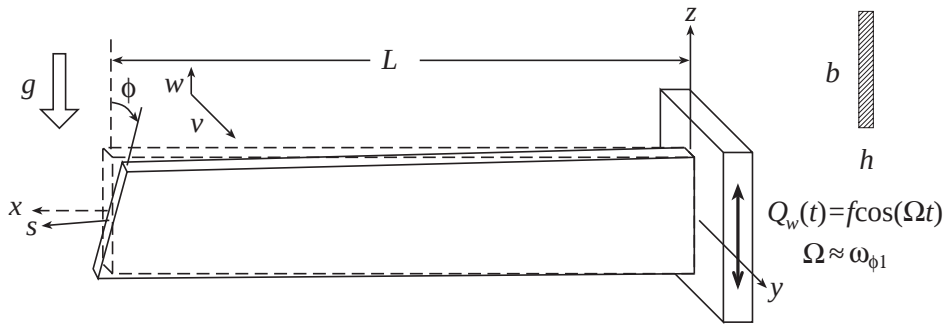

Figure 6.1: A schematic of a thin rectangular cantilever beam under fundamental parametric excitation.

Lagrangian. Furthermore, because, in the absence of damping, the governing equations are derivable from a Lagrangian and a virtual-work term, the coefficients in the modulation equations must exhibit certain symmetries.

6.2 Problem Formulation

The equations of motion and associated boundary conditions for the system considered here are obtained from Eqs. (2.103)-(2.111) by neglecting the rotatory inertia terms and setting $Q_u = Q_v = Q_\phi = 0$ and $Q_w = f\cos(\Omega t)$. As a result, we obtain

$$\begin{aligned} m\ddot{v} + c_v\dot{v} + D_\zeta v^{iv} &= -D_\xi\left(\phi' w' + v'' w'^2\right)'' - \left(D_\eta - D_\zeta\right)\left(\phi^2 v'' - \phi w''\right)'' \\ &\quad - D_\zeta\left[v'\left(v'v''\right)' + v'\left(w'w''\right)'\right]' + J_\xi\frac{\partial}{\partial t}\left(\dot{\phi}w' + \dot{v}'w'^2\right)' \\ &\quad - \frac{m}{2}\left\{v'\int_L^s\left[\frac{\partial^2}{\partial t^2}\int_0^s\left(v'^2 + w'^2\right)ds\right]ds\right\}' \end{aligned} \tag{6.1}$$

$$\begin{aligned} m\ddot{w} + c_w\dot{w} + D_\eta w^{iv} &= Q_w + D_\xi\left(\phi' v'' + v''^2 w'\right)' + \left(D_\eta - D_\zeta\right)\left(\phi^2 w'' + \phi v''\right)'' \\ &\quad - D_\eta\left[w'\left(w'w''\right)'\right]' - D_\zeta\left[w'\left(v'v''\right)'\right]' - J_\xi\left(\dot{\phi}\dot{v}' + \dot{v}'^2 w'\right)' \\ &\quad - \frac{m}{2}\left\{w'\int_L^s\left[\frac{\partial^2}{\partial t^2}\int_0^s\left(v'^2 + w'^2\right)ds\right]ds\right\}' \end{aligned} \tag{6.2}$$

$$J_\xi\ddot{\phi} + c_\phi\dot{\phi} - D_\xi\phi'' = D_\xi\left(v''w'\right)' + \left(D_\eta - D_\zeta\right)\left(v''w'' - \phi v''^2 + \phi w''^2\right) - J_\xi\frac{\partial}{\partial t}\left(\dot{v}'w'\right) \tag{6.3}$$

The associated boundary conditions are

$$v = 0, \quad v' = 0, \quad w = 0, \quad w' = 0, \quad \text{and} \quad \phi = 0 \quad \text{at the fixed end } s = 0, \tag{6.4}$$

and

$$D_\zeta v'' = -D_\xi \left(v''w'^2 + \phi' w'\right) - \left(D_\eta - D_\zeta\right)\left(\phi^2 v'' - \phi w'' - v'w'w''\right) \tag{6.5}$$

$$\begin{aligned} D_\zeta v''' = &-D_\xi \left(\phi' w' + w'^2 v''\right)' - \left(D_\eta - D_\zeta\right)\left(\phi^2 v'' - \phi w''\right)' \\ &- D_\zeta \left[v'\left(v'v''\right)' + v'\left(w'w''\right)'\right] + J_\xi \frac{\partial}{\partial t}\left(\dot\phi w' + w'^2 \dot v'\right) \end{aligned} \tag{6.6}$$

$$D_\eta w'' = \left(D_\eta - D_\zeta\right)\left(\phi^2 w'' + \phi v''\right) \tag{6.7}$$

$$\begin{aligned} D_\eta w''' = &D_\xi \left(w'v'^2 + v''\phi'\right) - D_\eta \left[w'\left(w'w''\right)'\right] - D_\zeta \left[w'\left(v'v''\right)'\right] \\ &+ \left(D_\eta - D_\zeta\right)\left(\phi^2 w'' + \phi v''\right)' - J_\xi \left(w'\dot v'^2 + \dot\phi \dot v'\right) \end{aligned} \tag{6.8}$$

$$D_\xi \phi' = -D_\xi \left(v''w'\right) \tag{6.9}$$

at the fixed end $s = L$. The Lagrangian and virtual-work term corresponding to Eqs. (6.1)-(6.9) are given by

$$\begin{aligned} \mathcal{L} = \frac{1}{2}\int_0^1 \Bigg\{ &m\left[\frac{1}{2}\frac{\partial}{\partial t}\int_0^s \left(v'^2 + w'^2\right) ds\right]^2 + m\left(\dot v^2 + \dot w^2\right) + J_\xi \left(\dot\phi + \dot v' w'\right)^2 \\ &- D_\eta \left(w''^2 + w'^2 w''^2\right) - D_\zeta \left(v''^2 + v'^2 v''^2 + 2v'v''w'w''\right) \\ &- D_\xi \left(\phi' + v''w'\right)^2 - \left(D_\eta - D_\zeta\right)\left[\phi^2\left(v''^2 - w''^2\right) - 2\phi v''w''\right] \Bigg\} ds \end{aligned} \tag{6.10}$$

$$\delta W = -\int_0^1 \left\{ c_v \dot v \delta v + c_\phi \dot\phi \delta\phi + \left[c_w \dot w - Q_w(t)\right]\delta w \right\} ds \tag{6.11}$$

6.3 Direct Perturbation Solution of the Partial-Differential Equations and Boundary Conditions

We use the method of multiple scales (Nayfeh, 1981) to determine a second-order uniform expansion for the solution of Eqs. (6.1)-(6.9). To this end, we introduce the nondimensional parameter $\epsilon \ll 1$

as a measure of smallness. An appropriate value in this case is $\epsilon = \frac{\omega_v}{\omega_\phi}$, where ω_v is the circular natural frequency of the first in-plane bending mode and ω_ϕ is the circular natural frequency of the first torsional mode.

Then, we see from the linear undamped response that, in order to accurately capture the interaction between the high- and low-frequency modes, we need to scale the linear in-plane bending stiffness term $D_\zeta v^{iv}$ as $\epsilon^2 D_\zeta v^{iv}$ in Eq. (6.1). Furthermore, we scale the damping and forcing terms so that their effects balance the effect of nonlinearities. So we scale c_v as ϵc_v, c_ϕ and c_w as $\epsilon^2 c_\phi$ and $\epsilon^2 c_w$, and set $Q_w(t) = \epsilon^2 f \cos(\Omega t)$.

Next, we seek a uniform expansions for v, w, and ϕ in the form of Eqs. (5.12)-(5.14). Substituting Eqs. (5.12)-(5.14) into Eqs. (6.1)-(6.9) and equating coefficients of like powers of ϵ, we obtain the following system of linear partial-differential equations and boundary conditions:

Order ϵ

$$mD_0^2 v_1 = 0 \tag{6.12}$$

$$J_\xi D_0^2 \phi_1 - D_\xi \phi_1'' = 0 \tag{6.13}$$

$$mD_0^2 w_1 + D_\eta w_1^{iv} = 0 \tag{6.14}$$

$$v_1 = 0, \quad v_1' = 0, \quad \phi_1 = 0, \quad w_1 = 0, \quad \text{and} \quad w_1' = 0 \quad \text{at } s = 0 \tag{6.15}$$

and

$$v_1'' = 0, \quad v_1''' = 0, \quad \phi_1' = 0, \quad w_1'' = 0, \quad \text{and} \quad w_1''' = 0 \quad \text{at } s = L \tag{6.16}$$

Order ϵ^2

$$\begin{aligned} mD_0^2 v_2 = &-2mD_0 D_1 v_1 + (D_\eta - D_\zeta)\left(\phi_1 w_1''\right)'' + J_\xi D_0\left[(D_0\phi_1) w_1'\right]' - D_\xi\left(\phi_1' w_1'\right)'' \\ &- c_v D_0 v_1 \end{aligned} \tag{6.17}$$

$$J_\xi D_0^2 \phi_2 - D_\xi \phi_2'' = -2J_\xi D_0 D_1 \phi_1 + (D_\eta - D_\zeta)\left(v_1'' w_1''\right) - J_\xi D_0\left[\left(D_0 v_1'\right) w_1'\right] + D_\xi\left(v_1'' w_1'\right)' \tag{6.18}$$

$$mD_0^2 w_2 + D_\eta w_2^{iv} = -2mD_0D_1w_1 + (D_\eta - D_\zeta)(\phi_1 v_1'')'' - J_\xi\left[(D_0\phi_1)(D_0v_1')\right]' + D_\xi(\phi_1'v_1'')' + f\cos(\Omega T_0) \tag{6.19}$$

$$v_2 = 0, \quad v_2' = 0, \quad \phi_2 = 0, \quad w_2 = 0, \quad \text{and} \quad w_2' = 0 \quad \text{at } s = 0 \tag{6.20}$$

and

$$v_2'' = 0, \quad D_\zeta v_2''' = -D_\xi\left(\phi_1'w_1'\right)' + J_\xi D_0\left[(D_0\phi_1)\,w_1'\right], \quad \phi_2' = 0, \quad w_2'' = 0, \quad \text{and} \quad D_\eta w_2''' = -J_\xi\left[(D_0\phi_1)(D_0v_1')\right] \quad \text{at } s = L \tag{6.21}$$

Order ϵ^3

$$\begin{aligned} mD_0^2v_3 = &-D_\zeta v_1^{iv} - m\left(2D_0D_1v_2 + D_1^2v_1 + 2D_0D_2v_1\right) - c_vD_0v_2 - c_vD_1v_1 \\ &- D_\xi\left(\phi_1'w_2' + \phi_2'w_1' + v_1''w_1'^2\right)'' - D_\zeta\left[v_1'\left(v_1'v_1''\right)' + v_1'\left(w_1'w_1''\right)'\right]' \\ &- (D_\eta - D_\zeta)\left(\phi_1^2v_1'' - \phi_1w_2'' - \phi_2w_1''\right)'' + J_\xi D_1\left[(D_0\phi_1)\,w_1'\right]' \\ &+ J_\xi D_0\left[(D_0\phi_2)\,w_1' + (D_1\phi_1)\,w_1' + (D_0\phi_1)\,w_2' + \left(D_0v_1'\right)w_1'^2\right]' \\ &- \frac{m}{2}\left[v_1'\int_L^s\int_0^s D_0^2(v_1'^2 + w_1'^2)dsds\right]' \end{aligned} \tag{6.22}$$

$$\begin{aligned} J_\xi D_0^2\phi_3 - D_\xi\phi_3'' = &-J_\xi\left(2D_0D_1\phi_2 + D_1^2\phi_1 + 2D_0D_2\phi_1\right) - c_\phi D_0\phi_1 - J_\xi D_1\left[\left(D_0v_1'\right)w_1'\right] \\ &- J_\xi D_0\left[\left(D_0v_1'\right)w_2' + \left(D_0v_2'\right)w_1' + \left(D_1v_1'\right)w_1'\right] + D_\xi\left(v_1''w_2' + v_2''w_1'\right)' \\ &- (D_\eta - D_\zeta)\left(\phi_1v_1''^2 - \phi_1w_1''^2 - v_1''w_2'' - v_2''w_1''\right) \end{aligned} \tag{6.23}$$

$$\begin{aligned} mD_0w_3 + D_\eta w_3^{iv} = &-m\left(2D_0D_1w_2 + D_1^2w_1 + 2D_0D_2w_1\right) - c_wD_0w_1 - D_\zeta\left[w_1'\left(v_1'v_1''\right)'\right]' \\ &- D_\eta\left[w_1'\left(w_1'w_1''\right)'\right]' + (D_\eta - D_\zeta)\left(\phi_1^2w_1'' + \phi_1v_2'' + \phi_2v_1''\right)'' + D_\xi\big(\phi_1'v_2'' \\ &+ \phi_2'v_1'' + v_1''^2w_1'\big)' - J_\xi\Big[(D_0\phi_1)(D_0v_2') + (D_0\phi_1)(D_1v_1') + (D_0\phi_2)(D_0v_1') \\ &+ (D_1\phi_1)(D_0v_1') + \left(D_0v_1'\right)^2w_1'\Big]' - \frac{m}{2}\left[w_1'\int_L^s\int_0^s D_0^2(v_1'^2 + w_1'^2)dsds\right]' \end{aligned} \tag{6.24}$$

$$v_3 = 0, \quad v_3' = 0, \quad \phi_3 = 0, \quad w_3 = 0, \quad \text{and} \quad w_3' = 0 \quad \text{at } s = 0 \tag{6.25}$$

and

$$\begin{aligned}
v_3'' = 0, \quad \phi_3' = 0, \quad w_3'' = 0,& \\
D_\zeta v_3''' = -D_\xi \left(\phi_1' w_2' + \phi_2' w_1' + v_1'' w_1'^2\right)' + (D_\eta - D_\zeta)\left(\phi_1 w_2''\right)' + J_\xi D_0 \Big[&(D_0\phi_1) w_2' \\
+ (D_0\phi_2) w_1' + (D_1\phi_1) w_1' + \left(D_0 v_1'\right) w_1'^2\Big] + J_\xi D_1 \left[(D_0\phi_1)\, w_1'\right],& \\
\text{and} \quad D_\eta w_3''' = (D_\eta - D_\zeta)\left(\phi_1 v_2''\right)' - J_\xi \Big[&(D_0\phi_1)(D_0 v_2') + (D_0\phi_1)(D_1 v_1') + (D_0\phi_2)(D_0 v_1') \\
+ (D_1\phi_1)(D_0 v_1') + \left(D_0 v_1'\right)^2 w_1'\Big] \quad \text{at } s = L&
\end{aligned} \tag{6.26}$$

6.3.1 First-Order Problem

Because of the presence of damping, the steady-state response of the beam will consist of only the modes that are directly excited by the forcing or indirectly excited by the zero-to-one internal resonance. Hence, the homogeneous solution

$$w_1(s, T_0, T_1, T_2) = \Phi_w(s)\left[A_w(T_1, T_2) e^{i\omega_w T_0} + \bar{A}_w(T_1, T_2) e^{-i\omega_w T_0}\right] \tag{6.27}$$

is assumed to die out as $t \to \infty$ since ω_w is neither commensurate with the forcing frequency Ω nor with the natural frequencies ω_v and ω_ϕ. Furthermore, the solutions for v_1 and ϕ_1 are expressed as

$$v_1(s, T_0, T_1, T_2) = \Phi_v(s)\eta(T_1, T_2) + V_1(s, T_1, T_2) T_0 \tag{6.28}$$

$$\phi_1(s, T_0, T_1, T_2) = \Phi_\phi(s)\left[A_\phi(T_1, T_2) e^{i\omega_\phi T_0} + \bar{A}_\phi(T_1, T_2) e^{-i\omega_\phi T_0}\right] \tag{6.29}$$

where η and A_ϕ are slowly time-varying functions, which will be determined at higher-order levels of approximation, and $\bar{A}_\phi$ is the complex conjugate of A_ϕ.

To ensure that the expansion for $v_1(s, T_0, T_1, T_2)$ remains uniform as T_0 becomes large, we set

$V_1(s, T_1, T_2) = 0$ in Eq. (6.28). Therefore, to first order, the in-plane bending oscillations are a function of the slow time scales, whereas the torsional oscillations are governed by both the fast and slow time scales. The functions $\Phi_v(s)$ and $\Phi_\phi(s)$ are the linear undamped mode shapes for cantilever beams and are given by

$$\Phi_v(s) = \kappa_v \left\{ \cosh\left(\frac{zs}{L}\right) - \cos\left(\frac{zs}{L}\right) + \frac{\cos(z) + \cosh(z)}{\sin(z) + \sinh(z)} \left[\sin\left(\frac{zs}{L}\right) - \sinh\left(\frac{zs}{L}\right) \right] \right\} \tag{6.30}$$

$$\Phi_\phi(s) = \kappa_\phi \sin\left[\frac{1}{2}(2n-1)\frac{\pi s}{L}\right], \quad n = 1, 2, \cdots \tag{6.31}$$

where z is a root of $1 + \cos(z)\cosh(z) = 0$. The mode shape $\Phi_w(s)$ can be obtained from Eq. (6.30) by replacing the subscript v by w. The first five roots are 1.8751, 4.6941, 7.8548, 10.9955, and 14.1372. The constants κ_v and κ_ϕ are chosen so that

$$\int_0^L \Phi_v^2 ds = 1 \qquad \text{and} \qquad \int_0^L \Phi_\phi^2 ds = 1 \tag{6.32}$$

which yield $\frac{1}{\sqrt{L}}$ and $\frac{\sqrt{2}}{\sqrt{L}}$, respectively. In addition, the corresponding circular natural frequencies are

$$\omega_v = z^2\sqrt{\frac{D_\zeta}{mL^4}}, \qquad \omega_w = z^2\sqrt{\frac{D_\eta}{mL^4}}, \qquad \text{and} \qquad \omega_\phi = \frac{1}{2}(2n-1)\frac{\pi}{L}\sqrt{\frac{D_\xi}{J_\xi}} \tag{6.33}$$

6.3.2 Second-Order Problem

We substitute Eqs. (6.28) and (6.29) into Eqs. (6.17)-(6.21) and obtain

$$mD_0^2 v_2 = 0 \tag{6.34}$$

$$J_\xi D_0^2 \phi_2 - D_\xi \phi_2'' = -2i\omega_\phi J_\xi \Phi_\phi \frac{\partial A_\phi}{\partial T_1} e^{i\omega_\phi T_0} + \text{cc} \tag{6.35}$$

$$mD_0^2 w_2 + D_\eta w_2^{iv} = \left[D_\xi (\Phi_\phi' \Phi_v'')' + (D_\eta - D_\zeta)(\Phi_\phi \Phi_v'')'' \right] \eta A_\phi e^{i\omega_\phi T_0} + \frac{1}{2} f e^{i\Omega T_0} + \text{cc} \tag{6.36}$$

$$v_2 = 0, \qquad v_2' = 0, \qquad \phi_2 = 0, \qquad w_2 = 0, \qquad \text{and} \qquad w_2' = 0 \qquad \text{at } s = 0 \tag{6.37}$$

$$v_2'' = 0, \qquad v_2'''' = 0, \qquad \phi_2' = 0, \qquad w_2'' = 0, \qquad \text{and} \qquad w_2'''' = 0 \qquad \text{at } s = L \tag{6.38}$$

where cc stands for the complex conjugate of the preceding terms. Eliminating the terms that produce secular terms in Eq. (6.35), we obtain

$$\frac{\partial A_\phi}{\partial T_1} = 0 \tag{6.39}$$

Therefore, A_ϕ is independent of the time scale T_1. However, the dependence of the function η on T_1 is still undetermined.

The solutions of Eqs. (6.34)-(6.38) are

$$\begin{aligned} &v_2(s, T_0, T_1, T_2) = 0, \quad \phi_2(s, T_0, T_1, T_2) = 0, \quad \text{and} \\ &w_2(s, T_0, T_1, T_2) = \Phi_w(s) A_w e^{i\omega_w T_0} + \Phi_1(s)\eta A_\phi e^{i\omega_\phi T_0} + \Phi_2(s) f e^{i\Omega T_0} + \text{cc} \end{aligned} \tag{6.40}$$

where the function $\Phi_1(s)$ is determined from the boundary-value problem

$$D_\eta \Phi_1^{iv} - m\omega_\phi^2 \Phi_1 = D_\xi(\Phi_\phi' \Phi_v'')' + (D_\eta - D_\zeta)(\Phi_\phi \Phi_v'')'' \tag{6.41}$$

$$\Phi_1 = 0 \quad \text{and} \quad \Phi_1' = 0 \qquad \text{at} \quad s = 0 \tag{6.42}$$

$$\Phi_1'' = 0 \quad \text{and} \quad \Phi_1''' = 0 \qquad \text{at} \quad s = L \tag{6.43}$$

and the function $\Phi_2(s)$ is determined from the boundary-value problem

$$D_\eta \Phi_2^{iv} - m\Omega^2 \Phi_2 = \frac{1}{2} \tag{6.44}$$

$$\Phi_2 = 0 \quad \text{and} \quad \Phi_2' = 0 \qquad \text{at} \quad s = 0 \tag{6.45}$$

$$\Phi_2'' = 0 \quad \text{and} \quad \Phi_2''' = 0 \qquad \text{at} \quad s = L \tag{6.46}$$

The general form of the functions $\Phi_1(s)$ and $\Phi_2(s)$ can be expressed as

$$\begin{aligned}\Phi_1(s) = &\sin\left[\frac{1}{2}(2n-1)\frac{\pi s}{L}\right]\left[B_1\sin\left(\frac{zs}{L}\right)+B_2\cos\left(\frac{zs}{L}\right)+B_3\sinh\left(\frac{zs}{L}\right)+B_4\cosh\left(\frac{zs}{L}\right)\right]\\ &+\cos\left[\frac{1}{2}(2n-1)\frac{\pi s}{L}\right]\left[B_5\sin\left(\frac{zs}{L}\right)+B_6\cos\left(\frac{zs}{L}\right)+B_7\sinh\left(\frac{zs}{L}\right)+B_8\cosh\left(\frac{zs}{L}\right)\right]\\ &+B_9\sin\left(\frac{r_1 s}{L}\right)+B_{10}\cos\left(\frac{r_1 s}{L}\right)+B_{11}\sinh\left(\frac{r_1 s}{L}\right)+B_{12}\cosh\left(\frac{r_1 s}{L}\right) \qquad (6.47)\end{aligned}$$

$$\Phi_2(s) = C_1\sin\left(\frac{r_2 s}{L}\right)+C_2\cos\left(\frac{r_2 s}{L}\right)+C_3\sinh\left(\frac{r_2 s}{L}\right)+C_4\cosh\left(\frac{r_2 s}{L}\right)-\frac{1}{2m\Omega^2} \qquad (6.48)$$

where $r_1 = \sqrt[4]{\frac{mL^4\omega_\phi^2}{D_\eta}}$ and $r_2 = \sqrt[4]{\frac{mL^4\Omega^2}{D_\eta}}$.

6.3.3 Third-Order Problem

To proceed further, we need to relate the excitation frequency Ω to the torsional natural frequency ω_ϕ. To this end, we introduce the detuning parameter σ so that

$$\Omega = \omega_\phi + \epsilon^2\sigma \qquad (6.49)$$

Then, substituting Eqs. (6.28), (6.29), and (6.40) into Eqs. (6.22)-(6.26) and using Eq. (6.49), we obtain

$$mD_0^2 v_3 = g(s,T_1,T_2) + \text{NST} \qquad (6.50)$$

$$J_\xi D_0^2\phi_3 - D_\xi\phi_3'' = h(s,T_1,T_2)e^{i\omega_\phi T_0} + \text{cc} \qquad (6.51)$$

where the functions g and h are defined in Appendix C and NST stands for terms that do not produce secular terms. The boundary conditions at the fixed end $s = 0$ are

$$v_3 = 0, \qquad v_3' = 0, \qquad \text{and} \qquad \phi_3 = 0 \qquad (6.52)$$

and the boundary conditions at the free end $s = L$ are

$$v_3'' = 0, \qquad \phi_3' = 0, \qquad \text{and} \qquad D_\zeta v_3''' = g_0(T_1,T_2) + \text{NST} \qquad (6.53)$$

where g_0 is defined in Appendix C.

Next, to determine the equations governing η and A_ϕ, we seek the solutions of Eqs. (6.50)-(6.53) in the form

$$v_3(s, T_0, T_1) = \psi(s, T_1) + \text{NST} \tag{6.54}$$

$$\phi_3(s, T_0, T_2) = \chi(s, T_2)e^{i\omega_\phi T_0} + \text{cc} + \text{NST} \tag{6.55}$$

where $\psi(s)$ is given by the boundary-value problem

$$D_\zeta \psi^{iv} - m\omega_v^2 \psi = g(s, T_1, T_2) \tag{6.56}$$

$$\psi(0) = 0, \quad \psi'(0) = 0, \quad \psi''(L) = 0, \quad \text{and} \quad D_\zeta \psi'''(L) = g_0(T_1, T_2) \tag{6.57}$$

and $\chi(s)$ is given by the boundary-value problem

$$D_\xi \chi'' + \omega_\phi^2 J_\xi \chi = -h(s, T_1, T_2) \tag{6.58}$$

$$\chi(0) = 0 \quad \text{and} \quad \chi'(L) = 0 \tag{6.59}$$

Following the argument presented in Section 5.2.3, we require the solutions of Eqs. (6.56)-(6.59) to be orthogonal to their respective adjoints $\psi^*(s) = \Phi_v(s)$ and $\chi^*(s) = \Phi_\phi(s)$. As a result, we obtain the following solvability conditions:

$$\int_0^L \Phi_v g ds - \Phi_v(L) g_0 = 0 \tag{6.60}$$

$$\int_0^L \Phi_\phi h ds = 0 \tag{6.61}$$

Substituting for the functions g, h, and g_0 from Appendix C into Eqs. (6.60) and (6.61), we obtain

the following modulation equations governing the behavior of $\eta(T_1)$ and $A_\phi(T_2)$:

$$m\frac{d^2\eta}{dT_1^2} = -c_v\frac{d\eta}{dT_1} - m\omega_v^2\eta + \alpha_1\eta^3 + 2\alpha_2\eta A_\phi\bar{A}_\phi + \alpha_3 f\left(A_\phi e^{-i\sigma T_2} + \bar{A}_\phi e^{i\sigma T_2}\right) \tag{6.62}$$

$$2i\omega_\phi J_\xi\frac{dA_\phi}{dT_2} = -i\omega_\phi c_\phi A_\phi + \beta_2\eta^2 A_\phi + \beta_3 f\eta e^{i\sigma T_2} \tag{6.63}$$

where the coefficients α_i and β_i are defined in Appendix C.

6.4 Perturbation Analysis Using the Method of Time-Averaged Lagrangian

We use the method of time-averaged Lagrangian as an alternate approach to obtaining the modulation equations governing the nonlinear dynamics of this system. To this end, we substitute Eqs. (5.12)-(5.14) directly into Eqs. (6.10) and (6.11), make use of the fact that $D_1A_\phi = 0$, $w_1 = 0$, $v_2 = 0$, and $\phi_2 = 0$, and obtain

$$\begin{aligned}\mathcal{L} = \frac{\epsilon^2}{2}\int_0^L \Big\{ & J_\xi(D_0\phi_1)^2 - D_\xi\phi_1'^2\Big\}ds + \frac{\epsilon^4}{2}\int_0^L \Big\{ m(D_1v_1)^2 + m(D_0w_2)^2 \\ & + 2J_\xi\Big[(D_0\phi_1)(D_0\phi_2) + (D_0\phi_1)(D_2\phi_1)\Big] - D_\eta w_2''^2 - D_\zeta\left[v_1''^2 + v_1'^2v_1''^2\right] \\ & - 2D_\xi\Big[\phi_1'\phi_3' + \phi_1'v_1''w_2'\Big] - (D_\eta - D_\zeta)\left[\phi_1^2v_1''^2 - 2\phi_1v_1''w_2''\right]\Big\}ds\end{aligned} \tag{6.64}$$

$$\delta W = -\epsilon^4\int_0^L\Big\{c_v(D_1v_1)\delta v_1 + c_\phi(D_0\phi_1)\delta\phi_1\Big\}ds \tag{6.65}$$

Next we substitute for v_1, ϕ_1, and w_2 from Eqs. (6.28), (6.29), and (6.40) in Eqs. (6.64) and (6.65), retain the slowly varying terms, and obtain the following time-averaged Lagrangian and virtual-work term:

$$\begin{aligned}\frac{<\mathcal{L}>}{\epsilon^4} = & \frac{1}{2}m\left(\frac{d\eta}{dT_1}\right)^2 - \frac{1}{2}m\omega_v^2\eta^2 + i\omega_\phi J_\xi\left(A_\phi\frac{d\bar{A}_\phi}{dT_2} - \bar{A}_\phi\frac{dA_\phi}{dT_2}\right) \\ & - \frac{1}{2}\nu_1\eta^4 + \nu_2\eta^2A_\phi\bar{A}_\phi + \nu_3 f\eta\left(A_\phi e^{-i\sigma T_2} + \bar{A}_\phi e^{i\sigma T_2}\right) + \text{constant} + \cdots\end{aligned} \tag{6.66}$$

$$\begin{aligned}\frac{<\delta W>}{\epsilon^4} &= -c_v\frac{d\eta}{dT_1}\delta\eta - i\omega_\phi c_\phi\left(A_\phi\delta\bar{A}_\phi - \bar{A}_\phi\delta A_\phi\right) + \cdots \\ &= Q_\eta\delta\eta + Q_\phi\delta A_\phi + \bar{Q}_\phi\delta\bar{A}_\phi\end{aligned} \tag{6.67}$$

where the ν_i are defined in Appendix C. Then, applying Hamilton's extended principle

$$\frac{d}{dT_1}\left[\frac{\partial < \mathcal{L} >}{\partial\left(\frac{d\eta}{dT_1}\right)}\right] - \frac{\partial < \mathcal{L} >}{\partial \eta} = Q_\eta \tag{6.68}$$

$$\frac{d}{dT_2}\left[\frac{\partial < \mathcal{L} >}{\partial\left(\frac{d\bar{A}_\phi}{dT_2}\right)}\right] - \frac{\partial < \mathcal{L} >}{\partial \bar{A}_\phi} = \bar{Q}_\phi \tag{6.69}$$

to Eqs. (6.66) and (6.67), we obtain the following modulation equations:

$$m\frac{d^2\eta}{dT_1^2} = -c_v\frac{d\eta}{dT_1} - m\omega_v^2\eta - 2\nu_1\eta^3 + 2\nu_2\eta A_\phi\bar{A}_\phi + \nu_3 f\left(A_\phi e^{-i\sigma T_2} + \bar{A}_\phi e^{i\sigma T_2}\right) \tag{6.70}$$

$$2i\omega_\phi J_\xi\frac{dA_\phi}{dT_2} = -i\omega_\phi c_\phi A_\phi + \nu_2\eta^2 A_\phi + \nu_3 f\eta e^{i\sigma T_2} \tag{6.71}$$

6.5 Response Analysis

Comparing Eqs. (6.70) and (6.71) with Eqs. (6.62) and (6.63), we find that the following symmetries must be satisfied:

$$\alpha_1 = -2\nu_1, \qquad \alpha_2 = \beta_2 = \nu_2, \qquad \text{and} \qquad \alpha_3 = \beta_3 = \nu_3 \tag{6.72}$$

Next, using the definitions $T_1 \equiv \epsilon t$ and $T_2 \equiv \epsilon^2 t$, substituting the Cartesian transformation

$$A_\phi = \frac{1}{2}\left(p - iq\right)e^{i\sigma T_2} \qquad \text{and} \qquad \bar{A}_\phi = \frac{1}{2}\left(p + iq\right)e^{-i\sigma T_2} \tag{6.73}$$

into Eqs. (6.70) and (6.71), and separating real and imaginary terms, we obtain a set of four first-order ordinary-differential equations that govern the modulations of η, ζ, p, and q as

$$\dot{\eta} = \epsilon\zeta \tag{6.74}$$

$$\dot{\zeta} = -\epsilon\left\{\frac{c_v}{m}\zeta + \omega_v^2\eta + \frac{2\nu_1}{m}\eta^3 - \frac{\nu_2}{2m}\eta\left(p^2 + q^2\right) - \frac{\nu_3}{m}pf\right\} \tag{6.75}$$

$$\dot{p} = -\epsilon^2\left\{\sigma q + \frac{c_\phi}{2J_\xi}p + \frac{\nu_2}{2\omega_\phi J_\xi}\eta^2 q\right\} \tag{6.76}$$

$$\dot{q} = -\epsilon^2 \left\{ -\sigma p + \frac{c_\phi}{2J_\xi} q - \frac{\nu_2}{2\omega_\phi J_\xi} \eta^2 p - \frac{\nu_3}{\omega_\phi J_\xi} \eta f \right\} \tag{6.77}$$

Alternatively, we can use the transformation

$$A_\phi = \frac{1}{2} a e^{i\theta} \qquad \text{and} \qquad \bar{A}_\phi = \frac{1}{2} a e^{-i\theta} \tag{6.78}$$

to express Eqs. (6.70) and (6.71) in polar form as

$$\dot{\eta} = \epsilon \zeta \tag{6.79}$$

$$\dot{\zeta} = -\epsilon \left\{ \frac{c_v}{m} \zeta + \omega_v^2 \eta + \frac{2\nu_1}{m} \eta^3 - \frac{\nu_2}{2m} \eta a^2 - \frac{\nu_3}{m} a f \cos\gamma \right\} \tag{6.80}$$

$$\dot{a} = -\epsilon^2 \left\{ \frac{c_\phi}{2J_\xi} a + \frac{\nu_3}{\omega_\phi J_\xi} \eta f \sin\gamma \right\} \tag{6.81}$$

$$a\dot{\gamma} = -\epsilon^2 \left\{ \sigma a + \frac{\nu_2}{2\omega_\phi J_\xi} \eta^2 a + \frac{\nu_3}{\omega_\phi J_\xi} \eta f \cos\gamma \right\} \tag{6.82}$$

where $\gamma = \theta - \epsilon^2 \sigma t$ and $a = \sqrt{p^2 + q^2}$.

To determine the equilibrium solutions, we set $\dot{\eta}$, $\dot{\zeta}$, $\dot{p}$, and $\dot{q} = 0$ in Eqs. (6.74)-(6.77). There are two possible solutions: (i) trivial fixed points where η, ζ, p, and $q = 0$ or (ii) nontrivial fixed points where $\zeta = 0$ but η, p, and $q \neq 0$. The stability of the fixed points can be examined from the eigenvalues λ_i of the Jacobian matrix of Eqs. (6.74)-(6.77). For this system, the characteristic equation is given by

$$\lambda^4 + \kappa_3 \lambda^3 + \kappa_2 \lambda^2 + \kappa_1 \lambda + \kappa_0 = 0 \tag{6.83}$$

Applying the Routh-Hurwitz criterion, we find that the equilibrium solutions are stable if

$$\kappa_3 > 0, \quad \kappa_2 \kappa_3 - \kappa_1 > 0, \quad \kappa_1(\kappa_2 \kappa_3 - \kappa_1) - \kappa_0 \kappa_3^2 > 0, \quad \text{and} \quad \kappa_0 > 0 \tag{6.84}$$

When $\kappa_0 = 0$, the equilibrium solutions undergo a static bifurcation. On the other hand, when $\kappa_1(\kappa_2 \kappa_3 - \kappa_1) - \kappa_0 \kappa_3^2 = 0$, the equilibrium solutions undergo a Hopf bifurcation.

For the trivial solution, the coefficients κ_i are given by

$$\kappa_0 = \epsilon^6\sigma^2\omega_v^2 + \frac{\epsilon^6 c_\phi^2\omega_v^2}{4J_\xi^2} + \frac{f^2\epsilon^6\sigma\nu_3^2}{mJ_\xi\omega_\phi} \tag{6.85}$$

$$\kappa_1 = \frac{\epsilon^5\sigma^2 c_v}{m} + \frac{\epsilon c_v c_\phi^2}{4mJ_\xi^2} + \frac{\epsilon^4 c_\phi\omega_v^2}{J_\xi} \tag{6.86}$$

$$\kappa_2 = \epsilon^4\sigma^2 + \frac{\epsilon^4 c_\phi^2}{4J_\xi^2} + \frac{\epsilon^3 c_v c_\phi}{mJ_\xi} + \epsilon^2\omega_v^2 \tag{6.87}$$

$$\kappa_3 = \frac{\epsilon c_v}{m} + \frac{\epsilon^2 c_\phi}{J_\xi} \tag{6.88}$$

Hence, it follows from Eq. (6.85) that the trivial solution loses stability when

$$f = \pm i\frac{\omega_v}{2\nu_3}\sqrt{\frac{m\omega_\phi}{J_\xi\sigma}}\sqrt{4J_\xi^2\sigma^2 + c_\phi} \tag{6.89}$$

or when

$$\sigma = -\frac{f^2\nu_3^2 \pm \sqrt{f^4\nu_3^4 - m^2c_\phi^2\omega_v^4\omega_\phi^2}}{2mJ_\xi\omega_v^2\omega_\phi} \tag{6.90}$$

which may be true only when $\sigma < 0$ in the first case and when $f^4\nu_3^4 - m^2c_\phi^2\omega_v^4\omega_\phi^2 > 0$ in the second case.

For the nontrivial fixed points, closed-form solutions are not readily available. Instead, we calculate them numerically using a pseudo-arclength continuation scheme (Nayfeh and Balachandran, 1995). It is worth noting, however, that the system (6.74)-(6.77) is invariant under the transformation $(\eta, \zeta, p, q) \Longleftrightarrow (\eta, \zeta, -p, -q)$. Hence, for any asymmetric solution, a second one can be obtained using this transformation.

6.6 Example

As an example, we consider an aluminum beam having the following properties: $E = 70$ GPa, $G = 26$ GPa, $L = 33.020\ cm$, $b = 2.520\ cm$, and $h = 0.076\ cm$. The corresponding quantities are $m = 0.052\ kg/m$, $J_\xi = 2.755 \times 10^{-6}\ kg \cdot m$, $D_\eta = 71.106\ N \cdot m^2$, $D_\zeta = 0.065\ N \cdot m^2$, and

Table 6.1: Values of the α_i, β_i, and ν_i for the aluminum beam considered.

Time-Averaged Lagrangian		Directly Attacking the Partial-Differential System			
ν_1	3072.39	α_1	-6144.77		
ν_2	42920.6	α_2	42920.6	β_2	42920.6
ν_3	0.332	α_3	0.332	β_3	0.332

$D_\xi = 0.095\ N \cdot m^2$. The circular natural frequencies are $\omega_{v1} = 35.934$ rad/s, $\omega_{\phi 1} = 872.97$ rad/s, and $\omega_{w1} = 1192.11$ rad/s. The damping coefficients were taken to be $c_v = 0.01\ N \cdot s/m^2$ and $c_\phi = 1 \times 10^{-4}\ N \cdot s$.

Values for the coefficients α_i, β_i, and ν_i are presented in Table 6.1. We note from Table 6.1 that the symmetries given by Eq. (6.72) are satisfied, which reflects the conservative nature of the system (6.1)-(6.9), in the absence of damping.

It follows from Eqs. (5.12), (5.14), (6.28), and (6.29) that the in-plane bending and torsional oscillations to second order are given by

$$v(s,t) = \epsilon \Phi_v(s)\eta(t) + \cdots \tag{6.91}$$

$$\phi(s,t) = \epsilon \Phi_\phi(s)\left[p(t)\cos(\omega_\phi t) + q(t)\sin(\omega_\phi t)\right] + \cdots \tag{6.92}$$

Therefore, it follows from Eqs. (6.91) and (6.92) that the nontrivial fixed points of Eqs. (6.74)-(6.77) correspond to the beam experiencing a static bending while at the same time oscillating periodically in torsion. However, since we are neglecting gravity effects and assuming the beam to be initially straight, we expect that this solution to be mostly unstable. This is apparent from Figures 6.2 and 6.3. On the other hand, limit-cycle solutions of Eqs. (6.74)-(6.77) correspond to the beam simultaneously oscillating periodically in bending and quasiperiodically in torsion.

In Figure 6.2, we present typical amplitude-response curves when $\sigma = -5$. As the forcing level is increased beyond $f = 10.187$, the trivial solution loses stability through a subcritical pitchfork bifurcation and the response of the beam becomes nontrivial. However, the branch of nontrivial fixed points is unstable, and hence we expect the trivial solution to jump up to a dynamic limit-cycle

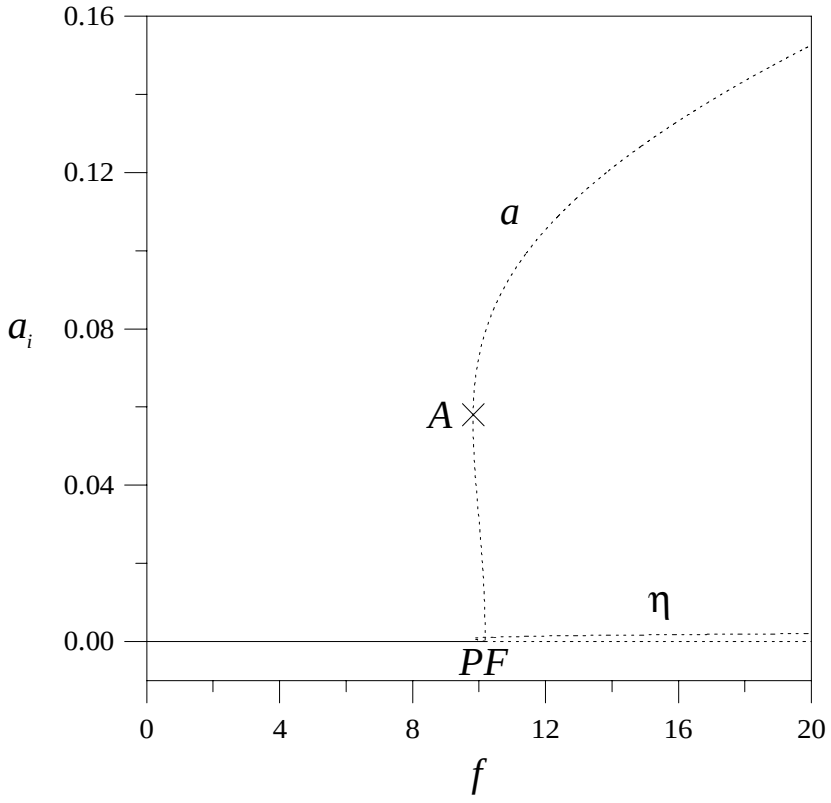

Figure 6.2: Amplitude-response curves when $\sigma = -5$: (—) Stable solutions, $(\cdots)$ saddles, and PF = pitchfork bifurcation

or chaotic solution. Around point A in Figure 6.2, the nontrivial solution undergoes a saddle-node bifurcation, at $f_{SN} = 9.821292345$, and briefly becomes stable. At $f = 9.821292404$, however, the nontrivial solution loses stability again as a pair of complex-conjugate eigenvalues crosses transversely the imaginary axis from the left- to the right-half of the complex plane, indicating a Hopf bifurcation. However, through long-term numerical integration, we were unable to determine the limit cycle emanating from the Hopf bifurcation. We suspect that the closeness of the supercritical Hopf bifurcation to the saddle-node probably caused the limit cycle to experience a cyclic-fold bifurcation and lose stability.

In Figure 6.3, we present frequency-response curves when $f = 10$. The trivial solution loses stability through a supercritical and a subcritical pitchfork bifurcation. The nontrivial solutions are again mostly unstable, and hence, at either pitchfork bifurcation point, the transition to a nontrivial response is a sudden jump to a branch of dynamic solutions. The behavior around point B in

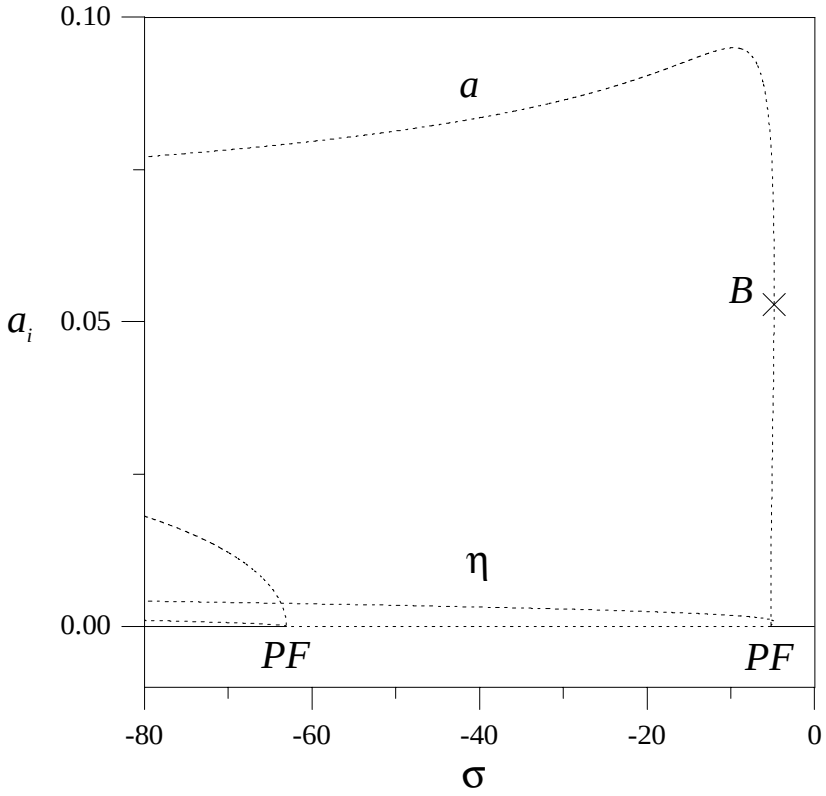

Figure 6.3: Frequency-response curves when $f = 10$: (—) Stable solutions, $(\cdots)$ saddles, and PF = pitchfork bifurcation

Figure 6.3 is similar to that at point A in Figure 6.2.

Next, we investigated the dynamic solutions of Eqs. (6.74)-(6.77), corresponding to Figure 6.2, when $\sigma = -5$. Using long-time integration, a combination of a two-point boundary-value program and Newton's scheme, and Floquet theory, we were able to determine two isolated branches, I and II, of dynamic solutions, as shown in Figure 6.4.

In Figure 6.5a, we present two-dimensional projections of the phase portraits onto the $\eta\zeta$- and pq-planes and an FFT of η of a symmetric limit cycle found on branch I for $f = 1$. As we decrease f beyond 0.73, the limit cycle loses stability through a cyclic-fold bifurcation and a jump to the trivial solution occurs. As f is increased, the symmetric limit cycle grows and deforms, as shown in Figure 6.5b for $f = 10$. As f is increased further, the limit cycle undergoes a symmetry-breaking bifurcation, as shown in part (c) for $f = 11$. The presence of odd and even harmonics in the FFT

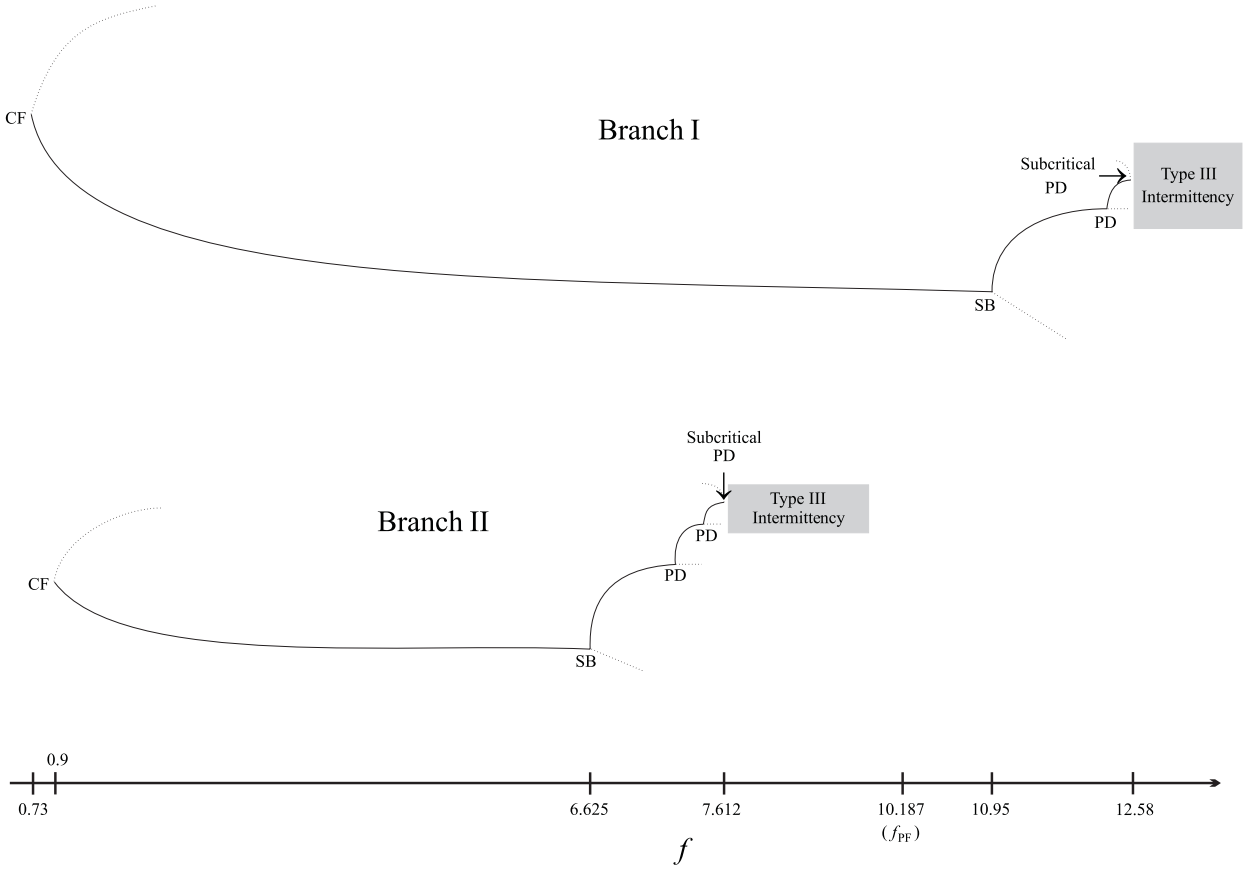

Figure 6.4: A schematic of the dynamic solutions found when $\sigma = -5$: (—) Stable limit cycles, $(\cdots)$ unstable limit cycles, PD = period-doubling bifurcation, SB = symmetry-breaking bifurcation, and CF = cyclic-fold bifurcation.

in part (c) indicates that the limit cycle is asymmetric. The limit cycle then undergoes a period-doubling bifurcation, as shown in part (d) for $f = 12.5$. The presence of subharmonics of order $\frac{1}{2}$ in the FFT in part (d) indicates that the limit cycle is period-two. As f is increased further, the limit cycle goes through a second period-doubling bifurcation, which is subcritical.

In Figure 6.6, we present time histories of η, ζ, p, and q for $f = 12.59$, just after the subcritical period-doubling bifurcation. It is clear from Figure 6.6 that the response starts out as a periodic limit cycle, but fairly quickly it becomes intermittently chaotic. In Figure 6.7, we present the time histories of the states over a long span of time. Because the intermittency resulted after a subcritical period-doubling bifurcation, it is of type III (Nayfeh and Balachandran, 1995).

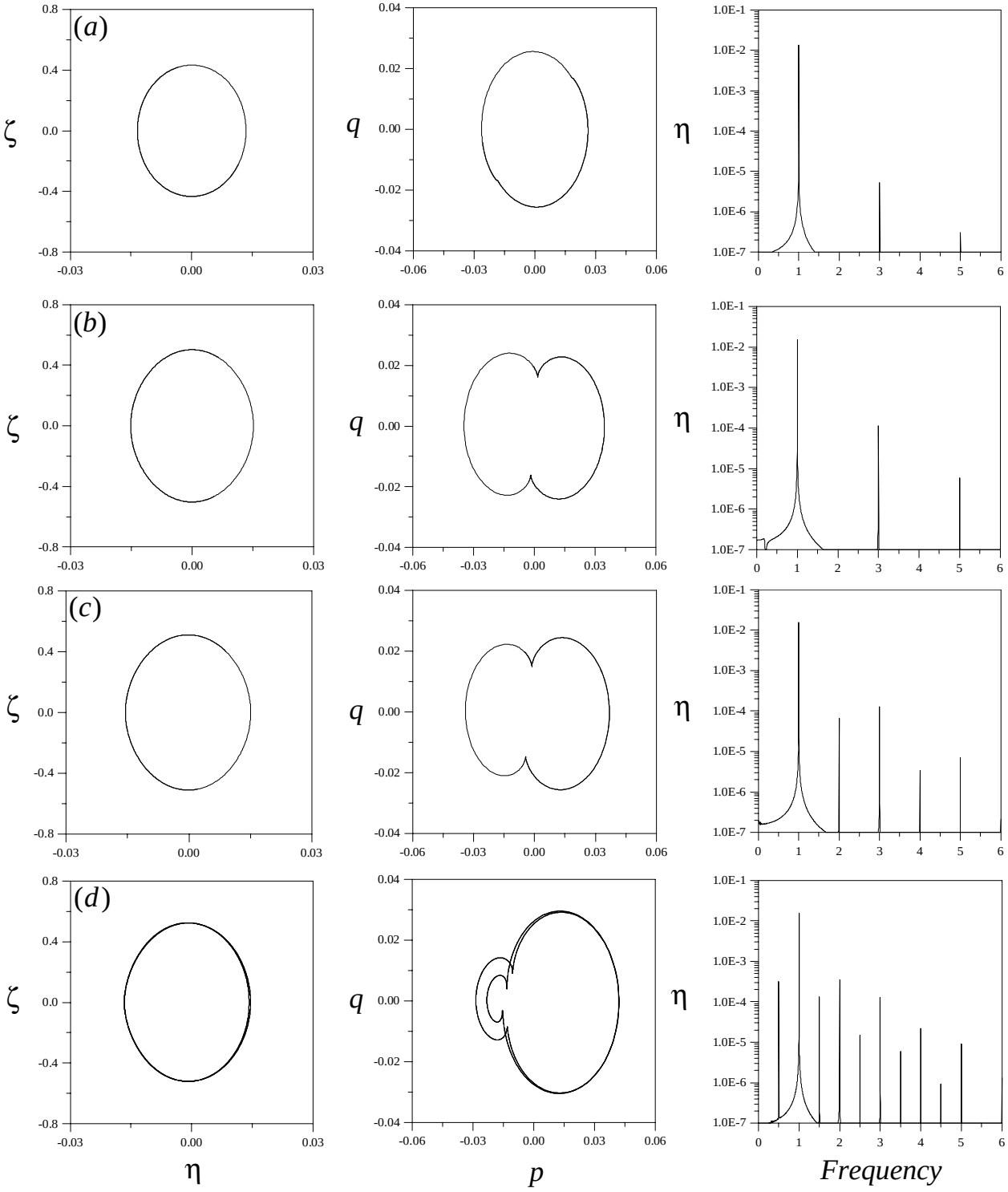

Figure 6.5: Two-dimensional projections of the phase portraits onto the $\eta\zeta$- and pq-planes and FFTs of η showing the dynamics occurring on Branch I as f is slowly varied. The corresponding values of f are $f_a = 1$, $f_b = 10$, $f_c = 11$, and $f_d = 12.5$.

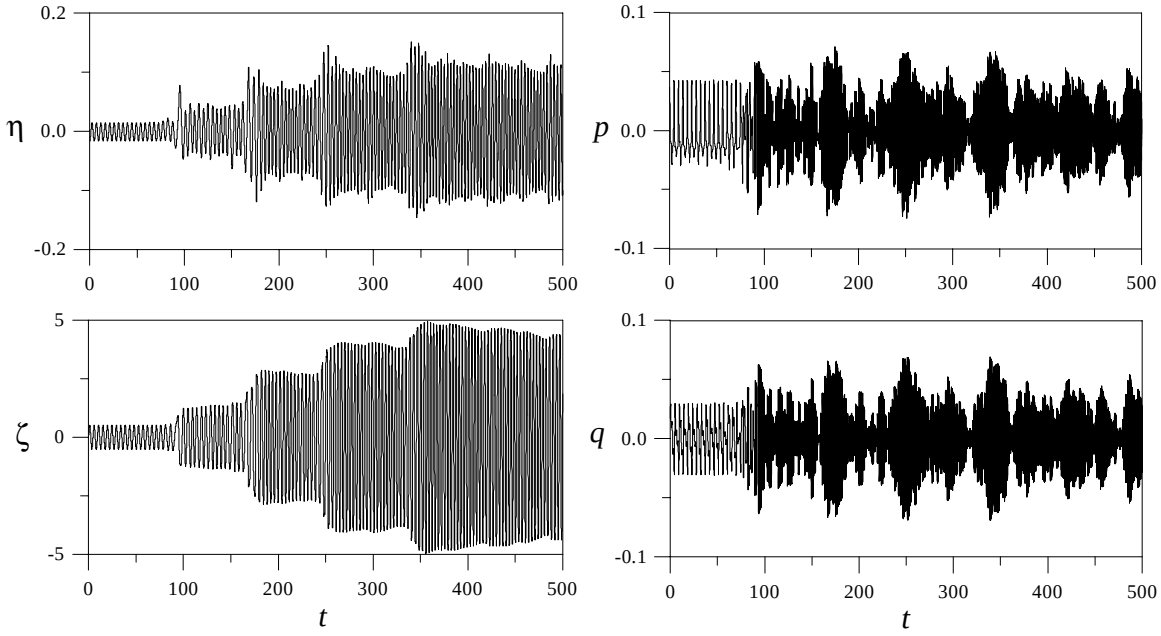

Figure 6.6: Close up of the time histories for η, ζ, p, and q at $f = 12.59$, showing the chaotic response that results as the limit cycle on branch I loses stability through a subcritical period-doubling bifurcation.

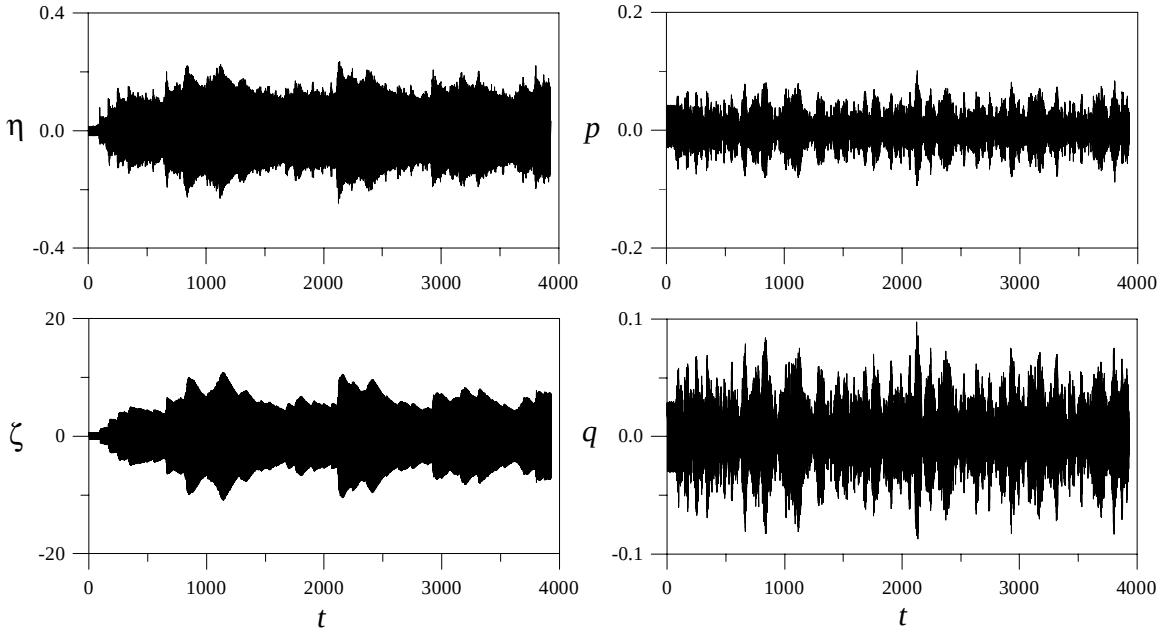

Figure 6.7: Long time histories for η, ζ, p, and q at $f = 12.59$ showing the chaotic response that results as the limit cycle on branch I loses stability through a subcritical period-doubling bifurcation.

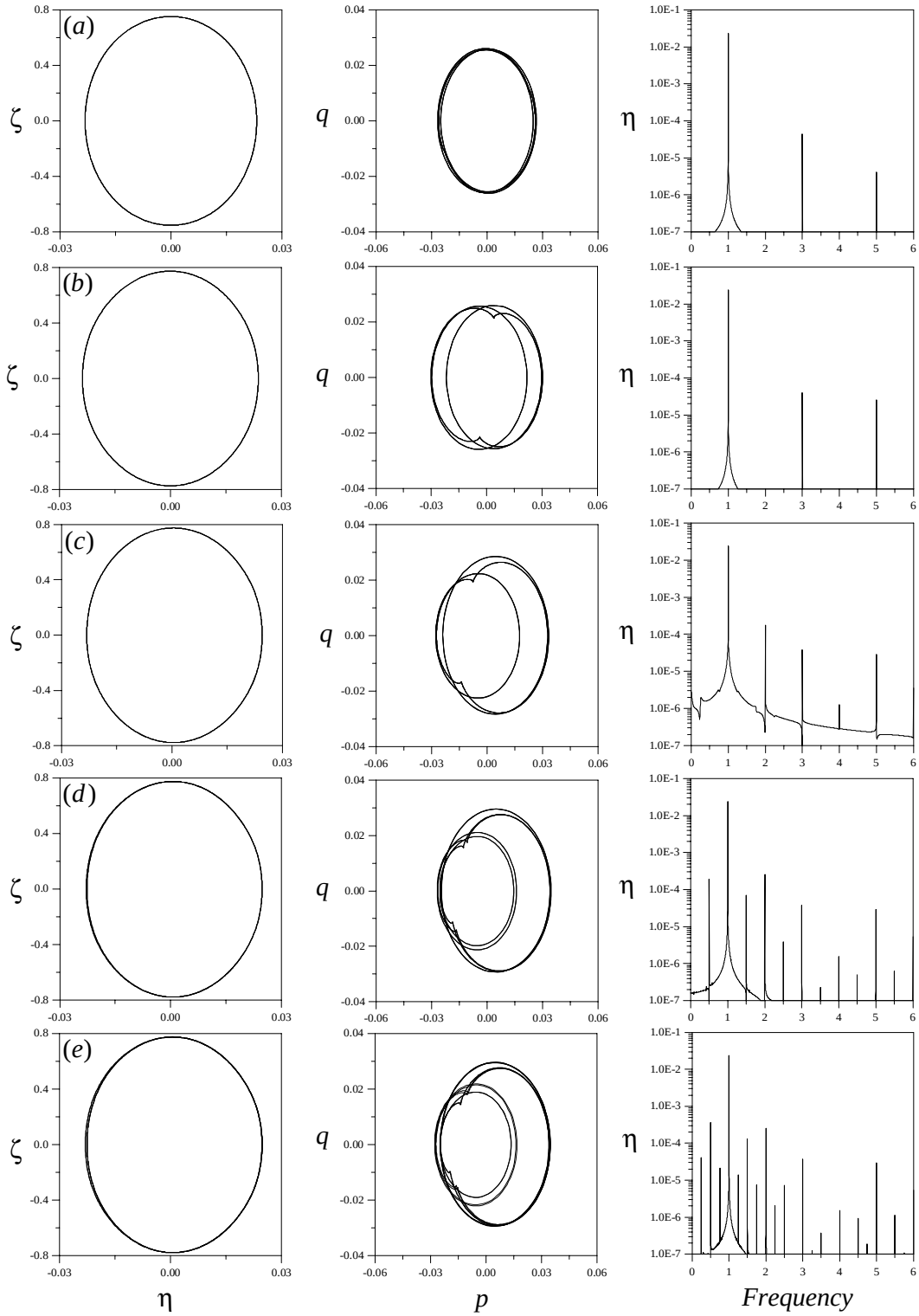

Figure 6.8: Two-dimensional projections of the phase portraits onto the $\eta\zeta$- and pq-planes and FFTs of η showing the dynamics occurring on Branch II as f is slowly varied. The corresponding values of f are $f_a = 1$, $f_b = 6$, $f_c = 7$, $f_d = 7.5$, and $f_e = 7.6$.

In Figure 6.8, we present phase portraits and FFTs of the dynamic solutions found on branch II. In part (a), we show a symmetric limit cycle for $f = 1$. As f is decreased below 0.9, the limit cycle undergoes a cyclic-fold bifurcation and a jump to the trivial solution occurs. As f is increased, the limit cycle grows and deforms, as shown in part (b) for $f = 6$. As f is increased further, the limit cycle undergoes a symmetry-breaking bifurcation and becomes asymmetric, as shown in part (c) for $f = 7$. The limit cycle then goes through a period-doubling bifurcation, as shown in part (d) for $f = 7.5$, which is soon followed by a second period-doubling bifurcation, as shown in part (e) for $f = 7.6$. Both of these period-doubling bifurcations are supercritical and the resulting period-two and period-four limit cycles are stable.

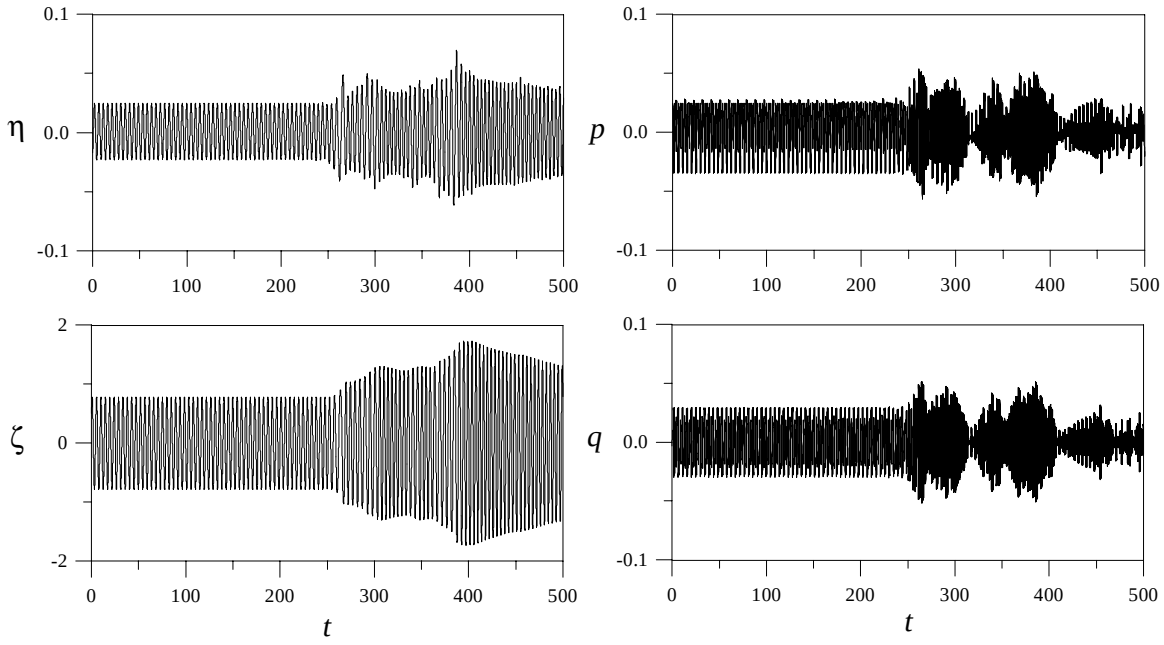

Figure 6.9: Close up of the time histories for η, ζ, p, and q at $f = 7.612$, showing the chaotic response that results as the limit cycle on branch II loses stability through a subcritical period-doubling bifurcation.

As f is slightly increased, the period-four limit cycle shown in Figure 6.8e undergoes another period-doubling bifurcation. Integrating the system numerically just after the bifurcation at $f = 7.612$, we obtain the time histories shown in Figure 6.9. The chaotic nature of the response indicates that the third period-doubling bifurcation is subcritical, causing the period-four limit cycle solution to lose stability and become intermittent of type III. In Figure 6.10, we present time histories that

show the chaotic response over a long period of time.

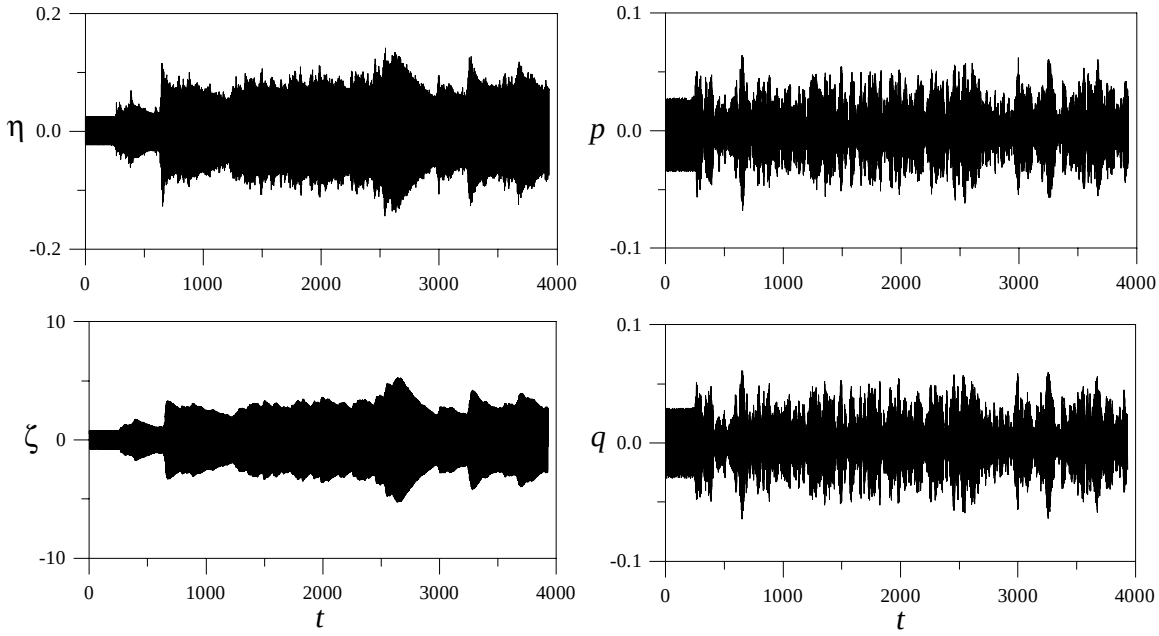

Figure 6.10: Long time histories for η, ζ, p, and q at $f = 7.612$ showing the chaotic response that results as the limit cycle on branch II loses stability through a subcritical period-doubling bifurcation.

Chapter 7

Symmetry in Composite Beams

We investigate the nonlinear response of symmetrically laminated composite beams. A two-to-one internal resonance between the out-of-plane bending motion and the in-plane bending and torsional motions is considered. Pai and Nayfeh (1991a, b) investigated this case by directly applying the method of multiple scales to a set of governing partial-differential equations and boundary conditions, which they derived by using a Newtonian approach (Pai, 1990). However, their modulation equations do not show any symmetry properties. In contrast, we consider the partial-differential equations and boundary conditions derived in Chapter 2 by using a variational approach. We apply the method of multiple scales directly to the governing partial-differential system to determine a set of ordinary-differential equations that govern the modulation of the interacting modes. In addition, we use the method of time-averaged Lagrangian and virtual work to determine a similar set of modulation equations. We show that both sets of modulation equations are the same. Furthermore, we show that these equations possess symmetry properties, reflecting the conservative nature of the system in the absence of damping and external excitations.

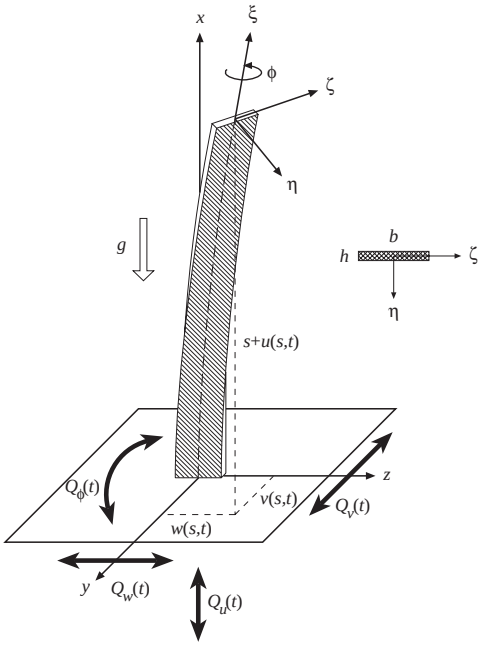

Figure 7.1: A schematic of a symmetrically laminated composite cantilever beam under external excitations.

7.1 Direct Perturbation Analysis of the Partial-Differential Equations of Motion and Boundary Conditions

In Chapter 2, we derived the equations of motion and associated boundary conditions for symmetrically laminated inextensional composite beams by using a variational approach. In dimensional form, these are given by Eqs. (2.90)-(2.100). Because it is more convenient to deal with a nondimensional system, we define the following:

$$
\begin{aligned}
s^* &= \frac{s}{L}, \quad c_v^* = \frac{c_v L^2}{\sqrt{mD_{33}}}, \quad \beta_{11} = \frac{D_{11}}{D_{33}}, \quad J_\xi^* = \frac{J_\xi}{mL^2}, \quad Q_v^* = \frac{L^3}{D_{33}} Q_v, \qquad t^* = \sqrt{\frac{D_{33}}{mL^4}}\, t \\
v^* &= \frac{v}{L}, \quad c_w^* = \frac{c_w L^2}{\sqrt{mD_{33}}}, \quad \beta_{22} = \frac{D_{22}}{D_{33}}, \quad J_\eta^* = \frac{J_\eta}{mL^2}, \quad Q_w^* = \frac{L^3}{D_{33}} Q_w, \qquad \beta_{33} = 1 \\
w^* &= \frac{w}{L}, \quad c_\phi^* = \frac{c_\phi}{\sqrt{mD_{33}}}, \quad \beta_{13} = \frac{D_{13}}{D_{33}}, \quad J_\zeta^* = \frac{J_\zeta}{mL^2}, \quad Q_\phi^* = \frac{L^2}{D_{33}} Q_\phi, \quad (Q_u^*)^* = \frac{L^3}{D_{33}} Q_u^*
\end{aligned}
\tag{7.1}
$$

Scaling the forcing terms, damping terms, and both quadratic and cubic nonlinear terms to be of order ϵ and neglecting the nonlinear rotary inertia terms, we obtain the nondimensional equations

of motion

$$\ddot{v} + \epsilon c_v \dot{v} + \beta_{33} v^{iv} + \beta_{13} \phi''' - J_\varsigma \ddot{v}'' = \epsilon \Big\{ Q_v(t) - \big[v'(s-1) \big]' Q_u(t) + H_v(s,t) \Big\} \tag{7.2}$$

$$\ddot{w} + \epsilon c_w \dot{w} + \beta_{22} w^{iv} - J_\eta \ddot{w}'' = \epsilon \Big\{ Q_w(t) - \big[w'(s-1) \big]' Q_u(t) + H_w(s,t) \Big\} \tag{7.3}$$

$$J_\xi \ddot{\phi} + \epsilon c_\phi \dot{\phi} - \beta_{11} \phi'' - \beta_{13} v''' = \epsilon \Big\{ Q_\phi(t) + H_\phi(s,t) \Big\} \tag{7.4}$$

where the asterisk has been dropped for convenience and the functions H_v, H_w, and H_ϕ are defined in Appendix D. The corresponding nondimensional boundary conditions are

$$v = 0, \qquad v' = 0, \qquad w = 0, \qquad w' = 0, \qquad \text{and} \qquad \phi = 0 \tag{7.5}$$

at the fixed end $s = 0$ and

$$\beta_{33} v'' + \beta_{13} \phi' = \epsilon B_{v1}(t) \tag{7.6}$$

$$\beta_{33} v''' + \beta_{13} \phi'' - J_\varsigma \ddot{v}' = \epsilon B_{v2}(t) \tag{7.7}$$

$$\beta_{22} w'' = \epsilon B_{w1}(t) \tag{7.8}$$

$$\beta_{22} w''' - J_\eta \ddot{w}' = \epsilon B_{w2}(t) \tag{7.9}$$

$$\beta_{11} \phi' + \beta_{13} v'' = \epsilon B_{\phi 1}(t) \tag{7.10}$$

at the free end $s = 1$ where the functions B_{v1}, B_{v2}, B_{w1}, B_{w2}, and $B_{\phi 1}$ are defined in Appendix D.

Next, we apply the method of multiple scales directly to Eqs. (7.2)-(7.10) to determine a uniform expansion of the response of the beam. To this end, we substitute

$$v(s,t) = v_0(s, T_0, T_1) + \epsilon v_1(s, T_0, T_1) + \cdots \tag{7.11}$$

$$w(s,t) = w_0(s, T_0, T_1) + \epsilon w_1(s, T_0, T_1) + \cdots \tag{7.12}$$

$$\phi(s,t) = \phi_0(s, T_0, T_1) + \epsilon \phi_1(s, T_0, T_1) + \cdots \tag{7.13}$$

into Eqs. (7.2)-(7.10), use Eqs. (3.6) and (3.7), equate terms of like powers of ϵ, and obtain

Order 1

$$D_0^2 v_0 + \beta_{33} v_0^{iv} + \beta_{13}\phi_0''' - J_\zeta D_0^2 v_0'' = 0 \tag{7.14}$$

$$D_0^2 w_0 + \beta_{22} w_0^{iv} - J_\eta D_0^2 w_0'' = 0 \tag{7.15}$$

$$J_\xi D_0^2 \phi_0 - \beta_{11}\phi_0'' - \beta_{13} v_0''' = 0 \tag{7.16}$$

$$v_0 = 0, \qquad v_0' = 0, \qquad w_0 = 0, \qquad w_0' = 0, \qquad \text{and} \qquad \phi_0 = 0 \tag{7.17}$$

at the fixed end $s = 0$ and

$$\beta_{33} v_0'' + \beta_{13}\phi_0' = 0, \qquad \beta_{33} v_0''' + \beta_{13}\phi_0'' - J_\zeta D_0^2 v_0' = 0, \qquad \beta_{22} w_0'' = 0,$$
$$\beta_{22} w_0''' - J_\eta D_0^2 w_0' = 0, \qquad \text{and} \qquad \beta_{11}\phi_0' + \beta_{13} v_0'' = 0 \tag{7.18}$$

at the free end $s = 1$.

Order ϵ

$$D_0^2 v_1 + \beta_{33} v_1^{iv} + \beta_{13}\phi_1''' - J_\zeta D_0^2 v_1'' = -2D_0 D_1 v_0 + 2J_\zeta D_0 D_1 v_0'' - c_v D_0 v_0 + Q_v(T_0, T_1)$$
$$- \left[v_0'(s-1)\right]' Q_u(T_0, T_1) + H_v(s, T_0, T_1) \tag{7.19}$$

$$D_0^2 w_1 + \beta_{22} w_1^{iv} - J_\eta D_0^2 w_1'' = -2D_0 D_1 w_0 + 2J_\eta D_0 D_1 w_0'' - c_w D_0 w_0 + Q_w(T_0, T_1)$$
$$- \left[w_0'(s-1)\right]' Q_u(T_0, T_1) + H_w(s, T_0, T_1) \tag{7.20}$$

$$J_\xi D_0^2 \phi_1 - \beta_{11}\phi_1'' - \beta_{13} v_1''' = -2J_\xi D_0 D_1 \phi_0 + Q_\phi(T_0, T_1) + H_\phi(s, T_0, T_1) \tag{7.21}$$

$$v_1 = 0, \qquad v_1' = 0, \qquad w_1 = 0, \qquad w_1' = 0, \qquad \text{and} \qquad \phi_1 = 0 \tag{7.22}$$

at the fixed end $s = 0$ and

$$\beta_{33} v_1'' + \beta_{13}\phi_1' = B_{v1}(T_0, T_1), \quad \beta_{33} v_1''' + \beta_{13}\phi_1'' - J_\zeta D_0^2 v_1' = 2J_\zeta D_0 D_1 v_0' + B_{v2}(T_0, T_1),$$
$$\beta_{22} w_1'' = B_{w1}(T_0, T_1), \qquad \beta_{22} w_1''' - J_\eta D_0^2 w_1' = 2J_\eta D_0 D_1 w_0' + B_{w2}(T_0, T_1), \quad \text{and}$$

$$\beta_{11}\phi_1' + \beta_{13}v_1'' = B_{\phi 1}(T_0, T_1) \tag{7.23}$$

at the free end $s = 1$.

7.1.1 First-Order Problem

We divide the first-order problem into two parts. The first part corresponds to the linearly coupled in-plane bending v_0 and torsional ϕ_0 motions, as described by Eqs. (7.14) and (7.16)-(7.18). The second part corresponds to the out-of-plane bending motion w_0, as described by Eqs. (7.15), (7.17), and (7,18). Next, we assume solutions for v_0, ϕ_0, and w_0 as

$$v_0 = \Phi_v(s)\left[A_v(T_1)e^{i\omega_v T_0} + \bar{A}_v(T_1)e^{-i\omega_v T_0}\right] = \Phi_v(s)\left[A(T_1)e^{i\omega T_0} + \bar{A}(T_1)e^{-i\omega T_0}\right] \tag{7.24}$$

$$\begin{aligned}\phi_0 &= \hat{\Phi}_\phi(s)\left[A_\phi(T_1)e^{i\omega_\phi T_0} + \bar{A}_\phi(T_1)e^{-i\omega_\phi T_0}\right] = \hat{\Phi}_\phi(s)\Gamma\left[A(T_1)e^{i\omega T_0} + \bar{A}(T_1)e^{-i\omega T_0}\right] \\ &= \Phi_\phi(s)\left[A(T_1)e^{i\omega T_0} + \bar{A}(T_1)e^{-i\omega T_0}\right]\end{aligned} \tag{7.25}$$

$$w_0 = \Phi_w(s)\left[A_w(T_1)e^{i\omega_w T_0} + \bar{A}_w(T_1)e^{-i\omega_w T_0}\right] = \Phi_w(s)\left[B(T_1)e^{i\rho T_0} + \bar{B}(T_1)e^{-i\rho T_0}\right] \tag{7.26}$$

where ω is the natural frequency of the in-plane bending and torsional motions, ρ is the natural frequency of the out-of-plane bending motion, and A and B are complex-valued functions. The functions $\Phi_v(s)$, $\Phi_\phi(s)$, and $\Phi_w(s)$ are the linear undamped mode shapes, which are governed by the following boundary-value problems:

$$\beta_{33}\Phi_v^{iv} + \omega^2 J_\zeta \Phi_v'' - \omega^2 \Phi_v + \beta_{13}\Phi_\phi''' = 0 \tag{7.27}$$

$$-\beta_{11}\Phi_\phi'' - \omega^2 J_\xi \Phi_\phi - \beta_{13}\Phi_v''' = 0 \tag{7.28}$$

$$\Phi_v = 0, \qquad \Phi_v' = 0, \qquad \text{and} \qquad \Phi_\phi = 0 \qquad \text{at } s = 0 \tag{7.29}$$

$$\Phi_v'' = 0, \qquad \Phi_\phi' = 0, \qquad \text{and} \qquad \beta_{33}\Phi_v''' + \beta_{13}\Phi_\phi'' + \omega^2 J_\zeta \Phi_v' = 0 \qquad \text{at } s = 1 \tag{7.30}$$

and

$$\beta_{22}\Phi_w^{iv} + \rho^2 J_\eta \Phi_w'' - \rho^2 \Phi_w = 0 \tag{7.31}$$

$$\Phi_w = 0 \qquad \text{and} \qquad \Phi'_w = 0 \qquad \text{at } s = 0 \tag{7.32}$$

$$\Phi''_w = 0 \qquad \text{and} \qquad \beta_{22}\Phi'''_w + \rho^2 J_\eta \Phi'_w = 0 \qquad \text{at } s = 1 \tag{7.33}$$

In-Plane Bending and Torsional Mode Shapes and Natural Frequencies

We rewrite Eqs. (7.27) and (7.28) in a differential operator form (Dokumaci, 1987; Bishop, Cannon, and Miao, 1989) as

$$L_1\Phi_v + L_2\Phi_\phi = 0 \tag{7.34}$$

$$L_3\Phi_v + L_4\Phi_\phi = 0 \tag{7.35}$$

where

$$L_1 = \beta_{33}D^4 + \omega^2 J_\zeta D^2 - \omega^2, \quad L_2 = \beta_{13}D^3, \quad L_3 = -\beta_{13}D^3, \quad L_4 = -\beta_{11}D^2 - \omega^2 J_\xi, \tag{7.36}$$

and $D^n(\,) = \frac{d^n}{ds^n}(\,)$. Applying the operator L_4 on Eq. (7.34) and the operator L_2 on Eq. (7.35), subtracting the two results, and assuming that $L_iL_j = L_jL_i$ (i.e., the L_i commute), we obtain

$$(L_4L_1 - L_2L_3)\,\Phi_v = 0 \tag{7.37}$$

Similarly, applying the operator L_3 on Eq. (7.34) and the operator L_1 on Eq. (7.35) and subtracting the two results, we obtain

$$(L_4L_1 - L_2L_3)\,\Phi_\phi = 0 \tag{7.38}$$

Hence, for nontrivial solutions of Φ_v and Φ_ϕ, we must have

$$L_4L_1 - L_2L_3 = 0 \tag{7.39}$$

Equations (7.37) and (7.38) can then be expressed as

$$\alpha_1 D^6\psi + \alpha_2 D^4\psi + \alpha_3 D^2\psi + \alpha_4\psi = 0 \tag{7.40}$$

where $\psi(s)$ denotes either Φ_v or Φ_ϕ and

$$\alpha_1 = \beta_{13}^2 - \beta_{11}\beta_{33} \tag{7.41}$$

$$\alpha_2 = -\omega^2 J_\zeta \beta_{11} - \omega^2 J_\xi \beta_{33} \tag{7.42}$$

$$\alpha_3 = -\omega^4 J_\xi J_\zeta + \beta_{11}\omega^2 \tag{7.43}$$

$$\alpha_4 = J_\xi \omega^4 \tag{7.44}$$

It follows from Eqs. (7.42) and (7.44) that α_2 is always negative while α_4 is always positive. Next, we substitute

$$\psi = e^{\hat{\lambda} s} \tag{7.45}$$

into Eq. (7.40), divide the result by α_1, and obtain

$$r^3 + \tau_1 r^2 + \tau_2 r + \tau_3 = 0 \tag{7.46}$$

where $r = \hat{\lambda}^2$ and the τ_i are real-valued constants defined as

$$\tau_1 = \frac{\alpha_2}{\alpha_1}, \qquad \tau_2 = \frac{\alpha_3}{\alpha_1}, \qquad \text{and} \qquad \tau_3 = \frac{\alpha_4}{\alpha_1} \tag{7.47}$$

Since Eq. (7.46) is cubic in r, it is possible for one to determine the solutions in closed-form. Defining

$$Q = \frac{3\tau_2 - \tau_1^2}{9} \qquad \text{and} \qquad R = \frac{9\tau_1\tau_2 - 27\tau_3 - 2\tau_1^3}{54} \tag{7.48}$$

we express the roots of Eq. (7.46) as (Spiegel, 1968)

$$r_1 = S + T - \frac{1}{3}\tau_1 \tag{7.49}$$

$$r_2 = -\frac{1}{2}(S+T) - \frac{1}{3}\tau_1 + i\frac{\sqrt{3}}{2}(S-T) \tag{7.50}$$

$$r_3 = -\frac{1}{2}(S+T) - \frac{1}{3}\tau_1 - i\frac{\sqrt{3}}{2}(S-T) \tag{7.51}$$

where $S = \sqrt[3]{R + \sqrt{Q^3 + R^2}}$ and $T = \sqrt[3]{R - \sqrt{Q^3 + R^2}}$. In addition, we define the *discriminant* $\Delta \equiv Q^3 + R^2$. Hence,

1. if $\Delta > 0$, then one root is real and the other two are complex conjugates,
2. if $\Delta = 0$, then all three roots are real and at least two are repeated, and
3. if $\Delta < 0$, then all three roots are real and distinct.

Furthermore, for the last case (i.e., $\Delta < 0$) and because $\alpha_2 < 0$ and $\alpha_4 > 0$, it follows that of the three *real* roots of Eq. (7.46), only one root is *positive* when $\alpha_1 < 0$, while two roots are *positive* when $\alpha_1 > 0$. In the first case, if we assume that $r_1 > 0$ while r_2 and $r_3 < 0$, then $\hat{\lambda}_1 = \pm\sqrt{r_1} = \pm\lambda_1$, $\hat{\lambda}_2 = \pm\sqrt{r_2} = \pm i\lambda_2$, and $\hat{\lambda}_3 = \pm\sqrt{r_3} = \pm i\lambda_3$ where the λ_i are *real*-valued constants. Then, it follows from Eq. (7.45) that the mode shapes have the form

$$\Phi_v(s) = \mathcal{E}_1 \cosh(\lambda_1 s) + \mathcal{E}_2 \sinh(\lambda_1 s) + \mathcal{E}_3 \cos(\lambda_2 s) + \mathcal{E}_4 \sin(\lambda_2 s) + \mathcal{E}_5 \cos(\lambda_3 s) + \mathcal{E}_6 \sin(\lambda_3 s) \quad (7.52)$$

$$\Phi_\phi(s) = \mathcal{F}_1 \cosh(\lambda_1 s) + \mathcal{F}_2 \sinh(\lambda_1 s) + \mathcal{F}_3 \cos(\lambda_2 s) + \mathcal{F}_4 \sin(\lambda_2 s) + \mathcal{F}_5 \cos(\lambda_3 s) + \mathcal{F}_6 \sin(\lambda_3 s) \quad (7.53)$$

On the other hand, in the second case, if we assume that $r_1 < 0$ while r_2 and $r_3 > 0$, then $\hat{\lambda}_1 = \pm\sqrt{r_1} = \pm i\lambda_1$ while $\hat{\lambda}_2 = \pm\sqrt{r_2} = \pm\lambda_2$ and $\hat{\lambda}_3 = \pm\sqrt{r_3} = \pm\lambda_3$. Hence, the mode shapes have the form

$$\Phi_v(s) = \mathcal{E}_1 \cos(\lambda_1 s) + \mathcal{E}_2 \sin(\lambda_1 s) + \mathcal{E}_3 \cosh(\lambda_2 s) + \mathcal{E}_4 \sinh(\lambda_2 s) + \mathcal{E}_5 \cosh(\lambda_3 s) + \mathcal{E}_6 \sinh(\lambda_3 s) \quad (7.54)$$

$$\Phi_\phi(s) = \mathcal{F}_1 \cos(\lambda_1 s) + \mathcal{F}_2 \sinh \lambda_1 s) + \mathcal{F}_3 \cosh(\lambda_2 s) + \mathcal{F}_4 \sinh(\lambda_2 s) + \mathcal{F}_5 \cosh(\lambda_3 s) + \mathcal{F}_6 \sinh(\lambda_3 s) \quad (7.55)$$

For the $[10^\circ_6/45^\circ_4/90^\circ_5]_s$ graphite-epoxy composite beam considered by Pai and Nayfeh (1991a, b), we find that $\Delta < 0$ and $\alpha_1 < 0$ and, hence, the mode shapes are given by Eqs. (7.52) and (7.53). Therefore, the results we present next will be specific to Eqs. (7.52) and (7.53). The same steps, however, are applicable if α_1 is greater than zero and, hence, the mode shapes are given by Eqs. (7.54) and (7.55).

Next, we require that Eqs. (7.52) and (7.53) satisfy the boundary-value problem governing Φ_v and Φ_ϕ. Substituting Eqs. (7.52) and (7.53) into either Eq. (7.27) or Eq. (7.28), we relate the coefficients $\mathcal{F}_i$ to the coefficients $\mathcal{E}_i$ by

$$\begin{aligned} &\mathcal{F}_1 = \Psi_1 \mathcal{E}_2, \qquad \mathcal{F}_3 = \Psi_2 \mathcal{E}_4, \qquad \mathcal{F}_5 = \Psi_3 \mathcal{E}_6, \\ &\mathcal{F}_2 = \Psi_1 \mathcal{E}_1, \qquad \mathcal{F}_4 = -\Psi_2 \mathcal{E}_3, \qquad \mathcal{F}_6 = -\Psi_3 \mathcal{E}_5 \end{aligned} \tag{7.56}$$

where

$$\Psi_1 = -\frac{\beta_{33}\lambda_1^4 + \omega^2 J_\zeta \lambda_1^2 - \omega^2}{\beta_{13}\lambda_1^3} = -\frac{\beta_{13}\lambda_1^3}{\beta_{11}\lambda_1^2 + \omega^2 J_\xi} \tag{7.57}$$

$$\Psi_2 = -\frac{\beta_{33}\lambda_2^4 - \omega^2 J_\zeta \lambda_2^2 - \omega^2}{\beta_{13}\lambda_2^3} = -\frac{\beta_{13}\lambda_2^3}{\beta_{11}\lambda_2^2 - \omega^2 J_\xi} \tag{7.58}$$

$$\Psi_3 = -\frac{\beta_{33}\lambda_3^4 - \omega^2 J_\zeta \lambda_3^2 - \omega^2}{\beta_{13}\lambda_3^3} = -\frac{\beta_{13}\lambda_3^3}{\beta_{11}\lambda_3^2 - \omega^2 J_\xi} \tag{7.59}$$

As a result, we rewrite the mode shape Φ_ϕ, which is defined by Eq. (7.53), as follows:

$$\begin{aligned} \Phi_\phi(s) = \Psi_1 \left[\mathcal{E}_2 \cosh(\lambda_1 s) + \mathcal{E}_1 \sinh(\lambda_1 s)\right] + \Psi_2 \left[\mathcal{E}_4 \cos(\lambda_2 s) - \mathcal{E}_3 \sin(\lambda_2 s)\right] \\ + \Psi_3 \left[\mathcal{E}_6 \cos(\lambda_3 s) - \mathcal{E}_5 \sin(\lambda_3 s)\right] \end{aligned} \tag{7.60}$$

Then, substituting Eqs. (7.52) and (7.60) into the boundary conditions given by Eqs. (7.29) and (7.30), we determine the coefficients $\mathcal{E}_2$-$\mathcal{E}_6$ in terms of $\mathcal{E}_1$. Furthermore, the last boundary condition yields a complicated characteristic equation in terms of λ_1, λ_2, and λ_3, which, when combined with Eq. (7.46), can be solved numerically for the natural frequency ω of the in-plane bending and torsional oscillations.

Out-of-Plane Bending Mode Shapes and Natural Frequencies

The mode shapes for the out-of-plane bending oscillations are governed by Eqs. (7.31)-(7.33). Substituting

$$\Phi_w(s) = e^{\hat{\nu} s} \tag{7.61}$$

into Eq. (7.31), we obtain

$$R^2 + \kappa_1 R - \kappa_2 = 0 \tag{7.62}$$

where $R = \hat{\nu}^2$ and κ_1 and κ_2 are constants defined as

$$\kappa_1 = \frac{\rho^2 J_\eta}{\beta_{22}} \qquad \text{and} \qquad \kappa_2 = \frac{\rho^2}{\beta_{22}} \tag{7.63}$$

The solutions of Eq. (7.62) are

$$R_1 = -\frac{\kappa_1}{2} + \sqrt{\left(\frac{\kappa_1}{2}\right)^2 + \kappa_2} \qquad \text{and} \qquad R_2 = -\frac{\kappa_1}{2} - \sqrt{\left(\frac{\kappa_1}{2}\right)^2 + \kappa_2} \tag{7.64}$$

Because κ_2 is greater than zero according to Eq. (7.63), it follows from Eq. (7.64) that $R_1 > 0$ while $R_2 < 0$. Hence, $\hat{\nu}_1 = \pm\sqrt{R_1} = \pm\nu_1$ whereas $\hat{\nu}_2 = \pm\sqrt{R_2} = \pm i\nu_2$ where ν_1 and ν_2 are *real*-valued constants. Accordingly, the solution of Eq. (7.31) can be expressed as

$$\Phi_w(s) = \mathcal{G}_1 \cosh(\nu_1 s) + \mathcal{G}_2 \sinh(\nu_1 s) + \mathcal{G}_3 \cos(\nu_2 s) + \mathcal{G}_4 \sin(\nu_2 s) \tag{7.65}$$

Next, using the first three boundary conditions from Eqs. (7.32) and (7.33), we determine the values of $\mathcal{G}_2$, $\mathcal{G}_3$, $\mathcal{G}_4$ in terms of $\mathcal{G}_1$ and obtain

$$\Phi_w(s) = \mathcal{G}_1 \left\{ \Big[\cosh(\nu_1 s) - \cos(\nu_2 s) \Big] - \left(\frac{\nu_1^2 \cosh\nu_1 + \nu_2^2 \cos\nu_2}{\nu_1^2 \sinh\nu_1 + \nu_1\nu_2 \sin\nu_2} \right) \left[\sinh(\nu_1 s) - \frac{\nu_1}{\nu_2} \sin(\nu_2 s) \right] \right\} \tag{7.66}$$

Then, substituting Eq. (7.66) into the second boundary condition in Eq. (7.33), we obtain a characteristic equation in terms of ν_1 and ν_2 which, along with Eq. (7.64), can be numerically solved to determine the natural frequency ρ of the out-of-plane oscillations.

Numerical Results

Following Pai and Nayfeh (1991a, b), we consider a graphite-epoxy composite beam with the lay-up $[10^\circ_6/45^\circ_4/90^\circ_5]_s$ and the following material properties: $E_1 = 1.92 \times 10^7\, psi$, $E_2 = E_3 =$

$1.56 \times 10^6\, psi$, $G_{23} = 5.23 \times 10^5\, psi$, $G_{12} = G_{13} = 8.20 \times 10^5\, psi$, $\nu_{23} = 0.49$, $\nu_{12} = \nu_{13} = 0.24$, and $\rho_0 = 96.1\, lbm/ft^3$. For a beam with the dimensions $L = 1.5\, ft$, $b = 0.37526\, in$, $h_{(k)} = 0.005\, in$, and $h = 2 \times 15 \times h_{(k)} = 0.15$, the bending and torsional rigidities are $D_{11} = 436.23\, lbf \cdot in^2$, $D_{22} = 5547.2\, lbf \cdot in^2$, $D_{33} = 1532.4\, lbf \cdot in^2$, and $D_{13} = 252.02\, lbf \cdot in^2$. The corresponding nondimensional stiffnesses and mass moments of inertia are

$$\begin{aligned} \beta_{11} &= 0.284671 & & J_\xi = 4.20062 \times 10^{-5} \\ \beta_{22} &= 3.61994 & \text{and} \quad & J_\eta = 3.62192 \times 10^{-5} \\ \beta_{13} &= 0.164461 & & J_\zeta = 5.78704 \times 10^{-6} \end{aligned} \tag{7.67}$$

Using *Mathematica*, we numerically calculated the nondimensional natural frequencies of the first bending and torsional modes to be

$$\omega = 3.34465987 \qquad \text{and} \qquad \rho = 6.68906 \tag{7.68}$$

The corresponding nondimensional mode shapes are given by

$$\begin{aligned} \Phi_v(s) = &-\cosh(1.87503s) + 0.734073\sinh(1.87503s) + \cos(1.87509s) - 0.734047\sin(1.87509s) \\ &- 4.62941 \times 10^{-8}\cos(0.0406291s) - 7.36223 \times 10^{-10}\sin(0.0406291s) \end{aligned} \tag{7.69}$$

$$\begin{aligned} \Phi_\phi(s) = &-0.794809\cosh(1.87503s) + 1.08274\sinh(1.87503s) + 0.795556\cos(1.87509s) \\ &+ 1.08379\sin(1.87509s) - 7.46689 \times 10^{-4}\cos(0.0406291s) \\ &+ 4.69522 \times 10^{-2}\sin(0.0406291s) \end{aligned} \tag{7.70}$$

$$\Phi_w(s) = \cosh(1.87497s) - 0.734054\sinh(1.87497s) - \cos(1.87508s) + 0.734007\sin(1.87508s) \tag{7.71}$$

where we arbitrarily took $\mathcal{E}_1 = -1.0$ in Eqs. (7.54) and (7.60) and $\mathcal{G}_1 = 1.0$ in Eq. (7.66).

7.1.2 Second-Order Problem

We consider directly exciting the beam along the y-direction (i.e., flapwise excitation). Therefore, we set $Q_w = 0$, $Q_\phi = 0$, $Q_u = 0$, and $Q_v = f\Omega^2\cos(\Omega T_0)$ in Eqs. (7.19)-(7.21). In addition,

we introduce the detuning parameters σ and δ to express the nearness of the primary and the two-to-one internal resonances as follows:

$$\Omega = \omega\,(1+\epsilon\sigma) \qquad \text{and} \qquad \rho = 2\omega\,(1+\epsilon\delta) \tag{7.72}$$

Then, we substitute Eqs. (7.24)-(7.26) into Eqs. (7.19)-(7.23), use Eq. (7.72), and obtain

$$D_0^2 v_1 + \beta_{33} v_1^{iv} + \beta_{13}\phi_1''' - J_\zeta D_0^2 v_1'' = H_v^*(s,T_1)e^{i\omega T_0} + \text{cc} + \text{NST} \tag{7.73}$$

$$J_\xi D_0^2 \phi_1 - \beta_{11}\phi_1'' - \beta_{13} v_1''' = H_\phi^*(s,T_1)e^{i\omega T_0} + \text{cc} + \text{NST} \tag{7.74}$$

$$D_0^2 w_1 + \beta_{22} w_1^{iv} - J_\eta D_0^2 w_1'' = H_w^*(s,T_1)e^{i\rho T_0} + \text{cc} + \text{NST} \tag{7.75}$$

where cc stands for the complex conjugate of the preceding terms, NST stands for the terms that do not produce secular terms, and the functions H_v^*, H_ϕ^*, and H_w^* are defined in Appendix D. The boundary conditions are

$$v_1 = 0, \qquad v_1' = 0, \qquad w_1 = 0, \qquad w_1' = 0, \qquad \text{and} \qquad \phi_1 = 0 \tag{7.76}$$

at the fixed end $s = 0$ and

$$\beta_{33} v_1'' + \beta_{13}\phi_1' = \text{NST}, \quad \beta_{33} v_1''' + \beta_{13}\phi_1'' - J_\zeta D_0^2 v_1' = B_{v2}^*(T_1)e^{i\omega T_0} + \text{cc} + \text{NST}, \quad \beta_{22} w_1'' = \text{NST},$$
$$\beta_{22} w_1''' - J_\eta D_0^2 w_1' = B_{w2}^*(T_1)e^{i\rho T_0} + \text{cc} + \text{NST} \quad \text{and} \quad \beta_{11}\phi_1' + \beta_{13} v_1'' = \text{NST} \tag{7.77}$$

at the free end $s = 1$, where the functions B_{v2}^* and B_{w2}^* are defined in Appendix D. We seek solutions of Eqs. (7.73)-(7.77) in the form

$$v_1 = V(s,T_1)e^{i\omega T_0} + \text{cc} + \text{NST} \tag{7.78}$$

$$\phi_1 = \Xi(s,T_1)e^{i\omega T_0} + \text{cc} + \text{NST} \tag{7.79}$$

$$w_1 = W(s,T_1)e^{i\rho T_0} + \text{cc} + \text{NST} \tag{7.80}$$

Substituting Eqs. (7.78)-(7.80) into Eqs. (7.73), (7.74), (7.76), and (7.77), we obtain the following

boundary-value problem governing V and Ξ:

$$\beta_{33}V^{iv} + J_\zeta\omega^2V'' - \omega^2V + \beta_{13}\Xi''' = H_v^* \tag{7.81}$$

$$-\beta_{11}\Xi'' - J_\xi\omega^2\Xi - \beta_{13}V''' = H_\phi^* \tag{7.82}$$

$$V = 0, \qquad V' = 0, \qquad \text{and} \quad \Xi = 0 \quad \text{at } s = 0 \tag{7.83}$$

$$V'' = 0, \quad \beta_{33}V''' + J_\zeta\omega^2V' + \beta_{13}\Xi'' = B_{v2}^*, \quad \text{and} \quad \Xi' = 0 \quad \text{at } s = 1 \tag{7.84}$$

Similarly, substituting Eqs. (7.78)-(7.80) into Eqs. (7.75)-(7.77), we obtain the following boundary-value problem governing W:

$$\beta_{22}W^{iv} + J_\eta\rho^2W'' - \rho^2W = H_w^* \tag{7.85}$$

$$W = 0 \quad \text{and} \qquad W' = 0 \qquad \text{at } s = 0 \tag{7.86}$$

$$W'' = 0 \quad \text{and} \quad \beta_{22}W''' + J_\eta\rho^2W' = B_{w2}^* \quad \text{at } s = 1 \tag{7.87}$$

Since the homogeneous boundary-value system given by Eqs. (7.81)-(7.84) has a nontrivial solution, the inhomogeneous system has a solution only if a solvability condition is satisfied. To determine this solvability condition, we take the inner product of Eq. (7.81) with the adjoint $V^*(s)$ and Eq. (7.82) with the adjoint $\Xi^*(s)$, add the two results, and obtain

$$\int_0^1 \Big\{\beta_{33}V^*V^{iv} + J_\zeta\omega^2V^*V'' - \omega^2V^*V + \beta_{13}V^*\Xi'''\Big\}ds + \int_0^1 \Big\{ -\beta_{11}\Xi^*\Xi'' \\ -J_\xi\omega^2\Xi^*\Xi - \beta_{13}\Xi^*V'''\Big\}ds = \int_0^1 V^*H_v^*ds + \int_0^1 \Xi^*H_\phi^*ds \tag{7.88}$$

Then, we transfer the derivatives to the adjoints through repeated integrations by parts and obtain

$$\int_0^1 \big(V^*H_v^* + \Xi^*H_\phi^*\big)ds = \Big[\beta_{33}\big(V^*V''' - V^{*\prime}V'' + V^{*\prime\prime}V' - V^{*\prime\prime\prime}V\big) + J_\zeta\omega^2\big(V^*V' - V^{*\prime}V\big) \\ - \beta_{11}\big(\Xi^*\Xi' - \Xi^{*\prime}\Xi\big) + \beta_{13}\big(V^*\Xi'' - V^{*\prime}\Xi' + V^{*\prime\prime}\Xi - \Xi^*V'' + \Xi^{*\prime}V'$$

$$- \Xi^{*\prime\prime} V)\Big]_{s=0}^{s=1} + \int_0^1 \Big\{ V\Big[\beta_{33} V^{*iv} + J_\zeta \omega^2 V^{*\prime\prime} - \omega^2 V^* + \beta_{13} \Xi^{*\prime\prime\prime}\Big] + \Xi\Big[- \beta_{11} \Xi^{*\prime\prime} - J_\xi \omega^2 \Xi^* - \beta_{13} V^{*\prime\prime\prime}\Big]\Big\} ds \tag{7.89}$$

To determine the adjoints, we consider the homogeneous problem (i.e., $H_v^* = 0$, $H_\phi^* = 0$, and $B_{v2}^* = 0$). The resulting system is similar to Eqs. (7.27)-(7.30) and, hence, the adjoints are $V^*(s) = \Phi_v(s)$ and $\Xi^*(s) = \Phi_\phi(s)$. Having defined the adjoints, we reduce Eq. (7.89) to the following solvability condition for $A(T_1)$:

$$\int_0^1 \left(\Phi_v H_v^* + \Phi_\phi H_\phi^*\right) ds - \Phi_v(1) B_{v2}^* = 0 \tag{7.90}$$

To determine the solvability condition for $B(T_1)$, we take the inner product of Eq. (7.85) with the adjoint $W^*(s)$, integrate by parts, and obtain

$$\int_0^1 W^* H_w^* ds = \Big[\beta_{22}\left(W^* W^{\prime\prime\prime} - W^{*\prime} W^{\prime\prime} + W^{*\prime\prime} W^\prime - W^{*\prime\prime\prime} W\right) + J_\eta \rho^2 \left(W^* W^\prime - W^{*\prime} W\right)\Big]_{s=0}^{s=1} + \int_0^1 \Big\{ W\Big[\beta_{22} W^{*iv} + J_\eta \rho^2 W^{*\prime\prime} - \rho^2 W^*\Big]\Big\} ds \tag{7.91}$$

Setting $H_w^* = 0$ and $B_{w2}^* = 0$ in Eq. (7.91), we find that the homogeneous problem is similar to Eqs. (7.31)-(7.33). Hence, the system is self-adjoint and $W^*(s) = \Phi_w^*(s)$. Accordingly, Eq. (7.91) reduces to the following solvability condition for $B(T_1)$:

$$\int_0^1 \Phi_w H_w^* ds - \Phi_w(1) B_{w2}^* = 0 \tag{7.92}$$

Substituting for H_v^*, H_ϕ^*, H_w^*, B_{v2}^*, and B_{w2}^* from Appendix D into Eqs. (7.90) and (7.92) and performing the spatial integrations, we obtain the following modulation equations governing the dynamics of the interacting modes:

$$2i\omega\Gamma_1 A^\prime = 2i\omega\Gamma_2 A - \Gamma_3 \bar{A} B e^{2i\omega\delta T_1} - 2\Gamma_4 A B \bar{B} - 3\Gamma_5 A^2 \bar{A} - \Gamma_6 e^{i\omega\sigma T_1} \tag{7.93}$$

$$2i\rho\Lambda_1 B^\prime = 2i\rho\Lambda_2 B - \Lambda_3 A^2 e^{-2i\omega\delta T_1} - 2\Lambda_4 A \bar{A} B - 3\Lambda_5 B^2 \bar{B} \tag{7.94}$$

where the Γ_i and Λ_i are defined in Appendix D.

7.2 Perturbation Analysis Using the Method of Time-Averaged Lagrangian

The Lagrangian and virtual-work term corresponding to Eqs. (7.2)-(7.10) are

$$\begin{aligned}\mathcal{L} = \frac{1}{2}\epsilon\int_0^1 \Bigg\{ &\left[\frac{\partial}{\partial t}\int_0^s \frac{1}{2}\left(v'^2+w'^2\right)ds\right]^2 + \frac{1}{\epsilon}\left(\dot{v}^2+\dot{w}^2\right) + J_\xi\left(\frac{1}{\epsilon}\dot{\phi}^2 + 2\dot{\phi}\dot{v}'w' + \dot{v}'^2w'^2\right)\\ &+ \frac{1}{\epsilon}\left(J_\eta\dot{w}'^2 + J_\zeta\dot{v}'^2\right) - \beta_{11}\left(\frac{1}{\epsilon}\phi'^2 + 2\phi'v''w' + v''^2w'^2\right) - \beta_{22}\Bigg(\frac{1}{\epsilon}w''^2 + \phi^2v''^2 - 2\phi v''w''\\ &- \phi^2w''^2 + w'^2w''^2\Bigg) - \beta_{33}\left(\frac{1}{\epsilon}v''^2 - \phi^2v''^2 + v'^2v''^2 + 2\phi v''w'' + 2v'v''w'w'' + \phi^2w''^2\right)\\ &- \beta_{13}\left(2\phi'v'' - \phi^2\phi'v'' + v'^2\phi'v'' + 2w'v''^2 + 2\phi\phi'w'' + 2v'w'\phi'w'' + 2\phi w'v''w''\right)\Bigg\}ds \quad (7.95)\end{aligned}$$

$$\begin{aligned}\delta W = \epsilon\int_0^1 \Bigg\{ &\left[Q_v - \left[v'(s-1)\right]'Q_u - c_v\dot{v}\right]\delta v + \left[Q_w - \left[w'(s-1)\right]'Q_u - c_w\dot{w}\right]\delta w\\ &+ \left[Q_\phi - c_\phi\dot{\phi}\right]\delta\phi\Bigg\}ds = \epsilon\int_0^1\left\{\left[f\Omega^2\cos(\Omega t) - c_v\dot{v}\right]\delta v - \left[c_w\dot{w}\right]\delta w - \left[c_\phi\dot{\phi}\right]\delta\phi\right\}ds \quad (7.96)\end{aligned}$$

In the absence of damping and external forces, the system is conservative; the original partial-differential equations of motion and associated boundary conditions are derivable from a Lagrangian. As a consequence, the modulation equations obtained in Section 7.2 are expected to contain some symmetry properties. However, without numerically calculating the values of the coefficients one cannot easily identify the symmetries in Eqs. (7.93) and (7.94).

To further emphasize this point, we use the method of time-averaged Lagrangian and virtual work to determine once again the modulation equations. The advantage of this approach is that the process is more straightforward and the symmetries in the modulation equations are readily apparent.

Therefore, we substitute Eqs. (3.6), (3.7), and (7.11)-(7.13) into Eqs. (7.95) and (7.96) and obtain

$$\begin{aligned}\mathcal{L} = \frac{1}{2}\int_0^1 \Bigg\{ &\left(D_0v_0\right)^2 + \left(D_0w_0\right)^2 + J_\xi\left(D_0\phi_0\right)^2 + J_\eta\left(D_0w_0'\right)^2 + J_\zeta\left(D_0v_0'\right)^2 - \beta_{11}\phi_0'^2 - \beta_{22}w_0''^2\\ &- \beta_{33}v_0''^2 - 2\beta_{13}\phi_0'v_0''\Bigg\}ds + \frac{1}{2}\epsilon\int_0^1\left\{\left[D_0\int_0^s\frac{1}{2}\left(v_0'^2+w_0'^2\right)ds\right]^2 + 2\left(D_0v_0\right)\left(D_1v_0\right)\right.\end{aligned}$$

$$+2\left(D_0v_0\right)\left(D_0v_1\right)+2\left(D_0w_0\right)\left(D_1w_0\right)+2\left(D_0w_0\right)\left(D_0w_1\right)+2J_\xi\Big[\left(D_0\phi_0\right)\left(D_1\phi_0\right)$$
$$+\left(D_0\phi_0\right)\left(D_0\phi_1\right)+\left(D_0\phi_0\right)\left(D_0v_0'\right)w_0'+\frac{1}{2}\left(D_0v_0'\right)^2w_0'^2\Big]+2J_\eta\Big[\left(D_0w_0'\right)\left(D_1w_0'\right)$$
$$+\left(D_0w_0'\right)\left(D_0w_1'\right)\Big]+2J_\zeta\Big[\left(D_0v_0'\right)\left(D_1v_0'\right)+\left(D_0v_0'\right)\left(D_0v_1'\right)\Big]-2\beta_{11}\Big[\phi_0'\phi_1'+\phi_0'v_0''w_0'$$
$$+\frac{1}{2}v_0''^2w_0'^2\Big]-2\beta_{22}\Big[w_0''w_1''+\frac{1}{2}\phi_0^2v_0''^2-\phi_0v_0''w_0''-\frac{1}{2}\phi_0^2w_0''^2+\frac{1}{2}w_0'^2w_0''^2\Big]-2\beta_{33}\Big[v_0''v_1''$$
$$-\frac{1}{2}\phi_0^2v_0''^2+\frac{1}{2}v_0'^2v_0''^2+\phi_0v_0''w_0''+v_0'v_0''w_0'w_0''+\frac{1}{2}\phi_0^2w_0''^2\Big]-2\beta_{13}\Big[\phi_0'v_1''+\phi_1'v_0''-\frac{1}{2}\phi_0^2\phi_0'v_0''$$
$$+\frac{1}{2}v_0'^2\phi_0'v_0''+w_0'v_0''^2+\phi_0\phi_0'w_0''+v_0'w_0'\phi_0'w_0''+\phi_0w_0'v_0''w_0''\Big]\Big\}ds+\cdots \tag{7.97}$$

$$\delta W=\epsilon\int_0^1\Big\{\left[f\Omega^2\cos\left(\Omega T_0\right)-c_vD_0v_0\right]\delta v_0-\left[c_wD_0w_0\right]\delta w_0-\left[c_\phi D_0\phi_0\right]\delta\phi_0\Big\}ds+\cdots \tag{7.98}$$

Next, we substitute Eqs. (7.24)-(7.26) into Eqs. (7.97) and (7.98), use Eq. (7.72), retain only the slowly-varying terms, and obtain the following time-averaged Lagrangian and virtual work:

$$\frac{<\mathcal{L}>}{\epsilon}=-i\omega\Pi_1\left(A\bar{A}'-A'\bar{A}\right)-i\rho\Pi_2\left(B\bar{B}'-B'\bar{B}\right)+\Pi_3\left(\bar{A}^2Be^{2i\omega\delta T_1}+A^2\bar{B}e^{-2i\omega\delta T_1}\right)$$
$$+2\Pi_4A\bar{A}B\bar{B}+3\Pi_5A^2\bar{A}^2+3\Pi_6B^2\bar{B}^2+\cdots \tag{7.99}$$
$$\frac{<\delta W>}{\epsilon}=-2i\omega\Pi_7\left(A\delta\bar{A}-\bar{A}\delta A\right)-2i\rho\Pi_8\left(B\delta\bar{B}-\bar{B}\delta B\right)+\Pi_9\left(\delta\bar{A}e^{i\omega\sigma T_1}+\delta Ae^{-i\omega\sigma T_1}\right)+\cdots$$
$$=Q_A^*\delta A+\bar{Q}_A^*\delta\bar{A}+Q_B^*\delta B+\bar{Q}_B^*\delta\bar{B}+\cdots \tag{7.100}$$

where the Π_i are defined in Appendix D. Then, using Hamilton's extended principle

$$\frac{d}{dT_1}\left(\frac{\partial<\mathcal{L}>}{\partial\bar{A}'}\right)-\frac{\partial<\mathcal{L}>}{\partial\bar{A}}=\bar{Q}_A^* \tag{7.101}$$
$$\frac{d}{dT_1}\left(\frac{\partial<\mathcal{L}>}{\partial\bar{B}'}\right)-\frac{\partial<\mathcal{L}>}{\partial\bar{B}}=\bar{Q}_B^* \tag{7.102}$$

yields the following modulation equations governing the dynamics of the interacting modes:

$$2i\omega\Pi_1A'=2i\omega\Pi_7A-2\Pi_3\bar{A}Be^{2i\omega\delta T_1}-2\Pi_4AB\bar{B}-6\Pi_5A^2\bar{A}-\Pi_9e^{i\omega\sigma T_1} \tag{7.103}$$
$$2i\rho\Pi_2B'=2i\rho\Pi_8B-\Pi_3A^2e^{-2i\omega\delta T_1}-2\Pi_4A\bar{A}B-6\Pi_6B^2\bar{B} \tag{7.104}$$

Table 7.1: Values of the Γ_i, Λ_i, and Π_i for the $[10^\circ_6/45^\circ_4/90^\circ_5]_s$ graphite-epoxy composite beam considered.

Time-Averaged Lagrangian		Directly Attacking the Partial-Differential System			
Π_1	-1.00005	Γ_1	-1.00005	Λ_1	-1.00008
Π_2	-1.00008	Γ_2	$0.49998c_v + 0.77663c_\phi$	Λ_2	$0.49996c_w$
Π_3	-20.68924	Γ_3	-41.37849	Λ_3	-20.68924
Π_4	-20.78901	Γ_4	-20.78901	Λ_4	-20.78901
Π_5	-19.50055	Γ_5	-39.00110	Λ_5	-9.28130
Π_6	-4.64065	Γ_6	$-0.39149f\Omega^2$		
Π_7	$0.49998c_v + 0.77663c_\phi$				
Π_8	$0.49996c_w$				
Π_9	$-0.39149f\Omega^2$				

Using integration by parts once, we note from Appendix D that

$$\Pi_1 \equiv -\int_0^1 \left(\Phi_v^2 + J_\zeta \Phi_v'^2 + J_\xi \Phi_\phi^2\right) ds = \int_0^1 \left(J_\zeta \Phi_v \Phi_v'' - \Phi_v^2 - J_\xi \Phi_\phi^2\right) ds - \left[J_\zeta \Phi_v \Phi_v'\right]_{s=1} \equiv \Gamma_1 \quad (7.105)$$

and

$$\Pi_2 \equiv -\int_0^1 \left(\Phi_w^2 + J_\eta \Phi_w'^2\right) ds = \int_0^1 \left(J_\eta \Phi_w \Phi_w'' - \Phi_w^2\right) ds - \left[J_\eta \Phi_w \Phi_w'\right]_{s=1} \equiv \Lambda_1 \quad (7.106)$$

Therefore, comparing Eqs. (7.103) and (7.104) with Eqs. (7.93) and (7.94), we find that

$$\begin{gathered} \Gamma_2 = \Pi_7, \qquad \Gamma_3 = 2\Pi_3, \qquad \Gamma_4 = \Pi_4, \qquad \Gamma_5 = 2\Pi_5, \qquad \Gamma_6 = \Pi_9, \\ \Lambda_2 = \Pi_8, \qquad \Lambda_3 = \Pi_3, \qquad \Lambda_4 = \Pi_4, \qquad \text{and} \qquad \Lambda_5 = 2\Pi_6 \end{gathered} \quad (7.107)$$

Furthermore, one can now easily deduce the following symmetries in the modulation equations:

$$\Gamma_3 = 2\Lambda_3 = 2\Pi_3 \qquad \text{and} \qquad \Gamma_4 = \Lambda_4 = \Pi_4 \quad (7.108)$$

For the $[10^\circ_6/45^\circ_4/90^\circ_5]_s$ graphite-epoxy composite beam, whose properties and mode shapes are

defined by Eqs. (7.67)-(7.71), we present in Table 7.1 values of the coefficients Γ_i, Λ_i, and Π_i. It is clear from the Table 7.1 that the properties given by Eqs. (7.107) and (7.108) are satisfied.

Chapter 8

Conclusions

8.1 Results

We investigated the nonlinear responses of cantilever beams to direct and parametric harmonic excitations. An emphasis was put on the importance of nonlinear modal interactions on the steady-state responses. Both inertia and geometric nonlinearities were accounted for in the governing equations of motion and associated boundary conditions. We assumed the beams to be relatively long and thin, and therefore we modeled them using the Euler-Bernoulli theory.

Using three successive Euler-rotation angles, principles of mechanics of composites, and a variational formulation, we derived the Lagrangian, equations of motion, and boundary conditions governing the nonlinear bending-bending-twisting vibrations of symmetrically laminated composite and isotropic metallic inextensional beams.

Unlike linear beam theory, an exact analytical solution of the nonlinear response is typically unattainable. However, for weak nonlinearities in the governing equations of motion and associated boundary conditions, perturbation methods can be used to determine uniform approximate solutions. Next, we summerize the results of the different investigations.

8.1.1 Bending-Bending Dynamics of Parametrically Excited Cantilever Beams

The nonlinear nonplanar response of a cantilever inextensional metallic beam to a principal parametric resonance of its flexural modes was investigated. The cross section of the beam is such that the excited mode is involved in a one-to-one internal resonance with a flexural mode in the orthogonal direction. The lowest torsional frequencies of the beams are much larger than the frequencies of the excited modes so that the torsional inertia can be neglected.

We used the inextensionality condition to express the longitudinal displacement $u(s,t)$ in terms of $v(s,t)$ and $w(s,t)$. Moreover, neglecting the rotational inertia, we expressed $\phi(s,t)$ in terms of $v(s,t)$ and $w(s,t)$. Substituting these expressions for $u(s,t)$ and $\phi(s,t)$ into the Lagrangian derived by Crespo da Silva and Glynn (1978a, b), we obtained a Lagrangian in terms of $v(s,t)$ and $w(s,t)$. Instead of following Nayfeh and Pai (1989) and applying the method of multiple scales to the equations derived by Crespo da Silva and Glynn (1978b), we applied the method of multiple scales to the Lagrangian to derive the modulation equations. These equations exhibit all of the symmetries found by Feng and Leal (1994).

Using a pseudo-arclength continuation scheme, we generated typical frequency-response curves. Calculating the eigenvalues of the Jacobian matrix, we assessed the stability of these responses. We found that, as the excitation frequency is slowly varied, the responses may undergo saddle-node bifurcations and subcritical and supercritical pitchfork and Hopf bifurcations. The normal form of the modulation equations were calculated in the vicinity of the Hopf bifurcations to assess the stability of the created limit cycles and determine whether the Hopf bifurcations are subcritical or supercritical. The effect of the bending stiffness ratio detuning on the loci of the bifurcation points was investigated and codimension-2 bifurcations were identified. A combination of a two-point boundary-value scheme and a Newton-Raphson procedure was used to calculate limit-cycle solutions of the modulation equations and then Floquet theory was used to assess their stability. We found that these limit cycles may undergo symmetry-breaking, cyclic-fold, and period-doubling bifurcations. The period-doubling bifurcations culminate in chaos. The chaotic attractors may undergo attracting-merging and boundary crises.

8.1.2 Nonlinear Nonplanar Dynamics of Directly Excited Cantilever Beams

The nonlinear nonplanar response of a cantilever inextensional metallic beam to a transverse base excitation of one of its flexural modes was investigated. The cross section of the beam is near-square, and hence the excited mode is involved in a one-to-one internal resonance with a flexural mode in the orthogonal direction. Because the system is similar to that discussed in Chapter 4, we only needed to modify the virtual-work term to account for the base excitation and hence, obtain the modulation equations. Using a pseudo-arclength scheme, we studied the influence of the forcing amplitude and the internal resonance detuning on the fixed points. We considered two cases: (i) the first bending modes, modes (1,1), are excited and (ii) the second bending modes, modes (2,2), are excited.

Because the system is directly excited, nontrivial single-mode fixed points exist as soon as the forcing amplitude f is increased from zero. As f increases beyond a threshold, the single-mode solution loses stability through a pitchfork bifurcation and two-mode solutions come about. For modes (1,1), we found that the excited mode may exhibit pseudo-saturation. For modes (2,2), the two-mode response may either continue to be stable while its amplitude increases monotonously or undergo Hopf bifurcations resulting in limit-cycle solutions.

Due to the nondimensionalizing scheme used, we found that the internal resonance detuning δ_2 does not affect the amplitude of the single-mode solutions. However, we showed that the influence of δ_2 on the amplitude of the two-mode solutions and the stability of both single-mode and two-mode solutions can be significant. Furthermore, we found that nonplanar oscillations are more likely to occur when $\delta_2 < 0$; that is, when the excitation is along the direction where the beam is stiffer in bending.

Using numerical integration, a shooting algorithm, and Floquet theory, we traced eleven branches of limit-cycle solutions for the case of modes (1,1). Two of the branches result from two supercritical Hopf bifurcations while the remaining nine are isolated. We found that the response can be complex, undergoing cyclic-fold, symmetry-breaking, and period-doubling bifurcations. The period-doubling bifurcations sometimes culminate in chaos and other times result in bubble structures.

A case where an asymmetric limit cycle underwent a homoclinic bifurcation near a saddle-focus

was analyzed. Following Shilnikov theory and using the symmetry of the modulation equations, we found that the response after the homoclinicity is a larger symmetric limit cycle. Other interesting behaviors found include attractor-merging and boundary crises.

8.1.3 Nonlinear Bending-Bending-Torsional Oscillations to Combination Parametric Excitations

The nonlinear bending-torsional oscillations of cantilever beams excited by combination parametric resonances were analyzed using two approaches. In the first approach, the method of multiple scales was applied directly to the partial-differential system to derive the modulation equations. In the second approach, the equations of motion were first discretized with respect to the linear undamped mode shapes and then the method of multiple scales was applied to obtain the modulation equations.

We considered two resonance cases, $\Omega \approx \omega_{v1} + \omega_{\phi 1}$ and $\Omega \approx \omega_{v2} + \omega_{\phi 1}$, and generated typical frequency- and amplitude-response curves. The results obtained with discretization are erroneous. This is because the discretization assumes that the spatial part of the solution at the higher orders is equal to the mode shapes of the undamped system. However, solving the partial-differential system, we saw that in general this is not true.

The analysis demonstrates that high-frequency low-amplitude torsional oscillations may activate low-frequency high-amplitude flexural oscillations through combination parametric resonances. The resulting overall motion of the beam in such cases may be sufficiently large and if ignored may be disastrous.

8.1.4 Transfer of Energy from High- to Low-Frequency Modes in the Bending-Torsion Oscillations

We investigated the transfer of energy from high- to low-frequency modes in the nonlinear bending-twisting response of cantilever beams. We assumed the beam to be relatively long, thin, and wide. We excited it transversely along its stiff direction at a forcing frequency near the first natural frequency of the fundamental torsional mode. We found that through the zero-to-one internal resonance, the first in-plane bending mode is activated.

We obtained the modulation equations using two approaches: (i) applying the method of multiple scales directly to the governing partial-differential system and (ii), using the method of time-averaged Lagrangian and virtual work. The results are identical and the symmetries exhibited by the system were obtained.

Using a pseudo-arclength scheme, we generated typical frequency- and force-response curves. We found that the trivial solution loses stability through supercritical and subcritical pitchfork bifurcations. The nontrivial fixed points, which for this system correspond to the beam statically bending while simultaneously oscillating periodically in torsion, were found to be mostly unstable. Hence, the oscillatory response of the beam is expected to be at least periodic in bending and quasiperiodic in torsion.

Using numerical integration, a shooting algorithm, and Floquet theory, we traced two branches of dynamic solutions. In both cases, as the forcing amplitude was increased, the symmetric limit cycle lost symmetry and then underwent a sequence of period-doubling bifurcations. For the limit cycle on the first branch, the period-two limit cycle underwent a subcritical period-doubling bifurcation. For the limit cycle on the second branch, the period-four limit cycle underwent a subcritical period-doubling bifurcation. In both cases, a type-3 intermittency occurred.

The dominant influence of the high-amplitude low-frequency response of the first in-plane bending mode on the periodic and chaotic responses of a beam excited by a high-frequency forcing demonstrates the importance of considering nonlinearities and the possible modal interactions they may produce.

8.1.5 Symmetry in Composite Beams

We used the Lagrangian and corresponding partial-differential equations of motion and associated boundary conditions derived in Chapter 2 to analyze the nonlinear responses of symmetrically laminated composite beams. A two-to-one internal resonance between the out-of-plane bending motion and the in-plane bending and torsional motions was considered. The main objective was to demonstrate that the modulation equations exhibit symmetry properties as the original system, in the absence of damping and external forces, is conservative and hence derivable from a Lagrangian.

This is contrary to the results of Pai and Nayfeh (1991a, b) whose modulation equations did not exhibit any symmetry properties.

We used two approaches to determine the equations that govern the dynamics of the interacting modes. In the first, we directly applied the method of multiple scales to the governing partial-differential equations and associated boundary conditions. In the second, we applied the method of multiple scales to the Lagrangian and virtual-work term. We then averaged the result and used Hamilton's extended principle to obtain the modulation equations. Comparing the two results, we found that one can easily deduce the symmetry in the modulation equations. Furthermore, we numerically calculated the coefficients for a $[10^\circ_6/45^\circ_4/90^\circ_5]$ graphite-epoxy composite beam and found that the results demonstrate these symmetry properties.

8.2 Recommendations for Future Work

8.2.1 External Combination, Subcombination, and Multifrequency Resonances

When the excitation is direct, an external combination resonance can occur in systems with quadratic nonlinearities when the excitation frequency $\Omega \approx |\omega_i \pm \omega_j|$ and in systems with cubic nonlinearities when $\Omega \approx |\omega_i \pm \omega_j + \omega_k|$ or $\Omega \approx |2\omega_i \pm \omega_j|$. Furthermore, external subcombination resonances can occur when $\Omega \approx \frac{1}{2}(\omega_i \pm \omega_j)$. Multifrequency resonant excitations occur when the external excitation is assumed to be the sum of two harmonics with incommensurate frequencies Ω_n and Ω_m such that $N\Omega_n \pm M\Omega_m \approx \omega_i$ or $\approx \omega_i \pm \omega_j$. In the presence of damping, all of the modes that are not directly excited or indirectly excited by an internal resonance will decay with time. Hence, the steady-state response of the system will consist of modes excited by the combination resonance (Sridhar, Nayfeh, and Mook, 1975; Nayfeh and Mook, 1979; Nayfeh, 1983c, 1984, and 1985; and Mook, HaQuang, and Plaut, 1986).

Although some work has been done to investigate such resonances in structures, none dealt with the nonplanar responses of cantilever beams. Nayfeh and Arafat (1998) investigated the nonlinear planar responses of cantilever beams to combination and subcombination resonances. Yamamoto, Yasuda, and Tei (1981, 1982) and Yasuda, Kato, and Masuda (1993) considered simply-supported

beams; Sridhar, Nayfeh, and Mook (1975) considered hinged-clamped beams; Yasuda and Hayashi (1982) considered clamped circular plates; and Popovic, Nayfeh, Oh, and Nayfeh (1995) considered a portal frame.

Therefore, analyzing the nonplanar responses of cantilever beams to combination resonances will further enhance our understanding of the modal interactions they can undergo. A possible scenario is the combination resonance $\Omega \approx \omega_v + \omega_\phi$.

8.2.2 Nonlinear Responses of Symmetrically Laminated Composite Beams

The response of monoclinic composite beams having a two-to-one internal resonance to direct excitations was investigated by Pai and Nayfeh (1990b, 1991a and b). However, their modulation equations did not exhibit any symmetric properties and, hence, did not reflect the conservative nature of the system in the absence of damping. Therefore, the results of their analysis are incorrect.

In contrast, we derived in Chapter 7 the modulation equations for the monoclinic composite beams considered by Pai and Nayfeh (1991a, b) and showed that they do in fact exhibit symmetry properties. Therefore, it would be worthwhile to use these results to perform a detailed analysis of the response of the beam.

Furthermore, the nonlinear modal interactions in symmetrically laminated composite beams that are parametrically excited have not been, to my knowledge, considered.

8.2.3 Nonlinear Responses of Asymmetrically Laminated Composite Beams

The investigation of nonlinear modal interactions in anisotropic composite beams, where all bending, stretching, and twisting modes are linearly and nonlinearly coupled, is an interesting yet challenging problem. If one can taylor the analysis to a specific material that is widely used in industry, the benefits could be tremendous.

Bibliography

Anderson, G. L., 1975, "On the Extensional and Flexural Vibrations of Rotating Beams," *International Journal of Non-Linear Mechanics*, Vol. 10, pp. 223-236.

Anderson, T. J., Balachandran, B., and Nayfeh, A. H., 1992, "Observations of Nonlinear Interactions in a Flexible Cantilever Beam," in *Proceedings of the 33rd AIAA/ASME/ASCE/AHS/ ASC Structures, Structural Dynamics and Materials Conference*, Dallas, Texas, April 13-15, pp. 1678-1686.

Anderson, T. J., Balachandran, B., and Nayfeh, A. H., 1994, "Nonlinear Resonances in a Flexible Cantilever Beam," *Journal of Vibration and Acoustics*, Vol. 116, pp. 480-484.

Ariaratnam, S. T., 1986, "Parametric Resonance," in *Proceedings of the Tenth U.S. National Congress of Applied Mechanics*, Austin, Texas, June 16-20, pp. 181-185.

Asmis, K. G., and Tso, W. K., 1972, "Combination and Internal Resonance in a Nonlinear Two-Degrees-of-Freedom System," *Journal of Applied Mechanics*, Vol. 39, pp. 832-834.

Bauchau, O. A., and Hong, C. H., 1988, "Nonlinear Composite Beam Theory," *Journal of Applied Mechanics*, Vol. 55, pp. 156-163.

Billah, K. Y., and Scanlan, R. H., 1991, "Resonance, Tacoma Narrows Bridge Failure, and Undergraduate Physics Textbooks," *American Journal of Applied Physics*, Vol. 59, pp. 118-124.

Bishop, R. E. D., Cannon, S. M., and Miao, S., 1989, "On Coupled Bending and Torsional Vibrations of Uniform Beams," *Journal of Sound and Vibration*, Vol. 131, pp. 457-464.

Bolotin, V. V., 1964, *The Dynamic Stability of Elastic Systems*, Holden-Day, San Francisco, California.

Burgreen, D., 1951, "Free Vibrations of a Pin-Ended Column with Constant Distance Between Pin Ends," *Journal of Applied Mechanics*, Vol. 18, pp. 135-139.

Cannon, J. T., and Dostrovsky, S., 1981, *The Evolution of Dynamics: Vibration Theory from 1687 to 1742*, Springer-Verlag, New York.

Cartmell, M. P., 1990, *Introduction to Linear, Parametric and Nonlinear Vibrations*, Chapman and Hall, London.

Cartmell, M. P., and Roberts, J. W., 1987, "Simultaneous Combination Resonances in a Parametrically Excited Cantilever Beam," *Strain*, Vol. 23, pp. 117-126.

Chin, C., and Nayfeh, A. H., 1996, "Bifurcations and Chaos in Externally Excited Circular Cylindrical Shells," *Journal of Applied Mechanics*, Vol. 63, pp. 565-574.

Chin, C., Nayfeh, A. H., and Mook, D. T., 1995, "The Response of a Nonlinear System With a Nonsemisimple One-to-One Resonance to a Combination Parametric Resonance," *International Journal of Bifurcation and Chaos*, Vol. 5, pp. 971-982.

Crespo da Silva, M. R. M., 1980, "On the Whirling of a Base-Excited Cantilever Beam," *Journal of the Acoustical Society of America*, Vol. 67, pp. 704-707.

Crespo da Silva, M. R. M., 1981, "Flap-Lag-Torsional Dynamic Modelling of Rotor Blades in Hover and in Forwards Flight, Including the Effect of Cubic Non-Linearities," *NASA Contractor Report*, NASA CR-166194.

Crespo da Silva, M. R. M., 1991, "Equations for Nonlinear Analysis of 3D Motions of Beams," *Applied Mechanics Review*, Vol. 44, pp. S51-S59.

Crespo da Silva, M. R. M., and Glynn, C. C., 1978, "Nonlinear Flexural-Flexural-Torsional Dynamics of Inextensional Beams. I. Equations of Motion," *Journal of Structural Mechanics*, Vol. 6, pp. 437-448.

Crespo da Silva, M. R. M., and Glynn, C. C., 1978, "Nonlinear Flexural-Flexural-Torsional Dynamics of Inextensional Beams. II. Forced Motions," *Journal of Structural Mechanics*, Vol. 6, pp. 449-461.

Crespo da Silva, M. R. M., and Glynn, C. C., 1979, "Non-Linear Non-Planar Resonant Oscillations in Fixed-Free Beams with Support Asymmetry," *International Journal of Solids and Structures*, Vol. 15, pp. 209-219.

Crespo da Silva, M. R. M., and Zaretzky, C. L., 1994, "Nonlinear Flexural-Flexural-Torsional Interactions in Beams Including the Effect of Torsional Dynamics. I: Primary Resonance," *Nonlinear Dynamics*, Vol. 5, pp. 3-23.

Crespo da Silva, M. R. M., Zaretzky, C. L., and Hodges, D. H., 1991, "Effects of Approximations on the Static and Dynamic Response of a Cantilever With a Tip Mass," *International Journal of Solids and Structures*, Vol. 27, pp. 565-583.

Cullimore, M. S. G., 1949, "The Shortening Effect, A Nonlinear Feature of Pure Torsion," in *Engineering Structures*, Academic Press, New York, pp. 153-164.

Dokumaci, E., 1978, "Pseudo-Coupled Bending-Torsion Vibrations of Beams under Lateral Parametric Excitation," *Journal of Sound and Vibration*, Vol. 58, pp. 233-238.

Dokumaci, E. 1987, "An Exact Solution for Coupled Bending and Torsion Vibrations of Uniform Beams Having Single Cross-Sectional Symmetry," *Journal of Sound and Vibration*, Vol. 119, pp. 443-449.

Dowell, E. H., Traybar, J., and Hodges, D. H., 1977, "An Experimental-Theoretical Correlation Study of Non-Linear Bending and Torsion Deformations of a Cantilever Beam," *Journal of Sound and Vibration*, Vol. 50, pp. 533-544.

Dugundji, J., and Mukhopadhyay, V., 1973, "Lateral Bending-Torsion Vibrations of a Thin Beam Under Parametric Excitation," *Journal of Applied Mechanics*, Vol. 40, pp. 693-698.

Evan-Iwanowski, R. M., 1965, "On the Parametric Response of Structures," *Applied Mechanics Reviews*, Vol. 18, pp. 699-702.

Feng, Z. C., and Leal, L. G., 1994, "Symmetries of the Amplitude Equations of an Inextensional Beam With Internal Resonance," *Journal of Applied Mechanics*, Vol. 62, pp. 235-238.

Glendinning, P., 1994, *Stability, Instability and Chaos: an Introduction to the Theory of Nonlinear Differential Equations*, Cambridge University Press, New York.

Haight, E. C., and King, W. W., 1970, "Stability of Parametrically Excited Vibrations of an Elastic Rod," *Developments in Theoretical and Applied Mechanics*, Vol. 5, pp. 677-713.

Haight, E. C., and King, W. W., 1972, "Stability of Nonlinear Oscillations of an Elastic Rod," *Journal of the Acoustical Society of America*, Vol. 52, pp. 899-911.

Hodges, D. H., and Dowell, E. H., 1974, "Nonlinear Equations of Motion for the Elastic Bending and Torsion of Twisted Nonuniform Rotor Blades," *NASA Technical Notes*, NASA TN D-7818.

Hodges, D. H., Crespo da Silva, M. R. M., and Peters, D. A., 1988, "Nonlinear Effects in the Static and Dynamic Behavior of Beams and Rotor Blades," *Vertica*, Vol. 12, pp. 243-256.

Hyer, M. W., 1979, "Whirling of a Base-Excited Cantilever Beam," *Journal of the Acoustical Society of America*, Vol. 65, pp. 931-939.

Ibrahim, R. A., and Hijawi, M., 1998, "Deterministic and Stochastic Response of Nonlinear Coupled Bending-Torsion Modes in a Cantilever Beam," *Nonlinear Dynamics*, Vol. 16, pp. 259-292.

Kar, R. C., and Sujata, T., 1990, "Parametric Instability of an Elastically Restrained Cantilever Beam," *Computers & Structures*, Vol. 34, pp. 469-475.

Kar, R. C., and Sujata, T., 1992, "Dynamic Stability of a Rotating, Pretwisted, and Preconed Cantilever Beam Including Coriolis Effects," *Computers & Structures*, Vol. 42, pp. 741-750.

Krishnaiyar, N. C., 1922, "On the Amplitude of Vibrations Maintained by Forces of Double Frequency," *The London, Edinburgh, and Dublin Philosophical Magazine and Journal of Science*, Vol. 43, pp. 503-510.

Lee, S. I., Lee, J. M., and Chang, S. I., 1997, "Nonlinear Modal Interactions of a Cantilever Beam with an Internal Resonance," in *Proceedings of the International Modal Analysis Conference (IMAC)*, Orlando, Florida, pp. 1614-1621.

Love, A. E. H., 1944, *A Treatise on the Mathematical Theory of Elasticity*, Dover, New York.

Mase, G. E., 1970, *Theory and Problems of Continuum Mechanics*, Schaum's Outline Series, McGraw-Hill, New York.

McDonald, P. H., 1955, "Nonlinear Dynamic Coupling in a Beam Vibration," *Journal of Applied Mechanics*, Vol. 22, pp. 573-578.

Meirovitch, L., 1997, *Principles and Techniques of Vibrations*, Prentice Hall, Upper Saddle River, New Jersey.

Mettler, E., 1967, "Stability and Vibration Problems of Mechanical Systems Under Harmonic Excitation," in *Dynamic Stability of Structures*, Herrmann, G., ed., Pergamon Press, New York, pp. 169-183.

Mook, D. T., HaQuang, N., and Plaut, R. H., 1986, "The Influence of an Internal Resonance on Non-Linear Structural Vibrations under Combination Resonance Conditions," *Journal of Sound and Vibration*, Vol. 104, pp. 229-241.

Nayfeh, A. H., 1973, *Perturbation Methods*, Wiley-Interscience, New York.

Nayfeh, A. H., 1981, *Introduction to Perturbation Methods*, Wiley-Interscience, New York.

Nayfeh, A. H., 1983, "Response of Two-Degree-of-Freedom Systems to Multifrequency Parametric Excitations," *Journal of Sound and Vibration*, Vol. 88, pp. 1-10.

Nayfeh, A. H., 1983, "Parametrically Excited Multidegree-of-Freedom Systems with Repeated Frequencies," *Journal of Sound and Vibration*, Vol. 88, pp. 145-150.

Nayfeh, A. H., 1983, "Combination Resonances in the Non-Linear Response of Bowed Structures to a Harmonic Excitation," *Journal of Sound and Vibration*, Vol. 90, pp. 457-470.

Nayfeh, A. H., 1984, "Quenching of a Primary Resonance by a Combination Resonance of Additive or Difference Type," *Journal of Sound and Vibration*, Vol. 97, pp. 65-73.

Nayfeh, A. H., 1985, "The Response of Non-Linear Single-Degree-of-Freedom Systems to Multi-frequency Excitations," *Journal of Sound and Vibration*, Vol. 102, pp. 403-414.

Nayfeh, A. H., 1987, "Parametric Excitation of Two Internally Resonant Oscillators," *Journal of Sound and Vibration*, Vol. 119, pp. 95-109.

Nayfeh, A. H., 1997, "On the Discretization of Weekly Nonlinear Spatially Continuous Systems," in *Differential Equations and Chaos Lectures on Selected Topics*, Ibragimov, N. H., Mahomed, F. M., Mason, D. P., and Sherwell, D., eds., pp 3-39.

Nayfeh, A. H., and Arafat, H. N., 1998, "Nonlinear Response of Cantilever Beams to Combination and Subcombination Resonances," *Shock and Vibration*, Vol. 5, pp. 277-288.

Nayfeh, A. H., and Balachandran, B., 1989, "Modal Interactions in Dynamical and Structural Systems," *Applied Mechanics Reviews*, Vol. 42, pp. S175-S201.

Nayfeh, A. H., and Balachandran, B., 1995, *Applied Nonlinear Dynamics*, Wiley-Interscience, New York.

Nayfeh, A. H., and Chin, C-M., 1995, "Nonlinear Interactions in a Parametrically Excited System with Widely Spaced Frequencies," *Nonlinear Dynamics*, Vol. 7, pp. 195-216.

Nayfeh, A. H., and Jebril, A. E. S., 1987, "The Response of Two-Degree-of-Freedom Systems with Quadratic and Cubic Non-Linearities to Multifrequency Parametric Excitations," *Journal of Sound and Vibration*, Vol. 115, pp. 83-101.

Nayfeh, A. H., and Mook, D. T., 1978, "A Saturation Phenomenon in the Forced Response of Systems With Quadratic Nonlinearities," in *Proceedings of the $VIII^{th}$ International Conference on Nonlinear Oscillations*, Prague, Czech Republic.

Nayfeh, A. H., and Mook, D. T., 1979, *Nonlinear Oscillations*, Wiley-Interscience Publication,

New York.

Nayfeh, A. H., and Mook, D. T., 1995, "Energy Transfer from High-Frequency to Low-Frequency Modes in Structures," in *ASME Special Combined Issue of the Journal of Mechanical Design and Journal of Vibration and Acoustics, 50th Anniversary of the Design Engineering Division*, Vol. 117, pp. 186-195.

Nayfeh, A. H., Mook, D. T., and Nayfeh, J. F., 1987, "Some Aspects of Modal Interactions in the Response of Beams," *Proceedings of the AIAA 28th Structures, Structural Dynamics and Materials Conference*, Monterey, California, April 6-8.

Nayfeh, A. H., and Pai, P. F., 1989, "Non-Linear Non-Planar Parametric Responses of an Inextensional Beam," *International Journal of Non-Linear Mechanics*, Vol. 24, pp. 139-158.

Nayfeh, A. H., and Zavodney, L. D., 1986, "The Response of Two-Degree-of-Freedom Systems with Quadratic Non-Linearities to a Combination Parametric Resonance," *Journal of Sound and Vibration*, Vol. 107, pp. 329-250.

Nayfeh, S. A., and Nayfeh, A. H., 1992, "Energy Transfer from High- to Low-Frequency Modes in Flexible Structures," *Nonlinear Vibrations*, ASME DE-Vol. 50/AMD-Vol. 144, pp. 89-97.

Nayfeh, S. A., and Nayfeh, A. H., 1993, "Nonlinear Interactions Between Two Widely Spaced Modes - External Excitation," *International Journal of Bifurcation and Chaos*, Vol. 3, pp. 417-427.

Nayfeh, S. A., and Nayfeh, A. H., 1994, "Energy Transfer from High- to Low-Frequency Modes in a Flexible Structure via Modulation," *Journal of Vibration and Acoustics*, Vol. 116, pp. 203-207.

Pai, P. F., 1990, *Nonlinear Flexural-Flexural-Torsional Dynamics of Metallic and Composite Beams*, Dissertation, Virginia Polytechnic Institute and State University, Blacksburg, Virginia.

Pai, P. F., and Nayfeh, A. H., 1990, "Non-Linear Non-Planar Oscillations of a Cantilever Beam Under Lateral Base Excitations," *International Journal of Non-Linear Mechanics*, Vol. 25, pp. 455-474.

Pai, P. F., and Nayfeh, A. H., 1990, "Three-Dimensional Nonlinear Vibrations of Composite Beams - I. Equations of Motion," *Nonlinear Dynamics*, Vol. 1, pp. 477-502.

Pai, P. F., and Nayfeh, A. H., 1991, "Three-Dimensional Nonlinear Vibrations of Composite

Beams - II. Flapwise Excitations," *Nonlinear Dynamics*, Vol. 2, pp. 1-34.

Pai, P. F., and Nayfeh, A. H., 1991, "Three-Dimensional Nonlinear Vibrations of Composite Beams - III. Chordwise Excitations," *Nonlinear Dynamics*, Vol. 2, pp. 137-156.

Pai, P. F., and Nayfeh, A. H., 1992, "A Nonlinear Composite Beam Theory," *Nonlinear Dynamics*, Vol. 3, pp. 273-303.

Popovic, P., Nayfeh, A. H., Oh, K., and Nayfeh, S. A., 1995, "An Experimental Investigation of Energy Transfer from a High-Frequency Mode to a Low Frequency Mode in a Flexible Structure," Journal of Vibration and Control, Vol. 1, pp. 115-128.

Rayleigh, J. W. S., 1945, *The Theory of Sound*, Vol. 1, Dover, New York.

Sathyamoorthy, M., 1982, "Nonlinear Analysis of Beams, Part I: A Survey of Recent Advances," *Shock and Vibration Digest*, Vol. 14, pp. 19-35.

Sathyamoorthy, M., 1982, "Nonlinear Analysis of Beams, Part II: Finite Element Methods," *Shock and Vibration Digest*, Vol. 14, pp. 7-18.

Serling, R. J., 1963, *The Electra Story*, Doubleday, Garden City, New York.

Seydel, R., 1994, *Practical Bifurcation and Stability Analysis*, Springer-Verlag, New York.

Shames, I. H., and Dym, C. L., 1985, *Energy and Finite Element Methods in Structural Mechanics*, Taylor & Francis, Bristol, Pennsylvania.

Shilnikov, L. P., 1965, "A Case of the Existence of a Denumerable Set of Periodic Motions," *Soviet Math. Dokl.*, Vol. 6, pp. 163-166.

Shilnikov, L. P., 1968, "On the Generation of a Periodic Motion from Trajectories Doubly Asymptotic to an Equilibrium State of Saddle-Type," *Math. USSR Sb.*, Vol. 6, pp. 427-438.

Shilnikov, L. P., 1970, "A Contribution to the Problem of the Structure of an Extended Neighborhood of a Rough Equilibrium State of Saddle-Type Focus," *Math. USSR Sb.*, Vol. 10, pp. 91-102.

Shyu, I.-M. K., Mook, D. T., and Plaut, R. H., 1993, "Whirling of a Forced Cantilevered Beam with Static Deflection. I: Primary Resonance," *Nonlinear Dynamics*, Vol. 4, pp. 227-249.

Shyu, I.-M. K., Mook, D. T., and Plaut, R. H., 1993, "Whirling of a Forced Cantilevered Beam with Static Deflection. II: Superharmonic and Subharmonic Resonances," *Nonlinear Dynamics*, Vol. 4, pp. 337-356.

Shyu, I.-M. K., Mook, D. T., and Plaut, R. H., 1993, "Whirling of a Forced Cantilevered Beam

with Static Deflection. III: Passage through Resonance," *Nonlinear Dynamics*, Vol. 4, pp. 461-481.

Southwell, R. V., 1941, *An Introduction to the Theory of Elasticity for Engineers and Physicists*, Oxford University Press, New York.

Spiegel, M. R., 1968, *Mathematical Handbook of Formulas and Tables*, Schaum's Outline Series, McGraw-Hill, New York.

Sridhar, S., Nayfeh, A. H., and Mook, D. T., 1975, "Nonlinear Resonances in a Class of Multi-Degree-of-Freedom Systems," *Journal of the Acoustical Society of America*, Vol. 58, pp. 113-123.

Streit, D. A., Bajaj, A. K., and Krousgrill, C. M., 1988, "Combination Parametric Resonance Leading to Periodic and Chaotic Response in Two-Degree-of-Freedom Systems with Quadratic Nonlinearities," *Journal of Sound and Vibration*, Vol. 124, pp. 297-314.

Tabaddor, M., and Nayfeh, A. H., 1997, "An Experimental Investigation of Multimode Responses in a Cantilever Beam," *Journal of Vibration and Acoustics*, Vol. 119, pp. 532-538.

Tezak, E. G., Nayfeh, A. H., and Mook, D. T., 1982, "Parametrically Excited Non-Linear Multidegree-of Freedom Systems with Repeated Natural Frequencies," *Journal of Sound and Vibration*, Vol. 85, pp. 459-472.

Thompson, J. M. T., and Stewart, H. B., 1986, *Nonlinear Dynamics and Chaos*, Wiley-Interscience, Chichester, England.

Timoshenko, S. P., 1921, "On the Correction for Shear of the Differential Equation for Transverse Vibrations of Prismatic Bars," *Philosophical Magazine*, Vol. 41, pp. 744-747.

Timoshenko, S. P., 1922, "On the Transverse Vibrations of Bars of Uniform Cross Section," *Philosophical Magazine*, Vol. 43, pp. 125-131.

Timoshenko, S. P., 1983, *History of Strength of Materials*, Dover, new York.

Timoshenko, S. P., and Goodier, J. N., 1970, *Theory of Elasticity*, McGraw-Hill, New York.

Tso, W. K., 1968, "Parametric Torsional Stability of a Bar Under Axial Excitation," *Journal of Applied Mechanics*, Vol. 35, pp. 13-19.

Tso, W. K., and Asmis, K. G., 1974, "Multiple Parametric Resonance in a Non-Linear Two Degree of Freedom System," *International Journal of Non-Linear Mechanics*, Vol. 9, pp. 269-277.

von Kármán, T., 1940, "The Engineer Grapples with Nonlinear Problems," *Bulletin of the Amer-*

ican Mathematical Society, Vol. 46, pp. 615-683.

Whitney, J. M., 1987, *Structural Analysis of Laminated Anisotropic Plates*, Technomic, Lancaster, Pennsylvania.

Woinowsky-Krieger, S., 1950, "The Effect of an Axial Force on the Vibration of Hinged Bars," *Journal of Applied Mechanics*, Vol. 17, pp. 35-36.

Yamamoto, T., Yasuda, K., and Tei, N., 1981, "Summed and Differential Harmonic Oscillations in a Slender Beam," *Bulletin of the JSME*, Vol. 24, pp. 1214-1222.

Yamamoto, T., Yasuda, K., and Tei, N., 1982, "Super Summed and Differential Harmonic Oscillations in a Slender Beam," *Bulletin of the JSME*, Vol. 25, pp. 959-968.

Yasuda, K., and Hayashi, N., 1982, "Summed and Differential Oscillations in a Circular Plate," *Bulletin of the JSME*, Vol. 25, pp. 1582-1590.

Yasuda, K., Kato, M., and Masuda, H., 1993, "Single-Mode and Multimode Combination Tones in a Nonlinear Beam," *JSME International Journal, Series C*, Vol. 36, pp. 17-25.

Zaretzky, C. L., and Crespo da Silva, M. R. M., 1994, "Experimental Investigation of Non-Linear Modal Coupling in the Response of Cantilever Beams," *Journal of Sound and Vibration*, Vol. 174, pp. 145-167.

Zaretzky, C. L., and Crespo da Silva, M. R. M., 1994, "Nonlinear Flexural-Flexural-Torsional Interactions in Beams Including the Effect of Torsional Dynamics. II: Combination Resonance," *Nonlinear Dynamics*, Vol. 5, pp. 161-180.

Zavodney, L. D., 1987, "Can the Modal Analyst Afford to Be Ignorant of Nonlinear Vibration Phenomena?," in *Proceedings of the Fifth International Modal Analysis Conference*, London, England, April 6-9, pp. 154-159.

Zavodney, L. D., and Nayfeh, A. H., 1989, "The Non-Linear Response of a Slender Beam Carrying a Lumped Mass to a Principal Parametric Excitation: Theory and Experiment," *International Journal of Non-Linear Mechanics*, Vol. 24, pp. 105-125.

Appendix A
Bending-Bending Oscillations of Beams

$$R_1 = 2\omega_{1m}\mu_1 \tag{8.1}$$

$$R_2 = -\frac{1}{2}\omega_{1m}\omega_{2n}\Gamma_6 + \frac{1}{4}\left[(1+\delta_0)\Gamma_3 + \frac{\delta_0^2}{\beta_\gamma}\Gamma_2 + \delta_0\Gamma_1\right] \tag{8.2}$$

$$R_3 = 2g\omega_{1m}^2\Gamma_7 \tag{8.3}$$

$$R_4 = 2\sigma\omega_{1m}^2 - \delta_2 z_m^4 \tag{8.4}$$

$$R_5 = \frac{1}{4}\left[2\omega_{1m}^2\Gamma_5 - 3\left(1+\delta_0\right)\Gamma_4\right] \tag{8.5}$$

$$R_6 = \frac{1}{2}\left[\left(1+\delta_0\right)\Gamma_3 + \frac{\delta_0^2}{\beta_\gamma}\Gamma_2 + \delta_0\Gamma_1\right] \tag{8.6}$$

$$E_1 = 2\omega_{2n}\mu_2 \tag{8.7}$$

$$E_3 = 2g\omega_{2n}^2\Lambda_7 \tag{8.8}$$

$$E_4 = 2\sigma\omega_{2n}^2 \tag{8.9}$$

$$E_5 = \frac{1}{4}\left[2\omega_{2n}^2\Lambda_5 - 3\Lambda_4\right] \tag{8.10}$$

$$E_8 = \Omega^2\Lambda_8 f \tag{8.11}$$

Appendix B
Bending-Bending-Torsional Oscillations of Beams to Combination Parametric Excitations

$$
\begin{aligned}
g(s,T_2) = & -2i\omega_v\Phi_v\left(\frac{dA_v}{dT_2}+\frac{c_v}{2}A_v\right) \\
& + \left\{2\omega_v^2\left(\Phi_v'\int_1^s\int_0^s\Phi_v'^2 dsds\right)' - 3\beta_y\left[\Phi_v'\left(\Phi_v'\Phi_v''\right)'\right]'\right\} \\
& \times A_v^2\bar{A}_v - \left\{\beta_\gamma\left[\Phi_\phi'(\Phi_1'+\Phi_2')\right]'' + 2\left(1-\beta_y\right)\left(\Phi_\phi^2\Phi_v''\right)''\right. \\
& \left. - \left(1-\beta_y\right)\left[\Phi_\phi(\Phi_1''+\Phi_2'')\right]'' - \omega_v\omega_\phi J_\xi\left[\Phi_\phi(\Phi_1'-\Phi_2')\right]'\right\} \\
& \times A_vA_\phi\bar{A}_\phi - \left[\beta_\gamma\left(\Phi_\phi'\Phi_3'\right)'' - \left(1-\beta_y\right)\left(\Phi_\phi\Phi_3''\right)''\right. \\
& \left. - \omega_v\omega_\phi J_\xi\left(\Phi_\phi\Phi_3'\right)'\right]\bar{A}_\phi e^{i\sigma T_2} \qquad (8.12) \\
h(s,T_2) = & -2i\omega_\phi\Phi_\phi\left(J_\xi\frac{dA_\phi}{dT_2}+\frac{c_\phi}{2}A_\phi\right) + \left[\left(1-\beta_y\right)\left(\Phi_v''\Phi_3''\right)\right. \\
& \left. - \omega_v\omega_\phi J_\xi\left(\Phi_v'\Phi_3'\right) + \beta_\gamma\left(\Phi_v''\Phi_3'\right)'\right]\bar{A}_v e^{i\sigma T_2} \\
& - \left\{\omega_v\omega_\phi J_\xi\left[\Phi_v'(\Phi_1'-\Phi_2')\right] - \left(1-\beta_y\right)\left[\Phi_v''(\Phi_1''+\Phi_2'')\right]\right. \\
& \left. + 2\left(1-\beta_y\right)\left(\Phi_\phi\Phi_v''^2\right) - \beta_\gamma\left[\Phi_v''(\Phi_1'+\Phi_2')\right]'\right\}A_\phi A_v\bar{A}_v \qquad (8.13)
\end{aligned}
$$

$$g_0(T_2) = -\Bigg[\Big\{\beta_\gamma\left[\Phi''_\phi(\Phi'_1+\Phi'_2)\right] - (1-\beta_y)\left[\Phi_\phi(\Phi'''_1+\Phi'''_2)\right] - \omega_v\omega_\phi J_\xi\left[\Phi_\phi(\Phi'_1-\Phi'_2)\right]\Big\}A_vA_\phi\bar{A}_\phi - \Big[(1-\beta_y)\left(\Phi_\phi\Phi'''_3\right) - \beta_\gamma\left(\Phi''_\phi\Phi'_3\right) + \omega_v\omega_\phi J_\xi\left(\Phi_\phi\Phi'_3\right)\Big]\bar{A}_\phi e^{i\sigma T_2}\Bigg]_{s=1} \tag{8.14}$$

$$\alpha_1 = \int_0^1 \Phi_v\left[\Phi'_\phi(\Phi'_1+\Phi'_2)\right]''ds - \left[\Phi_v\Phi''_\phi(\Phi'_1+\Phi'_2)\right]_{s=1} \tag{8.15}$$

$$\alpha_2 = \int_0^1 \Phi_v\left\{2\left(\Phi^2_\phi\Phi''_v\right)'' - \left[\Phi_\phi(\Phi''_1+\Phi''_2)\right]''\right\}ds + \left[\Phi_v\Phi_\phi(\Phi'''_1+\Phi'''_2)\right]_{s=1} \tag{8.16}$$

$$\alpha_3 = \int_0^1 \Phi_v\left[\Phi_\phi(\Phi'_2-\Phi'_1)\right]'ds + \left[\Phi_v\Phi_\phi(\Phi'_1-\Phi'_2)\right]_{s=1} \tag{8.17}$$

$$\alpha_4 = \int_0^1 \left[\Phi_v\left(\Phi'_\phi\Phi'_3\right)''\right]ds - \left[\Phi_v\left(\Phi''_\phi\Phi'_3\right)\right]_{s=1} \tag{8.18}$$

$$\alpha_5 = -\int_0^1 \left[\Phi_v\left(\Phi_\phi\Phi''_3\right)''\right]ds + \left[\Phi_v\left(\Phi_\phi\Phi'''_3\right)\right]_{s=1} \tag{8.19}$$

$$\alpha_6 = -\int_0^1 \left[\Phi_v\left(\Phi_\phi\Phi'_3\right)'\right]ds + \left[\Phi_v\left(\Phi_\phi\Phi'_3\right)\right]_{s=1} \tag{8.20}$$

$$\alpha_7 = 2\int_0^1 \left[\Phi_v\left(\Phi'_v\int_1^s\int_0^s \Phi'^2_v dsds\right)'\right]ds \tag{8.21}$$

$$\alpha_8 = 3\int_0^1 \Phi_v\left[\Phi'_v\left(\Phi'_v\Phi''_v\right)'\right]'ds \tag{8.22}$$

$$\alpha_9 = -\int_0^1 \Phi_\phi\left[\Phi''_v(\Phi'_1+\Phi'_2)\right]'ds \tag{8.23}$$

$$\alpha_{10} = \int_0^1 \Phi_\phi\Big\{2\left(\Phi_\phi\Phi''^2_v\right) - \left[\Phi''_v(\Phi''_1+\Phi''_2)\right]\Big\}ds \tag{8.24}$$

$$\alpha_{11} = \int_0^1 \left[\Phi_\phi\Phi'_v\left(\Phi'_1-\Phi'_2\right)\right]ds \tag{8.25}$$

$$\alpha_{12} = -\int_0^1 \left[\Phi_\phi\left(\Phi''_v\Phi'_3\right)'\right]ds \tag{8.26}$$

$$\alpha_{13} = -\int_0^1 \left[\Phi_\phi\left(\Phi''_v\Phi''_3\right)\right]ds \tag{8.27}$$

$$\alpha_{14} = \int_0^1 \left[\Phi_\phi\left(\Phi'_v\Phi'_3\right)\right]ds \tag{8.28}$$

$$\mu_i = \frac{1}{2}\int_0^1 c_i\Phi_i^2 ds, \qquad i = v,\ \phi \tag{8.29}$$

$$\delta_1 = \int_0^1 \Phi_v \left[(1-\beta_y) \left(\Phi_\phi \Phi''_w \right)'' - \beta_\gamma \left(\Phi'_\phi \Phi'_w \right)'' \right] ds \tag{8.30}$$

$$\delta_2 = \int_0^1 J_\xi \left[\Phi_v \left(\Phi_\phi \Phi'_w \right)' \right] ds \tag{8.31}$$

$$\delta_3 = -\int_0^1 \beta_y \Phi_v \left[\Phi'_v \left(\Phi'_v \Phi''_v \right)' \right]' ds \tag{8.32}$$

$$\delta_4 = -\frac{1}{2} \int_0^1 \Phi_v \left(\Phi'_v \int_1^s \int_0^s \Phi'^2_v ds ds \right)' ds \tag{8.33}$$

$$\delta_5 = -\int_0^1 (1-\beta_y) \left[\Phi_v \left(\Phi^2_\phi \Phi''_v \right)'' \right] ds \tag{8.34}$$

$$\delta_6 = \int_0^1 \Phi_w \left[(1-\beta_y) \left(\Phi_\phi \Phi''_v \right)'' + \beta_\gamma \left(\Phi'_\phi \Phi''_v \right)' \right] ds \tag{8.35}$$

$$\delta_7 = -\int_0^1 J_\xi \left[\Phi_w \left(\Phi_\phi \Phi'_v \right)' \right] ds \tag{8.36}$$

$$\delta_8 = \int_0^1 \Phi_w ds \tag{8.37}$$

$$\delta_9 = \int_0^1 \Phi_\phi \left[(1-\beta_y) \left(\Phi''_v \Phi''_w \right) + \beta_\gamma \left(\Phi''_v \Phi'_w \right)' \right] ds \tag{8.38}$$

$$\delta_{10} = -\int_0^1 J_\xi \left(\Phi_\phi \Phi'_v \Phi'_w \right) ds \tag{8.39}$$

$$\delta_{11} = -\int_0^1 (1-\beta_y) \left(\Phi_\phi \Phi_\phi \Phi''^2_v \right) ds \tag{8.40}$$

Appendix C

Transfer of Energy from High- to Low-Frequency Modes

$$
\begin{aligned}
g(s,T_1,T_2) = -\Big\{ & D_\zeta \Phi_v^{iv}\eta + m\Phi_v \frac{\partial^2 \eta}{\partial T_1^2} + c_v \Phi_v \frac{\partial \eta}{\partial T_1} + D_\zeta \left[\Phi_v' \left(\Phi_v' \Phi_v''\right)'\right]' \eta^3 \\
& + 2\left[D_\xi \left(\Phi_\phi' \Phi_1'\right)'' - (D_\eta - D_\zeta)\left(\Phi_\phi \Phi_1'' - \Phi_\phi^2 \Phi_v''\right)''\right] \eta A_\phi \bar{A}_\phi \\
& + \left[D_\xi \left(\Phi_\phi' \Phi_2'\right)'' - (D_\eta - D_\zeta)\left(\Phi_\phi \Phi_2''\right)''\right] f\left(A_\phi e^{-i\sigma T_2} + \bar{A}_\phi e^{i\sigma T_2}\right) \Big\}
\end{aligned} \tag{8.41}
$$

$$
\begin{aligned}
h(s,T_1,T_2) = -\Big\{ & 2i\omega_\phi J_\xi \Phi_\phi \frac{dA_\phi}{dT_2} + i\omega_\phi c_\phi \Phi_\phi A_\phi - \Big[(D_\eta - D_\zeta)\left(\Phi_v'' \Phi_1'' - \Phi_\phi \Phi_v''^2\right) \\
& + D_\xi \left(\Phi_v'' \Phi_1'\right)'\Big] \eta^2 A_\phi - \left[(D_\eta - D_\zeta)\left(\Phi_v'' \Phi_2''\right) + D_\xi \left(\Phi_v'' \Phi_2'\right)'\right] f\eta e^{i\sigma T_2} \Big\}
\end{aligned} \tag{8.42}
$$

$$
g_0(T_1,T_2) = -\Big\{ 2D_\xi \left(\Phi_\phi' \Phi_1'\right)' \eta A_\phi \bar{A}_\phi - D_\xi \left(\Phi_\phi' \Phi_2'\right)' f\left(A_\phi e^{-i\sigma T_2} + \bar{A}_\phi e^{i\sigma T_2}\right) \Big\}_{s=L} \tag{8.43}
$$

$$
\alpha_1 = -\int_0^L D_\zeta \Phi_v \left[\Phi_v' \left(\Phi_v' \Phi_v''\right)'\right]' ds \tag{8.44}
$$

$$
\alpha_2 = -\int_0^L \left[D_\xi \Phi_v \left(\Phi_\phi' \Phi_1'\right)'' - (D_\eta - D_\zeta)\Phi_v \left(\Phi_\phi \Phi_1'' - \Phi_\phi^2 \Phi_v''\right)''\right] ds + \left[D_\xi \Phi_v \left(\Phi_\phi' \Phi_1'\right)'\right]_{s=L} \tag{8.45}
$$

$$
\alpha_3 = -\int_0^L \left[D_\xi \Phi_v \left(\Phi_\phi' \Phi_2'\right)'' - (D_\eta - D_\zeta)\Phi_v \left(\Phi_\phi \Phi_2''\right)''\right] ds + \left[D_\xi \Phi_v \left(\Phi_\phi' \Phi_2'\right)'\right]_{s=L} \tag{8.46}
$$

$$
\beta_2 = \int_0^L \left[(D_\eta - D_\zeta)\left(\Phi_\phi \Phi_v'' \Phi_1'' - \Phi_\phi^2 \Phi_v''^2\right) + D_\xi \Phi_\phi \left(\Phi_v'' \Phi_1'\right)'\right] ds \tag{8.47}
$$

$$\beta_3 = \int_0^L \left[(D_\eta - D_\zeta) \left(\Phi_\phi \Phi_v'' \Phi_2'' \right) + D_\xi \Phi_\phi \left(\Phi_v'' \Phi_2' \right)' \right] ds \tag{8.48}$$

$$\nu_1 = \int_0^L D_\zeta \left(\Phi_v'^2 \Phi_v''^2 \right)^2 ds \tag{8.49}$$

$$\nu_2 = \int_0^L \left\{ m\omega_\phi^2 \Phi_1^2 - D_\eta \Phi_1''^2 - 2D_\xi \left(\Phi_\phi' \Phi_v'' \Phi_1' \right) - (D_\eta - D_\zeta) \left(\Phi_\phi^2 \Phi_v''^2 - 2\Phi_\phi \Phi_v'' \Phi_1'' \right) \right\} ds \tag{8.50}$$

$$\nu_3 = \int_0^L \left\{ m\omega_\phi^2 \Phi_1 \Phi_2 - D_\eta \Phi_1'' \Phi_2'' - D_\xi \left(\Phi_\phi' \Phi_v'' \Phi_2' \right) + (D_\eta - D_\zeta) \left(\Phi_\phi \Phi_v'' \Phi_2'' \right) \right\} ds \tag{8.51}$$

Appendix D
Symmetrically Laminated Composite Beams

$$
\begin{aligned}
H_v(s,t) = &-\beta_{11}\left(\phi' w' + v'' w'^2\right)'' - \left(\beta_{22}-\beta_{33}\right)\left(\phi^2 v'' - \phi w''\right)'' \\
&- \beta_{33}\left[v'\left(v' v''\right)' + v'\left(w' w''\right)'\right]' + \beta_{13}\Bigg[\frac{1}{2}\left(\phi'\phi^2\right)' - \left(w' w''\right)'\phi \\
&- \left(2v'' w'\right)' - \frac{1}{2} v'^2 \phi''\Bigg]' + J_\xi \frac{\partial}{\partial t}\left(\dot{\phi} w' + \dot{v}' w'^2\right)' \\
&- \frac{1}{2}\left\{v' \int_1^s \left[\frac{\partial^2}{\partial t^2}\int_0^s \left(v'^2 + w'^2\right) ds\right] ds\right\}' \qquad (8.52) \\
H_w(s,t) = &\ \beta_{11}\left(\phi' v'' + v''^2 w'\right)' + \left(\beta_{22}-\beta_{33}\right)\left(\phi^2 w'' + \phi v''\right)'' \\
&- \beta_{22}\left[w'\left(w' w''\right)'\right]' - \beta_{33}\left[w'\left(v' v''\right)'\right]' + \beta_{13}\Big[v''^2 - \left(\phi\phi'\right)' \\
&- w'\left(\phi v'\right)''\Big]' - J_\xi\left(\dot{\phi}\dot{v}' + \dot{v}'^2 w'\right)' \\
&- \frac{1}{2}\left\{w' \int_1^s \left[\frac{\partial^2}{\partial t^2}\int_0^s \left(v'^2 + w'^2\right) ds\right] ds\right\}' \qquad (8.53) \\
H_\phi(s,t) = &\ \beta_{11}\left(v'' w'\right)' + \left(\beta_{22}-\beta_{33}\right)\left(v'' w'' - \phi v''^2 + \phi w''^2\right) \\
&+ \beta_{13}\left[\frac{1}{2}\left(v'^2 v''\right)' - \frac{1}{2}\phi^2 v''' + v'\left(w' w''\right)' + \phi w'''\right] - J_\xi \frac{\partial}{\partial t}\left(\dot{v}' w'\right) \qquad (8.54)
\end{aligned}
$$

$$
B_{v1}(t) = -\beta_{11}\left(v'' w'^2 + \phi' w'\right) - \left(\beta_{22}-\beta_{33}\right)\left(\phi^2 v'' - \phi w'' - v' w' w''\right)
$$

$$+\beta_{13}\left(\frac{1}{2}\phi^2\phi' - \frac{1}{2}v'^2\phi' - \phi w'w'' - 2v''w'\right) \tag{8.55}$$

$$\begin{aligned} B_{v2}(t) = &-\beta_{11}\left(\phi'w' + w'^2v''\right)' - (\beta_{22}-\beta_{33})\left(\phi^2v'' - \phi w''\right)' \\ &-\beta_{33}\left[v'\left(v'v''\right)' + v'\left(w'w''\right)'\right] + \beta_{13}\left[\frac{1}{2}\left(\phi^2\phi'\right)' - \frac{1}{2}v'^2\phi'' \right. \\ &\left. -\phi\left(w'w''\right)' - 2\left(v''w'\right)'\right] + J_\xi\frac{\partial}{\partial t}\left(\dot{\phi}w' + w'^2\dot{v}'\right) \end{aligned} \tag{8.56}$$

$$B_{w1}(t) = (\beta_{22}-\beta_{33})\left(\phi^2w'' + \phi v''\right) - \beta_{13}\left[\phi\phi' + \left(\phi v'\right)'w'\right] \tag{8.57}$$

$$\begin{aligned} B_{w2}(t) = &\beta_{11}\left(w'v'^2 + v''\phi'\right) - \beta_{22}\left[w'\left(w'w''\right)'\right] - \beta_{33}\left[w'\left(v'v''\right)'\right] - J_\xi\left(w'\dot{v}'^2 + \dot{\phi}\dot{v}'\right) \\ &+(\beta_{22}-\beta_{33})\left(\phi^2w'' + \phi v''\right)' - \beta_{13}\left[w'\left(\phi v'\right)'' + \left(\phi\phi'\right)' - v''^2\right] \end{aligned} \tag{8.58}$$

$$B_{\phi1}(t) = -\beta_{11}\left(v''w'\right) + \beta_{13}\left(\frac{1}{2}\phi^2v'' - \frac{1}{2}v'^2v'' - \phi w'' - v'w'w''\right) \tag{8.59}$$

$$\begin{aligned} H_v^*(s,T_1) = &2i\omega\left(J_\zeta\Phi_v'' - \Phi_v\right)\frac{dA}{dT_1} - (i\omega c_v\Phi_v)A + \frac{f\Omega^2}{2}e^{i\omega\sigma T_1} + \left\{-\beta_{11}\left(\Phi_\phi'\Phi_w'\right)'' \right. \\ &\left. +(\beta_{22}-\beta_{33})\left(\Phi_\phi\Phi_w''\right)'' - 2\beta_{13}\left(\Phi_v''\Phi_w'\right)'' + J_\xi\omega^2\left(\Phi_\phi\Phi_w'\right)'\right\}\left(\bar{A}Be^{2i\omega\delta T_1}\right) \\ &+\left\{-\beta_{11}\left(\Phi_v''\Phi_w'^2\right)'' - \beta_{33}\left[\Phi_v'\left(\Phi_w'\Phi_w''\right)'\right]' - \beta_{13}\left[\left(\Phi_w'\Phi_w''\right)'\Phi_\phi\right]' \right. \\ &\left. -J_\xi\omega^2\left(\Phi_v'\Phi_w'^2\right)'\right\}\left(2AB\bar{B}\right) + \left\{-(\beta_{22}-\beta_{33})\left(\Phi_\phi^2\Phi_v''\right)'' - \beta_{33}\left[\Phi_v'\left(\Phi_v'\Phi_v''\right)'\right]' \right. \\ &\left. +\frac{\beta_{13}}{2}\left(\Phi_\phi'\Phi_\phi^2\right)'' - \frac{\beta_{13}}{2}\left(\Phi_v'^2\Phi_\phi''\right)' + \frac{2\omega^2}{3}\left(\Phi_v'\int_1^s\int_0^s\Phi_v'^2dsds\right)'\right\}\left(3A^2\bar{A}\right) \end{aligned} \tag{8.60}$$

$$\begin{aligned} H_\phi^*(s,T_1) = &-(2i\omega J_\xi\Phi_\phi)\frac{dA}{dT_1} - (i\omega c_\phi\Phi_\phi)A + \left\{\beta_{11}\left(\Phi_v''\Phi_w'\right)' + (\beta_{22}-\beta_{33})\left(\Phi_v''\Phi_w''\right) \right. \\ &\left. -J_\xi\omega^2\left(\Phi_v'\Phi_w'\right) + \beta_{13}\left(\Phi_\phi\Phi_w'''\right)\right\}\left(\bar{A}Be^{2i\omega\delta T_1}\right) + \left\{(\beta_{22}-\beta_{33})\left(\Phi_\phi\Phi_w'^2\right) \right. \\ &\left. +\beta_{13}\Phi_v'\left(\Phi_w'\Phi_w''\right)'\right\}\left(2AB\bar{B}\right) + \left\{-(\beta_{22}-\beta_{33})\left(\Phi_\phi\Phi_v'^2\right) + \frac{\beta_{13}}{2}\left(\Phi_v'^2\Phi_v''\right)' \right. \\ &\left. -\frac{\beta_{13}}{2}\left(\Phi_\phi^2\Phi_v'''\right)\right\}\left(3A^2\bar{A}\right) \end{aligned} \tag{8.61}$$

$$\begin{aligned} H_w^*(s,T_1) = &2i\rho\left(J_\eta\Phi_w'' - \Phi_w\right)\frac{dB}{dT_1} - (i\rho c_w\Phi_w)B + \left\{\beta_{11}\left(\Phi_\phi'\Phi_v''\right)' + (\beta_{22}-\beta_{33})\left(\Phi_\phi\Phi_v''\right)'' \right. \\ &\left. +\beta_{13}\left(\Phi_v'^2\right)' - \beta_{13}\left(\Phi_\phi\Phi_\phi'\right)'' + J_\xi\omega^2\left(\Phi_\phi\Phi_v'\right)'\right\}\left(A^2e^{-2i\omega\delta T_1}\right) + \left\{\beta_{11}\left(\Phi_v'^2\Phi_w'\right)' \right. \\ &\left. +(\beta_{22}-\beta_{33})\left(\Phi_\phi^2\Phi_w''\right)'' - \beta_{33}\left[\Phi_w'\left(\Phi_v'\Phi_v''\right)'\right]' - \beta_{13}\left[\Phi_w'\left(\Phi_\phi\Phi_v'\right)''\right]' - J_\xi\omega^2\left(\Phi_v'^2\Phi_w'\right)'\right\} \end{aligned}$$

$$\times \left(2A\bar{A}B\right) + \left\{ -\beta_{22}\left[\Phi'_w\left(\Phi'_w\Phi''_w\right)'\right]' + \frac{2\rho^2}{3}\left(\Phi'_w\int_1^s\int_0^s \Phi'^2_w ds ds\right)'\right\}\left(3B^2\bar{B}\right) \quad (8.62)$$

$$\begin{aligned} B^*_{v2}(T_1) = {} & \left[2i\omega J_\zeta \Phi'_v(1)\right]\frac{dA}{dT_1} + \left\{ -\beta_{11}\left(\Phi'_\phi\Phi'_w\right)' + \left(\beta_{22}-\beta_{33}\right)\left(\Phi_\phi\Phi''_w\right)' - 2\beta_{13}\left(\Phi''_v\Phi'_w\right)' \right. \\ & \left. + J_\xi\omega^2\left(\Phi_\phi\Phi'_w\right)\right\}_{s=1}\left(\bar{A}Be^{2i\omega\delta T_1}\right) + \left\{ -\beta_{11}\left(\Phi'^2_w\Phi''_v\right)' - \beta_{33}\left[\Phi'_v\left(\Phi'_w\Phi''_w\right)'\right] \right. \\ & \left. - \beta_{13}\left[\Phi_\phi\left(\Phi'_w\Phi''_w\right)'\right] - J_\xi\omega^2\left(\Phi'_v\Phi'^2_w\right)\right\}_{s=1}\left(2AB\bar{B}\right) + \left\{ -\left(\beta_{22}-\beta_{33}\right)\left(\Phi^2_\phi\Phi''_v\right)' \right. \\ & \left. - \beta_{33}\left[\Phi'_v\left(\Phi'_v\Phi''_v\right)'\right] + \frac{\beta_{13}}{2}\left(\Phi^2_\phi\Phi'_\phi\right)' - \frac{\beta_{13}}{2}\left(\Phi'^2_v\Phi''_\phi\right)\right\}_{s=1}\left(3A^2\bar{A}\right) \end{aligned} \quad (8.63)$$

$$\begin{aligned} B^*_{w2}(T_1) = {} & \left[2i\rho J_\eta \Phi'_w(1)\right]\frac{dB}{dT_1} + \left\{\beta_{11}\left(\Phi''_v\Phi'_\phi\right) + \left(\beta_{22}-\beta_{33}\right)\left(\Phi_\phi\Phi''_v\right)' - \beta_{13}\left(\Phi_\phi\Phi'_\phi\right)' + \beta_{13}\left(\Phi''^2_v\right)\right. \\ & \left. + J_\xi\omega^2\left(\Phi_\phi\Phi'_v\right)\right\}_{s=1}\left(A^2e^{-2i\omega\delta T_1}\right) + \left\{\beta_{11}\left(\Phi'_w\Phi''^2_v\right) - \beta_{33}\left[\Phi'_w\left(\Phi'_v\Phi''_v\right)'\right]\right. \\ & \left. + \left(\beta_{22}-\beta_{33}\right)\left(\Phi^2_\phi\Phi''_w\right)' - \beta_{13}\left[\Phi'_w\left(\Phi_\phi\Phi'_v\right)''\right] - J_\xi\omega^2\left(\Phi'^2_v\Phi'_w\right)\right\}_{s=1}\left(2A\bar{A}B\right) \\ & + \left\{ -\beta_{22}\left[\Phi'_w\left(\Phi'_w\Phi''_w\right)'\right]\right\}_{s=1}\left(3B^2\bar{B}\right) \end{aligned} \quad (8.64)$$

$$\Gamma_1 = \int_0^1 \left(J_\zeta\Phi_v\Phi''_v - \Phi^2_v - J_\xi\Phi^2_\phi\right)ds - \left[J_\zeta\Phi_v\Phi'_v\right]_{s=1} \quad (8.65)$$

$$\Gamma_2 = \int_0^1 \left(\frac{c_v}{2}\Phi^2_v + \frac{c_\phi}{2}\Phi^2_\phi\right)ds \quad (8.66)$$

$$\begin{aligned} \Gamma_3 = {} & \int_0^1 \left\{ -\beta_{11}\left[\Phi_v\left(\Phi'_\phi\Phi'_w\right)'' - \Phi_\phi\left(\Phi''_v\Phi'_w\right)'\right] + \left(\beta_{22}-\beta_{33}\right)\left[\Phi_v\left(\Phi_\phi\Phi''_w\right)'' + \left(\Phi_\phi\Phi''_v\Phi''_w\right)\right] \right. \\ & \left. - \beta_{13}\left[2\Phi_v\left(\Phi''_v\Phi'_w\right)'' - \left(\Phi^2_\phi\Phi'''_w\right)\right] + J_\xi\omega^2\left[\Phi_v\left(\Phi_\phi\Phi'_w\right)' - \left(\Phi_\phi\Phi'_v\Phi'_w\right)\right]\right\}ds + \left[\beta_{11}\Phi_v\left(\Phi'_\phi\Phi'_w\right)'\right. \\ & \left. - \left(\beta_{22}-\beta_{33}\right)\Phi_v\left(\Phi_\phi\Phi''_w\right)' + 2\beta_{13}\Phi_v\left(\Phi''_v\Phi'_w\right)' - J_\xi\omega^2\left(\Phi_v\Phi_\phi\Phi'_w\right)\right]_{s=1} \end{aligned} \quad (8.67)$$

$$\begin{aligned} \Gamma_4 = {} & \int_0^1 \left\{ -\beta_{11}\Phi_v\left(\Phi''_v\Phi'^2_w\right)'' - \beta_{33}\Phi_v\left[\Phi'_v\left(\Phi'_w\Phi''_w\right)'\right]' + \left(\beta_{22}-\beta_{33}\right)\left(\Phi^2_\phi\Phi''^2_w\right) - J_\xi\omega^2\Phi_v\left(\Phi'_v\Phi'^2_w\right)' \right. \\ & \left. - \beta_{13}\Phi_v\left[\left(\Phi'_w\Phi''_w\right)'\Phi_\phi\right]' + \beta_{13}\Phi_\phi\Phi'_v\left(\Phi'_w\Phi''_w\right)'\right\}ds + \left\{\beta_{11}\Phi_v\left(\Phi'^2_w\Phi''_v\right)' + \beta_{33}\Phi_v\left[\Phi'_v\left(\Phi'_w\Phi''_w\right)'\right]\right. \\ & \left. + \beta_{13}\Phi_v\left[\Phi_\phi\left(\Phi'_w\Phi''_w\right)'\right] + J_\xi\omega^2\left(\Phi_v\Phi'_v\Phi'^2_w\right)\right\}_{s=1} \end{aligned} \quad (8.68)$$

$$\Gamma_5 = \int_0^1 \left\{ -\beta_{33}\Phi_v\left[\Phi'_v\left(\Phi'_v\Phi''_v\right)'\right]' - \left(\beta_{22}-\beta_{33}\right)\left[\Phi_v\left(\Phi^2_\phi\Phi''_v\right)'' + \left(\Phi^2_\phi\Phi''^2_v\right)\right] + \frac{\beta_{13}}{2}\left[\Phi_v\left(\Phi'_\phi\Phi^2_\phi\right)''\right.\right.$$

$$- \Phi_v \left(\Phi_v'^2 \Phi_\phi''\right)' + \Phi_\phi \left(\Phi_v'^2 \Phi_v''\right)' - \left(\Phi_\phi^3 \Phi_v'''\right) \Big] + \frac{2\omega^2}{3} \Phi_v \left(\Phi_v' \int_1^s \int_0^s \Phi_v'^2 ds ds\right)' \Big\} ds$$
$$+ \left\{ \beta_{33} \Phi_v \left[\Phi_v' \left(\Phi_v' \Phi_v''\right)'\right] + \left(\beta_{22} - \beta_{33}\right) \Phi_v \left(\Phi_\phi^2 \Phi_v''\right)' - \frac{\beta_{13}}{2} \left[\Phi_v \left(\Phi_\phi^2 \Phi_\phi'\right)' - \left(\Phi_v \Phi_v'^2 \Phi_\phi''\right)\right] \right\}_{s=1} \tag{8.69}$$

$$\Gamma_6 = \int_0^1 \left(\frac{\Omega^2}{2} f \Phi_v\right) ds \tag{8.70}$$

$$\Lambda_1 = \int_0^1 \left(J_\eta \Phi_w \Phi_w'' - \Phi_w^2\right) ds - \left[J_\eta \Phi_w \Phi_w'\right]_{s=1} \tag{8.71}$$

$$\Lambda_2 = \int_0^1 \left(\frac{c_w}{2} \Phi_w^2\right) ds \tag{8.72}$$

$$\Lambda_3 = \int_0^1 \Big\{ \beta_{11} \Phi_w \left(\Phi_\phi' \Phi_v''\right)' + \left(\beta_{22} - \beta_{33}\right) \Phi_w \left(\Phi_\phi \Phi_v''\right)'' + \beta_{13} \left[\Phi_w \left(\Phi_v''^2\right)' - \Phi_w \left(\Phi_\phi \Phi_\phi'\right)''\right]$$
$$+ J_\xi \omega^2 \Phi_w \left(\Phi_\phi \Phi_v'\right)' \Big\} ds - \Big\{ \beta_{11} \left(\Phi_w \Phi_v'' \Phi_\phi'\right) + \left(\beta_{22} - \beta_{33}\right) \Phi_w \left(\Phi_\phi \Phi_v''\right)'$$
$$- \beta_{13} \left[\Phi_w \left(\Phi_\phi \Phi_\phi'\right)' - \left(\Phi_w \Phi_v''^2\right)\right] + J_\xi \omega^2 \left(\Phi_w \Phi_\phi \Phi_v'\right) \Big\}_{s=1} \tag{8.73}$$

$$\Lambda_4 = \int_0^1 \Big\{ \beta_{11} \Phi_w \left(\Phi_v''^2 \Phi_w'\right)' + \left(\beta_{22} - \beta_{33}\right) \Phi_w \left(\Phi_\phi^2 \Phi_w''\right)'' - \beta_{33} \Phi_w \left[\Phi_w' \left(\Phi_v' \Phi_v''\right)'\right]'$$
$$- \beta_{13} \Phi_w \left[\Phi_w' \left(\Phi_\phi \Phi_v'\right)''\right]' - J_\xi \omega^2 \Phi_w \left(\Phi_v'^2 \Phi_w'\right)' \Big\} ds - \Big\{ \beta_{11} \left(\Phi_w \Phi_w' \Phi_v''^2\right) - \beta_{33} \left[\Phi_w \Phi_w' \left(\Phi_v' \Phi_v''\right)'\right]$$
$$+ \left(\beta_{22} - \beta_{33}\right) \Phi_w \left(\Phi_\phi^2 \Phi_w''\right)' - \beta_{13} \left[\Phi_w \Phi_w' \left(\Phi_\phi \Phi_v'\right)''\right] - J_\xi \omega^2 \left(\Phi_w \Phi_v'^2 \Phi_w'\right) \Big\}_{s=1} \tag{8.74}$$

$$\Lambda_5 = \int_0^1 \Big\{ - \beta_{22} \Phi_w \left[\Phi_w' \left(\Phi_w' \Phi_w''\right)'\right]' + \frac{2\rho^2}{3} \Phi_w \left(\Phi_w' \int_1^s \int_0^s \Phi_w'^2 ds ds\right)' \Big\} ds$$
$$+ \left\{ \beta_{22} \left[\Phi_w \Phi_w' \left(\Phi_w' \Phi_w''\right)'\right] \right\}_{s=1} \tag{8.75}$$

$$\Pi_1 = - \int_0^1 \left(\Phi_v^2 + J_\zeta \Phi_v'^2 + J_\xi \Phi_\phi^2\right) ds \tag{8.76}$$

$$\Pi_2 = - \int_0^1 \left(\Phi_w^2 + J_\eta \Phi_w'^2\right) ds \tag{8.77}$$

$$\Pi_3 = \int_0^1 \Big[- J_\xi \omega^2 \left(\Phi_\phi \Phi_v' \Phi_w'\right) - \beta_{11} \left(\Phi_\phi' \Phi_v'' \Phi_w'\right) + \beta_{22} \left(\Phi_\phi \Phi_v'' \Phi_w''\right) - \beta_{33} \left(\Phi_\phi \Phi_v'' \Phi_w''\right)$$
$$- \beta_{13} \left(\Phi_w' \Phi_v''^2\right) - \beta_{13} \left(\Phi_\phi \Phi_\phi' \Phi_w''\right) \Big] ds \tag{8.78}$$

$$\Pi_4 = \int_0^1 \Big[J_\xi \omega^2 \left(\Phi_v'^2 \Phi_w'^2\right) - \beta_{11} \left(\Phi_v''^2 \Phi_w'^2\right) + \beta_{22} \left(\Phi_\phi^2 \Phi_w''^2\right) - 2\beta_{33} \left(\Phi_v' \Phi_v'' \Phi_w' \Phi_w''\right) - \beta_{33} \left(\Phi_\phi^2 \Phi_w''^2\right) - 2\beta_{13} \left(\Phi_v' \Phi_w' \Phi_\phi' \Phi_w''\right) - 2\beta_{13} \left(\Phi_\phi \Phi_w' \Phi_v'' \Phi_w''\right) \Big] ds \tag{8.79}$$

$$\Pi_5 = \int_0^1 \left[\frac{1}{3} \omega^2 \left(\int_0^s \Phi_v'^2 ds \right)^2 - \beta_{22} \left(\Phi_\phi^2 \Phi_v''^2\right) + \beta_{33} \left(\Phi_\phi^2 \Phi_v''^2\right) - \beta_{33} \left(\Phi_v'^2 \Phi_v''^2\right) + \beta_{13} \left(\Phi_\phi^2 \Phi_\phi' \Phi_v''\right) - \beta_{13} \left(\Phi_v'^2 \Phi_\phi' \Phi_v''\right) \right] ds \tag{8.80}$$

$$\Pi_6 = \int_0^1 \left[\frac{1}{3} \rho^2 \left(\int_0^s \Phi_w'^2 ds \right)^2 - \beta_{22} \left(\Phi_w'^2 \Phi_w''^2\right) \right] ds \tag{8.81}$$

$$\Pi_7 = \int_0^1 \left(\frac{c_v}{2} \Phi_v^2 + \frac{c_\phi}{2} \Phi_\phi^2 \right) ds \tag{8.82}$$

$$\Pi_8 = \int_0^1 \left(\frac{c_w}{2} \Phi_w^2 \right) ds \tag{8.83}$$

$$\Pi_9 = \int_0^1 \left(\frac{\Omega^2}{2} f \Phi_v \right) ds \tag{8.84}$$

Vita

Haider N. Arafat was born on March 16, 1968 in the city of Nablus on the West Bank. He lived in Amman, Jordan until May of 1986 where he graduated from Collège de la Salle/Frère high school. He then travelled to the United States to attend Albright College in Reading, Pennsylvania. In July of 1988, he transferred to the University of Michigan in Ann Arbor where he received a Bachelor of Science degree in Mechanical Engineering in December of 1990 and two Master of Science degrees in Mechanical Engineering and in Applied Mechanics in May of 1993. In August of 1993, he began a new journey in the small village of Blacksburg, Virginia where he joined the Department of Engineering Science and Mechanics at Virginia Polytechnic Institute and State University (Virginia Tech). After going through many hills and valleys, he got to the finish line on April 9, 1999 where he successfully defended his dissertation to receive a Doctor of Philosophy degree in Engineering Mechanics.